Impact of climate changes on the phenotype of Moroccan small mammals from Pleistocene to Anthropocene

Léa Terray


Université de Paris

École doctorale 474 : Frontières de l'Innovation en Recherche et Education

Laboratoires : Institut de Systématique, Evolution, Biodiversité - UMR 7205
Laboratoire des Sciences du Climat et de l'Environnement - UMR 8212 / UMR 8112

Impact of climate changes on the phenotype of Moroccan small mammals from Pleistocene to Anthropocene

Par Léa Terray

Thèse de doctorat en Ecologie, Evolution et Biologie Environnementale

Dirigée par Raphaël Cornette et Pascale Braconnot

Présentée et soutenue publiquement le 1er avril 2022

Devant un jury composé de

Lionel Hautier, CR CNRS, ISEM Montpellier	Rapporteur
Yannick Donnadieu, DR, CEREGE Aix-en-Provence	Rapporteur
Pierre Sepulchre, CR CNRS, CEA Paris-Saclay Orme des Merisiers	Examinateur
Antigoni Kaliontzopoulou, Auxiliary researcher, Universidade do Porto	Examinatrice
Sandrine Meylan, Professeure, IEES Paris	Examinatrice
Raphaël Cornette, Dr, MNHN Paris	Directeur
Pascale Braconnot, DR, CEA Paris-Saclay Orme des Merisiers	Co-Directrice

Impact of climate changes on the phenotype of Moroccan small mammals from Pleistocene to Anthropocene

Abstract *(english version)*

The climate and the environment determine the ecological context in which organisms live, at global and local scale respectively. The first refers to the physical characteristics of the atmosphere, while the second defines the surroundings of living organisms. In response to these external variations, organisms may display phenotypic changes. In this thesis, we explore the impact of both climate and environment on the phenotype of Moroccan small mammals. We consider two aspects of the phenotype: the morphological and the functional aspects. We confront two taxa, rodents and shrews, from El Harhoura 2 cave (Rabat, Morocco), an archeological site of exceptional taxonomic richness dated from late Pleistocene to mid-Holocene. We extend this timeline to current days, providing a phenotypic sequence covering the last 100 ka. In chapter 1, we assess the morphological variation in rodent's lower and upper first molars in relation to local environenmtental changes. We show that local paleoenvironments recorded by faunal assemblages are related with teeth morphology. In chapter 2, we examine the response of a functional trait, shrew's estimated bite force, to local paleoenvironmental changes. The functional trait appears to be a good indicator of transitions between arid and humid environments, supporting that functional traits may be relevant bio-paleoindicators. In chapter 3, we reconstruct global climate changes over the EH2 sequence using a set of paleoclimate simulations corresponding to the stratigraphical layers of EH2. The climate sequence described by simulations allows us to discuss and refine the chronological and paleoenvironmental context of our site. In chapter 4, we explore the covariation between the global climate changes simulated and the morphological and functional traits of rodents and shrews. All phenotypic traits are signifcantly related to climate variation, certainly through available ressources. The impact of climate on the morpho-functional aspects of the shrew mandible is not the same in present days as in the past, suggesting that another selective pressure might currently interfere with climate, as anthropic disturbances. Altogether, this work highlights the complexity of the phenotypic response to external variations (environmental and climatic). Our results support that environmental changes on EH2 triggered minor morphological and functional adjustements, thank to adaptation and phenotypic plasticity, suggesting a potential alternative behavioral response. Climate changes appear to have induced important morphological and functional responses, also through both adaptation and phenotypic plasticity. Standing at the intersection between biology and paleoclimatology, this study introduces a promising new way to address climate in evolutionary biology and archaeology.

Keywords – Phenotypic evolution, paleoclimates, rodents, shrews, geometric morphometrics, Morocco

Abstract *(version française)*

Le climat et l'environnement déterminent le contexte écologique dans lequel vivent les organismes, respectivement à l'échelle globale et locale. Le climat fait référence aux caractéristiques physiques de l'atmosphère tandis que l'environnement désigne le milieu de vie. En réponse à ces variations externes, les organismes peuvent présenter des changements phénotypiques. Dans cette thèse, nous explorons l'impact du climat et de l'environnement sur le phénotype des petits mammifères marocains. Nous considérons deux aspects du phénotype : le morphologique et le fonctionnel. Pour ce faire, nous avons étudié les restes de rongeurs et de musaraignes provenant du site archéologique El Harhoura 2 (Rabat, Maroc), exceptionel pour sa richesse spécifique. Ce site est daté du Pléistocène supérieur à l'Holocène moyen, et, pour étendre la chronologie jusqu'à nos jours, du matériel actuel a été ajouté, fournissant une séquence phénotypique couvrant les 100 derniers ka. Le chapitre 1 évalue la variation morphologique des premières molaires inférieures et supérieures des rongeurs en relation avec les changements environnementaux. Nous montrons que ces différences morphologiques sont liées à la variation paléoenvironnementale enregistrée par les assemblages fauniques. Le chapitre 2 examine la réponse d'un trait fonctionnel, la force de morsure estimée des musaraignes, aux changements paléoenvironnementaux. Ce trait semble être un bon indicateur des transitions entre les environnements arides et humides, ce qui confirme le potentiel des traits fonctionnels à être des indicateurs paleoenvironnementaux pertinents. Le chapitre 3 présente une reconstruction des changements climatiques à EH2. Nous avons produit un ensemble de simulations paleoclimatiques correspondant aux couches stratigraphiques de notre site. La séquence climatique décrite par ces simulations nous permet de discuter et d'affiner le contexte chronologique et paléoenvironnemental de EH2. Le chapitre 4 explore la covariation entre les variations climatiques simulées précédemment et les traits morphologiques et fonctionnels des rongeurs et des musaraignes. L'ensemble des traits phénotypiques est significativement impacté par les changements climatiques, certainement *via* les ressources disponibles. L'impact du climat sur les aspects morpho-fonctionnels de la mandibule de la musaraigne n'est pas le même aujourd'hui que par le passé, ce qui suggère que d'autres pressions sélectives pourraient actuellement être à l'oeuvre, possiblement liées aux perturbations anthropiques. Dans l'ensemble, ce travail souligne la complexité de la réponse phénotypique aux variations externes. Nos résultats suggèrent que les changements environnementaux à EH2 ont induit des variations morphologiques et fonctionnelles mineures, *via* adaptation et plasticité phénotypique, impliquant une éventuelle participation du comportement dans la réponse phénotypique. A l'inverse, les changements climatiques semblent avoir induit d'importantes réponses morphologiques et fonctionnelles, par adaptation et plasticité phénotypique. Se situant à l'intersection entre la biologie et la paléoclimatologie, cette étude introduit une nouvelle voie prometteuse d'aborder le climat en biologie évolutive et en archéologie.

Mots clés – Evolution phéntoypique, paléoclimats, rongeurs, musaraignes, morphométrie géométrique, Maroc

Résumé en français

Introdution et problématique

Le climat de la Terre n'a cessé de changer au cours des temps et continuera de le faire dans l'avenir. Comment les organismes vivants font-ils face à ces changements ? Cette question a fait l'objet d'un intérêt croissant de la part de la communauté scientifique au cours des dernières décennies, notamment dans le contexte du changement climatique actuel.

Le climat et l'environnement déterminent le contexte écologique dans lequel vivent les organismes. D'une part, l'environnement désigne leur milieu de vie, i.e. leur habitat. En context archéologique ou paléontologique, il est généralement inféré à partir d'indicateurs comme les assemblages fauniques, les indices de diversité ou les registres palynologiques. Ces indicateurs fournissent une estimation qualitative approximative du paysage, tels que le type de végétation possible, la couverture végétale et l'abondance des points d'eau. Ils fournissent une information à une échelle géographique très locale (l'échelle des communautés fauniques ou même des individus). D'autre part, le climat fait référence aux caractéristiques physiques de l'atmosphère. Les simulations paleoclimatiques peuvent apporter une estimation quantifiée des paléoclimats. Pour les simuler, elles s'appuient sur des modèles climatiques globaux qui modélisent la dynamique et la thermodynamique de l'atmosphère, de l'océan et des surfaces continentales et gelées, couplés aux cycles de l'eau et du carbone. Ces modèles décrivent les tendances à grande échelle des changements climatiques passés. A l'évidence, l'environnement est fortement conditionné par le climat. Cependant, d'autres facteurs l'influencent également, e.g. la topographie locale (la présence d'une colline, d'une falaise ou d'un lac) ou l'écologie des organismes de la localité.

En réponse à ces variations climatiques et environnementales, les organismes peuvent présenter des changements phénotypiques. La plupart des études abordant la question de l'impact du climat sur l'évolution des organismes au cours du temps se sont concentrées sur l'échelle macroévolutive. Cependant, sur de courtes périodes, les réponses premières des organismes sont plus généralement liées à la microévolution et/ou à la plasticité phénotypique, tel que mis en évidence par le changement climatique actuel. Pour évaluer la réponse globale des organismes au climat, nous avons donc considéré sans *a priori* ces niveaux de variations affectés par les changements climatiques. Nous avons choisit d'utiliser des groupes morphologiques comme unité de biodiversité. Ils permettent de

considérer les variations à plusieurs niveaux de diversité (inter- et intra-spécifique), ce qui en fait une approche pertinente pour caractériser la sélection liée à l'environnement qui agit à ces deux niveaux. Les variations morphologiques et fonctionelles peuvent être efficacement caractérisées *via* la morphométrie géométrique, un ensemble de méthodes qui permettent une quantification statistique et une visualisation des formes et, ainsi, d'identifier les trajectoires des changements morphologiques.

Au cours de ce travail de thèse, nous avons exploré l'impact du climat et de l'environnement sur le phénotype des petits mammifères marocains. Nous avons considéré deux aspects du phénotype : le morphologique et le fonctionnel. Pour ce faire, nous avons étudié les restes de rongeurs et de musaraignes provenant du site archéologique El Harhoura 2 (Rabat, Maroc), exceptionnel pour sa richesse spécifique. Ce site est daté du Pléistocène supérieur à l'Holocène moyen, et, pour étendre la chronologie jusqu'à nos jours, du matériel actuel a été ajouté, fournissant une séquence phénotypique couvrant les 100 derniers ka.

Les chapitres et leurs principaux résultats

Le chapitre 1 évalue la variation morphologique des premières molaires inférieures et supérieures des rongeurs en relation avec les changements environnementaux locaux. Comme unité phénotypique sans *a priori* nous avons utilisé des groupes morphologiques. Les paléoenvironnements sur El Harhoura 2 ont été très étudiés à travers les assemblages faunistiques et l'étude des isotopes. Globalement, les proxys environnementaux ont révélé une alternance d'environnements relativement humides et arides. *Via* un protocole d'acquisition semi-automatique, nous démontrons que la variation morphologique des molaires de rongeurs est liée à la variation paléoenvironnementale enregistrée par les assemblages fauniques et les isotopes. Les groupes morphologiques ne sont pas sensibles aux mêmes transitions environnementales et semblent en effet être des groupes écologiques transversaux entre les espèces. Principalement, les rongeurs ayant vécu dans des milieux plus humides présentent des molaires plus érodées, ce qui peut être dû à l'abrasion liée à un régime alimentaire fortement dominé par les plantes. Cependant, ces variations morphologiques ne concernent pas l'axe principal de variation phénotypique : elles ne correspondent pas à la partition faite par les groupes morphologiques, mais induisent des changements de forme au sein d'eux.

Les traits fonctionnels, parce qu'ils ne sont pas soumis aux mêmes pressions de sélection que les traits morphologiques, pourraient présenter une sensibilité différente aux changements climatiques. C'est pourquoi le chapitre 2 examine la réponse d'un trait fonctionnel, la force de morsure des musaraignes, aux changements paléoenvironnementaux locaux. Cette force de morsure est estimée à l'aide d'un modèle biomécanique. Les différents groupes morphologiques présentent chacun des caractéristiques fonctionnelles différentes. A chaque transition environnementale, d'importantes variations fonctionnelles sont observées. En particulier, la force de morsure estimée des musaraignes semble être un bon indicateur des transitions entre les environnements arides et humides. La nature complémentaire des indicateurs morphologiques et fonctionnels nous permet de mettre en évidence des évènements de convergence et de divergence fonctionnelle. Cependant, encore une fois, la réponse phénotypique détectée a principalement lieu au sein des groupes morphologiques.

Les deux premiers chapitres confirment que les variations environnementales locales ont un impact significatif sur le phénotype des rongeurs et des musaraignes. Cependant, elles n'affectent pas la variation phénotypique principale. Nous allons tester si les changements climatiques globaux impactent davantage les traits morphologiques et fonctionnels. Pour explorer cette piste, nous devons d'abord caractériser ces changements climatiques globaux au cours de la séquence à El Harhoura 2.

Le chapitre 3 présente une reconstruction des changements climatiques globaux à El Harhoura 2. Nous avons produit un ensemble de simulations correspondant aux couches stratigraphiques du site en utilisant le modèle LMDZOR6A. Les simulations décrivent une séquence climatique en deux phases à El Harhoura 2 : une humidification progressive suivie d'une transition abrupte vers un climat plus aride, puis un climat de moins en moins aride jusqu'à aujourd'hui. Nous démontrons également comment les simulations paléoclimatiques peuvent contribuer à affiner le contexte chronologique et paléoenvironnemental de notre site en évaluant la cohérence entre la séquence climatique décrite par les simulations et les proxys paléoenvironnementaux. Dans notre cas, la séquence climatique correspondant aux âges combinés US-ESR s'avère beaucoup plus cohérente avec les inférences paléoenvironnementales que celle correspondant aux âges OSL. Nos résultats permettent également de discuter des divergences qui existent entre les inférences paléoenvironnementales basées sur les assemblages de faune et celles basées sur les études isotopiques. S'ils sont plus cohérents avec les conclusions tirées de ces dernières,

ils mettent avant tout en évidence la différence d'échelle entre les informations fournies par chacun de ces indicateurs. Ce chapitre démontre que la combinaison de différentes sources de données environnementales et de simulations climatiques a un grand potentiel pour affiner le contexte paléoenvironnemental et chronologique des sites archéologiques et paléontologiques.

Le chapitre 4 explore les covariations entre le climat précédemment simulé et les traits morphologiques et fonctionnels des rongeurs et des musaraignes. Tous les traits phénotypiques covarient significativement avec les changements climatiques. Le stress hydrique, la température et l'insolation semblent avoir une implication plus importante dans ces covariations que les autres variables climatiques. Ces trois facteurs influençant la composition des communautés végétales, nous supposons qu'ils influencent indirectement le phénotype *via* les ressources disponibles. En ce qui concerne les dents de rongeurs, les changements de forme induits par le climat semblent liés à des variations dans leurs habitudes alimentaires entre des régimes plus ou moins faunivores et herbivores. Les groupes morphologiques révèlent un axe de variation proche du patron intraspécifique partagé par plusieurs espèces. Il semble traduire des ajustements morphologiques aux changements d'amplitude de variations saisonnière, *via* adaptation ou plasticité phénotypique développementale. Pour les musaraignes, la forme de mandibule associée à un régime plus généraliste est favorisée dans des conditions plus sèches et plus stressantes, à travers des processus de plasticité phénotypique et d'adaptation. L'impact du climat sur les aspects morpho-fonctionnels de la mandibule de la musaraigne n'est pas le même aujourd'hui que par le passé, ce qui suggère que d'autres pressions sélectives pourraient actuellement être à l'oeuvre, possiblement liées aux perturbations anthropiques.

Conclusions

Pour conclure, il est tout d'abord essentiel de revenir sur le sens évolutif et écologique du concept de groupes morphologiques, présent à travers toute la thèse. Les groupes morphologiques représentent des groupes d'individus trans-spécifiques qui diffèrent par leur forme et leurs capacités fonctionnelles. Ils sont distribués le long de l'axe principal de la variation phénotypique. Cet axe principal de variation phénotypique est partagé entre plusieurs espèces et semble lié à l'écologie alimentaire. Cela suggère, au moins en ce qui concerne les espèces étudiées, que les niches alimentaires sont distribuées au niveau de la

population et non de l'espèce. Des individus de différentes espèces peuvent partager une même niche alimentaire car ils consomment les mêmes ressources. Au contraire, des congénères peuvent occuper des niches alimentaires différentes et consommer des ressources différentes. Cette partition alimentaire est liée au fait que les espèces étudiées ici ont un régime alimentaire opportuniste.

Dans son ensemble, ce travail suggère que les changements climatiques globaux ont un impact sur la variation morphologique et fonctionnelle principale, alors que les changements environnementaux locaux affectent des axes de variation plus mineurs. L'environnement et le climat semblent avoir un impact différentiel sur le phénotype des organismes. L'environnement déterminant le milieu physique au sein duquel les organismes vivent, on s'attendrait à ce qu'il détermine le phénotype plus que le climat global et les conditions atmosphériques. Une explication possible est que les variations environnementales ont pu être tempérées par des ajustements comportementaux. Ces derniers permettent à un organisme de s’ajuster aux conditions de son environnement immédiat, et donc d'augmenter sa valeur sélective, sans modifier d'autres aspects de son phénotype tels que sa morphologie, ses capacités fonctionnelles ou sa physiologie. Par conséquent, le découplage environnement/climat que nous avons mis en évidence peut expliquer les différents aspects et intensités de la variation phénotypique.

Remerciements

En premier lieu, je souhaite remercier Lionel Hautier et Yannick Donnadieu d'avoir acceptés d'être les rapporteurs de ce travail, ainsi que Pierre Sepulchre, Antigoni Kaliontzopoulou et Sandrine Meylan d'en être les examinateur·trices. Je suis sincèrement honorée d'avoir un tel jury, et de sa diversité scientifique.

Ce manuscrit est avant tout le fruit d'échanges, tant scientifiques qu'humains, avec les personnes qui m'ont accompagnée au cours de ces trois dernières années.

Tout d'abord je tiens à remercier mon directeur de thèse, Raphaël Cornette, de m'avoir offert l'opportunité de réaliser cette thèse. Il a veillé au bon déroulement de ce travail, tout en me laissant la liberté de mener mes recherches où la curiosité m'appelait (sous condition de lui soumettre un argumentaire scientifique imparable). Raph, merci d'avoir pris sous ton aile le petit scarabée que je suis. Je te suis reconnaissante pour la confiance et le soutien que tu m'apportes, et ce depuis bien avant le début de la thèse. Merci. Enfin, tu vois le genre… !

Je voudrais également remercier vivement Pascale Braconnot, ma co-directrice de thèse. Elle m'a accompagnée tout au long de mon initiation tant conceptuelle que méthodologique au domaine de la paléoclimatologie. Pascale, merci d'avoir ouvert les portes virtuelles de la modélisation climatique à une néophyte intriguée. Je regrette que la période sanitaire ne m'ait pas permis de participer davantage à la vie du LSCE.

Je tiens à remercier les personnes qui m'ont accordée l'accès aux différentes sources de matériel de micromammifères : Roland Nespoulet and Mohamed A. El Hajraoui (directeurs de la Mission Archéologique franco-marocaine El Harhoura-Témara), Violaine Nicolas-Colin (collections actuelles, MNHN), Christine Steininger (collections fossiles, Wits University), Thalassa Matthews et Sarena Govender (collections fossiles, Iziko South African Museum) et Denis Geraads (fossiles de la région de Rabat-Témara).

J'aimerais témoigner ma profonde reconnaissance à Emmanuelle Stoetzel, pour son implication tout au long de cette thèse. Emma, merci d'avoir partagé avec moi ta passion de l'archéologie et tes grandes connaissances sur El Harhoura 2, ainsi que pour tes conseils et ta réactivité. Merci de m'avoir initiée au monde fascinant de l'archéologie.

J’aimerais exprimer ma gratitude à Elsem Ben Arous, qui a toujours répondu présente lorsque les datations stratigraphiques me donnaient du fil à retordre, ainsi qu’à Marion Segall pour ses conseils méthodologiques et conceptuels. Merci Eslem et Marion pour votre gentillesse et vos encouragements.

Merci également à David Nerini, Anthony Herrel et Masa Kageyama pour leur intérêt pour ce travail et pour leur aide, toujours dispensée avec bienveillance.

Je souhaite également remercier Philippe Grandcolas, directeur de l’ISYEB (UMR 7205), Violaine Llaurens, responsable de l’équipe Evolution et Développement des Variations Phénotypiques, ainsi que tous les membres de l’équipe de m’avoir accueillie ces trois dernières années. En particulier, merci à Arnaud Delapré et Céline Houssin pour leur disponibilité et leur immuable bonne humeur. Merci à Sylvianne Babin et Guzide Selcuk pour leur aide à la gestion des aspects administratifs de la thèse, ainsi qu’à Gilles Cottavoz, de l’équipe logistique, pour sa présence souriante.

Je tiens à remercier mes acolytes du fameux bureau de la « lose », sans qui ces trois années ne se ressembleraient pas : Charline pour ta bonne humeur et ton soutien moral indéfectible ; Ludo pour tes questionnements métaphysiques et politiques, qui nous font relativiser nos petits ennuis du quotidien ; Ariane pour ta pétillance et tes conseils capillaires ; Camille, maintenant membre émérite du bureau, pour ta constance à tout épreuve ; Ombeline, émérite parmi les émérites, pour ton humour toujours plus imprévisible ; Pierre, pour nos échanges sur les micromammifères, et pour me faire me sentir moins seule au milieu de ces groupies des papillons ; Vio, Erika et Maël pour tous ces bons moments. Merci à tous pour les instants de militantisme partagés, dont la colonne de la révolte restera l’éternel vestige (sous réverse de la durée de vie d’un autocollant). Pour votre soutien à travers les doutes et les remises en question. Pour cette gaieté et cette complicité inaltérable, même en période troublée de COVID, face auquel nous avons vaillamment pris les armes (virtuelles) et sommes partis en quête d’aventures (virtuelles) ! (*long live* la guilde du Renard Blanc)

Un grand merci également à Margot Michaud et Kévin Le Verger, pour les discussions de certains points importants de ce travail, mais surtout pour les échanges scientifiques toujours plus enrichissants.

Je tiens aussi à remercier mes amis qui ont pavé d’instants joyeux ces trois années, quelles que soient les circonstances : Joce, Cèb, Delphine, Cécilia, Clothilde ; ainsi que mes

compagnons investigateurs des innommables horreurs Lovecraftiennes Marjo, Louis, Rohan et Margot. Megann, merci pour ta présence joyeuse au quotidien, ton humour parfois douteux et ton assistance pour la fin de ce travail.

Et, en particulier, merci à mes parents, pour leur soutien indéfectible. Maman, merci pour ta présence quand le moral n'était pas toujours au beau fixe, et pour ton implication dans le sprint final de la thèse. Papa, encore merci pour tes suggestions avisées. C'était un plaisir de plonger dans la discipline qui occupe tes journées.

A vous tous, merci de m'avoir permis d'ajouter ma petite touche de pinceau sur la grande toile de la science.

Table of contents

Introduction

The Earth's climate has changed continuously over time and will continue to do so in the future (e.g., Paillard, 2001; Duplessy & Ramstein, 2013; Masson-Delmotte *et al.*, *in press*). How do living organisms react and eventually cope with these climate changes has been a growing topic in the scientific community over the past decades (e.g., Bown, Holroyd, & Rose, 1994; Angilletta, Jr & Dunham, 2003; Girard, Renaud, & Korn, 2004; Clavel & Morlon, 2017; Nogués-Bravo *et al.*, 2018), especially in the context of ongoing climate change induced by human activity (e.g., Renaud, Benammi, & Jaeger, 1999; Kaňuščák *et al.*, 2004; Parmesan & Matthews, 2005; Parmesan, 2006; Hendry, Farrugia, & Kinnison, 2008; Bickford *et al.*, 2010; Reed, Schindler, & Waples, 2011; Gardner *et al.*, 2011; Boutin & Lane, 2014; Radchuk *et al.*, 2019). Since the 17th century, we have entered a period of significant environmental changes, which marks the beginning of a new geological era characterized by human activity domination: the Anthropocene (Lewis & Maslin, 2015). The veracity of the Anthropocene is supported by a growing set of biotic, sedimentary and geochemical arguments (e.g., Zalasiewicz *et al.*, 2008; Lewis & Maslin, 2015; Young *et al.*, 2016; Masson-Delmotte *et al.*, *in press*). The numerous changes that occurred since our entry into this new era lead to a defaunation phenomenon (Young *et al.*, 2016) qualified as 6th extinction (Ceballos, Ehrlich, & Dirzo, 2017). Causes are of different nature, notably ecological and climatic, through fragmentation and habitat loss, the introduction of invasive species, the rise in atmospheric, land and water temperatures, etc. (Cassou & Guilyardi 2007).

To anticipate the consequences of the current climate changes on organismal biodiversity in the future, we need to understand the impact of climate variations on the evolution of organisms over time.

An integrative consideration of the phenotypic response

The fossil and paleoclimate archives can provide some insight into this issue. Most studies addressing the question of the impact of climate on the evolution of organisms over time have focused on the macroevolutionary scale. Macroevolutionary processes generate variations at interspecific level (Erwin, 2000; Hautmann, 2020). The impact of climate on

events such as diversifications and extinctions is undeniable (e.g., Elewa, 2008; Ezard *et al.*, 2011; Condamine, Rolland, & Morlon, 2013; Rolland *et al.*, 2014; Cyriac & Kodandaramaiah, 2017; Lewitus & Morlon, 2018). However, over short time spans such as the current climate period, macroevolution is rarely the first response to climate changes. The primary responses of organisms are usually mostly related to microevolution and phenotypic plasticity (Bown *et al.*, 1994; Sultan & Spencer, 2002; Girard *et al.*, 2004; Yazdi & Adriaens, 2011; Reed *et al.*, 2011; Vedder, Bouwhuis, & Sheldon, 2013; Boutin & Lane, 2014; Merilä & Hendry, 2014; Nogués-Bravo *et al.*, 2018), two processes that generate diversity within species (de Jong, 1995; Fusco, 2001). Microevolution refers to heritable changes within species and populations (e.g., Hansen & Martins, 1996; Hendry & Kinnison, 2001; Merilä, Sheldon, & Kruuk, 2001) while phenotypic plasticity can be defined as all non heritable changes induced by the environment in labile phenotypic traits of an organism (Via, 1993; Chevin, Collins, & Lefèvre, 2013). Therefore, responses to climate changes can occur at multiple evolutionary scales (macroevolution, microevolution and phenotypic plasticity). Thus, to assess the phenotypic response of organisms to climate changes, we choose to consider the phenotype without *a priori* about evolutionary scale.

The phenotype refers to all observable and measurable characteristics of an organism, i.e. its shape, size, color, ability to climb or foraging behavior for example (Houle, Govindaraju, & Omholt, 2010). They can be of various nature: morphological, functional, behavioral, physiological or phenological. The phenotype results from evolutionary processes at both intra- and interspecific scales: it is related to microevolution and phenotypic plasticity (Holt, 1990; Lande, 2009; Hoffmann & Sgrò, 2011; Boutin & Lane, 2014; Merilä & Hendry, 2014), but also to macroevolution (Erwin, 2000; Hautmann, 2020). The difference between intra- and interspecific levels is not always obvious because evolution is a continuous process. Microevolution and macroevolution are tightly linked processes. Macroevolutionary changes are guided by microevolutionary changes occurring at each generation (Hansen & Martins, 1996) and the decoupling between these two processes is debated (Simpson, 1944; Erwin, 2000; Arnold, Pfrender, & Jones, 2001; Hendry & Kinnison, 2001; Reznick & Ricklefs, 2009). Furthermore, an environmentally induced trait can evolve and become fixed through genetic assimilation, sometimes blurring the boundary between phenotypic plasticity and microevolution (Crispo, 2007; Lande, 2009; Aubret & Shine, 2009; Ehrenreich & Pfennig, 2016). To characterize the phenotypic response to climate changes, we chose to consider micro- and macroevolution as coupled

processes and addressed phenotypic evolution as a composite process implying both intra- or interspecific evolutions.

Morpho-functional traits constitute an important part of the phenotype (Arnold, 1983). They allow organisms to perform ecologically relevant interactions with their environment. Morphology has been demonstrated to be highly related to the environment: size is greatly related to temperature, precipitation and primary productivity (Renaud *et al.*, 1999; Wolf, Friggens, & Salazar-Bravo, 2009; Alhajeri & Steppan, 2016), skull shape displays several adaptations (Yazdi & Adriaens, 2011; Verde Arregoitia, Fisher, & Schweizer, 2017; Alhajeri, 2018), for example a wider tympanic bullae under desert conditions (Huang *et al.*, 2002; Alhajeri, Hunt, & Steppan, 2015), and the shape of teeth as well as the patterns of the tooth enamel reflect their dietary habits (Caumul & Polly, 2005; McGuire, 2010; Hautier, Lebrun, & Cox, 2012; Verde Arregoitia *et al.*, 2017). Performances (here used as a synonym of functional abilities) are also closely related to the environment. For example, bite force in shrews is related to the hardness and/or the size of the resources consumed (Young, Haselkorn, & Badyaev, 2007; Young, Sweeney, & Badyaev, 2010; Young & Badyaev, 2010), and a more maneuverable flight in bats, adjusted *via* wing loading, can be advantageous to track more patchy ressources under arid conditions (Conenna *et al.*, 2021). Variations in morphology and performance can be efficiently characterized throught the use geometric morphometric methods (Zelditch, 2004). They allow one to statistically quantify and visualize shape differences and, thus, to assess directions of shape change trajectories (Zelditch, 2004; Mitteroecker & Gunz, 2009). Since its development in the late 90s (e.g., Bookstein, 1996; Dryden & Mardia, 1998), geometric morphometrics has become a popular approach among biologists and is still in perpetual evolution (Adams, Rohlf, & Slice, 2013).

In addition to being greatly related to the environment, morphological and functional traits can provide complementary information as individuals with similar morphology can produce different functional outputs leading to functional divergence (Walker, 2007; Holzman *et al.*, 2011; Bergmann & McElroy, 2014). This is the case for herbivorous lizards whose lower jaws do not diverge morphologically from their carnivorous counterpart, but have higher values of mechanical advantage (Stayton, 2006). Conversely, individuals with different morphologies can produce similar functional outputs, resulting in functional convergence (Wainwright, 2005; Alfaro, Bolnick, & Wainwright, 2005; Young *et al.*, 2007, 2010; Bergmann & McElroy, 2014; Cruz *et al.*, 2021). For example, shrews with different

skeletal and muscular morphologies can display overlap in diet, implying similar feeding-related functional abilities (Young *et al.*, 2010; Cornette *et al.*, 2013). These multiple correspondences linking morphological and functional traits may be explained by the fact that these two kinds of traits are not under the exact same constraints. Indeed, selection can sometimes act primarily on fitness-related performance traits and only secondarily on the underlying morphological traits (Garland & Losos, 1994; Irschick *et al.*, 2008; Langerhans, & Reznick, 2010). The reverse is also observed, as in the case of feathers that evolved before flight, one of the main functions in which it is involved today (Ksepka, 2020). Form and function relationship is mediated by the fact that performance is not only related to morphology, but also by physiological, muscular and behavioral traits (Herrel *et al.*, 2008a; Chazeau *et al.*, 2013; Cornette, Tresset, & Herrel, 2015d; Tseng *et al.*, 2019; Brassard *et al.*, 2021). Thus, as morphological and functional traits can be partially decoupled, they could exhibit different responses to climate changes. It is therefore interesting to explore their respective responses to environmental and climate variations.

Paleoclimates and paleoenvironments

It is important to differentiate climate and environment. The climate is defined by the statistics of the physical characteristics of the atmosphere (Duplessy & Ramstein, 2013), while the environment is the surroundings of living organisms (Begon, Townsend, & Harper, 2006; Bhargava *et al.*, 2019). To some extent, they are related to each other, as the environment partly results from the climate conditions, but not only. Environment also depends on the type of soil, the local topography (e.g., the presence of a hill, a cliff or a lake) and the ecology of the organisms that share the environment and can participate to shape the landscape (Begon *et al.*, 2006; Jones, 2012; Bhargava *et al.*, 2019). Therefore, a region under the same climate conditions can present different types of micro-environments. Consequently, the climate and the environment can refer to external conditions at different geographic scales. This distinction has been accounted for and discussed throughout the thesis.

Most studies addressing the impact of past environments on organisms consider only indirect paleoenvironmental indicators. Those proxies are of various nature and deliver different information about environmental conditions. Oxygen and carbon isotopes (e.g., Anderson & Arthur, 1983; Bown *et al.*, 1994; Blois, McGuire, & Hadly, 2010; Ezard *et al.*, 2011; Jeffrey, 2016; Clavel & Morlon, 2017; Cyriac & Kodandaramaiah, 2017) are related

to temperature and water stress (Zachos *et al.*, 2001; Longinelli & Selmo, 2003; Levin *et al.*, 2006; Cramer *et al.*, 2011). Carbon isotopes can also reveal variations in the relative presence of C3, C4 and CAM plants (which refer to different metabolic carbon fixation pathways) because they have different signatures (O'Leary, 1988; Lin, 2013; Smiley *et al.*, 2016). These plant types are characteristic of more temperate, tropical and arid areas, respectively. Indicators such as faunal assemblages (e.g., Stoetzel *et al.*, 2011; Geraads *et al.*, 2013; Garcia-Ibaibarriaga *et al.*, 2018), diversity indices (e.g., Geraads *et al.*, 2013; Faith & Du, 2018; Ilieș *et al.*, 2020) or palynological records (e.g., Hooghiemstra *et al.*, 1992; Ibrahim *et al.*, 2020; Bolaji *et al.*, 2020) rely on animal and plant species' ecological preferences to provide paleoenvironmental reconstructions. All these paleoenvironmental indicators provide a rough estimation of the landscape, such as the plausible type of vegetation, the vegetation coverage, the abundance of water points and the overall temperature and precipitation conditions. They deliver information at a very local geographical scale (the scale of faunal communities or even individuals regarding isotopes), and thus, depict paleoenvironments more than paleoclimates.

The field of climatology, on the other hand, can provide a quantified and integrative estimate of climate. Climate simulations rely on physical models, that are sets of mathematical equations describing the evolution of the Earth system. The first climate models were created in the 40s, along with the first computers (Guillermot, 2011). Since then, the number and complexity of climate models have increased significantly, in parallel with the sophistication of atmospheric measurement devices and the development of supercomputers. Nowadays, global climate models can model the dynamic and thermodynamic of the atmosphere, the ocean and continental and frozen surfaces coupled with water and carbon cycles. Using these models, we can simulate the past climate of a given period by imposing particular boundaries and forcing conditions, i.e. limitations over space and time for certain parameters such as topography, orbital parameters, ice sheet coverage, atmospheric gas concentrations, etc. Those models depict the directions and large-scale patterns of past climate changes (Braconnot *et al.*, 2012). They give access to the average conditions over a period but also to seasonal variations. They have long been used to investigate past climate changes (Kutzbach & Otto-Bliesner, 1982; Braconnot *et al.*, 2012; Duplessy & Ramstein, 2013; Schmidt *et al.*, 2014; Harrison *et al.*, 2015). The use of climate models in biology remains confined to certain disciplines or topics, such as environmental niche modeling and their predicted evolution under future climate change

(e.g., Ramasamy, Das, & Ramesh, 2021; Gür, 2021; Meyer & Pie, 2021) or the past distribution and dispersal events of animal and plant species (e.g., Sepulchre, 2016; Porada *et al.*, 2016; Pohl *et al.*, 2018; Bernal *et al.*, 2019; Jaramillo *et al.*, 2020; Salles *et al.*, 2021). However, paleoclimatology combined with evolutionary biology could also lead to significant advances in understanding the links between climate and biodiversity in the past.

Rodents and shrews as study cases

We focused on two groups of small mammals: rodents and shrews (**Fig 1**). Rodents represent 41% of mammalian diversity with currently ~2277 species and are among the most ecologically diverse mammals (Nowak, 1999; Fabre *et al.*, 2012; Cox & Hautier, 2015). Shrews are less taxonomically diverse (currently ~385 species), but display an important morphological, functional and ecological diversity (Young *et al.*, 2007, 2010; Young & Badyaev, 2010).

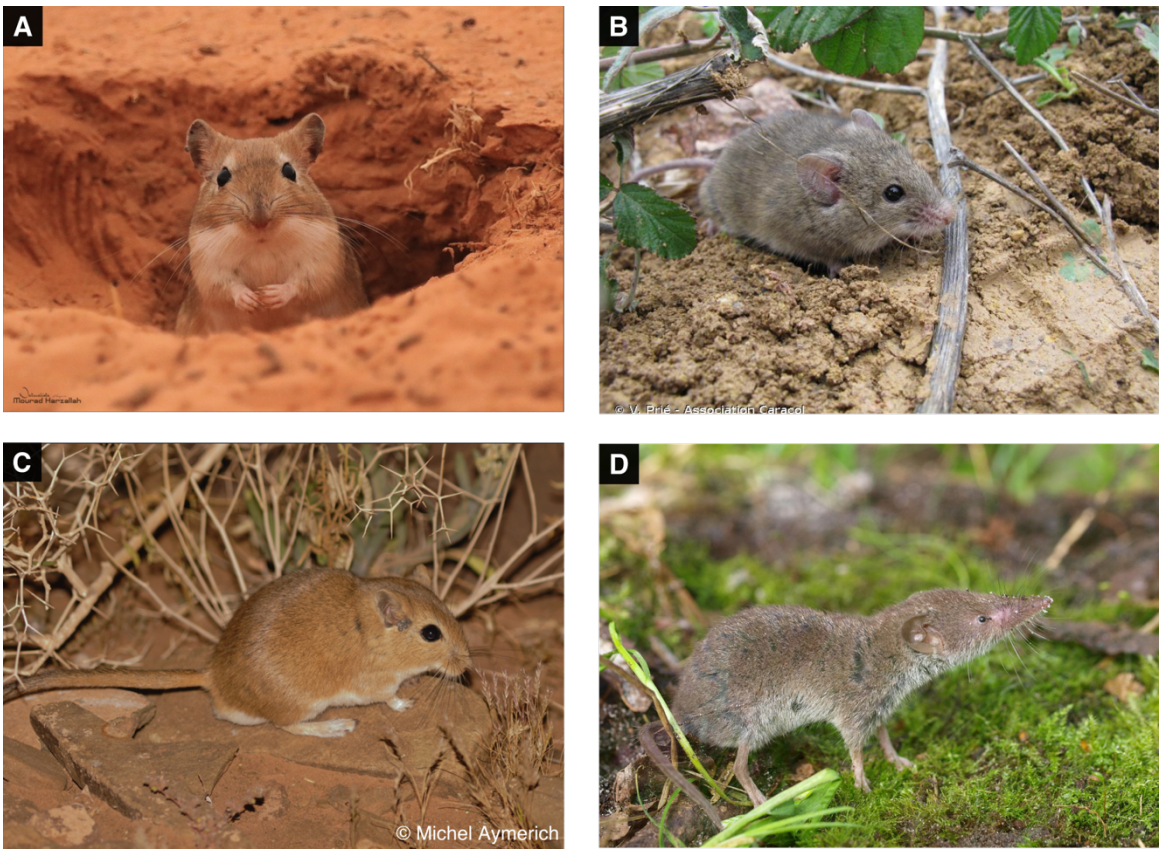

Fig. 1 Photographs of three species of rodents and one species of shrews that are studied in this thesis. A: *Meriones shawii*, B: *Mus spretus*, C: *Dipodillus campestris*, D: *Crocidura russula*.

Both inhabit a great variety of environments. They have a short life span and a short breeding cycle, which confer them a high adaptability. They have a low capacity of dispersion during their lifetime (e.g., of the order of a few dozens, at most hundreds of meters), which makes them very dependent on local conditions. In addition, they have opportunistic diets, feeding on available resources (seeds, fruits, plants and/or more occasionally insects for rodents; insects, invertebrates and/or small vertebrates for shrews) (Churchfield, 1990; Cox & Hautier, 2015). These characteristics make them very likely to display rapid responses to environmental and climatic changes.

El Harhoura 2, a relevant model site

We worked on remains from El Harhoura 2 cave (Rabat, Morocco), an archeological site of particular interest because of the incredible abundance of its faunal deposit and its taxonomic richness (Stoetzel, 2009; Stoetzel *et al.*, 2011) (**Fig 2**).

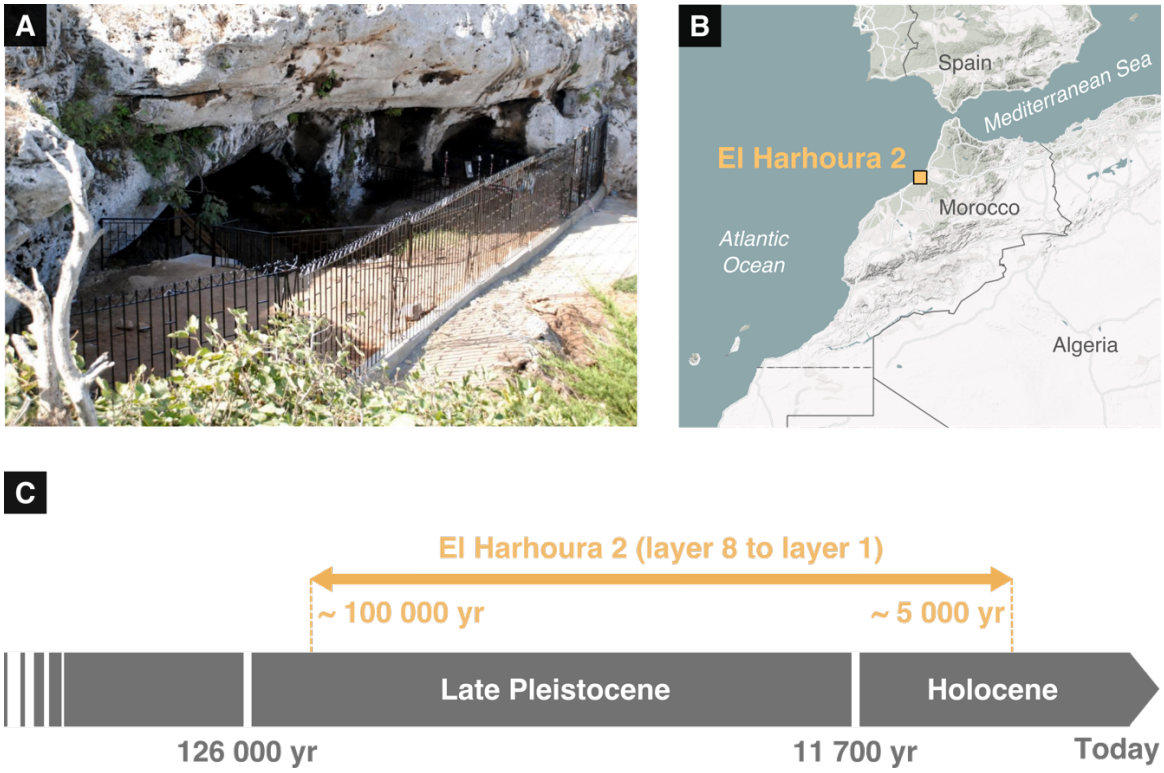

Fig. 2 Presentation of El Harhoura 2 cave. A: overview of El Harhoura 2 cave (© Roland Nespoulet). B: geographical location El Harhoura 2 cave. C: time period covered by El Harhoura 2 cave from layer 8 to layer 1.

The majority of small mammals species identified in this fossil record are still present in Morocco today. The stratigraphy of El Harhoura 2 is divided into 11 layers, among which the chronological and environmental context of eight layers is well known (Stoetzel, 2009, 2017; Stoetzel *et al.*, 2011; Nespoulet & El Hajraoui, 2012; Jacobs *et al.*, 2012; Janati-Idrissi *et al.*, 2012; Ben Arous *et al.*, 2020a,b; Marquer *et al.*, *in press*). This work focused on these eight layers, which cover a period from late Pleistocene to mid-Holocene (**Fig 2C**). By extending this timeline until today, it covers the past 100 ka, which have witnessed important climate changes including the last glacial-interglacial transition (~ 12 ka BP) (e.g., Hooghiemstra *et al.*, 1992; deMenocal, 1995, 2004; Le Houérou, 1997; Carto *et al.*, 2009; Trauth, Larrasoaña, & Mudelsee, 2009; Drake *et al.*, 2011; Drake, Breeze, & Parker, 2013; Blome *et al.*, 2012; Kageyama *et al.*, 2013; Couvreur *et al.*, 2020). Thus, it would eventually allow us to compare current climate and environmental changes to past important ones, and to assess if and how the phenotypic response differed since the beginning of the Anthropocene.

Currently, Morocco displays a rich mosaic of climate types because of its geographical location. It is subjected to Mediterranean influences in the north, oceanic in the west, continental in the center, and desertic in the south. El Harhoura 2 cave is located on the coastal strip (**Fig 2B**), where the oceanic influence dominates. The area is characterized by a Mediterranean climate. Thermal contrasts are moderate (day/night and summer/winter) and the precipitations are irregular and intense. This results in the existence of two distinct seasons: a dry summer and a mild, wet winter. Thus, when we mention more humid or arid climates on El Harhoura 2 throughout this thesis, it never means tropical or desert conditions. Climatic conditions may range from semi-arid (average annual precipitation between 400 and 600 mm) to sub-humid (average annual precipitation between 600 and 800 mm), and the landscape from Mediterranean to steppic at most. An overview of the type of environments that can be encountered in Morocco is presented in **Fig 3**.

Paleoenvironments on El Harhoura 2 have been well studied through faunal assemblages (Stoetzel *et al.*, 2011; Stoetzel, 2017) and isotopes survey (Jeffrey, 2016). However, palynological data for Morocco are lacking. Only few are available for the Maghreb, but they are mainly limited to Tunisia, and only for the last ~40ka. The only things we know are that the late Pleistocene flora in the area are identical to present ones, and only the vegetation boundaries fluctuate along a north-south gradient (Wengler *et al.*, 1992). Overall, environmental proxies revealed an alternation of relatively humid and arid

environments (Stoetzel, 2009; Stoetzel *et al.*, 2011, 2012a,b). The succession of paleoenvironments over the El Harhoura 2 sequence is further detailed and discussed throughout the chapters. Because of the mosaic-like structure of the landscape in the region, we may observe a strong decorrelation between the local environment on El Harhoura 2 and the global climate of the area.

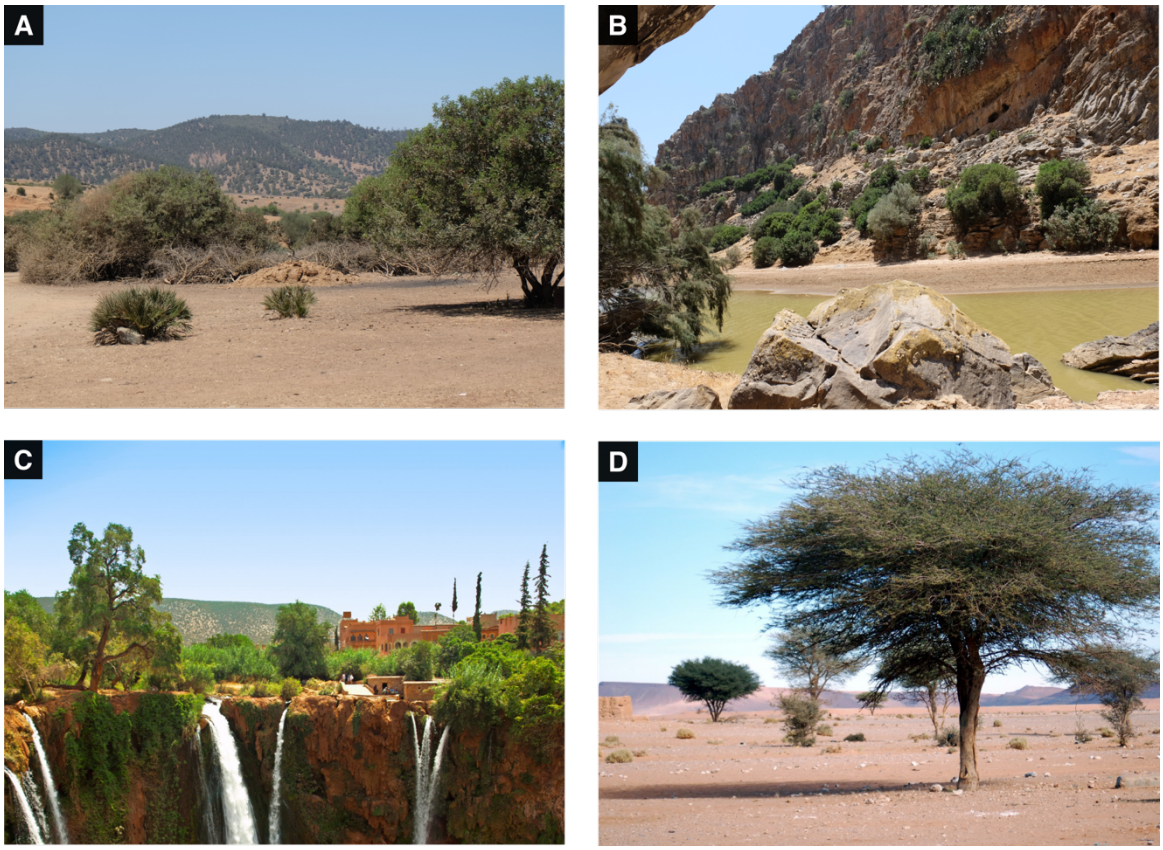

Fig. 3 Overview of the diversity of environments that can be encountered in Morocco nowadays. **A**: bushy area; **B**: oued; **C**: abundant vegetation; **D**: steppic landscape.

El Harhoura 2, because of its exceptional richness in micro-mammal remains and the variety of its paleoenvironmental and climate changes, is an ideal case study to investigate the relationship between both the phenotype and the environment, and the phenotype and the climate.

Objective and thesis structure

In this thesis, we explored the phenotypic response of small mammals from El Harhoura 2 through both their morphological and functional traits to environmental and climate changes over the last 100ka. To do so, we use a bi-disciplinary approach combining evolutionary biology and paleoclimatology. This thesis is divided into four chapters, each addressing a different aspect of our problematic (**Fig 4**).

In chapter 1, we address the impact of local environmental changes on rodent's teeth morphology. We present a taxon-free phenotypic approach that is used in all our analyses. This chapter is an article accepted with minor revisions in the Journal of Mammalian Evolution.

In chapter 2, we investigate the impact of local environmental changes on a functional trait: shrew's estimated bite force. This chapter is an article published in the Biological Journal of the Linnean Society.

In chapter 3, we explore the global climate changes that occurred over the El Harhoura 2 sequence through paleoclimate modeling. We assess the consistency between them and local environmental changes. This chapter is an article in review in Climate of the Past.

Finally, in chapter 4, we examine the impact of global climate changes on rodent's teeth morphology, shrew's mandible morphology and shrew's estimated bite force. This chapter is an article in preparation.

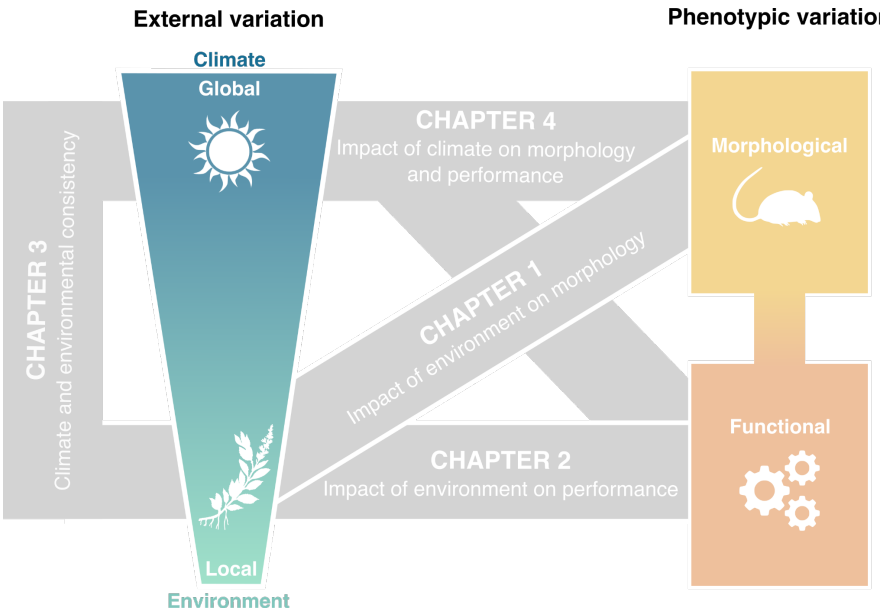

Fig. 4 Synthesis of the thesis structure.

CHAPTER 1

Phenotypic evolution over time and through local environmental changes

Léa Terray, Emmanuelle Stoetzel, David Nerini, Raphaël Cornette

Accepted with minor revisions in the Journal of Mammalian Evolution.

In the first chapter, we explore if and how morphological traits of rodents are impacted by local environmental changes. Upper and lower first molars are used as a proxy for the phenotype. To account for both intra- and interspecific variations, we use morphological groups (MG) as phenotypic units. This MG approach is used in the study of other groups such as foraminifera, but not so much on small mammals. In addition to shape and size, four shape indicators are computed: number of MGs, relative abundance in MGs, MGs disparity and MGs mean shape. We test the significance of phenotypic variation over time and through environments as depicted by paleoenvironmental indicators in the literature. To evaluate the potential of the MG approach, we confronte it to three widely used biodiversity indices: number of taxa, Shannon index and Simpson index.

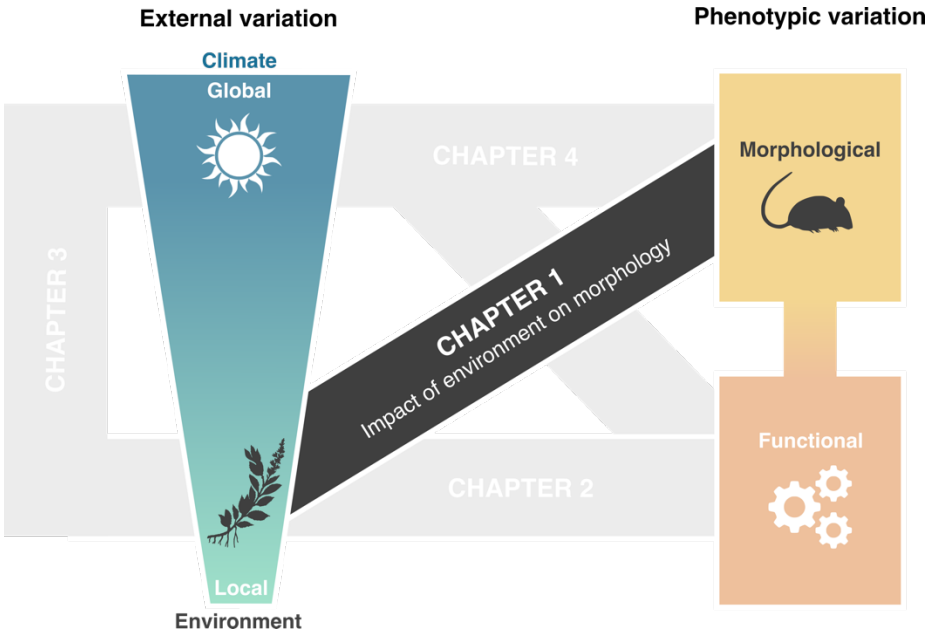

Diagram showing how chapter 1 fits into the thesis problematic.

Introduction

Environmental changes affect the surroundings of living organisms (vegetation, landscapes, etc.). Those changes can be gradual or abrupt, and often morphological variations at adaptative and/or phenotypical scale are observed in response to these new environmental conditions (Lande, 2009; Hoffmann & Sgrò, 2011; Clavel & Morlon, 2017). Most studies raising the issue of phenotypic evolution adopted species as phenotypic units to characterize phenotypic variation (e.g., Hendry *et al.*, 2008; Bickford *et al.*, 2010; Reed *et al.*, 2011; Gardner *et al.*, 2011; Boutin & Lane, 2014; Radchuk *et al.*, 2019). However individuals belonging to the same species may display distinct phenotypic responses to environmental conditions, especially in a complex environmental context (Sultan & Spencer, 2002). The concept of species itself, albeit discussed, defined as morphologically or genotypic similar grouping of individuals, implies the existence of individuals with intermediate morphologies (Mayr, 1942; Simpson, 1951; Mallet, 1995; Wheeler & Meier, 2000; Baker & Bradley, 2006). Those intermediate morphotypes can display a variety of responses to environmental changes. When the addressed problematic aims to identify patterns and/or characterize processes at another scale than species (as intraspecific scale) this partition may not be appropriate. In our case, that kind of approach is therefore not the most suitable way to evidence phenotypic evolution on multiple scales. In order to detect phenotypic responses to environmental changes, we thus need to adopt a taxonomy-free approach.

In the context of our study, morphology is a potential candidate criterion to define those taxonomy-free units. Morphology as a phenotypic unit is particularly used in the field of study of foraminifera (e.g., Nagy, 1992; Tyszka, 1994; Alperin, Cusminsky, & Bernasconi, 2011; Alegret, Thomas, & Lohmann, 2012; Khare *et al.*, 2017). This shape-based approach lays on setting morphological groups (MGs) instead of taxa as biodiversity units. This approach groups individuals solely on the basis of their morphology. It splits shape variability according to the main pattern of shape variation. In the context of foraminifera, Murray (1973, 2006) defined MGs as phylogenetically-independent groups of forms with similar test morphology. Since a test's form is closely related to their environment, this MG approach allows one to infer climatic conditions (Alperin *et al.*, 2011). Conversely, it can thus be a relevant way to characterize phenotypic responses to environmental changes when studied organisms are known to be good environmental indicators. The concept of MGs has been successfully extended to other study frameworks, such as soil biocrust in Read *et*

al. (2014) where they concluded MGs to be functional response groups to environmental disturbances. Moreover, the MG approach presents demonstrated advantages: 1) it allows rapid and ecologically informative survey of big morphological datasets; 2) it enables comparisons of assemblages of different ages; 3) taxonomic identification is not required; 4) MGs are independent of systematic relationship (Murray, 1973; Nagy, 1992; Murray, 2006; Read *et al.*, 2014). We extended Murray's definition and defined MGs as phylogenetic independent grouping of forms with similar morphology.

This study focuses on the Moroccan archeological site of El Harhoura 2 (EH2), a coastal cave located in the Rabat-Témara region. This site is of particular interest for the study of short-term phenotypic evolution related to environmental variations (Stoetzel, 2009; Stoetzel *et al.*, 2010, 2011, 2012b; Stoetzel, 2017; Stoetzel *et al.*, 2017). This region is submitted to complex climatic influences coming from the Atlantic Ocean to the West, the arid Sahara to the South, and the Mediterranean region to the North. EH2 covers a time period from the Late Pleistocene to the Holocene, during which important climatic fluctuations occurred in the area (e.g., Drake *et al.* 2011; Blome *et al.* 2012; Drake *et al.* 2013; Kageyama *et al.* 2013; Scerri 2017; Couvreur *et al.* 2020). This variable climatic context resulted in a succession of relatively humid/arid and open/closed environments at EH2 (Stoetzel, 2009; Stoetzel *et al.*, 2011, 2012b,a). This cave revealed an exceptional richness in small terrestrial vertebrate remains accumulated through owl pellets and/or carnivore feces which have been intensively studied over the past decade (e.g., Michel *et al.* 2009; Stoetzel 2009; Stoetzel *et al.* 2010, 2011, 2012b; Cornette *et al.* 2015; Stoetzel *et al.* 2017).

Among the small mammals of EH2, rodents are well represented in every layer. They are the most diverse group of living mammals (Carleton & Musser, 2005) and are known for being good paleoenvironmental indicators (e.g., Avery 1982, Fernandez-Jalvo *et al*. 1998, McGuire 2010, Belmaker and Hovers 2011, Verde Arregoitia *et al.* 2017, Royer *et al.* 2020, López-García *et al*. 2021). Rodents' morphology can thus reflect ecological similarities. Among most mammals, teeth display higher homoplasy than osteological parts (Evans et al., 2007; Brocklehurst and Benevento, 2020). Thus, rodents teeth may be a good proxy for rodents phenotype. Shape based grouping of fossil rodent incisors have been shown to reflect dietary ecology (Paine *et al.*, 2019), and molar crowns are strongly related to environment through diet (Wolf *et al.*, 2009; McGuire, 2010; Coillot *et al.*, 2013; Gómez

Cano, Hernández Fernández, & Álvarez-Sierra, 2013; Gomes Rodrigues, 2015a; Selig, Khalid, & Silcox, 2021).

We studied the phenotypic evolution of the rodents of EH2 cave through a MG approach to answer the following questions: did local environmental changes impact the phenotype of rodents? Do short-term phenotypic evolution occurred at different scales - intra- / interspecific - under changing environments? We used two complementary models: first lower molars (m1) and first upper molars (M1). In murine rodents', both display slightly different evolutionary rates of size and shape (Renaud & van Dam, 2002). First, we tested the influence of the environment on overall shape and size. Then, MGs were identified using a non-subjective grouping method: unsupervised clustering (Hastie, Tibshirani, & Friedman, 2009). For each dataset four shape indicators were computed to evaluate phenotypic diversity: number of MGs, relative abundance in MGs, MGs disparity and MGs mean shapes. MGs represent the main pattern of shape variation. We expect them not necessarily to reflect species, but to be representative of response groups toward environmental changes. The relative abundance in MGs (i.e. the relative proportion of representatives of each MG) may reveal shifts in morphs that dominate a population. Thus, the impact of environmental changes on the relative abundance in MGs will reveal if the environment drive or not the main pattern of shape variation in molars. Number of MGs and disparity should detect periods of decreasing/increasing/stable phenotypic diversity. Variations in mean shape should point out shifts in selected shapes and eventually convergence/divergence of MGs shapes in constraining environments. However, the MG approach often underestimate diversity and can be costly in information (Read *et al.*, 2014). Then, to assess confidence in our approach we compared its ability to characterize phenotypic evolution to widely used biodiversity indices in ecology and archeology (number of species, Shannon index and Simpson index) (e.g. Avery, 1982, Geraads et al. 2013, Meunier *et al.* 2020).

Material and Methods

El Harhoura 2 cave

The stratigraphy of the cave is structured in 11 layers numbered from top to bottom (**Fig 1**). Eight levels (L1 to L8) are well studied from their microfauna (Stoetzel *et al.*, 2011, 2013, 2017) and well dated (Jacobs *et al.*, 2012; Ben Arous *et al*., 2020a; Ben Arous *et al.*, 2020b), and were used in this study. The small mammal taxonomic study of the site reveals

the presence of at least eight rodent species: *Apodemus sylvaticus*, *Lemniscomys barbarus*, *Mus spretus*, *Dipodillus campestris*, *Meriones shawii*/, *Meriones grandis*, *Jaculus* cf. *orientalis* and *Eliomys* cf. *munbyanus* (Stoetzel *et al.*, 2011, 2013, 2017). We were not able to include *Jaculus* cf. *orientalis* and *Eliomys* cf. *munbyanus,* due to the lack of well-preserved teeth remains. Local paleoenvironmental information from EH2 is based on large and small vertebrates recovered from the archeological levels (El Hajraoui *et al.*, 2012; Stoetzel *et al.*, 2010, 2011, 2012b, 2014; Campmas *et al.*, 2015; Stoetzel, 2017). They show successive relatively humid (L 3, L4a, L6 and L8) and arid (L2, L5 and L7) phases. Late Pleistocene environments appear more open and less humid than today. Paleolandscapes are defined as open steppe or savanna-like land with patches of shrubland, woodland and water bodies. Water bodies cover greater areas during humid phases than arid phases.

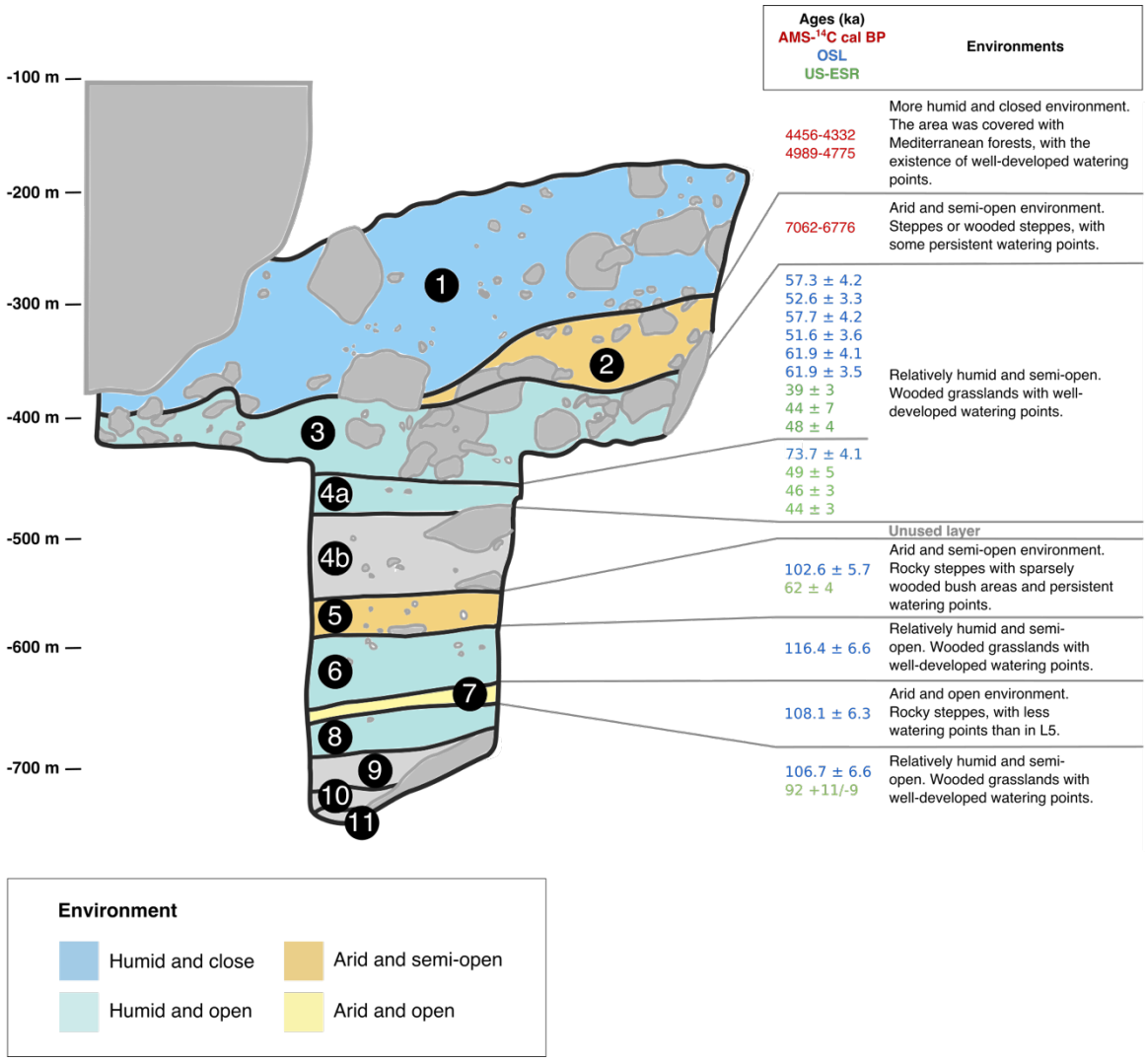

Fig. 1 Stratigraphy, age and characteristic environments of the eight layers of EH2 used in this study (Michel *et al*., 2009; Stoetzel, 2009; Jacobs *et al.*, 2012; Janati-Idrissi *et al*., 2012;

Nespoulet & El Hajraoui, 2012; Ben Arous *et al.*, 2020a, 2020b). Three dating methods were used: AMS-14C based on organic remains, US-ESR (Combined uranium series and Electron Spin Resonance) and OSL (Optical Stimulated Luminescence). Light blue layers: humid and semi-open environment; dark blue layers: humid and closed environment; light yellow layers: arid and open environment; dark yellow layers: arid and semi-open environment. Layers unused in this study are in grey (modified from Terray *et al*., 2021).

Data collection

We used 1133 m1 and 990 M1 housed at the Musée de l'Homme, Paris, France and the Institut National des Sciences de l'Archéologie et du Patrimoine, Rabat, Morocco. The sample is composed of six of the eight species present at EH2: *Meriones shawii*, *Meriones grandis* (referred in the following as the *Meriones shawii*/*grandis* complex because of their morphological proximity (Stoetzel *et al.*, 2017)), *Mus spretus* and *Dipodillus campestris* in abundance and occasionally *Lemniscomys barbarus* and *Apodemus sylvaticus*. The abundance of teeth per layer is indicated in **Table 1**.

Table. 1 Number of studied molars per layer of EH2. M1: upper first molars; m1: lower first molars.

Layers	m1	M1
L1	74	69
L2	45	43
L3	64	65
L4a	57	50
L5	157	118
L6	189	181
L7	314	227
L8	233	237
TOTAL	**1133**	**990**

Teeth photographs were taken using Nikon digital camera D 5500 coupled with AF-S Micro NIKKOR 60 mm and macro extension tubes. Picture taking was standardized: teeth were always placed so that the occlusal surface is horizontal. We obtained two categories of pictures: *in situ* teeth (when teeth are set in the mandible or the maxilla) and individualized teeth (when teeth are no longer encased in the bone). In the first case, masks

of teeth were manually extracted using the software Gimp v 2.10.6 (The GIMP Development Team, 2018). In the second case, masks extraction was semi-automatized using the software ImageJ 1.52j (Schneider, Rasband, & Eliceiri, 2012), through the use of the segmentation procedure of the MorphoLibJ plugin (Legland, Arganda-Carreras, & Andrey, 2016) which automatically detects objects on a picture. Difference between those two acquisition methods was tested and was not statistically significant (**Table S1**). The data acquisition protocol is summarized in **Fig. 2**. Finally, we extracted outlines from the masks using the library *Momocs* (Bonhomme *et al.*, 2014) in the free software R (R Development Core Team, 2018).

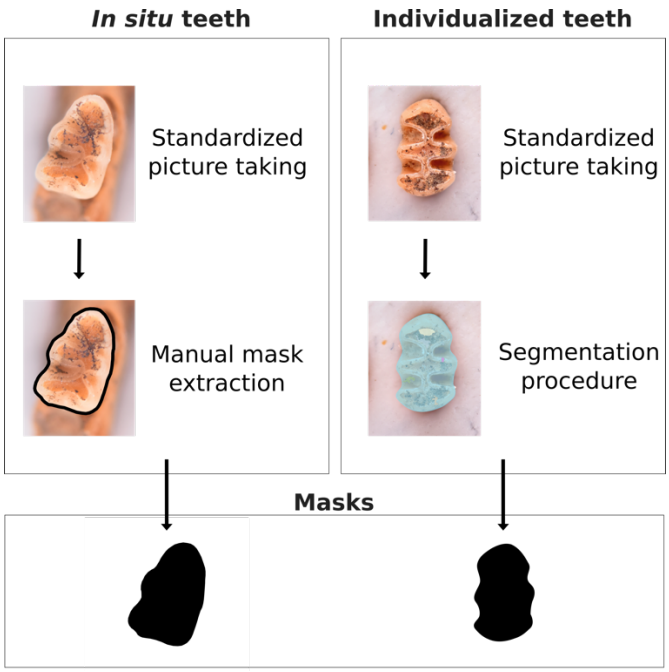

Fig. 2 Acquisition protocol from picture taking to masks extraction. The protocol depends on whether the teeth are individualized or not. Individualized teeth are no longer embedded in the bone. *In situ* teeth are those that are still set into the mandible or the maxilla.

Geometric morphometric analyses

Teeth shape was approximated through the 2D outlines of the teeth in occlusal view. Outlines have been taken at the base of the molar crown, which is less affected by age. This is especially the case for *Meriones* which have semi-hypsodont characteristics. As a consequence the occlusal surface and pattern varies importantly with the age of the individual (as discussed in Stoetzel *et al.*, 2017). Shape analyses were performed under the free software R (R Development Core Team, 2018). Fourier analysis is an efficient method

to describe teeth morphology (Renaud, 1999) and is less sensitive to wear than landmarks-based approach (Renaud *et al.*, 1999; Renaud, 2005).

The registration process proposed in this article relies on an algorithm of Functional Generalized Procrustes Analysis (FGPA) developed by David Nerini, one of our collaborator. It is an extension of the GPA algorithm that can be found in Dryden and Mardia (1998) (p. 90) but adapted in case where the outline of an object is considered as a continuous closed curve. The idea behind this landmark free method is to avoid the delicate choice of the number and the position of landmarks.

Consider an observed closed contour of tooth arriving as M pairwise observations $(x_1, y_1), \ldots, (x_M, y_M)$. We first consider that a contour line can be expressed as two curves $\big(X(t), Y(t)\big)$ that are supposed to be a linear combination of K known basis functions such that:

$$X(t) = \alpha_1 \phi_1(t) + \cdots + \alpha_K \phi_K(t)$$

$$\mathrm{Y}(t) = \beta_1 \phi_1(t) + \cdots + \beta_K \phi_K(t),$$

where the α_ks and β_ks are coefficients that must be estimated with regression on the sampled data. The time index t arbitrarily belongs to $[0; 2\pi]$. The basis functions $\phi_k, k = 1, \cdots, K$ are chosen by the practitioner and constitute a Fourier basis in our case. Other choices (B-splines, polynomials, …) can be relevant as well. The regression procedure is the same as that used in classical regression but in the functional case (see Ramsay and Silverman (2005) for more details). The number K of basis coefficients is arbitrarily fixed in such a way that a sufficient amount of curve variability is captured. In our case, we used 30 basis coefficients.

Once every contour line is expressed through its estimated Fourier coefficients, it is possible to apply the FGPA algorithm using these coefficients as inputs. Registration of closed curves involves translating, rescaling, rotating and changing the phase of the configurations relative to each other so as to minimize an objective function (a total sum of squares). The registration of the starting point (phase changing) between curves is the main difference compared to the original algorithm and is essential as shown in **Fig 3** in a landmark free method.

Let $Z_n = (X_n, Y_n)$ be a pair of functions parameterized in a Fourier basis and describing the contour line of a tooth. The FGPA algorithm is the following:

Algorithm 1: Algorithm for the FGPA

Input : A set of configurations $\{Z_1, \ldots, Z_N\}$
Output: A set of registered configurations $\{Z_N^P, \ldots, z_N^P\}$

Start
  Select : $\gamma \ll 1$
  Translation :
  The Z_n^P are the centered configurations of the Z_n
  Rotation, Scale & Phase :
  repeat
    for n=1,...,N **do**
      compute $\overline{Z}_{(-n)} = \frac{1}{N-1} \sum_{m \neq n} Z_m^P$
      impose $\| \overline{Z}_{(-n)} \| = 1$
      register Z_n^P over $\overline{Z}_{(-n)}$ by FOPA
      replace Z_n^P by its registered version
    end
  until $G(Z_1^P, \ldots, Z_N^P) < \gamma$
End

where $\overline{Z}_{(-n)}$ is the mean outline of all configurations except observation n, expression $\|.\|$ denotes the chosen norm in the space of the Z_ns, and FOPA is the Functional Ordinary Procrustes Analysis such as described in Dryden and Mardia (1998) (p. 84) but extended to the functional case (i.e. working with Fourier coefficients). The objective function $G(Z_1^P, \ldots, Z_N^P)$ denotes the objective function (a total sum of squares) that must be minimized. This algorithm converges in a couple of iterations and stops when $G(Z_1^P, \ldots, Z_N^P)$ goes underneath a fixed threshold γ.

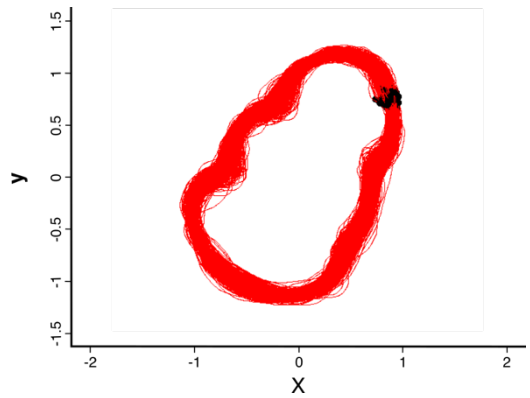

Fig. 3 Aligned outlines of right lower first molars with the registered starting point of each curve.

Once the contour lines have been registered, classical shape analyses can be achieved on the registered Fourier coefficients. We used all Fourier coefficients in following statistical analyses.

All subsequent treatments have been applied on the two datasets (m1 and M1) separately. To reduce data dimensionality in further analyses we performed principal component analyses on both datasets using the *PCA* function of the *FactoMineR* package (Lê, Josse, & Husson, 2008). We retained 95% of the shape variability, the latest principal components being usually considered as neglectable (Baylac & Frieß, 2005). In total, we used 20 principal components for the m1 dataset and 20 for the M1 dataset. As an estimate of the size, we used the surface area of the masks.

Clustering analyses

In order to partition datasets on the basis of their main pattern of shape variation and without any prior information, we performed unsupervised clustering analyses. We choose to explore two complementary clustering protocols (summarized in **Fig 4**):

1. Method 1 partitions the global variability into MGs and gives an overview of MGs evolution over time by retaining identity between MGs from one layer to another. The clustering was applied on the overall datasets.

2. Method 2 partitions variability on each layer separately. The clustering was applied independently on each layer. Thus, it does not allow us to follow MGs evolution over time because the relationship between MGs determined on different layers is not known. Consequently, part of our analyses could not be performed on MGs found with method 2.

Clustering analyses were performed using unsupervised morphological K-nearest neighbors method (KNN). KNN is a non-parametric classification (i.e. a method that is not based on statistical distributions) and therefore was applicable to both of our approaches (each of them implying highly varied sample sizes). KNN classification is based on the assumption: "tell me who your neighbors are, and I will tell you who you are". In other words, each shape object is affected to its nearest neighbors' clusters. Unsupervised KNN is implemented in the *clues* function of the *clues* package (Wang, Qiu, & Zamar, 2007). The dissimilarity measure used is Euclidean. In *clues* the number of clusters and K (the number of neighbors to consider) are estimated by the algorithm. The number of clusters is obtained thanks to a partition procedure preceded by a local shrinking procedure, in

which data points are "shrinked" toward a cluster center (Wang *et al.*, 2007). Then K is selected between 1 to n-1 (n being the number of objects) based on the more robust clustering result (Wang *et al.*, 2007). This robustness is assessed by the Silhouette index (SI) (Kaufman & Rousseeuw, 1990) which measures the strengths of clusters. SI is determined for each data point. It is comprised between -1 and 1. If SI>0 the data point is closer to its assigned cluster than to other clusters. If SI<0 the data point is misassigned to its cluster. If SI=0 the data point is at equal distance from its assigned cluster and neighboring clusters. To ensure that points are correctly allocated to clusters the average SI is calculated and must be strictly positive (Wang *et al.*, 2007). Clustering results and species are presented on PCA per layer in **Figure S1, S2, S3 and S4**. Size differences between MGs were tested using an one-factor ANOVA (analysis of variance) performed with the *aov* function of the *stats* library.

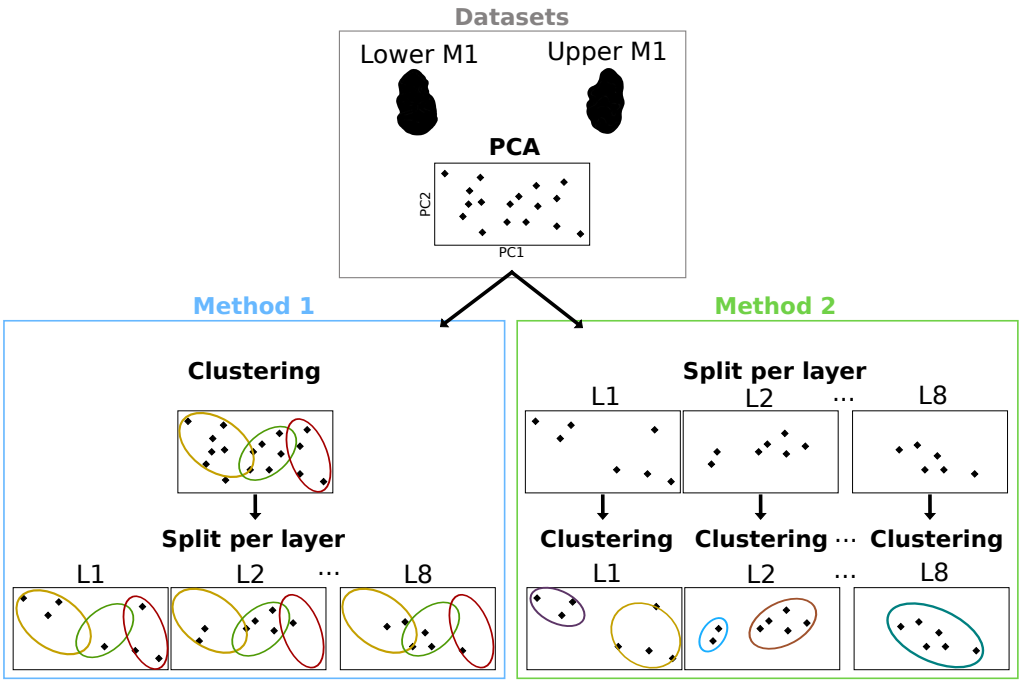

Fig. 4 Protocols of the two clustering methods.

Global shape and size variation

First, we assessed the impact of local environmental changes on the overall shape and size variation. We performed a multivariate analysis of variance (MANOVA) to test if shape is different depending on the environment using the *manova* function of the *stats* library, followed by pairwise Hotelling's T^2 tests (the multivariate alternative to the t-test) using

the *hotelling.test* function from the *Hotelling* library (Curran, 2017). Regarding size, we performed an one-factor analysis of variance (ANOVA) using the *aov* function of the *stats* library, followed by pairwise t-tests using the *pairwise.t.test* function of the *stats* library. To correct results for multiple testing we applied Bonferroni's criteria which consists in identifying the number of tests n, then performing each of the n tests not at the α level of significance, but at the α/n level. Visualisations of shape and size differences between environments are presented.

We studied more extensively the impact of local environmental changes on four shape indicators: number of MGs, relative abundances in MGs, MGs disparity and MGs mean shape.

Number of MGs

Number of MGs is the number of significant distinct morphological units in a dataset. It was obtained directly from the clustering analysis. We visualized variation in the number of MGs over time.

Relative abundance in MGs

MGs represent the main pattern of shape variation. Thus, the relative abundance in MGs may reveal shifts in the main morphs that composed a population. On each layer, we computed the percentage of individuals belonging to each groups. This indicator is only computed for MGs obtained with method 1, as MGs of method 2 have no continuity between layers. We tested the statistical significance of the variation in MGs abundances between types of environments and between EH2 layers by performing Friedman tests. This test is a rank sum test often used as an alternative to the one-factor ANOVA on paired samples when the normality assumptions are not met. We used the *friedman.test* function from the *stats* library.

Disparity

Disparity is the range of morphological variety in a group. It indicates changes in the amount of variation of a morphotype (Gould, 1989, 1991; Wills, Briggs, & Fortey, 1994; Foote, 1997). When considered independently of phylogenetic relationships a good

estimate of disparity is to quantify the amount of occupied morphospace (Wills *et al.*, 1994). As disparity estimator we used the median of the distances from the centroid of the group, a variance measure relatively insensitive to outliers (Guillerme *et al.*, 2020). Disparity was obtained thanks to the function *dispRity.per.group* from package *DispRity* (Guillerme, 2018). This function contains a bootstrap procedure to reduce effect of sample composition, a common issue when studying disparity (Butler *et al.*, 2012). Regarding sample size, variance is generally not biased by it (Foote, 1997) and no sample size correction has been applied. We tested the statistical significance of disparity variation between the types of environments and between EH2 layers. Regarding method 1 we performed Friedman tests using the *friedman.test* function from the *stats* library. Regarding method 2 we performed Kruskal-Wallis tests, a test similar to the Friedman test but adapted to independent samples. We used the *Kruskal.test* function from the *stats* library.

MGs mean shapes

Mean shape reflects changes in the global shape of a group over time. It could detect shape divergence in groups in some layers. To quantify shape variations we built a distance tree between mean shapes per MG per layer. We computed Mahalanobis distances and built the tree using the neighbor joining algorithm, an agglomerative clustering method. The distance between groups in the tree is proportional to the morphological differences. To do that, we used the functions *dist* from the package *stats* and *nj* from the package *ape* (Paradis, Claude, & Strimmer, 2004). Visualizations of mean shapes per MG were also obtained. The neighbor joining distance trees are only computed for MGs obtained with method 1, as MGs of method 2 have no continuity between layers. For each MG, we also tested the statistical significance of mean shapes variation between the types of environments and between EH2 layers. We performed MANOVA using the *manova* function of the *stats* library. When the MANOVA between environmental types was significant, we conducted pairwise Hotelling's T^2 tests using the *hotelling.test* function from the *Hotelling* library (Curran, 2017) and corrected them by applying Bonferroni's criteria.

Biodiversity indices

Biodiversity indices are frequently used in ecology, and some of them as the Shannon and Simpson indices are also often applied to rodents fossil assemblages (Avery, 1982; Geraads

et al., 2013; Meunier *et al.*, 2020). Those indices compute quantitative parameters about the structure of specific diversity of a faunal assemblage (as species richness, diversity and specific dominance). We choose three diversity indicators:

1. Number of taxa over time.

2. Shannon-Weaver index (H'), which allows estimation of the diversity of a community of organism. A value close to 0 indicates that only one species is represented or that most of organisms belong to one same species. The index is maximal when many species are represented and when organisms are well distributed among species (Blondel, Ferry, & Frochot, 1973; Hill, 1973). This index is sensitive to variations of abundance in rare species (Peet, 1974) and highly sensible to sample size when it is composed of less than 25 individuals (Cruz-Uribe, 1988) (which is not the case here).

3. Simpson index (D), which measures the probability that two randomly selected individuals are of the same species. We used the unbiased Simpson index (D') which is corrected for sample size, as suggested in Faith and Du (2018). It ranges from 0 (when diversity is maximal) to 1 (when diversity is minimal). The transformation 1-D' provides values that are easier to manipulate and interpret (Pielou, 1969; Hill, 1973). This index is sensitive to variations of abundance in more important species (Peet, 1974).

They were computed for rodents and the whole terrestrial microvertebrates based on data from Stoetzel (2009) and Stoetzel *et al*. (2011, 2012b).

Results

Clustering analyses

Clustering results for both methods and both datasets are summarized in **Table 2**. All values of SI means are in the range of (0,1), meaning data points are rightly assigned to their clusters.

With method 1, we identified three MGs in the m1 dataset. MG1 contains mainly *Mus spretus* teeth, but also some *Dipodillus campestris*, *Meriones shawii*/*grandis* and *Apodemus sylvaticus* teeth. MG2 and MG3 contain mostly *Meriones shawii*/*grandis* teeth, but also some *Dipodillus campestris* and *Mus spretus* teeth. In the M1 dataset, two MGs were identified. MG1 is transgeneric and contains *Mus spretus* and *Meriones shawii*/*grandis* teeth, while MG2 is mainly composed of *Meriones shawii*/*grandis* teeth.

MGs display significant different size for m1 (anova: p-value < 2e-16 ***; df = 2; F = 355) and M1 (anova: p-value < 2e-16 ***; df = 1; F = 70.57).

For method 2, we identified up to three MGs per layer in the m1 dataset. Except for L7, all layers display only two MGs. Half of the MGs is transgeneric, while the other half is mainly composed of *Meriones shawii*/*grandis* teeth. In the M1 dataset, up to five MGs were identified. As for m1, half of the MGs is transgeneric, while the other half is mainly composed of *Meriones shawii*/*grandis* teeth. MGs display significant different size for m1 (anova: p-value < 2e-16 ***; df = 1; F = 145.9) and M1 (anova: p-value < 2e-16 ***; df = 1; F = 95.82). The detailed composition of each MG is available in **Table S2**, **Table S3**, **Table S4** and **Table S5**.

Table. 2 Synthesis of clustering results of method 1 - one general clustering performed - and method 2 - one clustering performed per layer. M1: upper first molars; m1: lower first molars.

		m1	**M1**
Method 1	Number of clusters	3	2
	K-values	399	500
	SI means	0.15	0.19
Method 2	Number of clusters	up to 3	up to 5
	K-values	22 < K < 140	13 < K < 84
	SI means	0.14 < SI < 0.29	0.10 < SI < 0.20

Global shape and size variation

Overall shape variation is significantly different between EH2 layers for m1 (manova: p-value < 2.2e-16 ***, df = 7, F = 3.55, Pillai = 0.42) and M1 (manova: p-value < 2.2e-16 ***, df = 7, F = 3.49, Pillai = 0.47), and between environments for m1 (manova: p-value < 2.2e-16 ***, df = 3, F = 4.52, Pillai = 0.23) and M1 (manova: p-value < 2.2e-16 ***, df = 3, F = 4.45, Pillai = 0.25). Shape differences between environments are visualized in **Fig 5a** (m1) and **5b** (M1). Both m1 and M1 display slightly more marked lophs/cups outlines under more arid and open environments. Also, M1 have a wider mesial part, and m1 rounder mesial and distal parts.

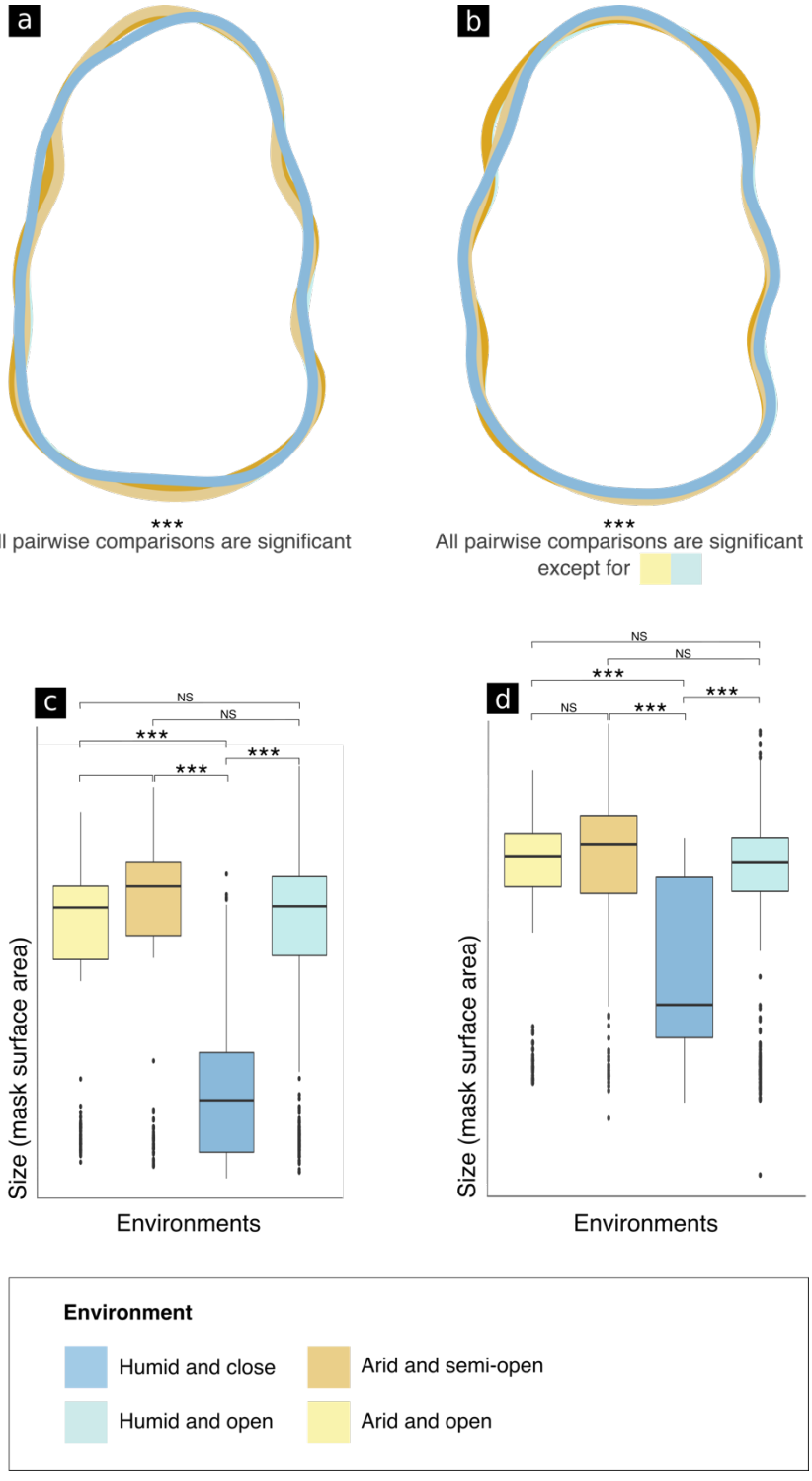

Fig. 5 Shape and size variations between environments. Shape changes are magnified by three to clarify visualization. **A**: Mean shape of the m1 in each environment; **B**: mean shape of the M1 in each environment; **C**: boxplot of m1 size between environments; **D**: boxplot of M1 size between environments.

Size variation is also significantly different between layers for m1 (anova: p-value < 2e-16 ***, df = 7, F = 19.35) and M1 (anova: p-value < 2e-16 ***, df = 7, F = 14.14), and between environments for m1 (anova: p-value < 2e-16 ***, df = 3, F = 37.5) and M1 (anova: p-value = 1.72e-15 ***, df = 3, F = 24.83). Size differences between environments are visualized in **Fig 5C** (m1) and **5D** (M1). For both m1 and M1 molars of individuals from humid and closed environments are much smaller than those of individuals from others environments. Among humid environments, molars from more closed environments are smaller, while among more arid environments molars from more closed environments are larger. Detailed results of pairwise Hotelling's T^2 tests performed on shape and pairwise t-tests performed on size are available in **Table S6**.

Number of MGs

Variation over time in the number of MGs is presented in **Fig 6** for m1and in **Fig 7** for M1. They are computed using both method 1 and method 2. For clarity, each analysis result is referred as "dataset-method", as in m1-method1. The number of MGs increases in m1-method 2 and M1-method2 in L7 (**Fig 6C**, **Fig 7C**), the only layer characterized by an open and arid environment. In M1-method2 there is also an additional MG in L5 (**Fig 7C**), a layer characterized by an arid and semi-open environment.

Relative abundance in MGs

The relative abundances of MGs are presented in **Fig 8**. There are computed only for method 1, as they require MGs identity between layers. The relative abundance of MGs significantly varies over EH2 layers for m1 (Friedman test: p-value = 0.018*, df = 7, X2 = 16.93) but not for M1 (Friedman test: p-value = 0.072, df = 7, X2 = 13). It is not related to local environmental changes neither for m1 (Friedman test: p-value = 0.12, df = 3, X2 = 5.8) nor M1 (Friedman test: p-value = 0.61, df = 3, X2 = 1.8).

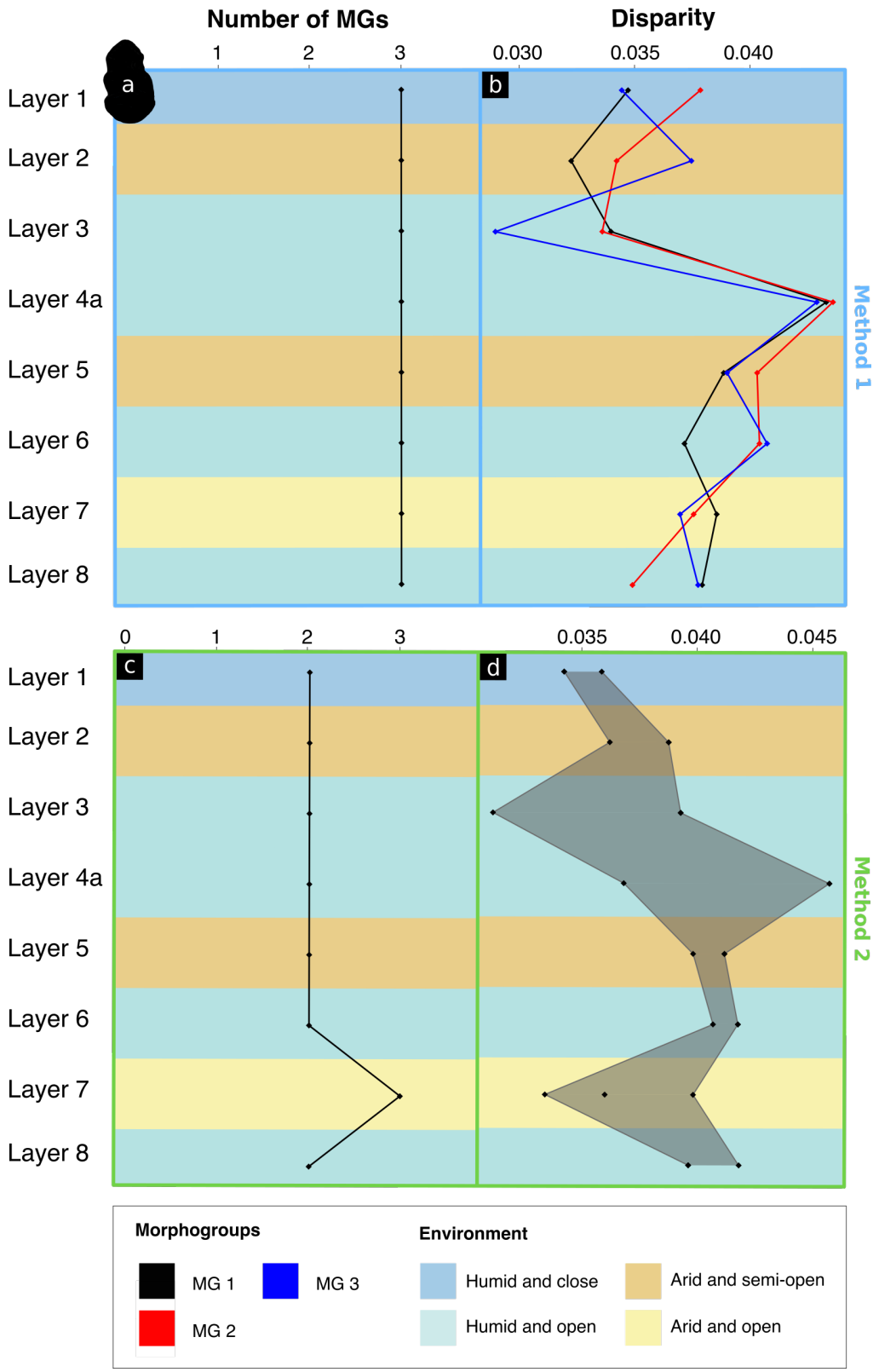

Fig. 6 Number of MGs and disparity of m1 (lower first molars) shape over the eight studied stratigraphic layers of EH2. Environmental conditions (Stoetzel, 2009; El Hajraoui *et al.*, 2012) are indicated by background colors. **A**: Number of MGs obtained with method 1; **B**: Disparity of MGs of method 1; **C**: Number of MGs obtained with method 2; **D**: Disparity of MGs of method 2.

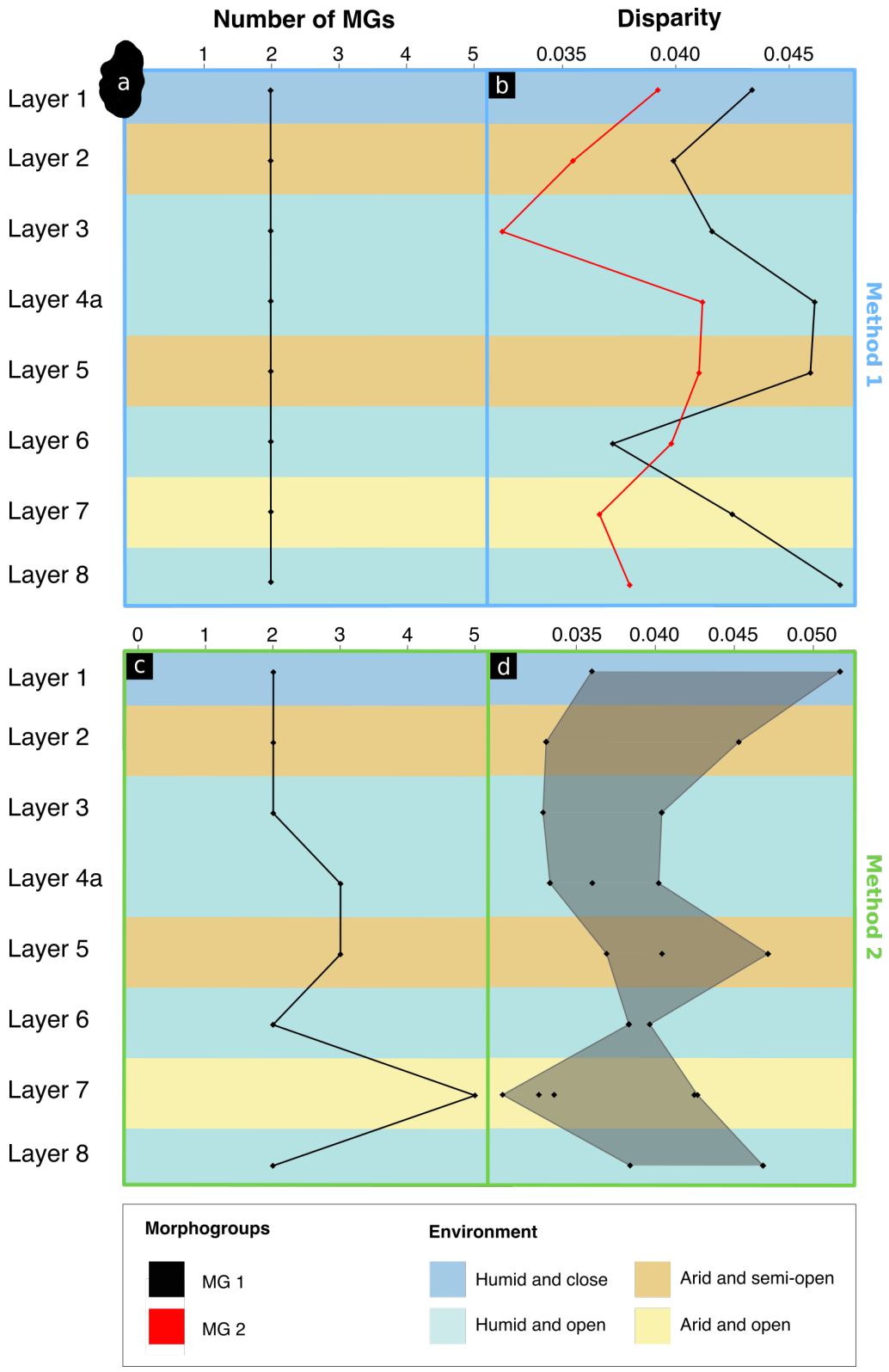

Fig. 7 Number of MGs and disparity of M1 (upper first molars) shape over the eight studied stratigraphic layers of EH2. Environmental conditions (Stoetzel, 2009; El Hajraoui *et al.*, 2012) are indicated by background colors. **A**: Number of MGs obtained with method 1; **B**: Disparity of MGs of method 1; **C**: Number of MGs obtained with method 2; **D**: Disparity of MGs of method 2.

Disparity

MGs disparity over time of m1 is presented in **Fig 6** and disparity of M1 in **Fig 7**. They are presented for both method 1 and method 2. Global disparity variation over EH2 layers is statistically significant for m1-method1 (Friedman test: p-value = 0.017*, df = 7, X2 = 17), but not for M1-method1 (Friedman test: p-value = 0.19, df = 7, X2 =10), m1-method2 (Kruskal-Wallis test: p-value = 0.21, df = 7, X2 = 9.66) nor M1-method2 (Kruskal-Wallis test: p-value = 0.78, df = 7, X2 = 3.97). In m1-method1 we observed a global increase in disparity from L8 to L4a, followed by an important drop between L4a and L3 and then slight increase until L1 shared by all MGs (**Fig 6D**). If we focus on MG's disparity, this pattern of variation is also present in one/several MGs of m1-method2 (**Fig 6D**) and in MG2 of M1-method1 (**Fig 7D**).

Variation of global disparity between environmental types are not statistically significant for m1-method1 (Friedman test: p-value = 0.45, df = 3, X^2 = 2.6), M1-method1 (Friedman test: p-value = 0.14, df = 3, X^2 = 5.4), m1-method2 (Kruskal-Wallis test: p-value = 0.21, df = 3, X^2 = 4.6) nor M1-method2 (Kruskal-Wallis test: p-value = 0.98, df = 3, X^2 = 0.19).

MGs mean shapes

Mean shape distance trees of MGs are presented in **Fig 8**. They are computed only for method 1, as they require MGs identity between layers. The MGs of method 1 do not display the same internal shape variability. In m1-method1, MG1 shows more similar mean shapes, while MG3 has more diverse mean shapes (**Fig 8A**). Similarly, in M1-method1 MG2 is composed of more similar mean shapes (except for the one in L1) than MG1 (**Fig 8B**). In L3, MGs of M1-method1 show more similar mean shapes than in other layers (**Fig 8B**).

Over EH2 layers, mean shape variation within each MG is statistically significant for m1-method1 (MANOVA: MG1: p-value = 1.68e-9 ***, df = 7, F = 1.91, Pillai = 0.53; MG2: p-value = 1.94e-8 ***, df = 7, F = 1.84, Pillai = 0.60; MG3: p-value = 4.31e-06 ***, df = 7, F = 1.67, Pillai = 0.95) and for M1-method1 (MANOVA: MG1: p-value = 4.76e-8 ***, df = 7, F =1.81, Pillai = 0.68; MG2: p-value < 2.2e-16 ***, df = 7, F = 3.069, Pillai = 0.64).

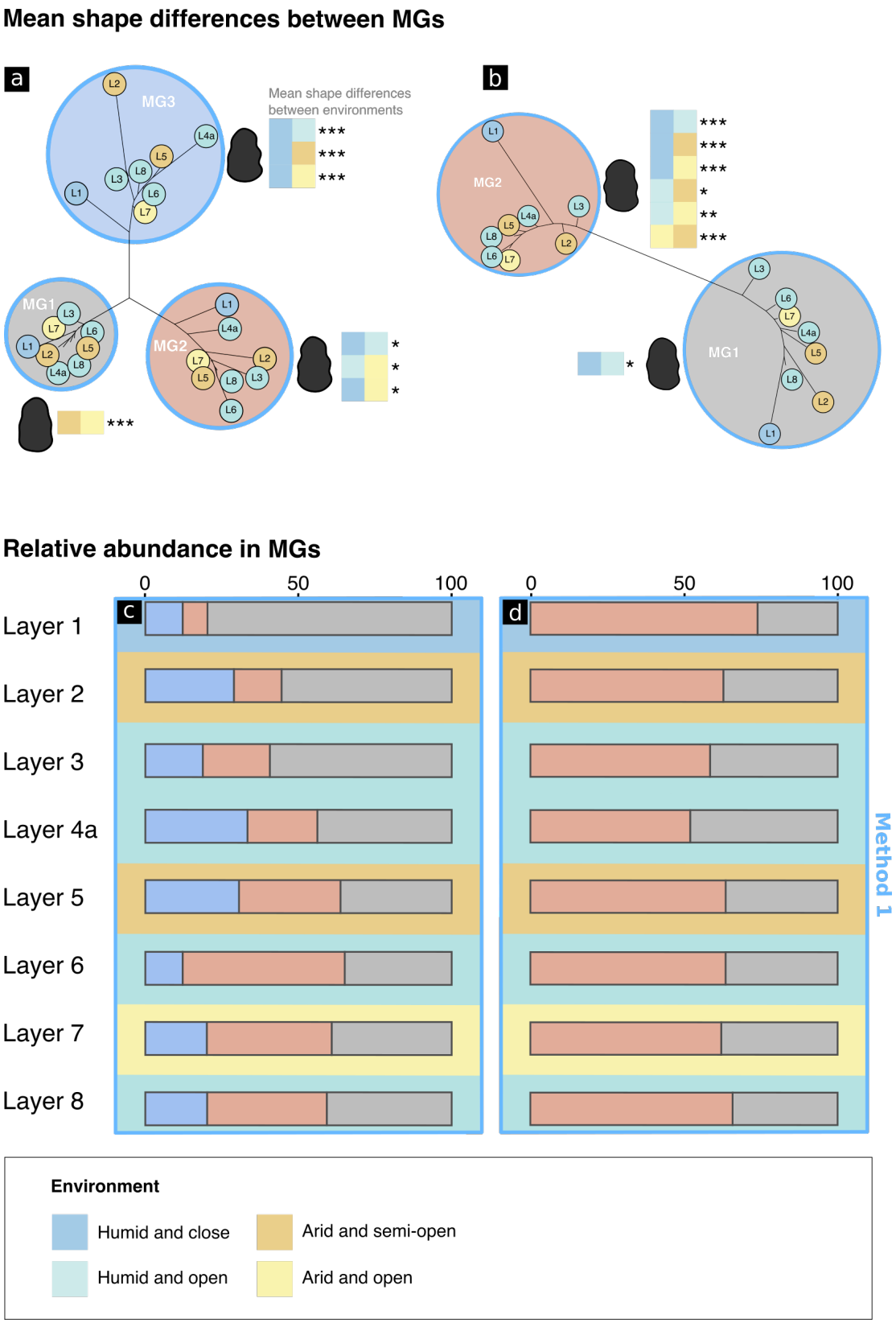

Fig. 8 MGs mean shape and relative abundance in MGs over the eight studied stratigraphic layers of EH2 (method 1). Environmental conditions (Stoetzel, 2009; El Hajraoui *et al.*, 2012) are indicated by background colors. **A**: Neighbor joining distance tree between mean shape of MGs per layer for m1 (lower first molars) and results of pairwise Hotelling's T^2

tests between environmental types per MGs; **B**: Neighbor joining distance tree between mean shape of MGs per layer for M1 (upper first molars) and results of pairwise Hotelling's T^2 tests between environmental types per MGs; **C**: Relative abundance in MGs (%) for m1; **D**: Relative abundance in MGs (%) for M1.

Variations between environmental types are also statistically significant for m1-method1 (MANOVA: MG1: p-value = 1.61e-09 ***, df = 8, F = 2.56, Pillai = 0.30; MG2: p-value = 0.00058 ***, df = 8, F = 1.73, Pillai = 0.24; MG3: p-value = 0.00093 ***, df = 8, F = 1.72, Pillai = 0.42) and for M1-method1 (MANOVA: MG1: p-value = 0.0023 **, df = 8, F = 1.63, Pillai = 0.26; MG2: p-value < 2.2e-16 ***, df = 8, F = 4.30, Pillai = 0.37). Mean shape differences between environments per MGs show that the different MGs are not sensible to the same environmental differences (**Fig 8A** and **8B**). for example, MG1 of m1-method1 is only sensible to transitions between humid and close environments and all other types of environments. MG1 of M1-method1 is very little sensitive to changes of environments while MG2 is highly sensible. Detailed results of pairwise Hotelling's T^2 tests are presented in **Table S7**.

Biodiversity indices

Biodiversity indices over the eight studied stratigraphic layers of EH2 are presented in **Fig 9**. All indicators display a continuous increase of diversity from L8 until L5-L4a, then a decrease until L2 and finally a second increase in L1 (**Fig 9**). This general trend is nuanced in L7 by a decrease of the number of taxa in terrestrial vertebrates (**Fig 9A**) and in L6 by a decrease in rodent diversity indicated by the Shannon and Simpson indices (**Fig 9B** and **Fig 9C**).

Discussion

We aimed to assess phenotypic evolution in EH2 cave rodents relatively to local environmental changes. To do so, we studied shape variation of rodents' teeth over time through an approach that set MGs instead of taxa as phenotypic units. First, we will discuss the evidenced phenotypic variation over time and through environmental changes. Then, we will discuss our methodological approach.

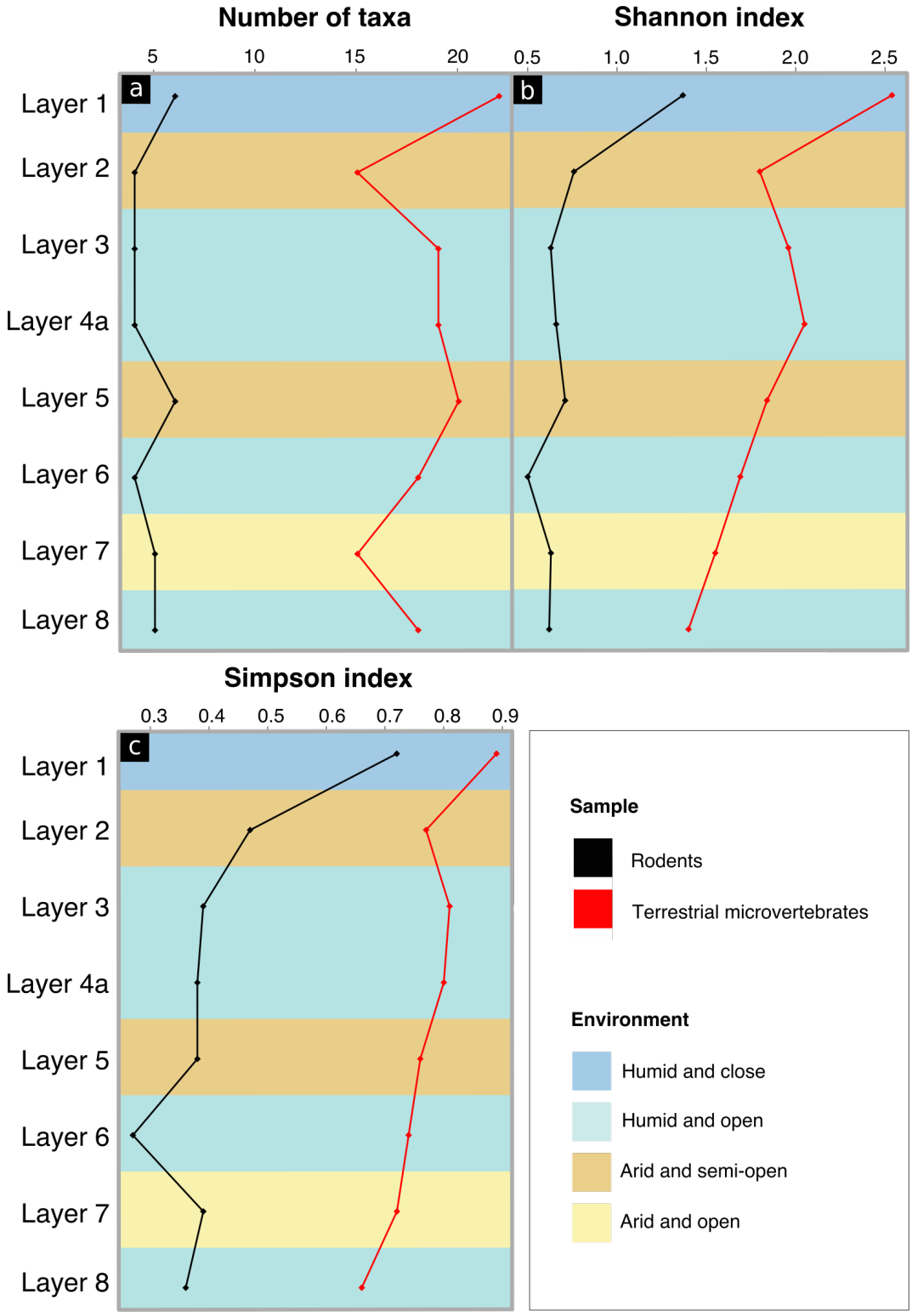

Fig. 9 Biodiversity indices over the eight studied stratigraphic layers of EH2. Environmental conditions (Stoetzel, 2009; El Hajraoui *et al.*, 2012) are indicated by background colors. **A**: Number of taxa; **B**: Shannon index; **C**: Simpson index.

Phenotypic variations under changing environments

We evidenced significant variations in the shape of rodents molars related to local environmental changes. Molars of individuals that lived under more humid environments display less marked outlines. This shape pattern indicates a more flat teeth surface, and thus more worned teeth. Renaud & Ledevin (2017) evidenced in the house mouse that softer food could induce more wearing, probably through tooth-tooth attrition or by a different tooth row occlusion. As rodents are opportunistic feeders (Nowak, 1999; Cox & Hautier, 2015), they may include softer invertabrates present under humid conditions to their diet. In addition, rodents may eat more plants under humid conditions, when vegetation can thrive, than under arid conditions, where they migth rely on others food ressources. An herbivorous dominated diet may lead to more worn and flat teeth because of plants abrasivity (Ungar *et al.*, 2021a).

We also evidenced environmental-related size variations. Molars of individuals from more humid and closed environments are much smaller than those of individuals from others environments. A humid and closed environments suggest a more abundant vegetation and a denser cover. A smaller size might ease mobility in dense environments, and be advantageous to escape from predators (Rieder, Newbold, & Ostoja, 2010).

These morphological variations, despite being significant, are not related to the main pattern of shape variation in molars. Indeed, the relative abundance in MGs, which represents the main pattern of morphological variation, is not related to environmental changes. However, mean shape variation within MGs is significantly different between environments. These results suggest that the shape response to local environmental changes occur within MGs. Relative abundance in MGs is nevertheless significant for m1 over the EH2 sequence. It might be related to other(s) selective pressure(s), as competition, which has been show to have a greater influence on molar shape than climate in the insular mouse (Ledevin *et al.*, 2016).

The main significant disparity variation consists in an increase from L8 to L4a followed by a huge diversity drop between L4a and L3 and then by an increase until L1 (around the Late Pleistocene-Holocene transition). It is illustrated by the disparity variations of the three MGs of m1-method1 and of MG2 of M1-method1, meaning important changes in the amount of variation within concerned morphotypes. The Shannon index of terrestrial

microvertebrates displays similar variation over time. This supports the idea that rodent teeth might be a good proxy to estimate variation in microvertebrate diversity. Moreover, it demonstrates that the exclusion of some rare species from our sampling (*Jaculus* cf *orientalis* and *Eliomys* cf *munbianus*) does not affect significantly our results.

Despite being significant over the EH2 sequence, none of the variation in disparity are signicantly related to environmental changes. This is surprising, as commonly variation in disparity has an ecomorphological meaning through the functional significance of morphological features (Ricklefs & Miles, 1994; Van Valkenburgh, 1994). In the case of teeth, because morphological changes can be related to environment through diet (Wolf *et al.*, 2009; McGuire, 2010; Coillot *et al.*, 2013; Gómez Cano *et al.*, 2013; Gomes Rodrigues, 2015a; Pineda-Munoz *et al.*, 2017), changes in disparity/diversity patterns are supported to reflect environmental variations (Erwin, 2007). Moreover, the fact that similar disparity trends in our results are displayed by two morphological features (m1 and M1) and are shared between MGs that include diverse species (*Meriones shawii/grandis*, *Dipodillus campestris* and *Mus spretus*) suggests that it is driven by (an) external disturbance(s). Moreover, other clades than rodents are also impacted: variations in shrew species composition have also been observed in the same layers (Cornette *et al.*, 2015c). Either disturbances of another nature - ecological or anthropogenic - must have caused those phenotypic changes, or there have been environmental changes that could not be detected through the usual markers used in paleoenvironmental inferences.

This mismatch might be explained by the fact that paleoenvironmental inferences can sometimes be questionable. At EH2, paleoclimatic fluctuations assessment were based on standard analyses of microvertebrate assemblages and were complemented by stable carbon (^{13}C) and oxygen (^{18}O) isotopes analyses on *Meriones shawii/grandis* teeth (Jeffrey, 2016). These analyses indicated that L11 to L7 (dated to MIS 5) encountered more humid conditions than today, while L6 to L3 (dating from MIS 5 to 3) were subjected to conditions similar to the present ones. This suggests a relatively open environment throughout the Late Pleistocene. L2 (dated to MIS 2) appears more arid, which is consistent with the MIS 2 aridification of the region. We thus observed some discrepancies with the previous paleoecological data, notably in L7, L6 and L5. Isotopic results indicate relatively humid conditions in L7 and L5 and more arid ones in L6, while faunal communities indicate the opposite. These discrepancies could be explained by different phenomena. One of these could be the differences in the signals recorded from a set of species communities and those

recorded from individuals within a single species (which can adapt differently to environmental changes) (Stoetzel *et al.*, 2019). Consequently, the paleoenvironmental signal at the individual or species/MG scales may be different than at the community scale.

Regarding the m1 dataset, the MG comprising *Mus spretus* (MG1) displays more similar mean shapes per layers than other MGs. This suggests a high morphological stability of this MG over time and environmental changes. It is consistent with the continuous presence of this species over the EH2 sequence, with no significant changes in terms of abundance over time (Stoetzel *et al.*, 2011), and a stability in morphology and size of molars from the Late Pleistocene to the Middle Holocene (Stoetzel *et al.*, 2013). This may be related to either a strong adaptability of this generalist species to environmental changes and/or a continuous presence of suitable habitats for this species in the Rabat-Temara region through the Late Quaternary (Lalis *et al.*, 2019). Geometric morphometric analysis of *Meriones* molars have shown that during the Late Pleistocene both *M. shawii* and *M. grandis* were present in western Morocco (Stoetzel *et al.*, 2017). Few changes occurred throughout this period despite several climatic changes, indicating that suitable habitats probably always occurred in the region, as it was the case for *Mus spretus*. But during the Middle Holocene, paleontological and morphometric analyses have highlighted a change in the faunal spectrum and species distribution accompanied by a clear demographic collapse (Lalis *et al.*, 2016; Stoetzel *et al.*, 2017). We therefore suggest that during the humid period of the Middle Holocene, when Mediterranean forests expanded, the semi-arid open steppe habitats, more suitable for *Meriones*, decreased drastically in the northern half of Morocco leading to population collapses and changes in their geographic distribution. Consequently, we hypothesize that *Mus spretus* may have been less affected by environmental changes than *Meriones shawii*/*grandis* and that the identified disturbance(s) in L4a must be of a climatic nature. This is supported by isotopes studies that display a higher $\delta^{13}C$ than the normal values observed at EH2, possibly indicating an important change in vegetation at this time (Jeffrey, 2016). Another possibility would be to relate this change in fauna with predator activity. Presence of variable non-human predators (especially canids, such as jackal and fox, and birds of prey) have been attested at EH2 cave and are suspected to be the main agent of modification for faunal remains (Stoetzel, 2009; Campmas *et al.*, 2015, 2017). Even if the microvertebrate diversity does not appear to be related to predator shift between levels (Stoetzel, 2009; Stoetzel et al. 2011), microevolutionary trends might have been affected, thereby influencing macroevolutionary trends (Hansen & Martins, 1996).

The combination of the different shape indicators can allow us to formulate hypotheses about evolution scenarios. This is the case for the phenotypic changes in M1-method1 that occurs in L3, and especially MG2. In this layer, there is a disparity drop combined with a mean shape convergence between the two MGs. Mean shapes represent clumps of forms in the occupied morphospace, and disparity the dispersal of those clumps. It is known that morphological clumps can represent local optima surrounded by less fit alternatives (Erwin, 2007). Shift in mean shapes should then happen when there is shift in ecology and so in optima. Moreover, changes in disparity patterns can reveal patterns of morphological selectivity (Erwin, 2007). Thus, reduction in disparity combined with a mean shape shift towards a particular morphotype can be interpreted as the selection of a form that is advantageous with respect to environmental conditions. Then, we can hypothesize that a morphological selective event occurred in L3, resulting in a shape convergence between the two MGs.

In L7 in m1-method 2 and M1-method 2 an increase in the number of MGs coupled with a decrease in the disparity of some MGs is observed. The presence of a new morphotype might have reinforced competition for resources resulting in each morphotype in a convergence toward its mean shape, reducing each group's disparity. Faunal variations in this layer were also observed in shrews with a particular species composition in the layer (Cornette *et al.*, 2015c). It might be explained by a particularly arid and open environment at this time (Stoetzel, 2009; El Hajraoui *et al.* 2012). However, isotope studies disagree with this hypothesis and suggest more humid conditions (Jeffrey, 2016). The hypothesis of an arid climate in L7, as in L5, is mainly supported by species abundance and the presence of *Jaculus* cf. *orientalis*. But this steppic species can also be considered as an indicator of more continental conditions (i.e. shoreline retreat caused by a sea-level drop) rather than particularly arid conditions. Consequently, some arguments question the paleoenvironmental inferences in L7 based on faunal communities, even if it is almost undeniable that an environmental change occurred.

In L6, MG1 of M1-method1 display a huge disparity drop. An important fact to underline is that L7 and L6 (as for L4a and L3) are very close layers in datation (Jacobs *et al*., 2012; Janati-Idrissi *et al*., 2012; Ben Arous *et al*., 2020a, 2020b). Thus, it is not excluded that these phenotypic variation have a unique cause. We must also have to keep in mind that two species, which we know are present in these deep layers, have not been included in this study (*Jaculus* cf. *orientalis* in L5 and L7 and *Eliomys* cf. *munbyanus* in L5 and L8).

Therefore, the importance of these trends might be under-estimated by this bias in the sampling.

Lower and upper molars, two complementary models

Shapes of the two biological objects - m1 and M1 - globally reflects similar evolutionary patterns as is has been observed in other rodents species (e.g. Renaud *et al*., 1999). More diversity was identified among m1, but more varied trends was displayed by M1. This last result is expected as M1 are known for being more reflective of environmental variations than m1 (Renaud, 1999; Gómez Cano *et al.*, 2013). Statistical tests of mean shape differences between environmental types show indeed that M1 are more sensible to environmental changes than m1. But also, eventually less informative because they are less specific to particular environmental transitions. Each of the biological models allowed us to detect different particular trends: different phenotypic responses within one species in the case of m1, and for M1 a morphological selective event in L3. Those two phenotypic proxies thus provide complementary information leading to a better understanding of rodents' phenotypic evolution.

Biological interpretation of the MGs

The MGs are taxon-free groups of specimens with more similar teeth shape and significant different size. They revealed to be also characterized by phenotypic evolutionary characteristics. For example, MGs of m1-method1 display different mean shapes similarities between layers. This could be interpreted as different degrees of morphological stability over time and through varied environments. MG1 displays more similar mean shapes, possibly implying high resistance to external variations. Conversely MG2 have more different mean shapes between layers, suggesting that this MG may be more plastic. Moreover, MGs are not equally sensible to all environmental changes, suggesting that they are responsive to different environmental parameters. Thus, MGs seem to have different responses to disturbances. They might be interpreted as taxon-free ecological response groups, which can be expected from the fact that rodents are ecological opportunists with flexible diet and habitat preference (Nowak, 1999; Alhajeri & Steppan, 2018).

We detected more phenotypic variations than what is evidenced by conventional indicators of biodiversity, although our results remain consistent with the latter. This may be

explained by the fact that during the Late Quaternary environmental changes were less abrupt in North Africa than in Europe and no major faunal turnover was observed. The geographical location of the EH2 cave also implies that fauna and vegetation are strongly influenced by the Atlantic climate, which was probably the case during the whole Quaternary. This includes lesser variations in humidity and temperature on the coast than in the interior of the continent, as well as regional faunal differences (Stoetzel, 2017; Stoetzel *et al.*, 2019). In sum, only minor changes in microvertebrate communities were observed throughout the EH2 sequence (Stoetzel *et al.*, 2011; Stoetzel, 2013, 2017). This means that a 'common pool' of species was preserved through time with only a few differences in the composition and proportions of species. Microvertebrates underwent low amplitude environmental changes, although alternations between arid and humid periods was recorded at EH2. The landscapes would have been characterized by a mosaic of habitats with only the relative cover of the different habitats changing over time. Most of these changes have certainly been too subtle to be detected by the classic biodiversity indices.

In an archeological context this approach may represent another way of apprehending phenotypic diversity. It is recognized that in archeology global diversity is often underestimated because of the difficulty to identify some taxa (Stoetzel, 2009). Moreover, even regarding current taxa taxonomy can be unstable as for the *Meriones shawii*/*grandis* complex, the systematic of which was very controversial during a long time (Carleton & Musser, 2005; Darvish, 2011; Lalis *et al.*, 2016; Stoetzel *et al.*, 2017). The MG approach is independent of identification, and in some cases unsupervised clustering proved to better evaluate phenotypic diversity than species (Quenu *et al.*, 2020). Moreover, the association of geometric morphometrics and machine learning has repeatedly proven its ability for phenotype discrimination (Dubey *et al.*, 2006; Bocxlaer & Schultheiß, 2010; Cornette *et al.*, 2015c; Guillaud, Cornette, & Béarez, 2016; Mapp *et al.*, 2017; Soda, Slice, & Naylor, 2017; Fang *et al.*, 2018; Quenu *et al.*, 2020). As a consequence, it might be a complementary local diversity indicator to species, as it does not carry the same information and potentially represent ecological groups.

However, this approach has the disadvantage of being a relative rather than an absolute characterization of phenotypic diversity, which sometimes could lead to an underestimation of the overall diversity when compared with other localities (Read *et al.*, 2014). Moreover, we have to keep in mind that *Jaculus* cf. *orientalis* (present in L5 and L7) and *Eliomys* cf.

munbyanus (present in L5 and L8) were not considered in the present study because of the lack of usable teeth for geometric morphometric analyses, which could have led to an underestimation of the diversity in the deepest levels.

Herein, the MG approach was addressed through two complementary methods. The major difference between the two is that: method 1 partitions the variability once on the overall dataset while method 2 does it layer by layer. By pooling remains from different layers, the partitioning protocol of method 1 implies that phenotypic evolution occurring in MGs over time is less important than the phenotypic difference between MGs. It is questionable whether this hypothesis is fully satisfied. First, the number of MGs varies greatly between the two methods. Then, phenotypic evolution has already been brought to light over the studied time interval (i.e. between layers). Indeed, morphological differences have been observed in remains of one same taxon between old and recent layers. Those differences have been imputed to the presence of "primitive" morphological characters in old layers (Stoetzel, 2009). Yet, the overall similarity of trends between the two methods suggests that it is doubtful that these phenotypic changes are equally or more important than phenotypic differences between MGs. The case of EH2 rodents seems to meet in some extent the assumption implied by method 1. However, this is not the case for any data set, and the MG approach will only be applicable to a limited number of cases.

Conclusion

We evidenced phenotypic variations in response to local environmental changes. MGs appear to be phenotypic response units representing ecological groups that are transversal between species. Local environmental changes do not impact the main pattern of shape variation, but induce changes within MGs. However, the impact of the environment on the phenotype might be underestimated. Discrepancies between paleoenvironmental proxies suggest the existence of some uncertainties in paleoenvironmental inferences that might blur the environmental signal. A lead for future investigations may be to look at functional characteristics of MGs in addition to morphological ones. Because they represent more directly the ability of individuals to perform ecological relevant tasks they might allow one to obtain a better characterization of the phenotypic responses to environmental changes.

Supplementary material

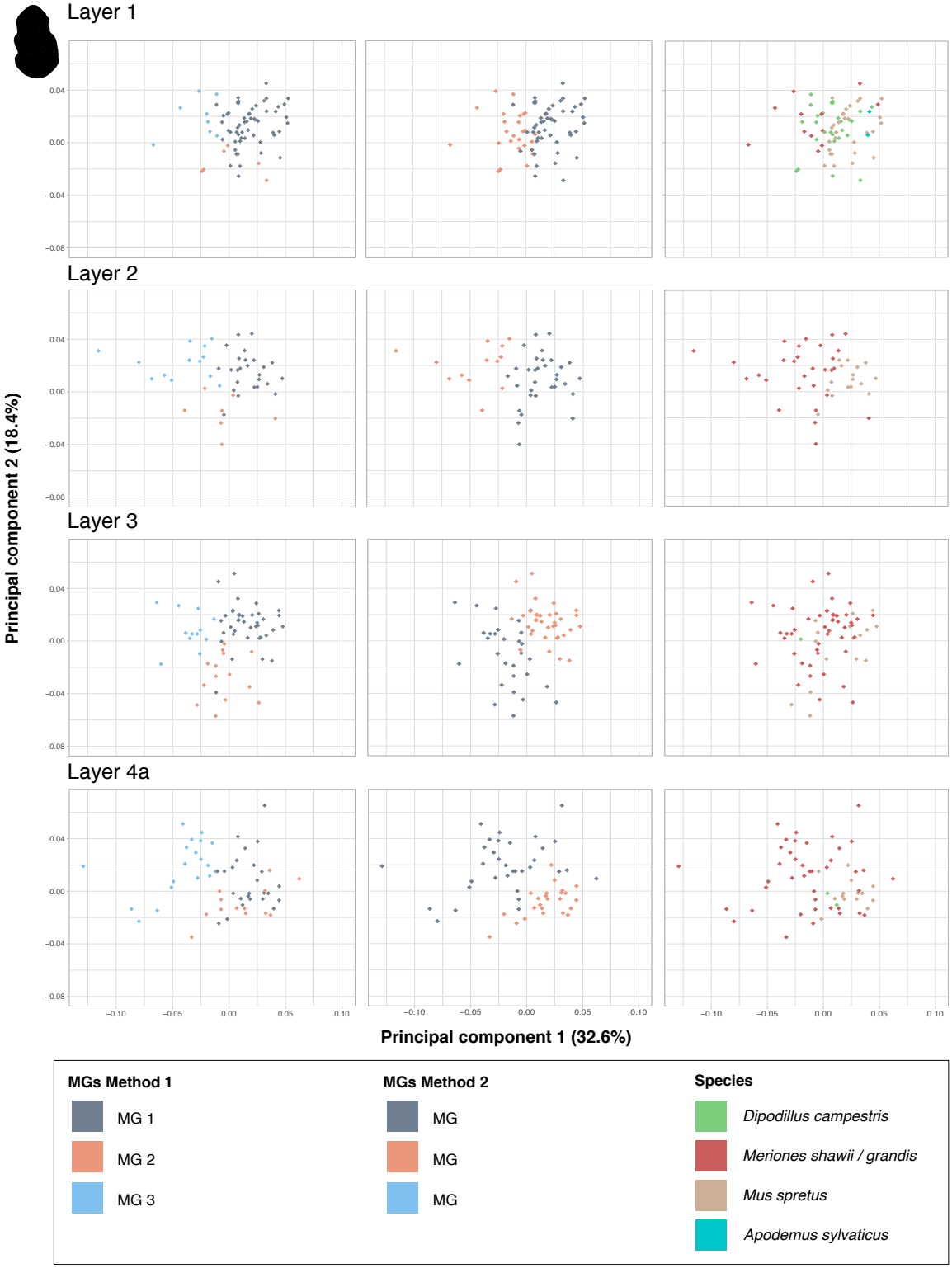

Fig. S1 Clustering results of method 1 and 2 and species of lower molars (m1) presented on the PCA split per layer. Layers 1 to 4a are presented.

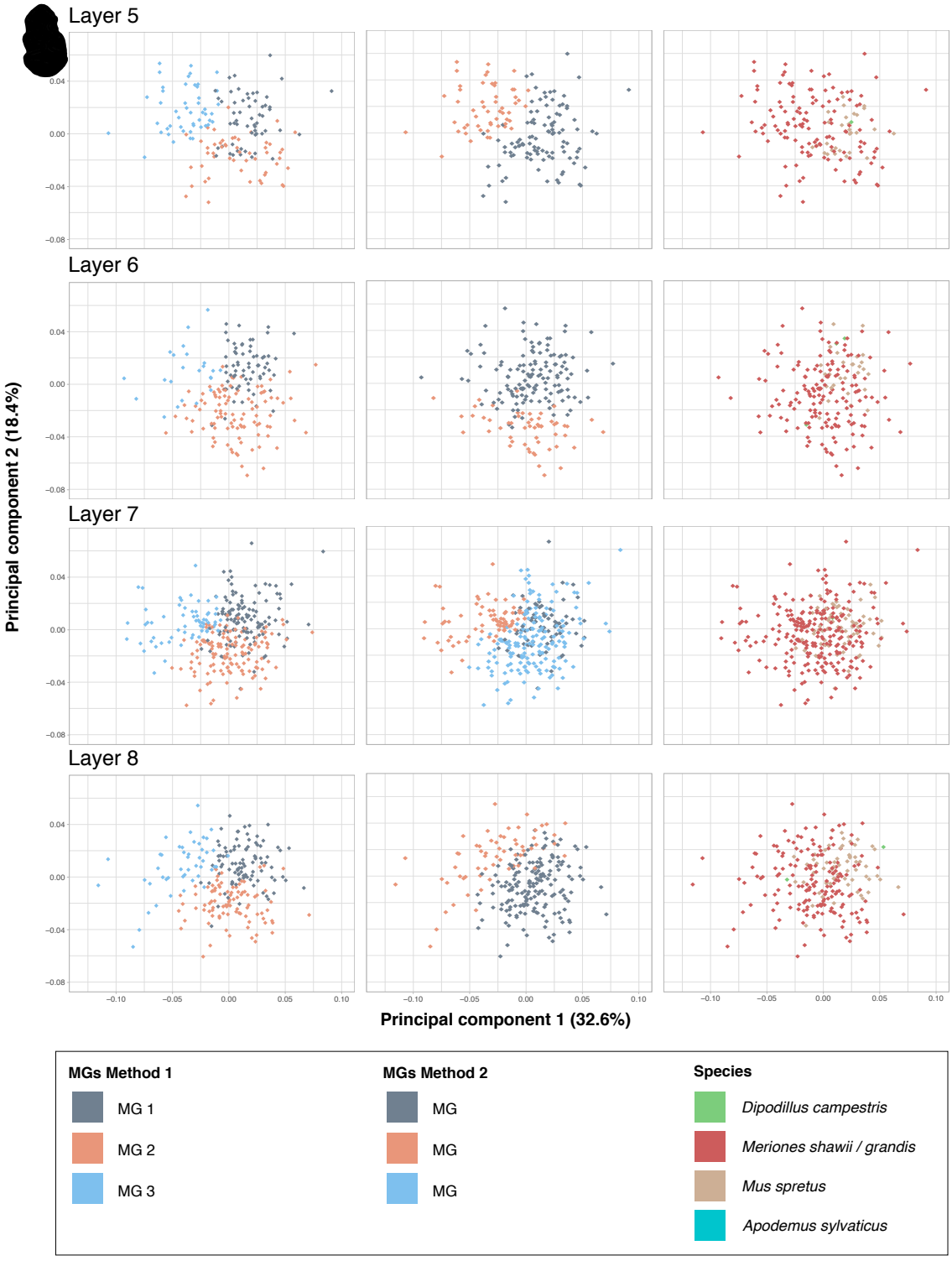

Fig. S2 Clustering results of method 1 and 2 and species of lower molars (m1) presenting on the PCA split per layer. Layers 5 to 8 are presented.

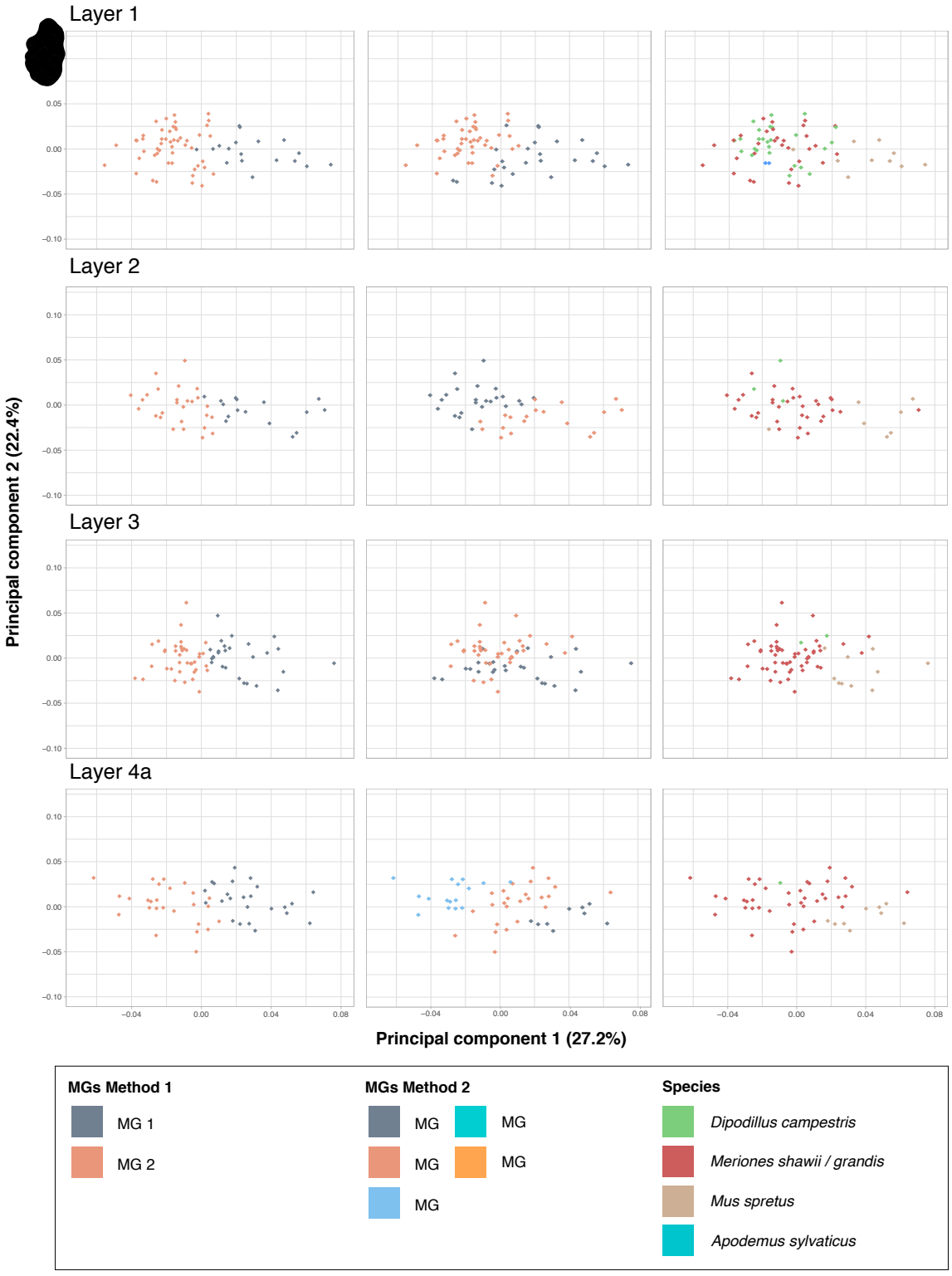

Fig. S3 Clustering results of method 1 and 2 and species of upper molars (M1) presenting on the PCA split per layer. Layers 1 to 4a are presented.

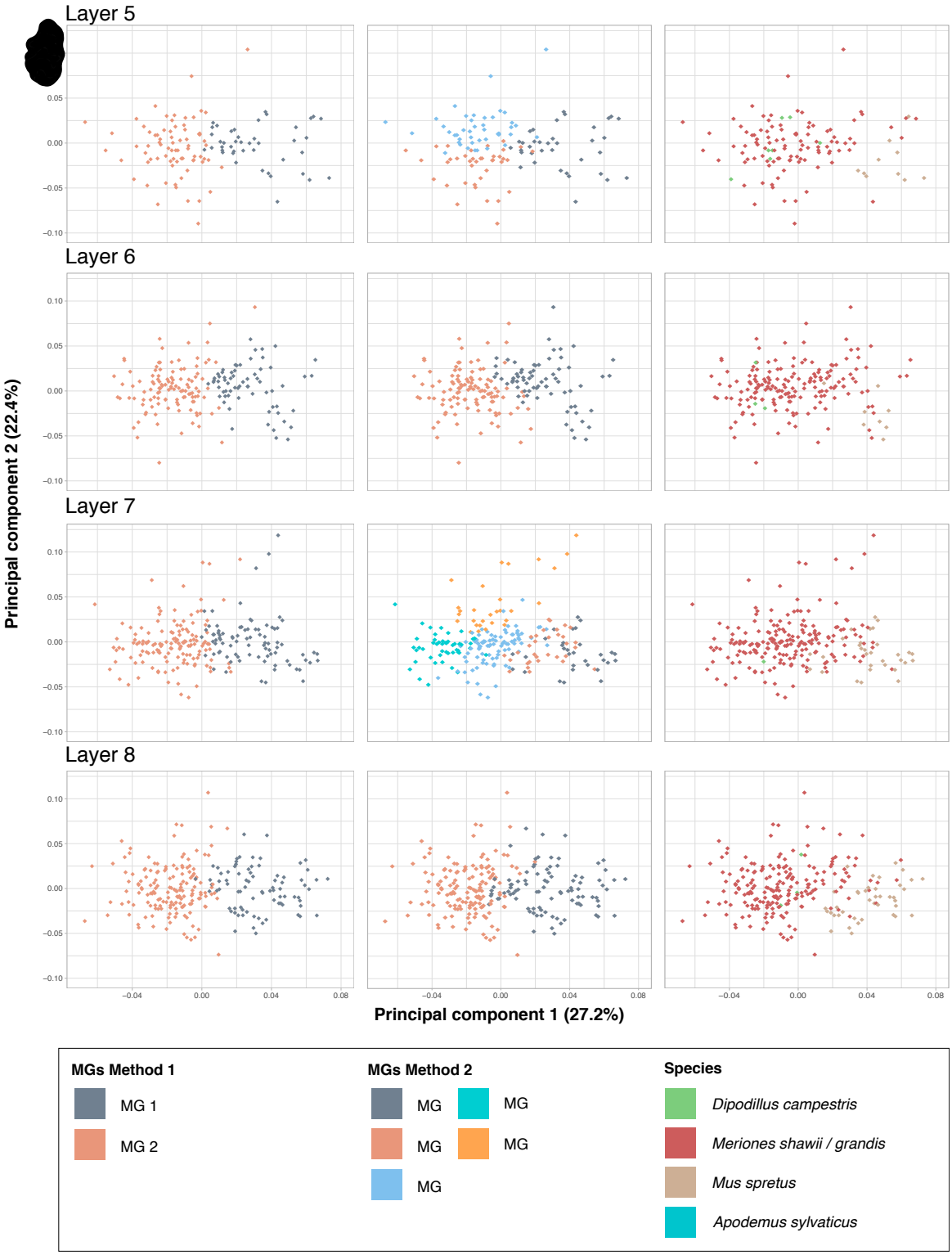

Fig. S4 Clustering results of method 1 and 2 and species of upper molars (M1) presenting on the PCA split per layer. Layers 5 to 8 are presented.

Table. S1 Statistical tests of the difference between the two acquisition methods (manual and semi-automatized). Test A: one m1 of *Mus spretus* was acquired twenty times (ten times with the manual acquisition method, and ten with the semi-automatized method). Test B: ten teeth (m1 and M1) of *Mus spretus* were acquired two times (one time with the manual acquisition method, and one with the semi-automatized method). In both tests, difference between the two acquisition methods was tested using a MANOVA (multivariate analysis of variance) with the *MANOVA* function of the *Momocs* package (Bonhomme *et al.*, 2014). NS is indicated when the result is non-statistically significant.

	Wilks'Lambda	**P-value**
Test A	0.055	0.077 NS
Test B	0.83	0.95 NS

Table. S2 Species composing the MGs identified on the m1 dataset with method 1.

	MG1	**MG2**	**MG3**
L1	45 % *M.spretus* 38 % *D. campestris* 8 % *M. shawii/grandis* 3 % *A. sylvaticus*	50 % *D. campestris* 50 % *M. shawii/grandis*	22 % *D. campestris* 67 % *M. shawii/grandis*
L2	64 % *M.spretus* 36 % *M. shawii/grandis*	100 % *M. shawii/grandis*	100 % *M. shawii/grandis*
L3	40% *M.spretus* 60 % *M. shawii/grandis*	14 % *M.spretus* 86 % *M. shawii/grandis*	8 % *D. campestris* 92 % *M. shawii/grandis*
L4a	56 % *M.spretus* 8 % *D. campestris* 36 % *M. shawii/grandis*	100 % *M. shawii/grandis*	100 % *M. shawii/grandis*
L5	51 % *M.spretus* 2 % *D. campestris* 47 % *M. shawii/grandis*	100 % *M. shawii/grandis*	100 % *M. shawii/grandis*
L6	42 % *M.spretus* 5 % *D. campestris* 53 % *M. shawii/grandis*	100 % *M. shawii/grandis*	100 % *M. shawii/grandis*
L7	56 % *M.spretus* 1 % *D. campestris* 43 % *M. shawii/grandis*	100 % *M. shawii/grandis*	100 % *M. shawii/grandis*
L8	62 % *M.spretus* 1 % *D. campestris* 37 % *M. shawii/grandis*	100 % *M. shawii/grandis*	2 % *M.spretus* 2 % *D. campestris* 96 % *M. shawii/grandis*

Table. S3 Species composing the MGs identified on the M1 dataset with method 1.

	MG1	**MG2**
L1	55% *M. spretus*	45% *D. campestris*
	17% *D. campestris*	4% *L. barbarus*
	28% *M. shawii/grandis*	51% *M. shawii/grandis*
L2	38% *M.spretus*	4% *M.spretus*
	62% *M. shawii/grandis*	11% *D. campestris*
		85% *M. shawii/grandis*
L3	37% *M.spretus*	3% *D. campestris*
	4% *D. campestris*	97% *M. shawii/grandis*
	59% *M. shawii/grandis*	
L4a	37% *M.spretus*	4% *D. campestris*
	63% *M. shawii/grandis*	96% *M. shawii/grandis*
L5	23% *M.spretus*	8% *D. campestris*
	2% *D. campestris*	92% *M. shawii/grandis*
	74% *M. shawii/grandis*	
L6	12% *M.spretus*	3% *D. campestris*
	88% *M. shawii/grandis*	97% *M. shawii/grandis*
L7	36% *M.spretus*	1% *D. campestris*
	64% *M. shawii/grandis*	99% *M. shawii/grandis*
L8	50% *M.spretus*	2% *D. campestris*
	50% *M. shawii/grandis*	98% *M. shawii/grandis*

Table. S4 Species composing the MGs identified on the m1 dataset with method 2.

	MG	**MG**	**MG**
L1	8% *M. shawii/grandis* 51% *M. spretus* 36% *D. campestris* 5% *A. sylvaticus*	40% *M. shawii/grandis* 8% *M. spretus* 36% *D. campestris*	-
L2	50% *M. shawii/grandis* 50% *M. spretus*	100% *M. shawii/grandis*	-
L3	69% *M. shawii/grandis* 28% *M. spretus* 3% *D. campestris*	74% *M. shawii/grandis* 26% *M. spretus*	-
L4a	38% *M. shawii/grandis* 54% *M. spretus* 8% *D. campestris*	97% *M. shawii/grandis* 3% *M. spretus*	-
L5	71% *M. shawii/grandis* 28% *M. spretus* 1% *D. campestris*	100% *M. shawii/grandis*	-
L6	77% *M. shawii/grandis* 21% *M. spretus* 2% *D. campestris*	100% *M. shawii/grandis*	-
L7	5% *M. shawii/grandis* 93% *M. spretus* 2% *D. campestris*	100% *M. shawii/grandis*	100% *M. shawii/grandis*
L8	65% *M. shawii/grandis* 34% *M. spretus* 1% *D. campestris*	96% *M. shawii/grandis* 2% *M. spretus* 2% *D. campestris*	-

Table. S5 Species composing the MGs identified on the M1 dataset with method 1.

	MG	**MG**	**MG**	**MG**	**MG**
L1	40% *M. spretus* 40% *M. shawii/grandis* 20% *D. campestris*	48% *M. shawii/grandis* 48% *D. campestris* 4% *L. barbarus*	-	-	-
L2	4% *M. spretus* 83% *M. shawii/grandis* 13% *D. campestris*	38% *M. spretus* 62% *M. shawii/grandis*	-	-	-
L3	95% *M. shawii/grandis* 5% *D. campestris*	38% *M. spretus* 62% *M. shawii/grandis*	-	-	-
L4a	100% *M. spretus*	100% *M. shawii/grandis*	94% *M. shawii/grandis* 6% *D. campestris*	-	-
L5	28% *M. spretus* 69% *M. shawii/grandis* 3% *D. campestris*	92% *M. shawii/grandis* 8% *D. campestris*	93% *M. shawii/grandis* 7% *D. campestris*	-	-
L6	11% *M. spretus* 89% *M. shawii/grandis*	97% *M. shawii/grandis* 3% *D. campestris*	-	-	-
L7	100% *M. spretus*	100% *M. shawii/grandis*	99% *M. shawii/grandis* 1% *D. campestris*	100% *M. shawii/grandis*	100% *M. shawii/grandis*
L8	43% *M. spretus* 57% *M. shawii/grandis*	98% *M. shawii/grandis* 2% *D. campestris*	-	-	-

Table. S6 Results of pairwise tests between environmental types on global shape and size. For shape we performed Hotelling's T^2 and for size t-tests. AO: Arid and Open; ASO: Arid and Semi-Open; HC: Humid and Close; HO: Humid and Open. ***Bold/italic***: the difference between the tested layers is statistically significant (p-values < 0.008 according to Bonferroni's criteria).

		AO	ASO	HC
Shape				
m1				
ASO	P-value	***2.76e-05***	-	
	T^2	***60.59***		
HC	P-value	***~0***	***3.49e-14***	-
	T^2	***184.84***	***139.72***	
HO	P-value	***0.0012***	***0.00028***	***~0***
	T^2	***46.50***	***51.63***	***177.60***
M1				
ASO	P-value	***2.63e-05***	-	
	T^2	***62.36***		
HC	P-value	***~0***	***7.90e-10***	-
	T^2	***192.92***	***107.51***	
HO	P-value	0.014	***0.0051***	***~0***
	T^2	37.64	***41.73***	***186.92***
Size				
m1				
ASO	P-value	0.58	-	
HC	P-value	***<2e-16***	***<2e-16***	-
HO	P-value	1.00	0.81	***<2e-16***
M1				
ASO	P-value	1	-	
HC	P-value	***7.5e-14***	***2.1e-14***	-
HO	P-value	1	1	***1.2e-14***

Table. S7 Results of pairwise Hotelling's T^2 tests between environmental types on mean shape of each MGs of m1-method1 and M1-method1. AO: Arid and Open; ASO: Arid and Semi-Open; HC: Humid and Close; HO: Humid and Open. ***Bold/italic***: the difference between the tested layers is statistically significant (p-values < 0.008 according to Bonferroni's criteria).

		AO	ASO	HC
m1				
MG1				
ASO	P-value	0.33	-	
	T^2	24.75		
HC	P-value	***3.91e-07***	***4.61e-05***	-
	T^2	***88.72***	***73.66***	
HO	P-value	0.055	0.41	***2.92e-10***
	T^2	33.48	22.22	***105.91***
MG2				
ASO	P-value	0.067	-	
	T^2	0.067		
HC	P-value	***0.0065***	0.13	-
	T^2	***50.056***	42.63	
HO	P-value	***0.0048***	0.073	***0.0044***
	T^2	***43.92***	32.73	***46.67***
MG3				
ASO	P-value	***4.76e-05***	-	
	T^2	***77.043***		
HC	P-value	0.034	0.040	-
	T^2	51.86	51.57	
HO	P-value	0.23	0.067	0.12
	T^2	28.18	35.74	35.35
M1				
MG1				
ASO	P-value	0.062	-	
	T^2	36.96		
HC	P-value	0.048	0.029	-
	T^2	42.019	51.54	
HO	P-value	0.42	0.031	***0.0048***
	T^2	22.22	37.12	***46.56***
MG2				
ASO	P-value	***1.097e-06***	-	
	T^2	***78.66***		
HC	P-value	***~0***	***5.18e-06***	-
	T^2	***202.41***	***81.87***	
HO	P-value	***0.00078***	***0.0053***	***~0***
	T^2	***49.54***	***42.72***	***172.81***

CHAPTER 2

The contribution of functional traits to the understanding of paleoenvironmental changes

Léa Terray, Emmanuelle Stoetzel, Anthony Herrel, Raphaël Cornette

Published (2021) in the Biological Journal of the Linnean Society.

DOI: 10.1093/biolinnean/blab057

In the previous chapter, we evaluated the response of morphological traits to local environmental variations and defined a phenotypic approach through the characterization of MGs. The MGs are characterized by different shape and size and do not respond to the same environmental changes: they seem to act as ecological groups. We demonstrated that shape is partly related to local environmental changes, but that these changes do not drive to the main pattern of shape variation evidenced by morphological groups. Indeed, these responses occur within MGs and local environmental changes do not significantly affect variation in disparity or relative abundance in MGs. Morphological traits are impacted by local environmental changes, but less than expected. Functional traits, that may be under different constraints than morphological traits, might display a stronger response to local environmental changes. In chapter 2, we explore how a functional trait, estimated bite force, is related to local environmental changes depicted by paleoenvironmental indicators from the literature. Because modularity may explain the relationship between the variation in mandible shape and the variation in estimated bite force, we also investigate variations in the degree of modularity of the mandible. In further MGs analyses in this thesis we use only method1. Indeed, in chapter 1 trends are overall similar between method 1 and method 2, method 1 evidenced more statistically significant phenotypic variations and because MGs identity between layers is preserved, it allows one to explore more phenotypic indicators.

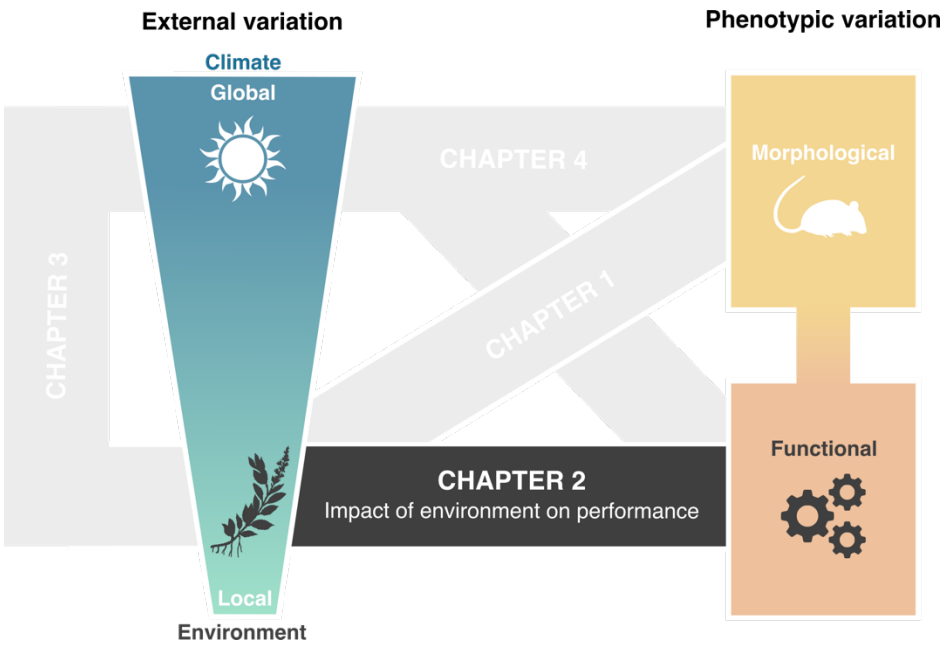

Diagram showing how chapter 2 fits into the thesis problematic.

Introduction

Performance traits, provide a direct link between ecology, morphology, and fitness (Arnold, 1983; Wainwright, 1994). They reflect the ability of individuals to perform ecologically relevant tasks (Irschick *et al.*, 2008) and are subjected to selection (Irschick *et al.*, 2008). In animals, performance traits are dependent on skeletal structures, variation in muscular anatomy, contractile physiology, and variation in biomechanical traits such as lever arms. Consequently, the relationship between morphological and functional traits is complex (Wainwright, 1994; Irschick *et al.*, 2008). Different morphological traits can generate similar functional outputs by redundancy (Alfaro *et al.*, 2005), which may lead to functional convergence in organisms living in environments requiring similar performance abilities (Wainwright, 2005; Young *et al.*, 2007, 2010). Conversely, one morphological trait can affect different performance traits through trade-offs and facilitation. Trade-offs occur when there is a conflicting demand on a phenotypic trait through its differential implication in several performance traits (Garland & Losos, 1994; Van Damme *et al.*, 2003; Walker, 2007, 2010; Langerhans, 2009; Holzman *et al*., 2011; Vanhooydonck *et al*., 2011). Facilitation, on the other hand, occurs when a similar demand is exerted on a phenotypic trait by several different performance traits (Walker, 2007). Therefore, a complex "many-to-many" morphology-performance relationship may exist (Bergmann & McElroy, 2014), implying that morphological and functional traits may not respond similarly to changes in the environment. Thus, functional traits may be relevant candidates to function as ecological indicators, complementary to morphological traits.

Feeding is the function related to dietary ecology (Schwenk, 2000). Bite force is a performance trait implicated in feeding. It is a performance trait directly linked to diet through the mechanical demands imposed by variation in the mechanical properties of food items (Anderson *et al*., 2008; Herrel *et al.*, 2008; Dumont *et al*., 2009; Santana *et al*., 2010; Maestri *et al.*, 2016). Changes in diet associated with bite force are considered one of the main drivers of diversification in mammals (Christiansen & Wroe, 2007; Monteiro & Nogueira, 2011). Thus, bite forces may be a powerful ecological proxy and have been widely used to characterize dietary ecology in vertebrates (e.g. Freeman, 1979; Losos, 1992; Herrel *et al*., 2002; Huber, 2005; Kerr *et al*., 2017).

Studies on bite force in fossil taxa are common as they may provide insights into the behavioural ecology of extinct taxa (e.g. Erickson *et al*., 1996; Therrien, 2005; Wroe *et al.*, 2005; Lappin *et al*., 2017; Rinderknecht *et al*., 2019). However, to our knowledge,

estimates of bite force have only rarely been applied to better understand paleoenvironmental variation. Commonly, such inferences rely on community compositions and/or the characterization of particular morphotypes (e.g., Fernandez-Jalvo *et al.*, 1998; Stoetzel *et al.*, 2011; Comay, Weissbrod & Dayan, 2019; Royer *et al.*, 2020; López-García *et al.*, 2021). These approaches associate a particular biological feature to a specific environment. However, an organism's dietary ecology can be more accurately inferred from bite force than by categorical ecological classifications (Santana *et al.*, 2010). Thus, bite force has a strong potential to contribute meaningfully to understand paleo-environmental variation.

Functional aspects are also important determinants of morphological integration. This concept defines the covariation patterns that exist between morphological traits (Badyaev & Foresman, 2000, 2004; Young & Badyaev, 2006; Klingenberg, 2008; Klingenberg & Marugán-Lobón, 2013). As a result of selection on performance, traits implicated in a same function interact strongly, making them vary together (Klingenberg, 2008). This may be particularly the case when they are linked through muscle insertions providing physical and mechanical links between structures (Cheverud, Routman, & Irschick, 1997; Mezey, Cheverud, & Wagner, 2000; Klingenberg, Mebus, & Auffray, 2003; Klingenberg, 2004). Thus, changes in the strength of integration in the feeding apparatus could be related to changes in bite force. Moreover, the less the modules in a structure like the mandible covary together (i.e. the more modular they are), the more disparate are the organisms that can be produced (Goswami *et al.*, 2014). Modularity patterns may consequently also be related to bite force disparity. Moreover, changes in modularity are known to respond to environmental stresses (Badyaev & Foresman, 2000). In the light of these facts, modularity in the feeding apparatus may also be a relevant indicator for understanding variation in paleoenvironments.

The Moroccan archaeological site El Harhoura 2 (EH2) is located in the Rabat-Témara region, on the North-Atlantic coast of Morocco. It is divided into 11 archeo-stratigraphical levels covering a time period from the Late Pleistocene to the Holocene. Phenotypic evolution related to environmental variation has been extensively studied at this site (Stoetzel, 2009; Stoetzel *et al.*, 2010, 2011, 2012b, 2013; Stoetzel, 2017; Stoetzel *et al.*, 2017). Small mammals such as rodents and shrews are a relevant model to consider paleoenvironmental variation (e.g. Valenzuela *et al.*, 2009; McGuire, 2010; Escudé *et al.*, 2013; Verde Arregoitia, Fisher & Schweizer, 2017). The biogeography and ecological

characteristics of species (such as diet, habitat, soil), as well as the global composition of the small vertebrate communities in the different studied levels, allowed paleoenvironmental inferences at EH2 (e.g. Stoetzel *et al.*, 2011, 2013, 2017). Among the remains recovered at EH2, shrew mandibles have been given peculiar attention (Cornette *et al.*, 2015a,c). Mandible shape is known for being highly plastic and often varies with environmental conditions in these animals (Badyaev & Foresman, 2000; Caumul & Polly, 2005; Cornette *et al.*, 2015a,c; Souquet *et al.*, 2019).

In the present study, we sought to understand the relationship between the morphology of the mandible in shrews, its modularity, and the estimated bite force over time. We further explored whether a functional trait (bite force) can provide relevant information for the understanding of paleoenvironments. Our approach is divided in three steps. 1) To evaluate global morphological diversity, shrews were divided into morphological groups (MGs). This characterization of biodiversity was chosen instead of species. MGs allow to consider variations at several levels of diversity (inter- and intra-specific), which makes it a relevant approach to characterize environment-related selection which acts at both levels (Erwin, 2000; Lande, 2009; Boutin & Lane, 2014; Hautmann, 2020). We expected identified MGs to be functional response units to changes in the environment, as has been suggested in previous studies (Read *et al.*, 2014; Khare *et al.*, 2017). 2) Bite force was estimated through the mechanical potential. Because performance and morphology are not strictly related, selection can apply differently at both levels of organization (Irschick *et al.*, 2008). Thus, quantifying variation in the mechanical potential may allow us to detect selection events undetectable through morphological proxies. 3) Finally, variation in modularity was characterized. An increase in modularity in shrew mandibles may allow morphological diversification within a population utilizing the same resources irrespective of selection on function (Young *et al.*, 2007, 2010) and as such be associated with variation in the environment.

Material and methods

El Harhoura 2 cave and data collection

El Harhoura 2 cave (33°57'08.9" N / 6°55'32.5" W) is an archaeological site located on the Moroccan Atlantic coast, a few km south of Rabat. The cave was occupied by Middle Stone Age, Later Stone Age, and Neolithic human populations and has yielded numerous

archaeological material as well as the remains of large and small vertebrates (Nespoulet *et al.*, 2008; El Hajraoui *et al.*, 2012; Stoetzel *et al.*, 2014). From top to bottom, the stratigraphy of EH2 cave is structured in 11 layers. Eight of these levels are well dated and were included in this study (L1, L2, L3, L4a, L5, L6, L7, L8) (Jacobs *et al.*, 2012; Jacobs & Roberts, 2012; Janati-Idrissi *et al.*, 2012; Ben Arous *et al.*, 2019, 2020a). Paleoenvironmental data were deduced from faunal communities (Stoetzel, 2009; Stoetzel *et al.*, 2011, 2012b,a, 2014). An alternation of humid and arid periods has been documented and the landscape was mainly dominated by steppes with an increase in more wooded areas and water ponds during humid periods (**Fig 1**, the same as **Fig 1** in chapter 1).

The material studied here is temporarily housed at the Muséum National d'Histoire Naturelle, Paris, France. It was sampled during the 2005-2009 excavation campaigns of the El Harhoura-Témara Archaeological Team (dir. R. Nespoulet and M.A. El Hajraoui). Four species of white-toothed shrews are represented: the material is largely dominated by *Crocidura russula* but *C. lusitania*, *C. tarfayensis* and *C. whitakeri* were also present (Cornette *et al.*, 2015a,c). Among archaeological remains complete mandibles are rare and most of the material is fragmented. Nevertheless, mandible fragments also carry relevant morphological and paleoenvironmental information (Cornette *et al.*, 2015a,c) and can be used to increase the sample. Here we used complete mandibles (Clpt) and three types of mandible fragments (A, B, C). Chosen fragments are those whose shape best enables species to be distinguished (Cornette *et al.*, 2015a). Fragmentation patterns are illustrated in **Fig 2**. Extant material (Act) of the same four species from the Rabat area was added to extend the time line to present day. The number of complete and fragmented mandibles studied is indicated in **Table 1**. Data acquisition is described in Cornette *et al*. (2015a).

Geometric morphometrics

Two dimensional geometric morphometric analyses were used. All mandibles could not be analyzed together because remains from various fragmentation patterns are not directly comparable. We performed separate shape analyses for each fragment type (Cplt, A, B and C) following the same protocol. Mandibles were analyzed through a landmark and sliding semi-landmark based approach allowing the description of the shape of biological relevant areas without anatomical landmarks (Bookstein, 1996; Zelditch, 2004; Gunz, Mitteroecker, & Bookstein, 2005; Cornette *et al.*, 2013). Landmark locations for each fragment type are

indicated in **Fig 2**. Semi-landmarks were slid to minimise the bending energy. Generalized Procrustes Analyses (GPA) were performed on each data set (Cplt, A, B and C) to remove effects of translation, rotation, and scale and make objects comparable (Rohlf & Slice, 1990).. Resulting shape coordinates are the Procrustes residuals. These two last steps were performed using the *gpagen* function of the *geomorph* package (Adams & Otárola-Castillo, 2013) in R version 3.6.3 (2020-02-29). To reduce data dimensionality, principal component analyses were performed on Procrustes residuals for each data set (Cplt, A, B and C) and we retained 95% of shape variation for the following analyses (Baylac & Frieß, 2005). All analyses were performed using R version 3.6.3 (2020-02-29).

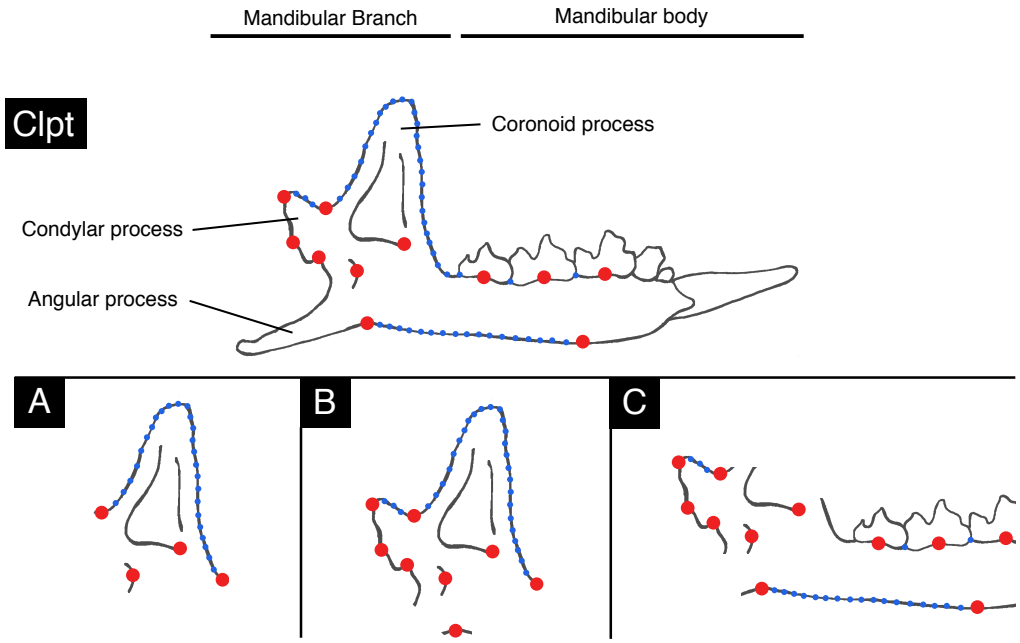

Fig. 2 Types of fragments and their landmark (red points) and semi-landmark (blue points) locations. Clpt: complete mandibles; **A**: fragmented mandibles of type A; **B**: fragmented mandibles of type B; **C**: fragmented mandibles of type C.

Morphological groups

To assess shape diversity, mandibles were partitioned into morphological groups. First, complete mandibles (Clpt) were clustered based on their shape. To do so a morphological K-nearest neighbor method (KNN) was used. This method is adapted to small datasets, as is the case here, because it is a non-parametric classification. In this algorithm, each shape object is assigned to its nearest neighbor cluster. The *clues* function of the *clues* package

(Wang, Qiu & Zamar 2007) proposes an unsupervised KNN, meaning that the number of clusters is inferred from the data itself, favoring the most robust partitioning of the dataset. The robustness of the clusters is assessed by the Silhouette index (SI) (Kaufman & Rousseeuw, 1990) which measures the strength of the clusters. SI is comprised between -1 and 1. The more SI is close to 1 (i.e. SI>0), the more data points are correctly assigned to their clusters, and conversely the more SI is close to -11 (i.e. SI<0), the more data points are mis-assigned (Wang *et al.*, 2007).

Table. 1 Abundance of remains studied (complete and fragmented mandibles).

Layer	Clpt	A	B	C	TOTAL
Act	16	-	-	-	**16**
L1	2	1	-	2	**5**
L2	2	4	1	2	**9**
L3	3	1	1	1	**6**
L4a	2	1	-	1	**4**
L5	10	-	2	3	**15**
L6	10	2	4	9	**25**
L7	9	7	13	10	**39**
L8	-	6	10	11	**27**
TOTAL					**146**

To visualize the morphological groups identified, the morphospace of complete mandibles (Cplt) was plotted using the three first axes of the principal component analysis computed on the Cplt data set. Deformations along axes were computed using the function "PlotRefToTarget" from the "geomorph" package (Adams & Otárola-Castillo, 2013). Thin-plate spline deformation grids representing differences between the extreme shapes of each axis and the global mean shape of Cplt mandibles were generated.

Next, we tested the robustness of the morphological groups identified on complete mandibles (Clpt) for each fragmentation pattern. Artificial A, B and C fragments were computed from complete mandibles (Clpt) and strengths of the clusters based on fragments

were assessed using SI. This was achieved using the *get_Silhouette* function of the *clues* package (Wang *et al.*, 2007).

Finally, the belonging of true A, B and C mandible fragments to the morphological groups was determined *a posteriori* using the KNN classification algorithm with the *knn* function of the *class* package (Venables & Ripley, 2002). Mean shapes of each morphological group were computed from complete mandibles (Clpt) using the functions "mshape" and "warpRefOutline" of the "Geomorph" package (Adams & Otárola-Castillo, 2013).

Mechanical potential

The mechanical potential as used in this study is the ratio of the muscle moment arm to the jaw outlever. As such it is dependent on the geometry of the skull and mandible and the insertion of the masticatory muscles (Herrel *et al.*, 2008a; Chazeau *et al.*, 2013; Manhães, Nogueira, & Monteiro, 2017; Ginot *et al.*, 2018, 2019). In particular, mandible shape is known for being a good estimator of bite force (Brassard *et al.*, 2020a,c). As a proxy for overall mechanical potential, we choose the mechanical potential of the temporalis muscle. This is one of the main muscles involved in bite force generation in shrews (Herrel *et al.*, 2008a; Santana *et al.*, 2010; Brassard *et al.*, 2020a). It was estimated based on the moment arm of the temporalis, computed from the mandible shape. The biomechanical model is presented in **Fig 3**. It is defined as MP = A / B, where: A is the moment arm of the temporalis, B the jaw out-lever and MP the mechanical potential of the temporalis. MP was computed for complete mandibles (Clpt) from Procrustes residuals.

However, MP does not reflect the phenotype in nature: because it is computed from Procrustes residuals, it does not account for size variation in the data set, nor for compensatory effects of musculature. Moreover, it only considers a single force - the temporalis muscle - which is applied uniformly (Young *et al.*, 2007). All these parameters are important drivers of the mechanical potential, in particular size (Wroe *et al.*, 2005; Freeman & Lemen, 2008; Herrel *et al.*, 2008a; Chazeau *et al.*, 2013; Manhães *et al.*, 2017; Ginot *et al.*, 2018, 2019; Brassard *et al.*, 2020a). In order to increase the accuracy of our estimate of bite force, we corrected MP to take size into account.

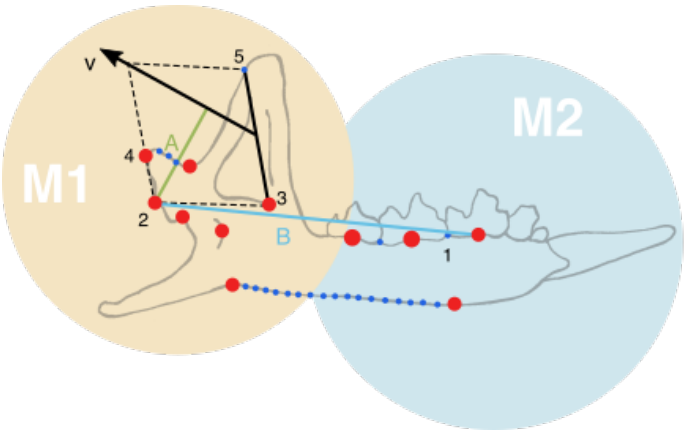

Fig. 3 Biomechanical model used to estimate the mechanical potential of the temporalis muscle (MP) from mandible shape. V is the vector that starts at mid distance between landmarks 3 and 5 and has for direction the intersection between the line passing through landmarks 3 and 4 and the parallel of the line passing through landmarks 2 and 3 passing through 5. A is the moment arm of the temporalis (the distance between the landmark 2 and the vector). B is the jaw out-lever (the distance between landmarks 1 and 2). M1 and M2 are the definitions of the two hypothesized modules of the mandible from the literature (Cheverud *et al.*, 1997; Mezey *et al.*, 2000; Klingenberg *et al.*, 2003; Klingenberg, 2004) and landmarks implicated (C fragmentation pattern). M1: ascending ramus module; M2: alveolar region module.

It is known that MP is linearly correlated to mandible/skull size in some mammals, including shrews (Nogueira, Peracchi, & Monteiro, 2009; Cornette *et al.*, 2015b; Manhães *et al.*, 2017; Ginot *et al.*, 2018; Brassard *et al.*, 2020a). As MP is computed from mandible shape, this means that it has an allometric component, i.e. even if MP is size-free, a part of the MP results from the influence of size. To confirm this assumption in our data set, we tested it on complete mandibles (Cplt) by performing a regression of the log-transformed centroid size on the log-transformed MP using the *lm* function of the *stats* package. Centroid size (Csize) is a size estimator widely used in geometric morphometrics. It is defined as the square root of squared distances of all landmarks of a mandible from its centroid (Klingenberg, 2016).

Corrected MP (cMP) was subsequently expressed as: cMP = MP + f(size) **(1)**, where MP is the mechanical potential and f(size) the part of cMP due to size. It is also known that $\log_{10}$ bite force is linearly correlated to size (Wroe *et al.*, 2005; Chazeau *et al.*, 2013; Manhães *et al.*, 2017; Ginot *et al.*, 2019; Brassard *et al.*, 2020a). Thus, for cMP to be a good estimator of bite force, log-transformed cMP must also be linearly correlated to size. So, in **(1)** we have f(size) = a*size + b **(2)**. The objective here is to determine a and b.

We assume that the allometric part of MP is proportional to the influence of size on MP. Thus, *a* and *b* of **(2)** can be found by performing a linear regression of size on MP. However, our data have a temporal component that we need to consider, otherwise, we may lose part of this temporal information as MP and size are both related to time. We performed a multivariate regression of size and time on MP. Log-transformed values of MP and Csize were used. *a* and *b* of **(2)** were defined with the parameters of this regression: *a* as the coefficient of log(Csize) and *b* as the intercept. We obtained: log(cMP) = log(MP) + *a**log(Csize) + *b* **(3)**.

To evaluate whether cMP is a good estimator of bite force, we assessed its reliability on a dataset of simulated data:

1. 1000 bite forces and associated sizes were simulated. Values were randomly generated according to a normal distribution using the *rnorm* function of the *stats* package, with for bite forces the constraint of a mean of 0.3 and a standard deviation of 0.15, and for size a mean of 3500 and a standard deviation of 500. Those constraints aimed to generate a dataset as close as possible to what is observed for the species present in our data set.

2. MP was computed using **(3)**, where cMP was replaced by bite force values and with *a* and *b* arbitrarily fixed (to represent the "real" relation between MP, bite force and size in the simulated dataset). 30 couples of *a* and *b* were randomly generated using the *rnorm* function of the *stats* package and tested. They were computed in order to be similar to the *a* and *b* found previously. As the correlation between $\log_{10}$ bite force and size is strictly positive (Wroe *et al.*, 2005; Chazeau *et al.*, 2013; Manhães *et al.*, 2017; Ginot *et al.*, 2019; Brassard *et al.*, 2020a), *a* should be strictly positive and was generated with the constraint of a mean of 3 and a standard deviation of 3. *b* was generated with the constraint of a mean of 0 and a standard deviation of 5, to test positive and negative values. Tested couples of *a* and *b* are presented in **Table S1**. To simulate measurement error, Gaussian noise was added to computed MP (error tested at 0.01, 0.05 and 0.1).

3. cMP were calculated using **(3)**, with *a* and *b* found previously.

4. For each pair of values in the simulated dataset, we tested whether the relation between the bite force of individuals was respected by cMPs (for example, if we have two individuals X and Y such that: bite force X > bite force Y, we must also have cMP X > cMP Y). Thus, variation in cMP reflects, in a relative way, variation in bite force. Mean,

min and max scores of reliability among the 30 *a* and *b* couples were computed for the three measurement error estimates.

To obtain the cMP of fragmented mandibles (A, B and C) we predicted it from the cMP of complete ones (Clpt) according to the following protocol. First, to evaluate the reliability of the prediction, we performed covariation analyses between artificial fragments generated from the complete mandibles (Clpt) corresponding to fragmentation patterns (A, B and C) and cMP. We used two-block Partial Least Squares Analyses (2B-pls) which assesses the covariance between two sets of variables. This step was done using the *two.b.pls* function of the *geomorph* package (Adams & Otárola-Castillo, 2013), which performs a 2B-pls adapted to shape data. Then, cMP of fragmented mandible was predicted using the *plsr* function of the *pls* package (Mevik & Wehrens, 2007). This function allows prediction based on the covariation between the two variables.

Shapes associated with the strongest and weakest cMP were computed. Those shapes were estimated based on the linear regression of cMP on shapes of complete mandibles (Cplt) using *procD.lm* of the *geomorph* package (Adams & Otárola-Castillo, 2013). They were then computed with the *warpRefOutline* function of the same package.

Changes of cMP through time were investigated in two ways:

1) global cMP per layer. Differences between layers were tested through pairwise comparisons testing using the *pairwise.t.test* function of the *stats* package which correct for multiple testing.

2) cMP per morphological group per layer.

For both, standard deviation was computed on each layer as a measure of variance.

Modularity

As the abundance of complete mandibles (Clpt) per layer was not sufficient, the modularity analysis was performed based on the C fragmentation pattern on complete (Clpt) and C fragments. We divided the mandible into two modules *a priori* according to the hypothesized primary developmental modules defined in the literature (Cheverud *et al.*, 1997; Mezey *et al.*, 2000; Klingenberg *et al.*, 2003; Klingenberg, 2004) (**Fig 3**).

To quantify the modular structure of the mandible, we computed the Covariance Ratio (CR) per layer. CR compares the global covariation between hypothesized modules relatively to

the covariation within those modules (Adams, 2016). The modularity hypothesis (independence of the hypothesized modules) is verified when CR<1. This measure is unaffected by sample size or the number of variables (Adams, 2016). It was performed using the *modularity.test* function of the *geomorph* package (Adams & Otárola-Castillo, 2013).

Results

Morphological groups

Three morphological groups were detected among complete mandibles (Clpt). We obtained an SI=0.15, meaning that the morphological partitions obtained with the clustering are correct. This partitioning was also valid for A, B, and C fragments (A fragments: SI=0.1; B fragments: SI=0.09; C fragments: SI=0.1).

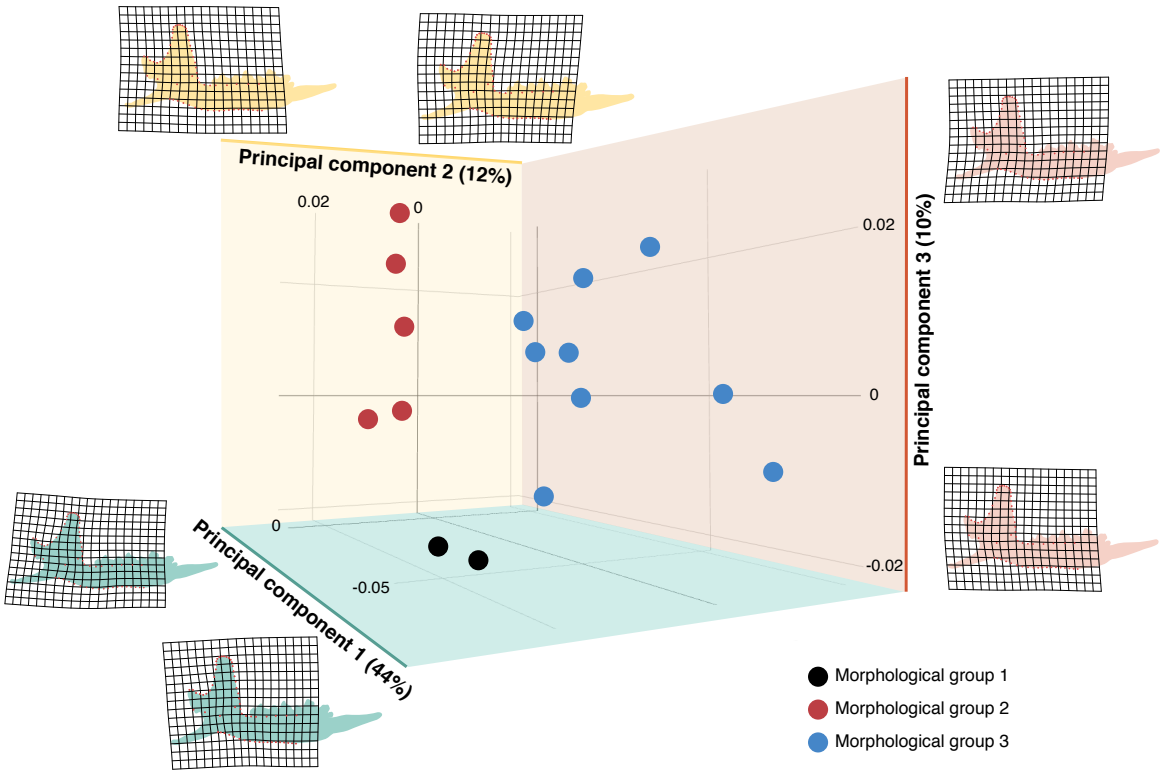

Fig. 4 Principal component analysis on complete mandibles (Cplt).

A visualization of the morphological groups on the principal component analysis of complete mandibles (Cplt) and their deformations along major axes is presented in **Fig 4**.

Mean shapes of the morphological groups are presented in **Fig 5**. The first group (illustrated in grey in **Fig 5**) has an elongated mandibular body, a more anteriorly inclined coronoid and a more dorsally oriented condylar process compared to the average mandible shape. The second group (illustrated in red in **Fig 5**) displays a shape similar to the mean shape. The third group (illustrated in blue in **Fig 5**) has a short mandibular body, a coronoid process that is slightly more posteriorly inclined, and a condylar process that is more ventrally oriented.

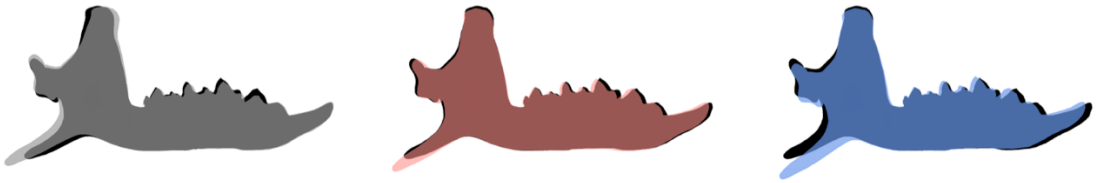

Fig. 5 Mean shapes of the three morphological groups (in grey, red and blue) compared to the global mean shape (in black) of complete mandibles (Clpt).

Mechanical potential

Log-transformed MP revealed to be weakly and negatively correlated to log-transformed Csize (R^2=0.014, P=0.0029**, 52 degrees of freedom). The multivariate regression **(3)** was also significant (R^2=0.12, P=0.023*, 50 degrees of freedom). We obtained a=0.30 (coefficient of log-transformed Csize) and b=-3.47 (intercept). The reliability scores of cMP based on the simulated data are indicated in **Table 2**.

Table. 2 Reliability scores of cMP for the three tested measure errors.

Measure error	0.01	0.05	0.1
Mean	82%	82%	81%
Max	98%	96%	93%
Min	66%	66%	66%

The 2B-pls results showed that cMP is well related to A, B, and C fragments generated from complete mandibles (Clpt) (2B-pls: A fragments, r-pls=0.66, P<0.05; B fragments, r-pls=0.75, P<0.05; C fragments, r-pls=0.64, P<0.05), ensuring the reliability of predicted cMPs for fragments.

Mean shapes associated with the strongest and weakest cMP are presented in **Fig 6**. The shape associated with the weakest cMP (left in **Fig 6**) is characterized by an elongated mandibular body and a short mandibular branch compared to the global average shape of the mandible. On the contrary, the shape associated with the strongest cMP (right in **Fig 6**) displays a short mandibular body and a long mandibular branch.

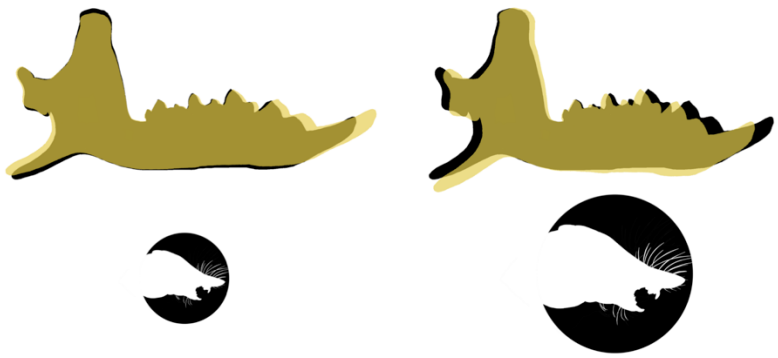

Fig. 6 Mean shapes associated with the strongest (right) and weakest (left) cMP (in yellow) compared to the global mean shape (in black) of complete mandibles (Clpt). Strength of the cMP is symbolized by the size of the shrew drawing under the models.

Global changes in cMP through the El Harhoura 2 sequence are presented in **Fig 7A**. In L7, a period characterized by an open and arid environment, a great variability in cMPs co-exist compared to other layers (**Fig 7B**). An important increase in average cMP is observed from L7 to L5 and then cMP decreases until present resulting in cMP values similar to those observed in L7 (**Fig 7A**). However, pairwise testing indicates that only the cMP of L5-L7 and Act-L5 are significantly different (P<0.05).

Changes in cMP per morphological group through time are presented in **Fig 7B**. Not all morphological groups show the same variation in cMP over time, nor the same degree of variability. However, the three groups display a higher variability in L7. Overall, one of the morphological groups (indicated in blue in **Fig 7B**) has a higher cMP than the others.

The two other groups (indicated in red and black in **Fig 7B**) display similar cMP values. In L5 the cMP of the three morphological groups converges toward high cMP values. Then, starting from L5, there is a drop of mandible shape diversity with the disappearance of one morphological group. In L4a and L3, the two remaining groups show a divergence in cMP towards respectively lower and higher values. In L2 a second diversity drop occurs with the disappearance of another group. From then onwards only one morphological group is consistently present, the two others show only few occurrences.

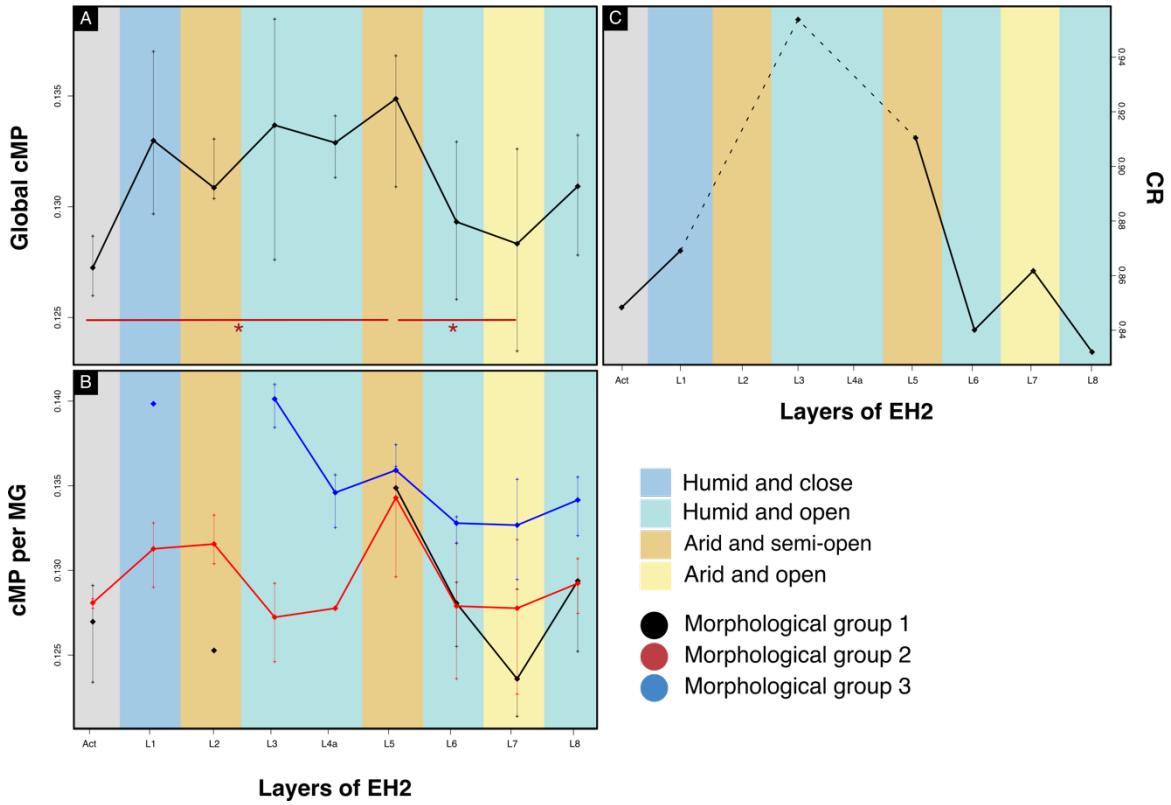

Fig. 7 Global changes in cMP (A), cMP per morphological groups (B) and CR (C) of the shrews of EH2, from L8 until current day. Environmental conditions (Stoetzel, 2009; El Hajraoui *et al.*, 2012) are indicated by background colors. For cMP, standard deviation is indicated for each point. **A**: layers displaying significant different cMP are indicated in red. **B**: Black is the first morphological group; red is the second morphological group; blue is the third morphological group. **C**: Dotted lines indicate missing values.

Modularity

Changes in CR over time are presented in **Fig 7C**. CR was not statistically significant in L2 and L4a. There are two main changes in CR values, first a slight increase in L7

(CR=0.86, P<0.05) followed by a strong increase from L5 to L3, with a peak in L3 (CR=0.95, P<0.05).

Discussion

In this study, we aimed [1] to investigate the relationship between shrew mandible morphology, modularity, and estimated biting forces (cMP) over time and [2] to evaluate whether a performance trait (bite force) could provide relevant information in the understanding of paleoenvironments. To do so, we explored mandible shape diversity in archaeological shrews, and computed the covariation ratio and estimated mechanical potential over time. First, we discuss the meaning of morphological groups and the benefits of this approach. Next, we focus on the relation between mandible shape and mechanical potential. Finally, we address the variation in these traits over time and compare them to environmental inferences from the literature to assess their potential relevance for paleo-environmental studies.

Morphological groups

Over the considered period, up to three morphological groups of mandibles were found among the four shrews species present at EH2 (*Crocidura russula*, *C. whitakeri*, *C. tarfayensis* and *C. lusitania*) (Cornette *et al.*, 2015a,c). The assessed morphological diversity is consequently above the species level. Simplification of information is a risk of the morphological group approach (Read *et al.*, 2014), but it provides access to a partition of variability that is potentially more informative ecologically than taxonomically when the studied biological object is sensitive to environmental change (Alperin *et al.*, 2011; Read *et al.*, 2014; Khare *et al.*, 2017), which is the case for shrew mandibles (Badyaev & Foresman, 2000; Young *et al.*, 2010). The morphological groups reveal variations in the number of morphotypes independent of the number of species. For example, in the recent layers of EH2 (from L4a until today) only one or two morphological groups are present per layer whereas all four species are still present suggesting morphological convergence across these species (Cornette *et al.*, 2015c). The morphological groups are characterized by different functional outputs and in their response to environmental changes. Except in L5, they display a different cMP and show different trends over time, especially from L4a and L3. To sum up, morphological groups are characterized by differences in morphology,

functional output, and their response to environmental change. Thus, they represent morphological and functional response units to external variation.

Nevertheless, because we used only three of the five types of mandible fragments that were used in Cornette *et al*. (2015a, c), we reduced the initial sampling which can result in a potential loss of diversity. However, unused fragments were the least informative and reliable and could have introduced uncertainties into the results of this study which is why we chose to exclude them.

Mandible shape and mechanical potential

The relation between rostrum elongation and mechanical potential is intuitive as a longer rostrum increases the jaw out-lever and consequently results in a lower mechanical potential. This is illustrated by the negative correlation between MP and mandible size. This type of relation between MP and mandible size has also been observed in other mammals (e.g. Casanovas-Vilar & van Dam (2013) for squirrels, Nancy A., (1982) for felids). This implies that the smallest specimens have a higher mechanical potential than the largest ones. Mechanical potential and size are both important drivers of bite force. These results suggest that the relative importance of these drivers varies between small and large specimens. Conformations may be a more important driver of bite force than size in small specimens compared to large ones. Nevertheless, the weakness of this correlation suggest that the specimens used here are rather uniform in size.

Concerning the mandibular branch, our results are consistent with Young *et al.* (2007) who found that a high mechanical potential was associated with a greater distance between the condylar and the coronoid processes. This is related to muscles of the masticatory apparatus: the coronoid process is the place of insertion of the temporalis muscle, the condylar process of the external pterygoid and the angular process of the internal pterygoid and the masseter. They all participate in generating bite force and impact bone shape in shrews (Furió *et al.*, 2010; Cornette *et al.*, 2015c).

In the light of the previous, the mean shapes of morphological groups display morphological features that can be related to their mechanical potential. The group displaying the highest mechanical potential (in blue on **Fig 4, 5** and **7**) is the one with the shortest mandibular body and the closest condylar and coronoid processes, which are morphological and functional particularities related to hard diet specialists in shrews

(Young *et al.*, 2007). Conversely the group with the weakest mechanical potential (in grey **Fig 5** and in black on **Fig 4** and **7**) displays features characteristic of soft diet specialists in shrews (Young *et al.*, 2007). The third group (in red on **Fig 4, 5** and **7**) showing average features likely regroups generalist shrews. Thus, morphological groups appear to highlight ecological specialisations.

Modularity might be a key concept to understand the link between morphological and functional variation. Three main decreases in modularity (i.e. increases in CR) are observed in the sequence at EH2 in L7, L5, and L3. In L7, the three morphological groups display unusual variability in cMP (it is important to note that this is the layer with the largest sample). In L5, the three morphological groups show remarkably similar cMPs, meaning similar functional outputs. Finally, in L3, the two morphological groups display highly divergent functional outputs. Each decrease in modularity (i.e., increase in CR) in the mandible is associated with an increase in the ability of a form to produce more diverse functional outputs, allowing either divergence (as in L7 and L3) or convergence (as in L5) in the cMP. These are in contradiction with Young *et al.* (2010) and Young *et al.* (2007), who found that extensive modularity allowed shrews with more diverse morphologies to produce a similar functional output. However, Young et al. (2010) underlined that adaptive responses are highly variable, even at a population level, which may explain the difference observed in comparison to our results. Maybe the adaptive strategy here implies a different relation between mechanical potential and the modularity of the mandible. A possibility might involve variation in skull shape which was not studied here (Cornette *et al.*, 2015c).

Mechanical potential as a paleoenvironmental indicator

When considering both global and per morphological group changes in cMP, four important functional variations were detected over time in L7, in L5, during L4a-L3 and in L2. Three of these (in L7, L5 and L2) match transitions from humid to arid environments (Stoetzel, 2009; Stoetzel *et al.*, 2011).

In L7 we observed a high morphological diversity (with the presence of the three morphological groups), the co-existence of highly diverse cMPs (**Fig 7A** and **B**) and a decrease in modularity (**Fig 7C**). An increase in the diversity in cMP could be caused by a release of selective pressures on this trait, allowing shrews with diverse abilities to survive. This could be due to the availability of more diverse resources in the environment of L7

than in those of other layers. However, the environment in L7 is characterized by an open and dry environment of arid steppes, and seems to present less ecological diversity than some other layers (Stoetzel, 2009; El Hajraoui *et al.*, 2012). Another hypothesis might be that a lack of resources drives character displacement in shrews with forms becoming highly specialized in the consumption of different resources. Moreover, the masseter and the medial pterygoid muscles also participate in generating bite force (Herrel *et al.*, 2008a; Santana *et al.*, 2010; Brassard *et al.*, 2020c,a). Yet, these muscles are implicated in the consumption of different types of resources, as in bats where the masseter allows the consumption of more soft resources (Santana *et al.*, 2010). Moreover, functional variation is accompanied by a decrease in modularity. Variation in the degree of covariation between mandibular modules in shrews may be related to stressful environmental conditions (Badyaev & Foresman, 2000, p. 200). In the light of this fact, it is more likely that during the period covered by L7, shrews endured particularly stringent environmental conditions, with fewer and/or different available resources than before. As shrews are opportunistic, they might have switched their diet during this period inducing a release on the functioning of the temporalis muscle. However, as L7 is the layer with the largest sample this may bias our observations.

In L5, the cMP of two morphological groups greatly increases and the cMP of the three groups converges toward high values (**Fig 7A and B**). Pairwise testing indicates that global cMP is significantly different in L5 compared to L7 and present day (**Fig 7A**), and consequently supports the hypothesis of a cMP convergence towards high values in L5. This functional convergence is not associated with a convergence of the morphological groups, which is not surprising as those two types of convergence (functional and morphological) can be independent (Stayton, 2006). The group of soft diet shrews (in black on **Fig 7B**) is possibly subjected to a selection causing large sized specimens to produce the highest mechanical potential (as illustrated in **Fig S1**). Here we have a case of functional redundancy: three distinct morphologies producing similar functional outputs (Alfaro *et al.*, 2005). This is observed in environmental conditions requiring similar performance abilities: distinct morphologies are then able to adapt to similar functional demands (Wainwright, 2005; Young *et al.*, 2007, 2010). This functional convergence could be explained by an increase in the selective pressures caused by fewer or different resources compared to previous layers, as the transition to L5 is towards a more arid environment (Stoetzel, 2009; El Hajraoui *et al.*, 2012).

In L4a, the morphological group of soft diet shrews is not present anymore. It must have disappeared during the previous arid period during which soft resources may have been scarce. It is known that the insect cuticle becomes harder under dryer environments (Klocke & Schmitz, 2011). The cMP of the two remaining groups diverged distinctly. The supposed strong selection pressure(s) leading previously to the functional convergence in L5 must have eased. This is congruent with existing environmental inferences, as the environment in L4a is hypothesized to be very similar with conditions in L6 (Stoetzel, 2009; El Hajraoui *et al.,* 2012). In L3, the divergence between cMP of the two groups increases. We can hypothesize that those two shrew morphotypes were subject to functional divergence. Each group of shrews may have specialized in the acquisition of a different food resource. The group displaying high cMP specializing in hard, large objects, requiring mechanical potential with an important contribution from the temporalis, and the other group specializing on softer, smaller items, which requires less contribution of the temporalis. This divergence might be caused by competition occurring among shrews. Such a competition has been suggested between *Crocidura russula* and other shrews species at EH2 at the exact same period (Cornette *et al.*, 2015c), and shrew dietary specialization might be a response to competition (Smith & Remington, 1996). In L2, a second diversity drop is observed with the disappearance of the group of hard diet specialists. As in L5, this event occurred following an arid period during which less diverse resources may have been available. Only the group of generalist shrews is continuously present up to present.

Interestingly, extant shrews display a particularly weak cMP. This may be caused by the recent deterioration of climatic conditions linked to the increase of human pressure (Lewis & Maslin, 2015). Once again, it might be explained by a release of selective pressures on the temporalis resulting from a switch in diet (Santana *et al.*, 2010). Another explanation might be a selection towards weaker cMP. This is counter-intuitive, however, as selection for lower performance likely only occurs when the trait is energetically expensive to maintain or involved in trade-offs with other more relevant trait (Irschick *et al.*, 2008). The energy previously allocated to the mechanical potential of the temporalis might have been reallocated to another performance trait under stronger selection in the novel environment.

Conclusion

To conclude, results of the present study illustrate the relevance of functional traits to detect paleoenvironmental transitions. Estimated bite forces showed variation in relation to

paleoenvironmental changes over the considered period (Late Pleistocene - Holocene), with a particular sensibility to transition between arid and humid environments. The complementary nature of morphological and functional indicators allowed to infer and discuss the possible evolutionary and ecological processes involved. Functional traits have a great potential for refining paleoenvironmental and paleoecological inferences. Moreover, they appear to be relevant indicators paleoenvironmental transitions and offer a range of opportunities to explore the impact of environmental changes on extinct organisms.

Supplementary material

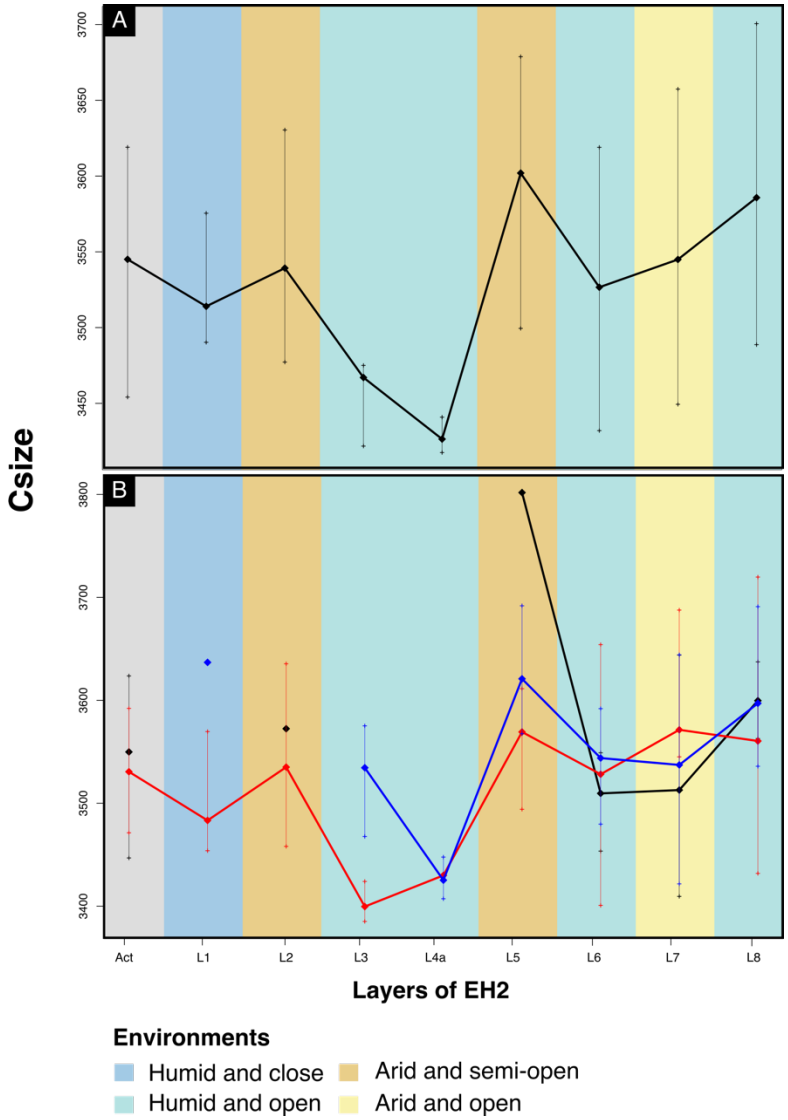

Fig. S1 Global changes in Csize (A) and Csize per morphological groups (B) of the shrews of EH2, from L8 until current day. Environmental conditions (Stoetzel, 2009; El Hajraoui *et al.*, 2012) are indicated by background colors. Standard deviation is indicated for each point. B: Black is the first morphological group; red is the second morphological group; blue is the third morphological group.

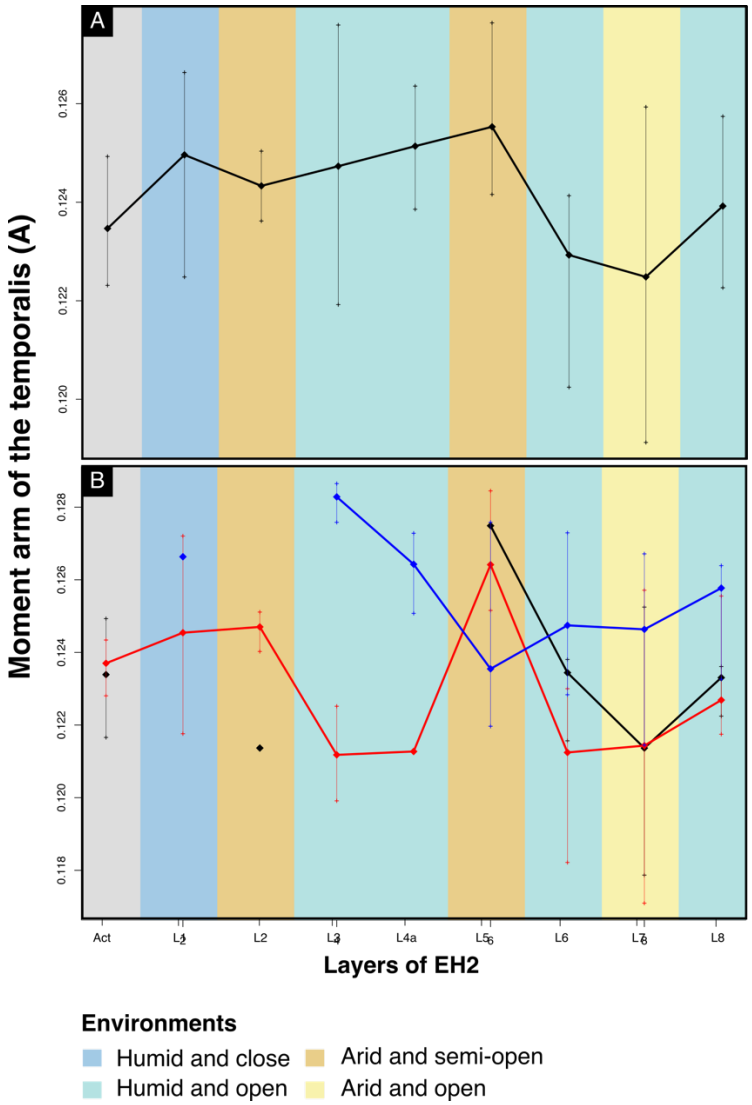

Fig. S2 Global changes in the moment arm of the temporalis (A on Figure 3) (A) and lever arm of the temporalis per morphological groups (B) of the shrews of EH2, from L8 until current day. Environmental conditions (Stoetzel, 2009; El Hajraoui *et al.*, 2012) are indicated by background colors. Standard deviation is indicated for each point. B: Black is the first morphological group; red is the second morphological group; blue is the third morphological group.

Table. S1 Couples of *a* and *b* tested on the simulated data set of bite forces and cMPs to assess the reliability of cMP as an estimator of bite force.

a	***b***
3.64	0.87
6.97	9.11
2.30	4.38
1.60	2.63
5.74	-2.40
8.56	-7.38
0.89	-1.81
7.09	5.49
1.89	-1.52
1.35	5.30
0.42	2.27
4.44	1.08
2.21	4.32
2.01	-6.27
5.74	-1.78
0.92	3.07
4.55	-5.31
3.34	0.82
5.90	0.86
7.90	4.29
0.40	-3.71
1.64	-7.20
1.03	9.24
0.38	-2.87
2.82	-4.73
4.60	-3.80
1.64	1.13
4.73	2.03
5.78	1.55
5.58	-0.37

CHAPTER 3

The use of paleoclimatic simulations to refine the environmental and chronological context of archeological/paleontological sites

Léa Terray, Masa Kageyama, Emmanuelle Stoetzel, Eslem Ben Arous, Raphaël Cornette and Pascale Braconnot

In review in Climate of the Past.

In the two previous chapters we assessed the response of morphological traits, rodent's teeth shape, and a functional trait, shrew's estimated bite force to local environmental variations. We evidenced that both morphological and functional variations are related to local environmental changes, but less than expected. Indeed, these responses mainly occur within MGs and do not concern the main axis of phenotypic variability. Thus, local environmental changes do not seem to be the main drivers of phenotypic variation. Maybe global climate changes are a more important driver of the phenotype than local environmental changes, and are related to the main axis of phenotypic variation. To explore this hypothesis, we need first to characterize the global climate changes over the EH2 sequence. One way to access global paleoclimate variations is through paleoclimate modeling. In this chapter, we reconstruct the climate state on each layer of EH2 with the help of a dedicated set of state-of-the-art paleoclimate simulations. We illustrate how paleoclimate simulations can contribute significantly to refine the chronological and paleoenvironmental contexts of archeological and paleontological sites. To do so, we confront the climate sequences resulting from two datation methods, combined US-ESR and OSL and assess the consistency between the climate sequence described by simulations and paleoenvironmental proxies.

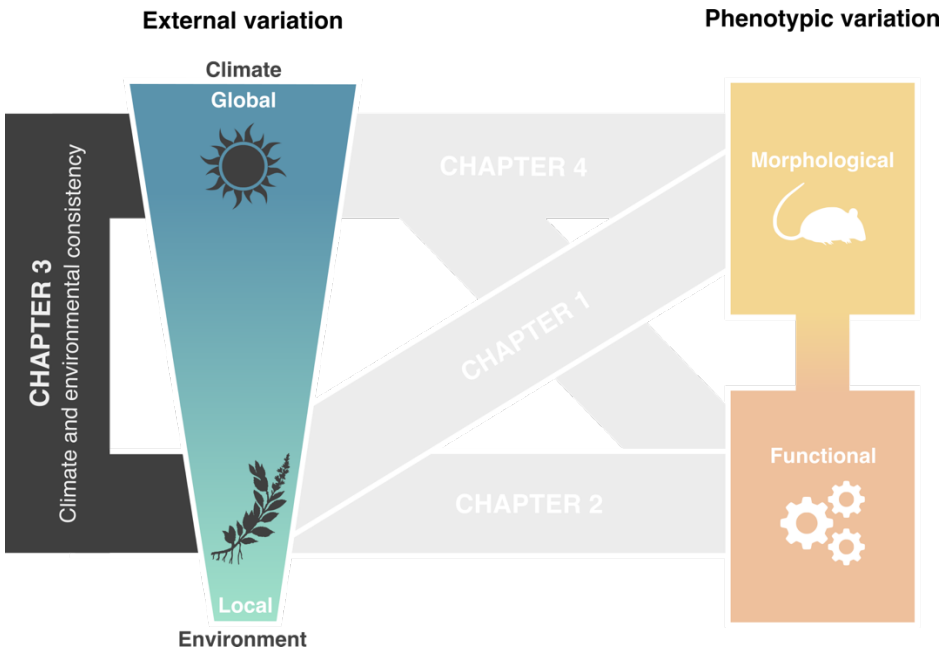

Diagram showing how chapter 3 fits into the thesis problematic.

Introduction

Reconstructing paleoenvironments is a key step to assess the ecological context and understand the evolutionary history of past organisms, and, hence, the link between their phenotype and environment. Commonly used methods to infer paleoenvironments rely on the organisms themselves, such as the qualitative presence/absence of species (e.g., Tchernov, 2002; Avery, 2007; Denys *et al.*, 2018), the association of certain taxa with their preferred modern habitat (e.g., Fernandez-Jalvo *et al.*, 1998; Stoetzel *et al.*, 2011), their relative abundances (e.g., Peters & Bork, 1999; Matthews, 2000; Belmaker & Hovers, 2011b; Comay & Dayan, 2018) or variations in the amount of stable isotopes in organic tissues (e.g., Anderson & Arthur, 1983; Tieszen, 1991; Royer *et al.*, 2013). These approaches allow one to characterize the local environment in which organisms lived. However, drastic discrepancies can be observed between these proxies (e.g., Jeffrey, 2016; Davis & Pineda-Munoz, 2016). Relying on the chronological context can also help to understand global environmental conditions. However, depending on the dating method used, the age of the stratigraphic layers may vary and this also leads to discrepancies in the chronoclimatic reconstructions (Ben Arous *et al.*, 2020a).

Besides paleoenvironmental reconstructions, paleoclimate modeling is another field for which one of the objectives is to describe past environments. To do so, it uses a climate model to simulate paleoclimates using physical laws that describe the dynamics and thermodynamics of the atmosphere, ocean, and continental and frozen surfaces coupled with water and carbon cycles. These models efficiently describe the time evolution and large-scale patterns of past climate changes (Braconnot *et al.*, 2012). They characterize past climates through quantified variables and have long been used to investigate past environmental changes (Kutzbach & Otto-Bliesner, 1982; Braconnot *et al.*, 2012; Duplessy & Ramstein, 2013; Schmidt *et al.*, 2014; Harrison *et al.*, 2015). Conversely to paleoenvironment proxies, paleoclimate simulations are much more influenced by large scale climate processes because they rely on the global dynamic of the Earth's climate system.

We propose to combine these two fields and to use climate simulations to discuss and refine the environmental and chronological context of El Harhoura 2 (EH2) cave, an archeological site located on the North-Atlantic coast of Morocco. What are the paleoclimate changes described by climate simulations over the sequence at EH2? Are they consistent with paleoenvironmental inferences available in the literature made from faunal assemblages

and isotopes? To answer these questions, we produced a set of climate simulations corresponding to EH2 stratigraphic layers. In order to discuss the chronological framework, we assessed the consistency between the climatic sequences described by simulations according to the varied dating methods and paleoenvironmental proxies from previous studies, such as isotopes and faunal assemblages. We thus expect that the congruence between paleoclimate simulations and paleoenvironmental proxies will allow us to distinguish between those two dating hypotheses. We then discussed the previously raised discrepancies between the different paleoenvironmental proxies in the light of the results of climate simulations.

Material and methods

El Harhoura 2 cave

The archeological site EH2 is located on the Moroccan Atlantic coast in the Rabat-Témara region (33°57'08.9" N / 6°55'32.5" W). Dating, stratigraphic and paleoenvironmental informations are summarized in **Fig 1**. This site is dated from the Late Pleistocene to the mid-Holocene. Its stratigraphy is currently divided into 11 layers (each layer is abbreviated in "L" followed by the layer number), among which the first eight are well studied and considered in this paper. These layers have revealed an impressive taxonomic richness and delivered an important amount of large and small vertebrate remains (Michel *et al.*, 2009b; Stoetzel *et al.*, 2011, 2012b). The site was used several times as a model to explore the relationship between the past diversity, the phenotype of organism and their environments (Stoetzel *et al.*, 2010, 2011, 2012a, 2013, 2017; Campmas *et al.*, 2015; Cornette *et al.*, 2015c; Terray *et al.*, 2021).

At EH2, paleoenvironments have mainly been inferred based on two different kinds of proxies: species presence and isotopes. Regarding species presence, environments were reconstructed using palaeoecological indices such as the Taxonomic habitat index (THI), which is a method based on the habitat preference of small vertebrates (Stoetzel, 2009; Stoetzel *et al.*, 2011, 2014). The presence and/or abundance of particular taxa can also be a strong indicator of certain types of environment, such as amphibians for more humid contexts, or gerbils and jerboas for more arid contexts. Isotope-based inferences were performed by Jeffrey (2016) on *Meriones* teeth from Layers 2 to 8 of EH2. They provide varied indications about paleoenvironments such as aridity, relative humidity, seasonal

variations and vegetal cover (Longinelli & Selmo, 2003; Navarro *et al.*, 2004; Royer *et al.*, 2013). Some inconsistencies were observed between species and isotopes based proxies on certain stratigraphic layers of the site (Jeffrey, 2016; Stoetzel *et al.*, 2019). On two layers (5 and 7), while THI indicates arid conditions, isotopes suggest a more humid and temperate climate. Given the mosaic-like landscape described at EH2 and the fact that the two methods do not deliver the same information (more global for faunal communities, at the scale of a limited number of individuals of a single species for isotopes), such inconsistencies are not surprising, but they make it difficult to reliably infer the global environmental conditions of the site.

The current climatic context of EH2 is complex. Morocco, due to its geographical location, has a rich mosaic of climate types (Sobrino & Raissouni, 2000). In particular, the Rabat-Témara region, where the cave is located, is under various climatic influences: from the Atlantic Ocean in the west, the arid Sahara in the south and the Mediterranean region in the north. Its climate is marked by a strong annual and interannual variability with a hot and dry summer during which precipitations are almost absent and evaporation is particularly high, and a cool and short winter, which is also the rainy season (Sobrino & Raissouni, 2000; Lionello, Malanotte, & Boscolo, 2006). The site has also recorded important climatic fluctuations over time (e.g., Hooghiemstra *et al.*, 1992; deMenocal, 1995, 2004; Le Houérou, 1997; Carto *et al.*, 2009; Trauth *et al.*, 2009; Drake *et al.*, 2011, 2013; Blome *et al.*, 2012; Kageyama *et al.*, 2013; Couvreur *et al.*, 2020). The Late Pleistocene - Holocene period (Marine Isotopic Stages (MIS) 5 to 1) is marked by significant global climate changes, which resulted in a succession of relatively humid/arid and open/closed environments at EH2 (Stoetzel, 2009; Stoetzel *et al.*, 2011, 2012a,b). As a result, paleolandscapes of the Late Pleistocene are described as open steppe or savanna-like lands with patches of shrubs, woodlands and water bodies, the latter expanding during wet periods, especially during the mid-Holocene.

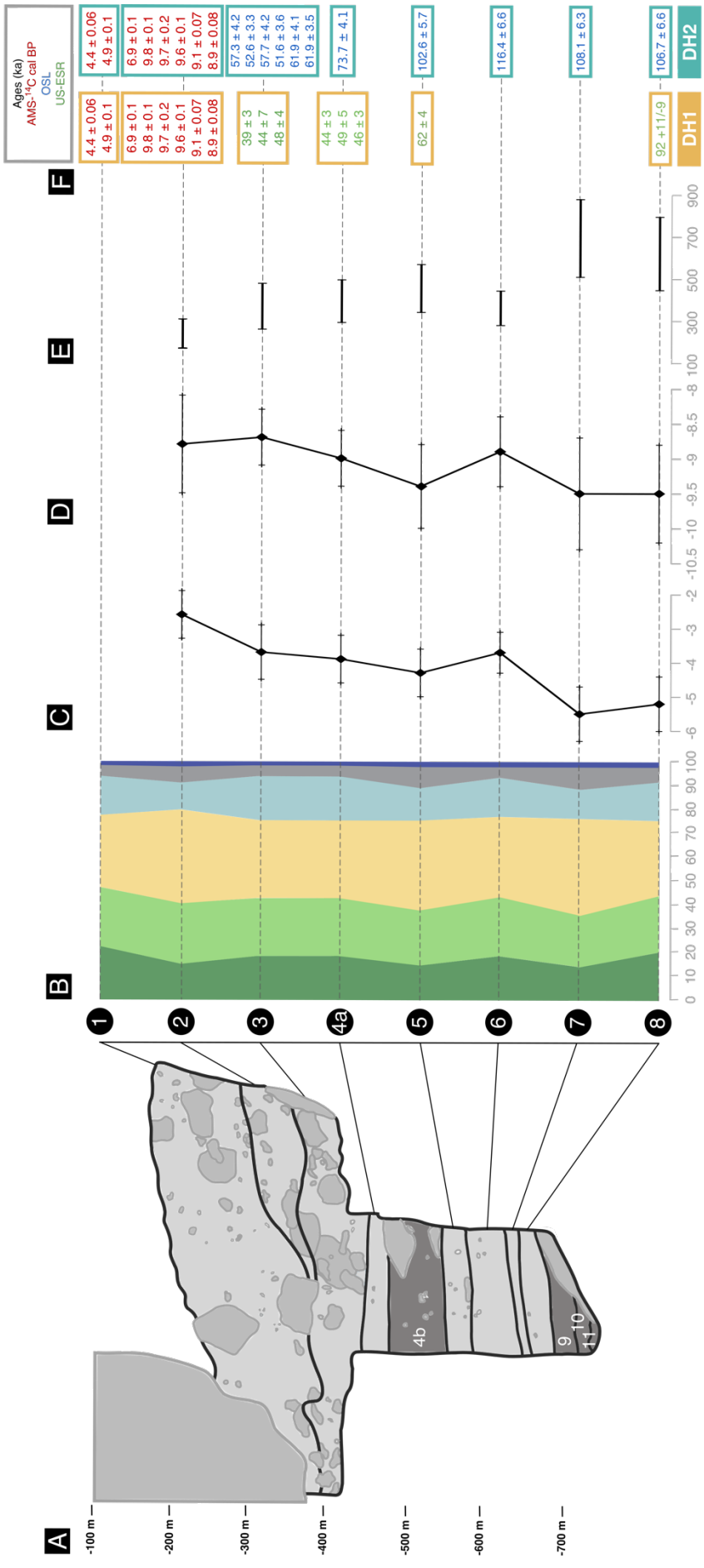

Fig. 1. Summary diagram displaying stratigraphy, paleoenvironmental proxies and the two dating hypotheses of El Harhoura 2 (EH2). **A**: stratigraphy of EH2, unused layers are in dark grey; **B**: relative % of THI values (adapted from Stoetzel *et al.* (2014) and Jeffrey (2016)); **C**: mean $\delta^{18}O$ values in *Meriones* teeth (from Jeffrey (2016)); **D**: mean $\delta^{13}C$ values in *Meriones* teeth (from Jeffrey (2016)); **E**: Mean Annual Precipitations (MAP; from Jeffrey (2016)); **F**: dating hypotheses DH1 and DH2 for the different layers of EH2 (Nespoulet & El Hajraoui, 2012; Jacobs *et al.*, 2012; Janati-Idrissi *et al.*, 2012; Ben Arous *et al.*, 2020b, a; Marquer et al., *in press*).

All of the eight studied layers have been dated (Ben Arous *et al.*, 2020a). Three different methods were used: OSL (Optical Stimulated Luminescence) (Jacobs & Roberts, 2012; Jacobs *et al.*, 2012), combined US-ESR (combination of uranium series and electron spin resonance methods) (Janati-Idrissi *et al.*, 2012; Ben Arous *et al.*, 2020b) and AMS-^{14}C (radiocarbon dating) (Nespoulet & El Hajraoui, 2012; Marquer *et al.*, *in press*). However, important discrepancies appear between methods when applied to the same layer, as for the L3 dated at approximately 40 ka using combined US-ESR, but at 60 ka using OSL (**Fig 1**). In addition, when two consecutive layers are dated with different methods, those dating can be inconsistent with the relative position of the layers as it is the case for the L6 dated at 108 ka using OSL and the L7 dated at 62 ka using combined US-ESR (**Fig 1**).

Thus, two dating hypotheses emerge by combining dates consistent with the relative position of the layers. These dating hypotheses are referred to in this paper as DH1 and DH2 (DH for Dating Hypothesis) and are presented in **Fig1**.

Paleoclimate simulations

Pre-existing ensemble of global coupled simulations

Climate simulations representative of key periods identified in EH2 layers were available to infer the climatic conditions at EH2. They have been run with different versions of the IPSL (IPSL for Institut Pierre-Simon Laplace) global coupled model (Marti *et al.*, 2010; Dufresne *et al.*, 2013; Boucher *et al.*, 2020). All versions consider the interactive coupling between ocean, atmosphere, land-surface and sea-ice components, as well as an interactive carbon cycle. The exact complexity, spatial and vertical resolutions vary depending on model version. The different simulations also differ by prescribed Earth's orbit parameters, atmospheric trace gases composition and ice-sheet configuration in order to represent the climate conditions of the different periods (**Table 1**). First, we used a total of six pre-existing global coupled simulations:

- For the climate in L1 we used the reference mid-Holocene IPSL simulation (mean age estimated at ~6ka) run as part of the PMIP4-CMIP6 ensemble of simulations (Kageyama *et al.*, 2017; Braconnot *et al.*, 2021). It is called *CM6mh* in the following and has been performed with IPSL-CM6A-LR (Boucher *et al.*, 2020). The atmosphere has a resolution of 144 points in longitude, 143 points in latitude and

79 vertical levels (144x143xL79). The ocean has a nominal 1° resolution with a refined grid in the equatorial region and 75 vertical levels.

- For the climate in L2, L3 (DH1, DH2), L4a (DH1, DH2) and L5 (DH1) we used, respectively, the *CM5AEH01* (early Holocene, mean age estimated at ~9ka), *MIS3mBB6* (mid-MIS3, mean age estimated at ~40ka), *MIS4dB6* (late MIS4, mean age estimated at ~60ka) and *MIS4mB6* (mid-MIS4, mean age estimated at ~66ka) simulations (Le Mézo *et al.*, 2017) performed with IPSL-CM5A-LR (Dufresne *et al.*, 2013), the previous version of the IPSL coupled model. This model version has a lower resolution than IPSL-CM6A-LR with only 96 points in longitude, 96 points in latitude and 39 vertical levels (96x96xL39 in the following). The ocean grid has a nominal 2° resolution with 31 vertical levels.
- For the climate in L5 (DH2), L6 (DH2), L7 (DH2) and L8 (DH1, DH2) we used the *lig115k* simulation (MIS5d, mean age estimated at ~115ka) (Sicard personal communication) performed with IPSL-CM5A2-LR 96x96xL39 (Sepulchre *et al.*, 2020). This model version is close to IPSL-CM5A-LR , but benefits from a retuning of the model to correct a model cold bias.

Unfortunately, these simulations are not directly comparable because they were performed using different versions of the IPSL model. Indeed, we will illustrate that these different versions, when used to simulate the current climate, showed different biases when compared to observations. This is due to the fact that the various versions of the model are characterized by different physical representations, resolutions and tuning as detailed above. The differences between these simulations for the periods of interest for EH2 (**Fig 1**) could then result from the difference in bias between the various versions of the model rather than representing significant climate differences between periods.

Thus, in order to make more reliable comparisons between periods, we ran an entirely new set of simulations for the key periods of EH2: *midH* (for the mid-Holocene period), *earlyH* (for the early Holocene period), *midMIS3* (for the mid MIS3 period), *lateMIS4* (for the late MIS4 period), *midMIS4* (for the mid MIS4 period) and *MIS5d* (for the MIS5d period). Configuration details for this new set of simulations are summarized in **Table 1**.

Model

To be consistent, we ran these new simulations using a unique model: LMDZOR6A. This model is a sub-configuration of the coupled model IPSL-CM6v1.11-LR, it integrates only the atmosphere-land surface component of the IPSL-CM6A-LR coupled model. It was chosen because it best simulates the regional climate in our area of interest (**Fig S1** and **S2**). It also has the finest spatial and vertical resolution and an improved representation of atmospheric and land surface processes.

First, with LMDZOR6A, we produced a control simulation *Ctrl,* which is similar to an existing *clim_pdControl* experiment (also performed with LMDZOR6A; see **Table 1** for details), and represents the present day climate. The Sea Surface Temperature (SST) boundary conditions used in *Ctrl* (as in *clim_pdControl*) are SSTs used for Atmospheric Model Intercomparison Project (AMIP) simulations, which are simply a mean annual cycle of SST estimated from current observations and repeated in time. This *Ctrl* simulation will be considered as the reference for the current climate in our ensemble of new atmospheric simulations. Then, to produce other simulations, the same experimental set up as in *Ctrl* was used, but orbital parameters, gas concentrations, ice-sheet and other land-surface conditions were prescribed as in the corresponding coupled simulations listed above (see **Table 1**). Note also that boundary conditions files of pre-existing (coupled) simulations were interpolated on a 143x144xL79 grid to be compatible with the grid of LMDZOR6A.

Sea-surface boundary conditions

When using the atmospheric component LMDZOR6A alone, the SSTs have to be prescribed. However, no SST reconstructions are available for the periods of interest for EH2. Consequently, we imposed the simulated SSTs for these periods from the pre-existing coupled simulations. However, these SSTs are subjected to different biases due to different model versions as noted above, and these different SST biases may deteriorate the simulation of other variables of interest and complicate the intercomparison between our new LMDZOR6A simulations.

To explore the consequences of these SST biases on the simulated climatology of other variables of interest for EH2, we first ran three test simulations with LMDZOR6A: *Ctrl_CM5ASST*, *Ctrl_CM5A2SST* and *Ctrl_CM6ASST* (see **Table 1**). They are similar to *Ctrl* except that we replaced the default SSTs (the AMIP SSTs) with the SSTs simulated

by each of the three coupled model versions for the current climate. We found significant differences between the results of *Ctrl_CM5ASST*, *Ctrl_CM5A2SST* and *Ctrl_CM6ASST*, which can be attributed exclusively to the differences in the SST biases (see discussion and **Fig 3** and **4** below).

These tests demonstrate that the SSTs from the pre-existing coupled simulations must be corrected before using them as boundary conditions in our new LMDZOR6A simulations. To this end, we first estimated the SST biases of the three coupled model versions by comparing the SSTs simulated by each coupled model for the current climate with the AMIP SSTs (issued from observations). For each coupled simulation, we finally corrected the simulated SST by removing the SST bias corresponding to the model version used. In other words, corrected SSTs were obtained according to the formula:

$$SSTcor = SSTsim + (SSTamip - SSTmod)$$

Where SSTsim are the SSTs from the coupled simulation, SSTamip are the AMIP SSTs, SSTmod the SSTs of the model version for current days and SSTcor the corrected SSTs, which will be used as boundary conditions in our new LMDZOR6A simulations. The underlying hypothesis in this correction scheme is that the SST bias, e.g. SSTmod - SSTamip, is stationary in time.

In total, we ran ten LMDZOR6A simulations as summarized in **Table 1**. The length of all these new simulations is 50 years. Three monitoring variables were first used to validate the (energy budget of the) simulations: bils (surface total heat flux), nettop (net dn radiative flux at top of the atmosphere) and mrso (total soil moisture). Bils and nettop allow to ensure that the energy balance of the system has reached equilibrium, and mrso allows to verify the stabilization of the hydrological reservoir. On average, the model reaches equilibrium after eight years of simulation and at local scale on EH2 after 17 years (**Fig S3**). This fast adjustment is due to the fact that LMDZOR6A is an atmospheric model. Consequently, we worked on the last 30 years of each LMDZOR6A simulation.

Table. 1. Forcing and boundary conditions of the ten simulations produced in this study.

New simulations										
Name	***Ctrl***	***Ctrl_CM6ASST***	***Ctrl_CM5ASST***	***Ctrl_CM5A2SST***	***midH***	***earlyH***	***midMIS3***	***lateMIS4***	***midMIS4***	***MIS5d***
Model	LMDZOR6A	LMDZOR6A	LMDZOR6A	LMDZOR6A	LMDZOR6A	LMDZOR6A	LMDZOR6A	LMDZOR6A	LMDZOR6A	LMDZOR6A
Initial simulations										
Name	-	-	-	-	CM6mh	CM5AEH01	MIS3mB6	MIS4dB6	MIS4mB6	lig115k
Model	-	-	-	-	IPSL-CM6A-LR	IPSL-CM5A-LR	IPSL-CM5A-LR	IPSL-CM5A-LR	IPSL-CM5A-LR	IPSL-CM5A2-LR
Date	Actual	Actual	Actual	Actual	~ 6 kyr BP	~ 9 kyr BP	~ 40 kyr BP	~ 60 kyr BP	~ 66 kyr BP	~ 115 kyr BP
Orbital parameters*										
Eccentricity	Same as *clim_pdControl*	Same as *clim_pdControl*	Same as *clim_pdControl*	Same as *clim_pdControl*	0.018682	0.01935	0.016715	0.024345	0.021311	0.041421
Obliquity (degrees)	Same as *clim_pdControl*	Same as *clim_pdControl*	Same as *clim_pdControl*	Same as *clim_pdControl*	24.105	24.231	23.441	22.391	22.493	22.404
Perihelion – 180	Same as *clim_pdControl*	Same as *clim_pdControl*	Same as *clim_pdControl*	Same as *clim_pdControl*	0.87	303.03	102.7	80.09	174.82	110.88
Solar constant (W/m2)	Same as *clim_pdControl*	Same as *clim_pdControl*	Same as *clim_pdControl*	Same as *clim_pdControl*	Same as *clim_pdControl*	Same as *clim_pdControl*	1365.6537	1365.6537	1365.6537	1361.20
Gaz concentration										
Carbon dioxide (ppm)	Same as *clim_pdControl*	Same as *clim_pdControl*	Same as *clim_pdControl*	Same as *clim_pdControl*	264	287	205	230	195	274
Methane (ppb)	Same as *clim_pdControl*	Same as *clim_pdControl*	Same as *clim_pdControl*	Same as *clim_pdControl*	597	791	500	450	450	505
Nitrous oxide (ppb)	Same as *clim_pdControl*	Same as *clim_pdControl*	Same as *clim_pdControl*	Same as *clim_pdControl*	262	275	260	230	217	251
SST	Same as *clim_pdControl*	tsol_oce from *CMIP6-IPSLCM6A-LR*	tsol_oce from *CMIP5-IPSLCM5A-MR*	tsol_oce from *CMIP6-IPSLCM5A2-LR*	tsol_oce from *CM6mh* (corrected)	tsol_oce from *CM5AEH01* (corrected)	tsol_oce from *MIS3mB6* (corrected)	tsol_oce from *MIS4dB6* (corrected)	tsol_oce from *MIS4mB6* (corrected)	tsol_oce from *lig115k* (corrected)
Geography	Same as *clim_pdControl*	Same as *clim_pdControl*	Same as *clim_pdControl*	Same as *clim_pdControl*	Same as *CM6mh*	Same as *CM5AEH01*	Same as *MIS3mB6*	Same as *MIS4dB6*	Same as *MIS4mB6*	Same as *lig115k*
Vegetation	Same as *clim_pdControl*	Same as *clim_pdControl*	Same as *clim_pdControl*	Same as *clim_pdControl*	Same as *CM6mh*	Same as *CM5AEH01*	Same as *MIS3mB6*	Same as *MIS4dB6*	Same as *MIS4mB6*	Same as *lig115k*
* The term "orbital parameters" refers to variations in the eccentricity of the Earth and longitude of perihelion as well as changes in its axial inclination (obliquity).										

Climate variations through EH2 sequence

We then focused on describing the climate at EH2 cave and its variations over time according to the two dating hypotheses DH1 and DH2. To characterize the large scale climate over the area, we worked on the mean annual cycle of the four grid cells containing EH2. From simulations *Ctrl*, *midH, earlyH, midMIS3, lateMIS4, midMIS4* and *MIS5d,* we extracted nine outputs variables that are likely to directly or indirectly (through available resources) influence organisms morphology. We selected: *tsol* (temperature at surface) (Gillooly *et al.*, 2001; Yom-Tov & Geffen, 2006; Ebrahimi-Khusfi, Mirakbari, & Khosroshahi, 2020), *precip* (precipitations) (Yom-Tov & Geffen, 2006; Alhajeri & Steppan, 2016; Ebrahimi-Khusfi *et al.*, 2020), *qsurf* (specific humidity) (Hovenden, Vander Schoor, & Osanai, 2012; Alhajeri & Steppan, 2016), *w10m* (wind speed at 10 meters) (McNeil, 1991; Tanner, Kapos, & Healey, 1991; Chapman *et al.*, 2011; Pellegrino *et al.*, 2013), *sols* (solar radiation at surface) (Monteith, 1972; Fyllas *et al.*, 2017), *drysoil_frac* (fraction of visibly dry soil) (Paz, Pineda-García, & Pinzón-Pérez, 2015) and *humtot* (total soil moisture) (Paz *et al.*, 2015). Two additional variables were computed. The diurnal temperature range *tsol_ampl_day* (Alhajeri & Steppan, 2016) computed from *tsol_max* (day maximum temperature) and *tsol_min* (day minimum temperature) as: *tsol_max – tsol_min*; and the hydric stress *hyd_stress* (Martínez-Blancas & Martorell, 2020) computed from *evapot* (potential evaporation) and *evap* (evaporation) as: *evapot – evap*. List of abbreviations and units for these variables are provided in **Table 2**. For each variable, we worked on a seasonal cycle averaged computed on the last 30 years of simulation. More precisely, we explored variations in monthly means (mean value of the variable) and monthly standard deviations (amplitude of seasonal variation).

Climate variations over the EH2 sequence are presented on a common scale to ease the reading and better visualize covariation between climate variables (all climate variables were centered and reduced). In addition, to visualize climate proximity/differences between EH2 layers we used principal component analysis (Jolliffe & Cadima, 2016). It allows us to visualize EH2 layers into a climate-space (of reduced dimension) by presenting the data along the leading principal components of the analysis. These are new uncorrelated variables that successively maximize variance. They are computed from the eigenvectors and eigenvalues of the covariance/correlation matrix (correlation matrix in our case, as all the variables are standardized). The proximity of layers in the climate-space simply represents the similarity between the climate of the layers.

Table. 2 List of the climate variables used in this study, with their abbreviations and units.

Short variable name	Complete variable name	Unit
tsol	temperature at surface	C°
tsol_ampl_day	diurnal temperature range	C°
precip	precipitations	$mm.month^{-1}$
qsurf	specific humidity	$kg.kg^{-1}$
w10m	wind speed at 10 meters	$m.s^{-1}$
sols	solar radiation at surface	$W.m^{-2}$
drysoil_frac	fraction of visibly dry soil	%
humtot	total soil moisture	$kg.m^{-2}$
hyd_stress	hydric stress	$mm.day^{-1}$

We tested the congruence between paleoenvironmental information available in the literature and our results from climatic simulations. As climate variables, we used the principal components obtained before, and as paleoenvironmental proxies we used isotopes ($\delta^{18}O$ and $\delta^{13}C$) means (Jeffrey, 2016), reconstructed mean annual precipitations (Jeffrey, 2016) and percentages of represented habitats indicated by the THI (Stoetzel *et al.*, 2014) presented in **Fig 1**. First, to test the global covariance between climate simulations and paleoenvironmental proxies we carried out a two-block Partial Least Squares (2B-pls) analysis, a method for exploring the patterns of covariation between two sets of variables (Sampson, Streissguth, & Bookstein, 1989; Streissguth *et al.*, 1993). Axes of maximum covariance between the two blocks are generated, thus reducing data dimensionality. A coefficient (r-PLS) is computed and represents the strength of covariation. The r-PLS is in the range of (0,1). The closer the r-PLS is to one, the stronger the covariation. P-values indicating the statistical significance of r-PLS were calculated based on 1000 permutations against the null hypothesis (absence of covariation between the two sets of variables). Then, to refine our results, we performed pairwise correlation tests. Regarding the THI, the oasis habitat was not tested because its percentage of presence does not vary over the EH2 sequence.

All operations on NetCDF files (the standard file format for the outputs of the IPSL models) were performed using CDO (Climate Data Operators) (Schulzweida, 2019). Maps, plots

and analyses were produced using the R free software (R Development Core Team, 2018) and the libraries *ncdf4* (http://dwpierce.com/software), *raster* (Hijmans & van Etten, 2012), *FactoMineR* (Lê *et al.*, 2008), *corrplot* (Wei & Simko, 2021) and *ggplot2* (Wickham, 2015).

Results

Paleoclimate simulations

In **Fig 2** we first present the differences in SST biases between the three model versions for the current climate (see **Table 1** for details of the models) of North Africa and Europe. Regarding IPSL-CM6A-LR, there is a global cold bias up to -4°C and a hot bias in boreal summer on the Mediterranean Sea compared to AMIP's SST. IPSL-CM5A-LR shows a rather homogeneous and stronger cold bias up to -6°C. As for IPSL-CM5A2-LR, which has been tuned for reducing the severe cold bias found in IPSL-CM5A-LR, the bias is more dependent on seasonality with a cold bias still up to -5°C in boreal winter and spring, and a hot bias over Europe during boreal summer and autumn.

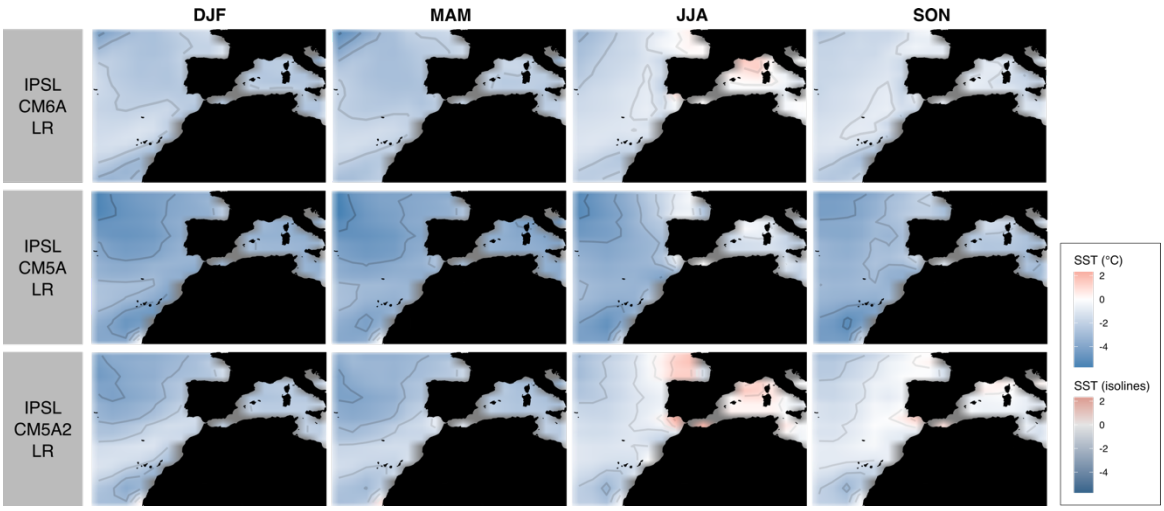

Fig. 2 Sea surface temperature (SST) biases of IPSL-CM5A-LR, IPSL-CM5A2-LR and IPSL-CM6A-LR relative to AMIP's SST (issued from current observations) (unit: °C). The seasons are DJF: December, January, February (winter); MAM: March, April, May (spring); JJA: June, July, August (summer); SON: September, October, November (autumn).

To assess to what extent these differences in SST biases impact the simulated climate, maps and curves comparing outputs of *Ctrl* with outputs of *Ctrl_CM5ASST*, *Ctrl_CM5A2SST* and *Ctrl_CM6ASST* are presented in **Fig 3** and **4**. Remember that all these simulations have been performed with the same model, LMDZOR6A, so the differences between these different simulations can be solely attributed to the different SST biases illustrated in **Fig 2.** We choose two metrics that are generally used to describe climatology: temperature (ts) and precipitations (pr) (Boucher *et al.*, 2020). In each case, a cold bias of ~ -5°C is observed over our area of interest. Some dry biases in precipitation are also noticed in winter. IPSL-CM5A-LR presents the strongest cold bias, up to -6 °C consistent with **Fig 2** and possible oceanic influences on EH2**.** IPSL-CM5A2-LR displays highly variable seasonal biases, with a cold one that reaches -6°C in winter and a hot one that reaches 2°C in summer, again consistent with **Fig 2**. Finally, the EH2 climate simulated with the SSTs from IPSL-CM6A-LR is the closest to the climate simulated with the AMIP SSTs in *Ctrl*.

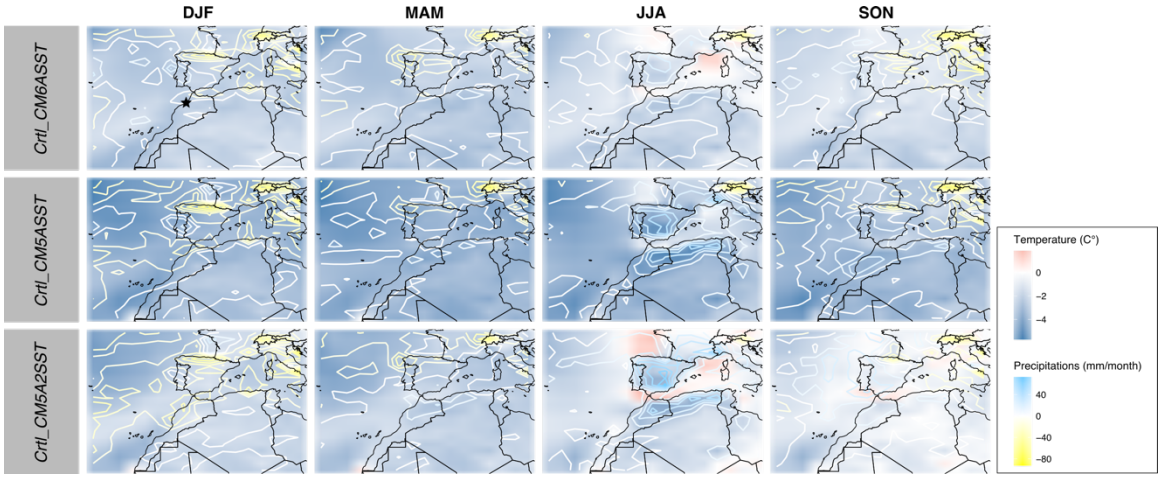

Fig. 3 Maps of EH2 region showing the impact of SST biases on the simulated current climate. Temperature (unit: °C) and precipitation (unit: mm/month) simulated with *Ctrl_CM5ASST*, *Ctrl_CM5A2SST* and *Ctrl_CM6ASST* are presented in contrast with those of *Ctrl*. The differences are estimated from the last 30 years of each simulation. EH2 cave location is represented by the star in the upper left panel. DJF: December, January, February (winter); MAM: March, April, May (spring); JJA: June, July, August (summer); SON: September, October, November (autumn).

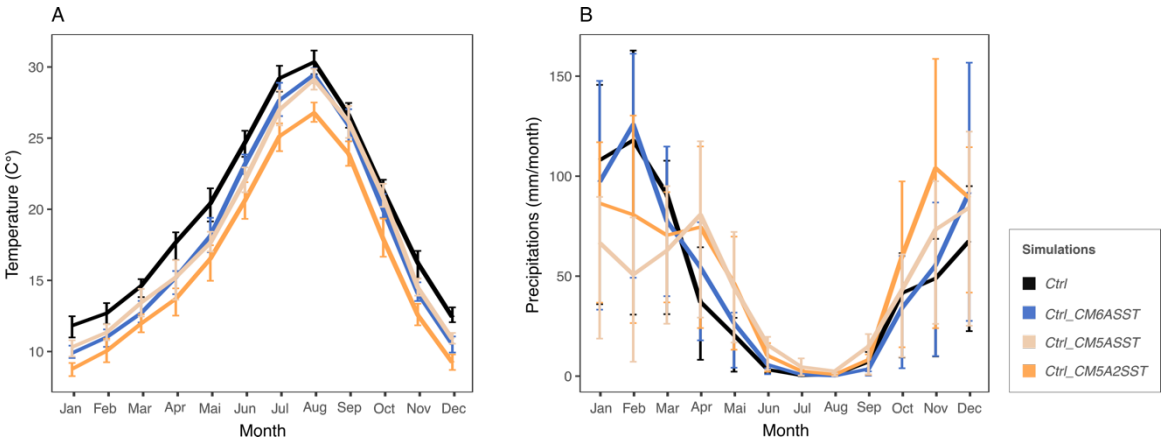

Fig. 4 Graph of seasonal variations in temperature (unit: °C) (A) and precipitation (unit: mm/month) (B) averaged from the four grid cells containing EH2 cave in *Ctrl_CM6ASST*, *Ctrl_CM5ASST*, *Ctrl_CM5A2SST* and *Ctrl*. Interannual variation over the averaged 30 years period is also shown by quartiles.

Outputs of *midH, earlyH, midMIS3, lateMIS4, midMIS4* and *MIS5d* for the region of EH2 are presented in **Fig 5**. Plots of monthly precipitations and temperatures are available in **Fig 6**. From ~115ka until ~40ka, the climate was colder than currently with less and less seasonal variation. ~66ka and ~40ka are also marked by more important precipitation, especially during winter. Starting from ~9ka the seasonal temperature variation is more important. Conditions in winter and spring are similar to the current climate, but a hotter autumn and a much warmer summer characterized this period. At ~6ka, climate conditions are close from today, but with a slightly more important seasonal temperature variation. A one-month shift is observed in the annual maximum temperature between *Ctrl*, *midH, earlyH, lateMIS4, MIS5d* (maximum temperature reached in August) and *midMIS3, midMIS4* (maximum temperature reached in July). There are also important changes in the magnitude of the seasonal temperature variation from June to October and of the seasonal precipitation variation from October to May (**Fig 6**). Those tendencies are induced by differences in the obliquity of Earth's orbit and clearly separate interglacial climate (*Ctrl, midH, earlyH*) from glacial climate (*midMIS3, lateMIS4, midMIS4, MIS5d*).

Climate variations through EH2 sequence

Interpreting the results of paleoclimate simulations through the two dating hypotheses DH1 and DH2 allows us to describe hypothetical climatic changes over EH2 layers. These two hypothetical climate sequences are presented in **Fig 7**, the two principal components

analyses focusing on DH1 and DH2, respectively, are shown in **Fig 8**. To visualize how climate variables structure the climate-space of these two principal component analyses, biplots are available in **Fig S4.**

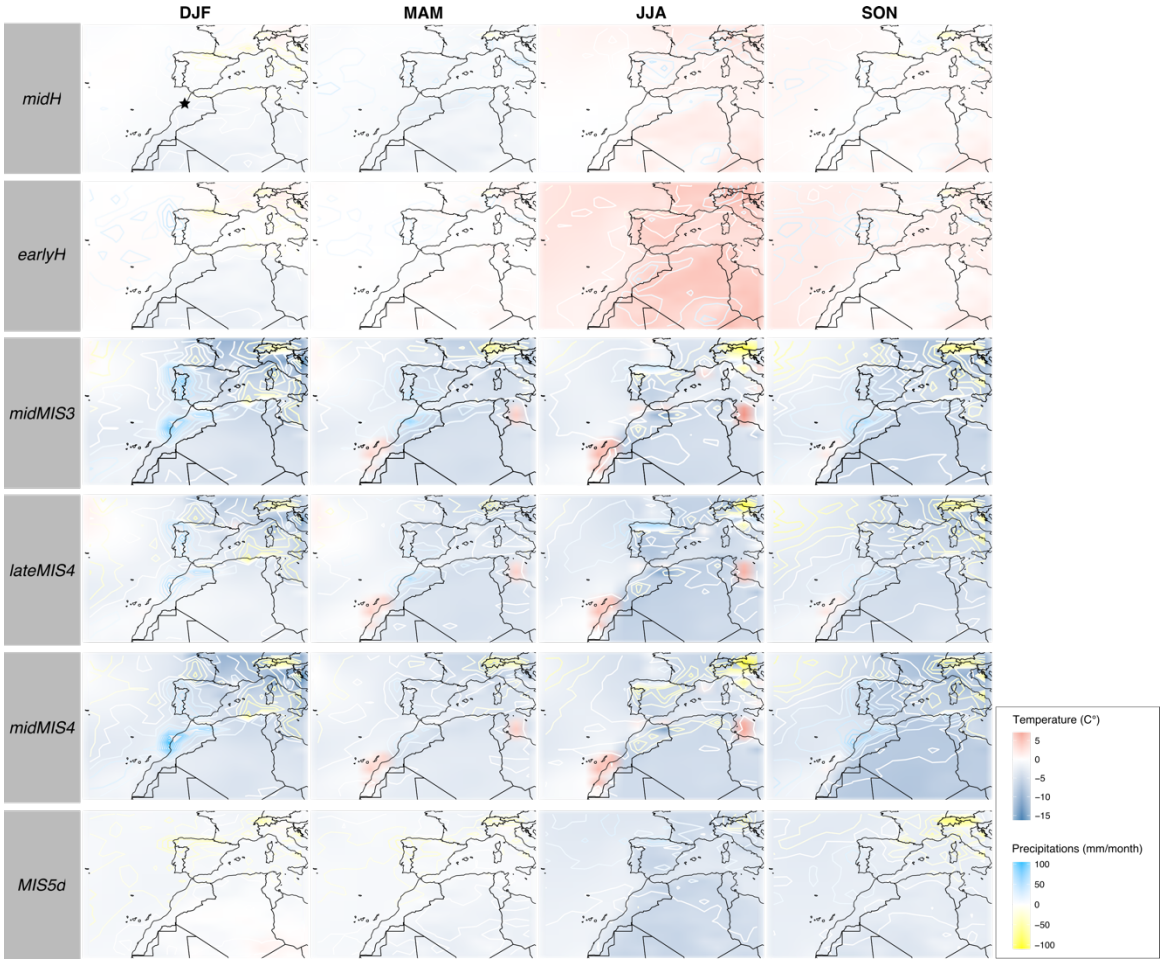

Fig. 5 Paleoclimatic reconstruction on EH2. Maps of temperature (unit: °C) and precipitation (unit: mm/month) simulated with *midH, earlyH*, *midMIS3*, *lateMIS4, midMIS4* and *MIS5d* are presented in contrast to *Ctrl* (the reference for current climate in our set of simulations). EH2 cave location is represented by a star in the upper left panel. DJF: December, January, February (winter); MAM: March, April, May (spring); JJA: June, July, August (summer); SON: September, October, November (autumn).

Based on DH1, our results indicate four major climate transitions (**Fig 7**). The first occurs between L8 and L5. In L5 the climate is wetter and colder with more precipitation, more soil humidity, increased wind speed, less hydric stress and less portions of dry soil. Humidity, precipitations and wind speed also show an important seasonal variability. The second transition, less marked, is between L5 and L4a. Climate in L4a is rather similar to

the climate in L5, but precipitations and humidity have increased. Seasonal variations are globally more pronounced. The third transition is between L3 and L2. The climate changes drastically between these two periods, with hotter and drier conditions in L2. Temperature, solar radiation, water stress and soil dryness all increase importantly, coupled with an important decrease in precipitation, soil moisture and wind speed. All these changes are consistent with aridification or desertification from L2. Surprisingly, however, specific humidity is enhanced, which is partly consistent with the decrease in precipitation and wind speed at this coastal location, and may possibly be linked to important changes of the atmospheric circulation patterns over this region from L2. The last climatic transition, more subtle, is between L1 and Act. The environment in Act seems closer to the one in L8 with more seasonal variability in temperature, solar radiation and water stress (**Fig 7**).

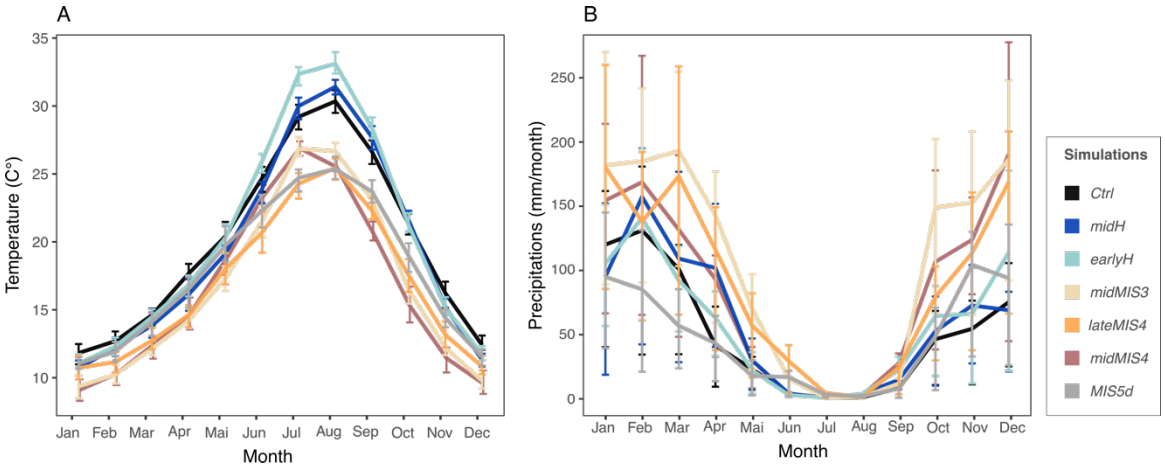

Fig. 6 Graph of monthly variations in temperature (unit: °C) and precipitation (unit: mm/month) averaged from the four grid cells containing EH2 cave in the different simulations. Interannual variation over the averaged 30 years is visualized by quartiles.

Overall, it seems there is an alternation of two main climate types. This partition is confirmed by the principal component analysis shown in **Fig 8**. The first principal component explains 65.85% of the observed variance (of the standardized variables) and splits the layers of EH2 into two climate regimes. The first regroups L3, L4a and L5 and is defined by humid and windy conditions with a high seasonal variability. The second includes Act, L1, L2 and L8 and is characterized by hot and dry conditions. The second axis, explaining 30.28% of the variability, divides the latter group into two subgroups: L1 and L2 with high seasonal variability, and Act and L8 with a lower seasonal variability.

Regarding DH2, we observe three important and abrupt climatic transitions (**Fig 7**). The first happened between L5 and L4a. In L4a, the climate is much windier and temperatures are colder with a substantial increase of diurnal temperature range. Precipitations and soil moisture increase importantly while hydric stress decreases. The climate also presents an overall higher seasonal variability. These tendencies persist in L3. The second transition is between L3 and L2. The soil is drier and the hydric stress increases greatly as well as solar radiation and temperature. Precipitation and soil moisture are less important. Conditions in L1 are close from those in L2, a bit colder with a less marked water stress. The last climate transition, more smooth than the previous ones, occurs between L1 and Act and is mainly marked by a global decrease of seasonal variations.

Results associated with DH2 suggest that three types of climate succeeded one another at EH2. The first group is composed of L8, L7, L6 and L5, the second by L3 and L4a and the third by L2, L1 and Act. As for DH1, this partition is supported by the principal component analysis results presented in **Fig 8**. The first principal component, which explains 52.10% of the observed variance, separates the group containing L8, L7, L6 and L5 with the one composed of L3 and L4a. The second principal component, explaining 42.35% of the observed variance, separates the group of L2, L1 and Act from others. L8, L7, L6 and L5 are characterized by a hot and dry climate and a low seasonal variation. L3 and L4a are defined by a wet and windy climate, with important precipitations and high seasonal variability. Finally, L2, L1 and Act present a hot environment associated with an important water stress.

Results of 2B-pls and correlations between climate variables and paleoenvironmental proxies are presented in **Fig 9**. Regarding DH1, 2B-pls shows that there is a statistically significant covariation between THI values and all climate variables, and between isotope data and the second principal component (climate variables contributing to the second principal component are indicated in **Fig 8**). Specifically, this second principal component is positively correlated with $\delta^{18}O$ mean, maximum and minimum values and $\delta^{13}C$ maximum values. Conversely, DH2 presents no statistically significant result for 2B-pls nor correlations.

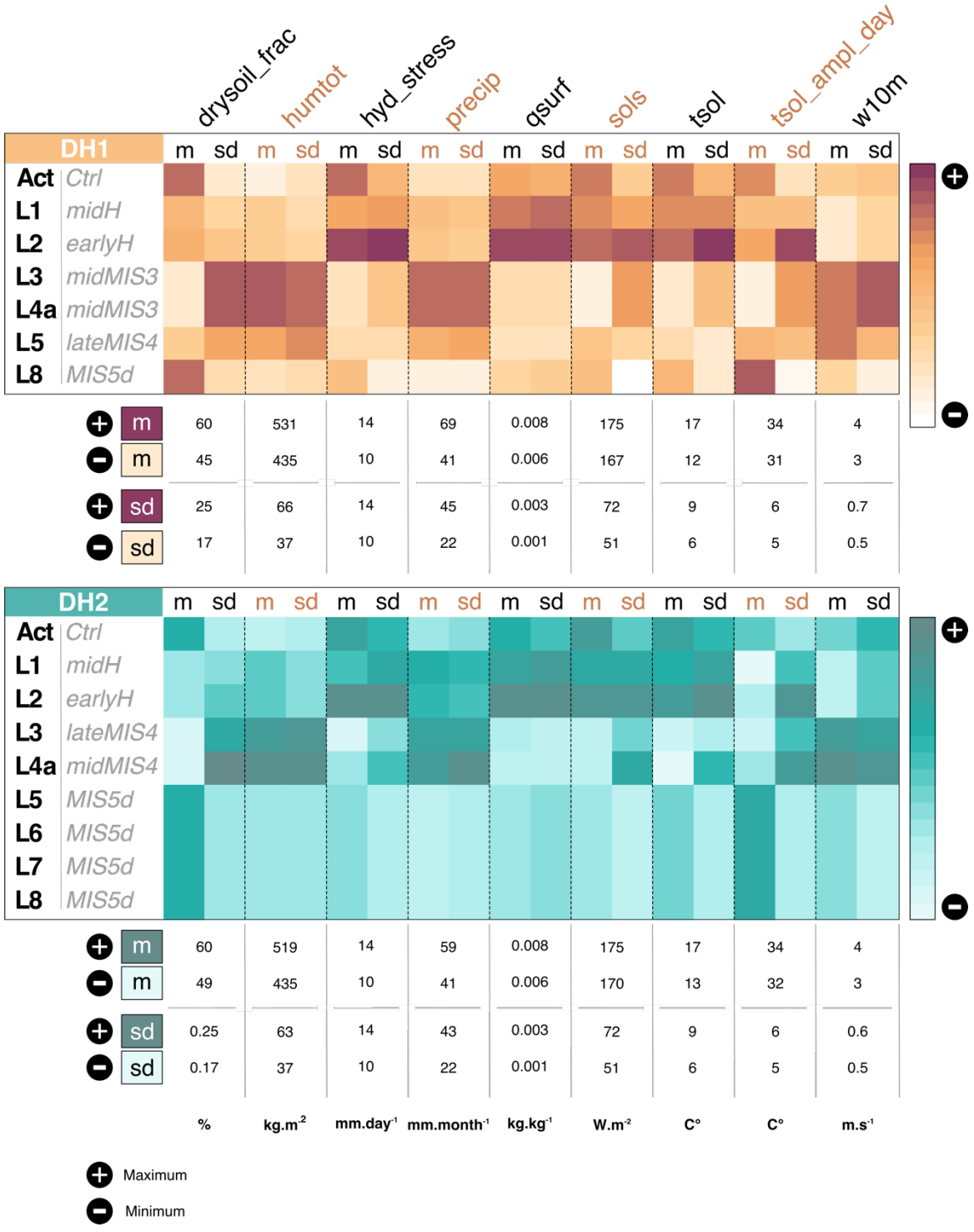

Fig. 7 Climatic variation over the EH2 sequence according to DH1 (Dating Hypothesis 1; upper), and DH2 (Dating Hypothesis 2; lower). Climate variables are centered and reduced and share a common scale. Maximum/minimum refers to the maximum/minimum value for all simulations. "L" is the abbreviation for Layer, "Act" for Actual, "m" for mean and "sd" for standard deviation.

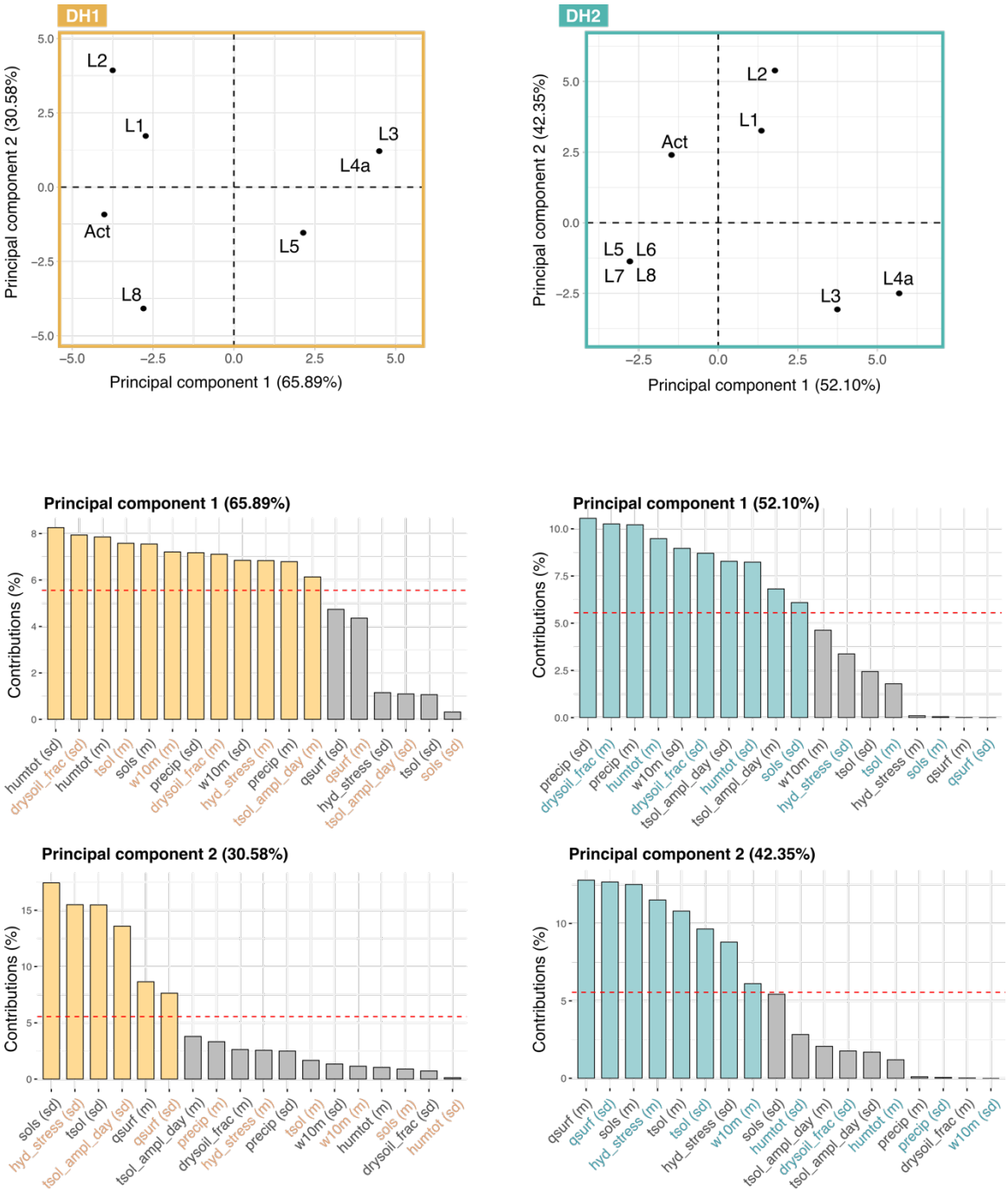

Fig. 8 Principal component analyses performed on climate variables according to DH1 (Dating Hypothesis 1; upper), and DH2 (Dating Hypothesis 2; lower). The contributions of the (standardized) climate variables to the two first principal components are presented (variables above the horizontal red line contribute significantly). "L" is the abbreviation for Layer and "Act" for Actual.

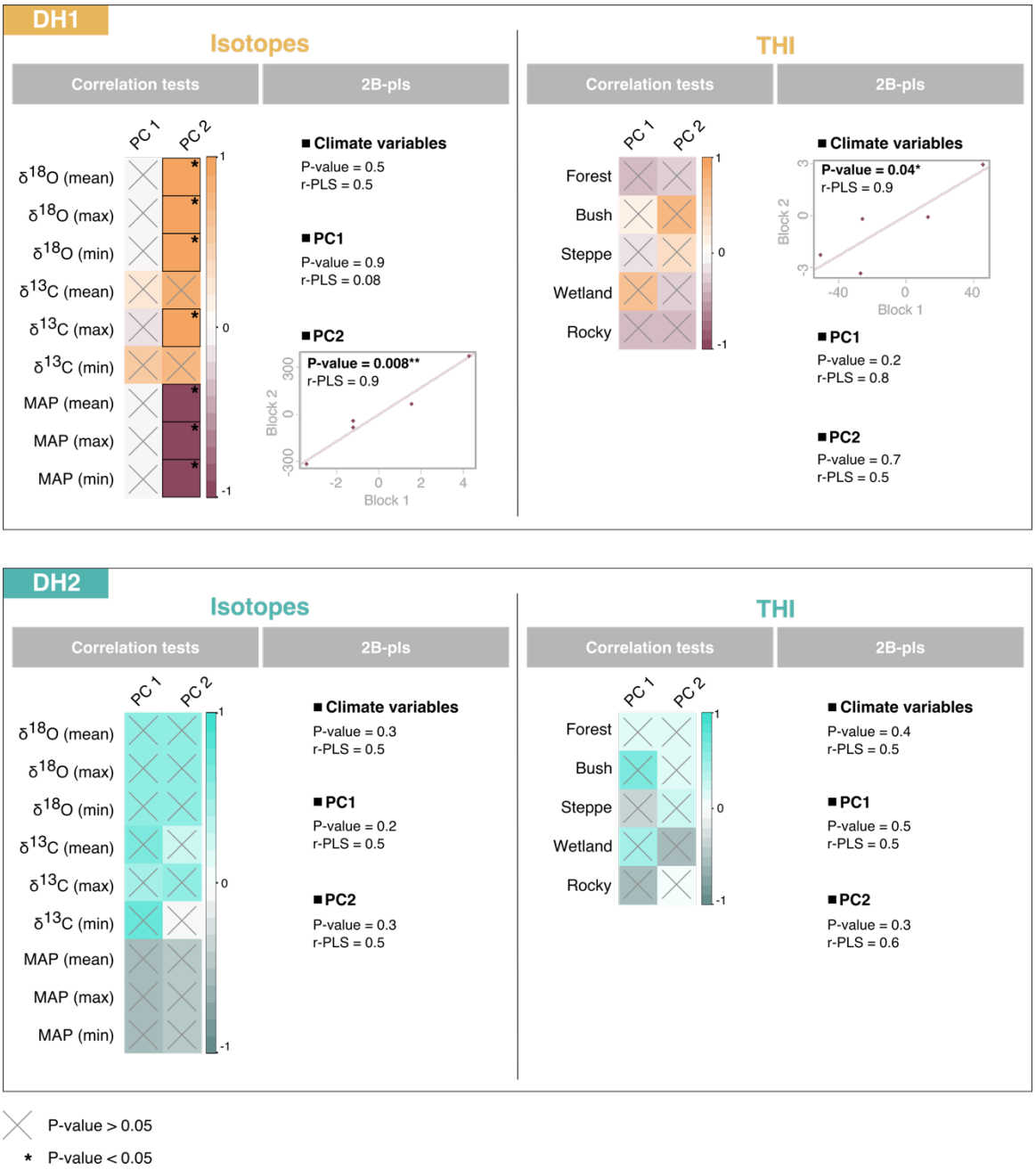

Fig. 9 Graphical representation of the 2B-pls and correlations between isotopes (Jeffrey, 2016) and THI values (Stoetzel *et al.*, 2014) and climate variables according to DH1 (Dating Hypothesis 1; upper panel), and DH2 (Dating Hypothesis 2; lower panel). Crosses indicate cases where correlation is not significant (p-value > 0.05) and colors represent the strength of the correlations. "L" is the abbreviation for Layer, "m" for mean and "sd" for standard deviation. $\delta^{18}O$: mean $\delta^{18}O$ values in *Meriones* teeth (from Jeffrey (2016)); $\delta^{13}C$: mean $\delta^{13}C$ values in *Meriones* teeth (from Jeffrey (2016)); MAP: Mean Annual Precipitations (from Jeffrey (2016)); Forest, Bush, Steppe, Wetland, Rocky: relative % of representation according to the THI (from Stoetzel *et al.* (2014) and Jeffrey (2016)).

Discussion

We have illustrated in this chapter that paleoclimate simulations allow us to discuss several important climate changes at EH2 over the Late Pleistocene to mid-Holocene period. The described climate transitions vary significantly depending on the chronological framework. Regarding DH1, there is an alternation of two main climate types. The climate of L1, L2 and L8 is relatively similar to the current climate Act, dry and hot with significant seasonal variation, defined as semi-arid. On the contrary, the climate of L3, L4a and L5 is more humid and colder with important and irregular precipitations, like a temperate climate. The succession revealed by DH2 is quite different, with the presence of three main climate types and rapid transitions between them. The climate from L8 to L5 is dry, the climate of L3 and L4a is humid with important precipitations and the climate in L2, L1 and Act is semi-arid.

The climate sequences described by DH1 and DH2 are not equally congruent with paleoenvironmental proxies from the literature. Indeed, several statistically significant correlations and covariation were found between the climate of DH1 and the paleoenvironmental proxies, while none were found for DH2. Thus, our results suggest that, with respect to EH2, combined US-ESR dating may be more reliable than OSL dating. As this dating process relies on quartz grains and that their chronology and origin is difficult to establish in the context of karstic coastal caves (as discussed in Ben Arous *et al.* (2020a)), OSL ages might have been overestimated.

Isotopes are correlated to particular climate variables of DH1. Both $\delta^{18}O$ and $\delta^{13}C$ are mainly related to seasonal variation in temperature and water stress. It is known that a high amount of $\delta^{18}O$ is an indicator of aridity (Longinelli & Selmo, 2003; Levin *et al.*, 2006). As the temperature increases, evaporation is more intense and because ^{16}O is a lighter isotope than ^{18}O, it will evaporate preferentially. Then the ratio between ^{16}O and ^{18}O changes, leading to an increase in the $\delta^{18}O$. It is then consistent to observe a $\delta^{18}O$ correlated with temperature and water stress. The $\delta^{13}C$ can reveal variations in the relative presence of C3, C4 and CAM plants (which refer to different metabolic carbon fixation pathways) because they have different signatures (O'Leary, 1988; Lin, 2013; Smiley *et al.*, 2016). C3 plants are associated with temperate climate, C4 plants have an advantage in tropical environments (which is not the case here) and CAM are found in arid areas. Because CAM have greater $\delta^{13}C$ values than C3 plants, it is meaningful that higher $\delta^{13}C$ values are related to an increase in the seasonal variation of temperature and water stress. On the contrary to

isotopes, related to particular climate variables, the THI is globally related to climate variations described by DH1. It is not surprising, as isotopes reveal fluctuations in particular variables that are temperature and precipitation provided by a limited number of individuals of a single species, while THI is an estimate of the global type of the environment provided by the whole microvertebrate communities. Thus, they do not deliver information at the same resolution.

The large differences between the climate simulations and the fact that they provide a physical consistent view of the relationships between the different climatic variables allow us to discuss the inconsistencies existing between paleoenvironmental proxies at EH2. The two major ones concern L5 and L7. In both cases, isotope surveys and mean annual precipitation reconstructions from Jeffrey (2016) indicate humid conditions with important precipitation. On the contrary, the THI as well as the presence of the steppic species *Jaculus* cf. *orientalis* (often used as an indicator of particularly arid conditions) and the scarcity of aquatic species support a dry climate (Stoetzel, 2009; Stoetzel *et al.*, 2014). Large mammals would also support this last hypothesis, with an increase in the representation of gazelles and alcelaphines, and a decrease in the representation of bovines in both layers (Stoetzel *et al.*, 2012a, 2014). Unfortunately, no combined US-ESR ages are available for L7 to date. Considering that climate conditions in L8 are dry with less precipitations than currently, we could hypothesize a similar climate for L7. In that case, this would support inferences from faunal assemblages. Nevertheless, we cannot exclude that a microclimatic event could have induced particular climatic conditions on L7. Concerning L5, the climate described by DH1 agrees with isotope surveys (Jeffrey, 2016). These conclusions are supported by the abundance of *Crocidura russula*, a shrew species associated with Mediterranean climates (Cornette *et al.*, 2015c). In addition, *Jaculus* cf. *orientalis* can also be considered as an indicator of more continental conditions, such as the distance from the coastline, rather than a marker of arid environments.

An important difference is noticed between the climate described by DH1 and the THI. DH1 describes an arid climate on L1, in contradiction with the composition of small and large mammal communities that indicates a humid environment. This inconsistency could be explained by the location of EH2: the cave is subjected to a complex climatic influence, as described previously. Because global climate models describe general climate characteristics, in L1 period, the region could have been arid, but a local climate phenomenon could have generated a wet environment in the surroundings of EH2.

While our results seem conclusive, it is important to notice that our approach has some limitations. First, the climate model used has many forced parameters: sea ice temperature, aerosol concentration and vegetation are prescribed in the model and are not allowed to vary. Therefore, the vegetation feedback for example is not included in the model.

The second issue relates to the compatibility of the spatial and temporal resolution of a climate simulation and a stratigraphic layer of an archeological site. The spatial resolution of the atmospheric grid of the IPSL-CM6A-LR model is 157 km on average (Boucher *et al.*, 2020). Consequently, the four cell grids used in this study cover a quite wide area. Conversely, EH2 represents a precise locality, and most species whose presence was recorded have a lifetime dispersal range largely inferior to 157km (e.g., the jird *Meriones shawii* has a home range estimated between 200-1000 m^2 (Ghawar *et al.*, 2015)). Then, the climate described by current global simulations might be a bit too coarse to faithfully describe microclimate variations at EH2. This may induce a mismatch between climate variables and other paleoenvironmental proxies.

The difference in temporal resolution between a stratigraphic layer and a paleoclimate simulation raises even more concerns. The older the dated layer, the higher the dating uncertainty is. For EH2, this uncertainty goes until 11 ka on L8. If we compare the dates estimated by different methods, the difference is much more significant. For example, it is the case for L3 dated at ~40 ka by combined US-ESR and at ~60 by OSL (i.e. a difference of 20 ka). Radical climate changes can occur in 20 ka: ~60 ka places L3 in a ice age while ~40 ka places it in an interglacial. As this paper demonstrates by comparing DH1 and DH2, those differences in estimated dates can result in completely different climate sequences. EH2 was an ideal case of investigation because a lot of studies focusing on the dating of its stratigraphic layers are available in the literature (e.g., Jacobs *et al.*, 2012; Janati-Idrissi *et al.*, 2012; Ben Arous *et al.*, 2020a,b). However, for archeological and paleontological sites, whose chronological framework is less referenced, it can lead to a completely wrong climate description. Furthermore, layers are not necessarily snapshots representing the faunal assemblages, cultural presence, etc. of specific moments in the past. A layer is a stratigraphic/sedimentary unit that can cover shorter or longer periods and undergoes microclimatic variations that cannot be disentangled.

Conclusion

The use of climate simulations allowed us to provide a quantified description of the paleoclimate at El Harhoura 2. Our results enabled us to discuss the validity of the varied dating methods used: in our case, the climate sequence corresponding to combined US-ESR ages was much more consistent with paleoenvironmental inferences from the simulations than those corresponding to OSL ages. Regarding discrepancies between paleoenvironmental inferences based on faunal assemblages and isotopic studies, our results are more consistent with conclusions drawn from the latter. But more than that, they highlighted the difference in scale between the information provided by each of these indicators. This study demonstrates that the combination of different sources of environmental data and climate simulations has a great potential for refining the paleoenvironmental and chronological context of archeological and paleontological sites.

Supplementary material

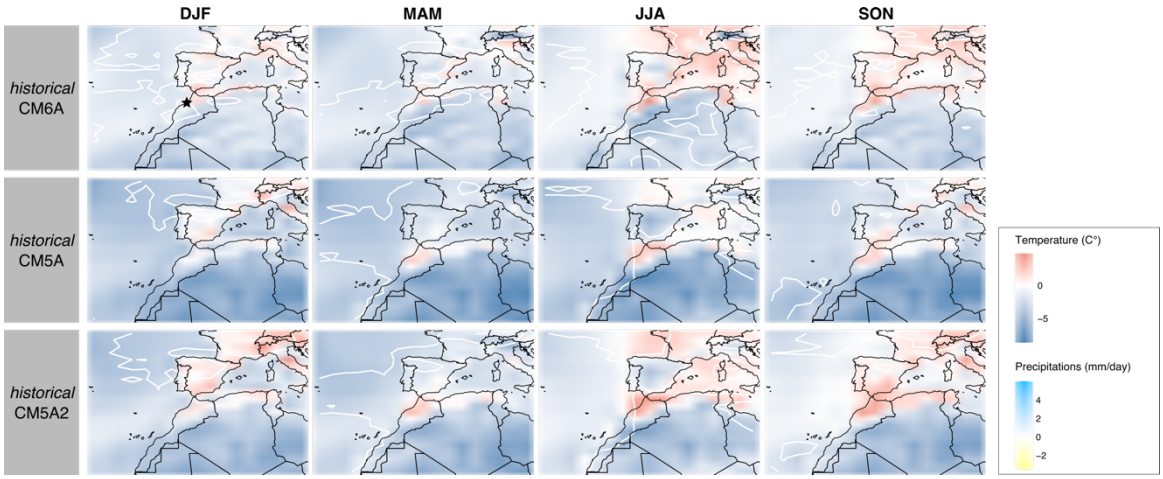

Fig. S1 Maps of EH2 region comparing temperature and precipitation of the *historical* simulations of IPSL-CM5A-LR, IPSL-CM5A2-LR and IPSL-CM6A-LR with ERAi temperature and GPCP precipitation, which are state-of-the-art datasets for analysis of observed temperature and precipitation during the recent period (more details below). IPSL-CM5A2-LR was upgraded to have improved computing performance, a reduced global cold bias compared to IPSL-CM5A-LR and it better handles past geological configurations (Sepulchre *et al.*, 2020). On the other hand, IPSL-CM6A-LR has a vastly improved climatology in contrast to previous versions of the model, but has been mainly developed and tested under present day climate (Boucher *et al.*, 2020). Model outputs of the *historical* simulations are stored on CICLAD (Calcul Intensif pour le Climat, l'Atmosphère et la Dynamique). As a reference for current climate, we used monthly data from the global atmospheric reanalysis ERA-interim for temperature (Berrisford *et al.*, 2011) and from the GPCP v2.3 (Global Precipitation Climatology Project) for precipitations (Adler *et al.*, 2018). Data were averaged on 30 seasonal cycles (1980-2009). Red areas designate higher simulated than reanalyzed temperatures while blue areas indicate lower temperatures. Light blue isolines represent areas subject to more precipitation in the simulation outputs than is reanalyzed, while the yellow isolines indicate areas with less precipitation. EH2 cave location is represented by the star in the upper left panel. DJF: December, January, February (winter); MAM: March, April, May (spring); JJA: June, July, August (summer); SON: September, October, November (autumn).

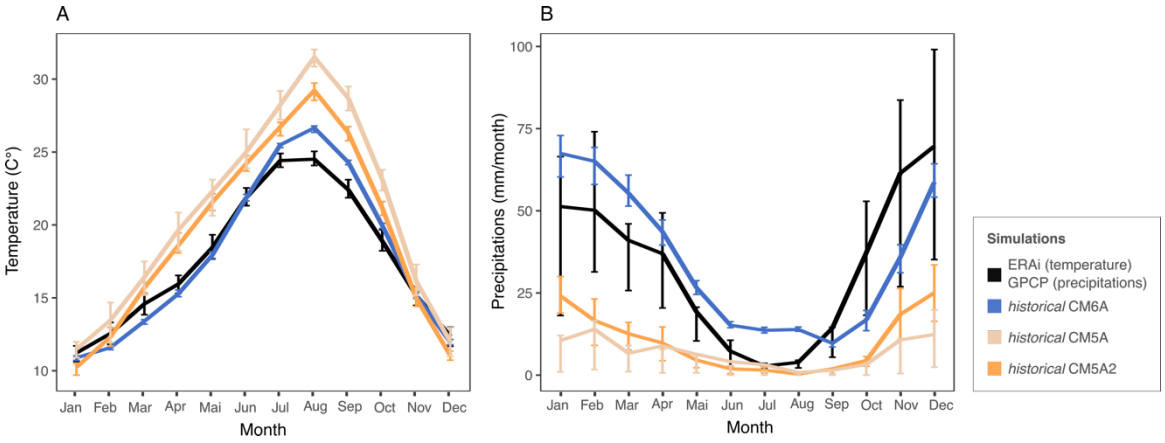

Fig. S2 Graph of monthly variations in temperature and precipitation of the *historical* simulations of IPSL-CM5A-LR, IPSL-CM5A2-LR and IPSL-CM6-LR models and ERAi temperature and GPCP precipitation on the four grid cells containing EH2 cave in each dataset. Interannual variation over the averaged 30 years is visualized by quartiles.

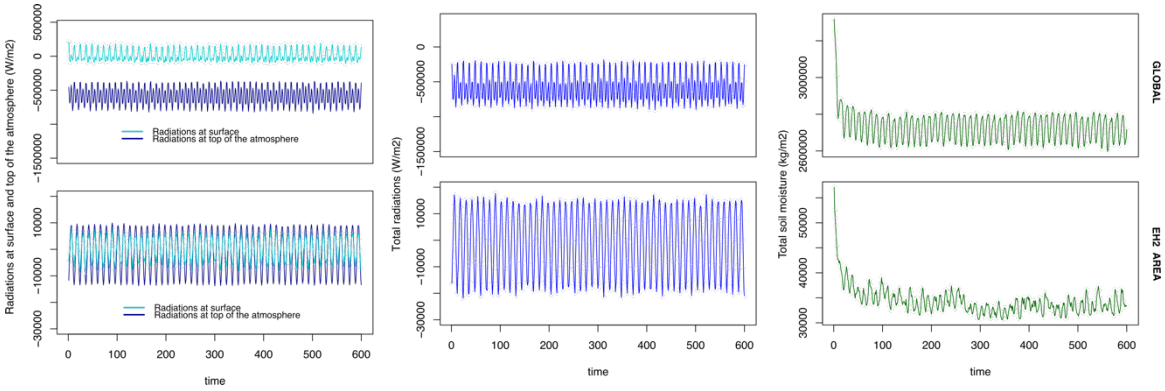

Fig. S3 Monitoring variables for energy budgets in *Ctrl* for the globe and in the EH2 region: radiations at top of the atmosphere (nettop), radiations at surface (bils), total radiations (nettop + bils) and total soil moisture (mrso).

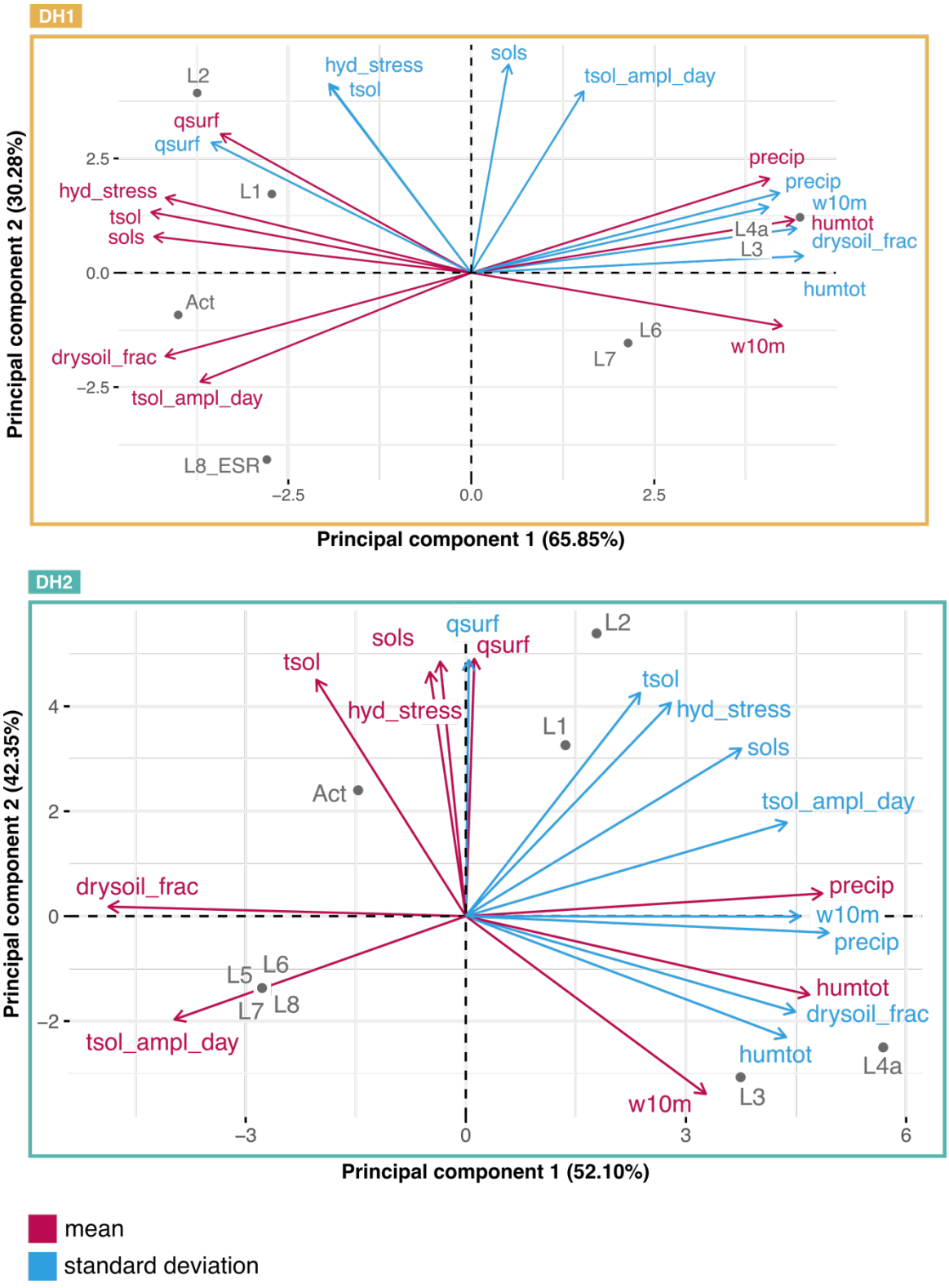

Fig. S4 Biplots of El Harhoura 2 layers and climate variables according to DH1 (Dating Hypothesis 1; upper panel) and DH2 (Dating Hypothesis 2; lower panel).

CHAPTER 4

How global climate variations impact the phenotype of rodents and shrews?

Léa Terray, Emmanuelle Stoetzel, David Nerini, Pascale Braconnot* and Raphaël Cornette*

* Equal authorship

This chapter is an article *In Prep.*

In the previous chapter, we found that combined US-ESR datings seem more reliable in the case of our site. Global climate variations described by simulations are overall congruent with local environmental changes suggested by paleoenvironmental proxies (isotopes and faunal assemblages), but also display notable differences. Indeed, instead of the alternation of more humid/arid conditions suggested by paleoenvironmental indicators, simulations describe a two-phase climate sequence: a progressive humidification from L8 to L3 followed by an abrupt transition toward a more arid climate and a less and less arid climate from L2 until today. Because of these differences, the global climate might have a different impact on the phenotype than the local environment. In chapter 4, we explore the covariation between these global climate changes and morphological and functional traits of rodents and shrews.

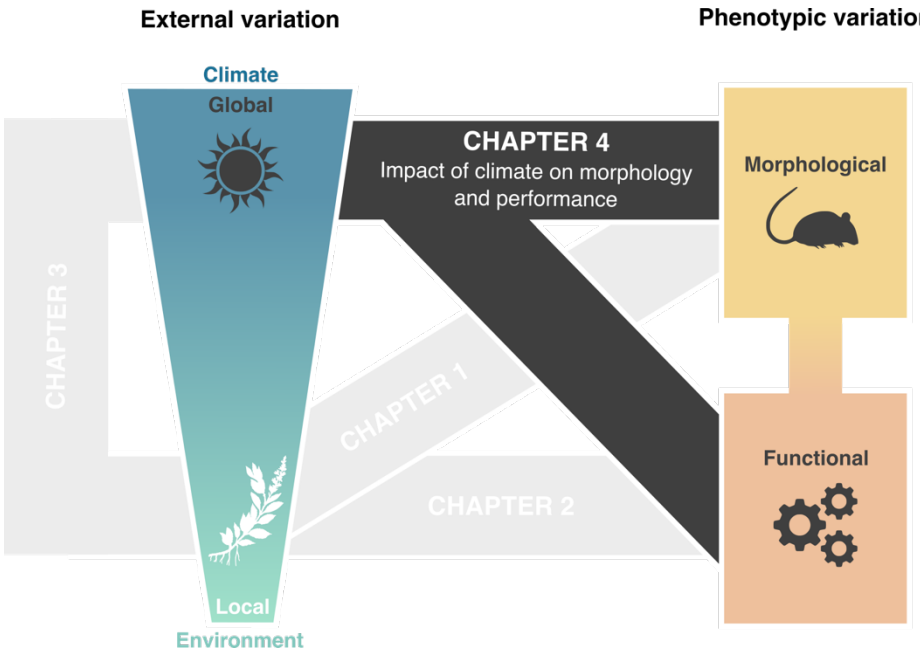

Diagram showing how chapter 4 fits into the thesis problematic.

Introduction

Evidences about past global climate changes driving macroevolutionary changes such as extinctions and diversifications in mammals are numerous (e.g., Douady *et al.*, 2003; Blois *et al.*, 2010; Finarelli & Badgley, 2010). However, the impact of these global climate changes on the phenotype of organisms is less known, while the phenotypic response is one of the primary responses to climate changes (Karell *et al.*, 2011; Boutin & Lane, 2014; Merilä & Hendry, 2014). Exploring those phenotypic responses in the past is the key for understanding the responses of organisms since the entry into the Anthropocene, the current geological era, characterized by human-induced climate change (Zalasiewicz *et al.*, 2008; Lewis & Maslin, 2015). In this chapter, we investigated what are the phenotypic responses of North African small mammals to global climate changes that occurred over the last 100ka.

We focused on rodents and shrews from the archeological site El Harhoura 2 (EH2; Rabat, Morocco), covering a period from late-Pleistocene to mid-Holocene, and extended our time line until today by considering current Moroccan specimens. Small mammals such as rodents and shrews are good models to evaluate the impact of paleoenvironmental variation on the phenotype (Valenzuela *et al.*, 2009; McGuire, 2010; Escudé *et al.*, 2013; Verde Arregoitia *et al.*, 2017). This site served many times as a model to investigate the relationship between diversity, the phenotype of organism and the environment they lived in (Stoetzel *et al.*, 2010, 2011, 2012a, 2017; Campmas *et al.*, 2015; Cornette *et al.*, 2015c; Terray *et al.*, 2021). It covers a wide range of climate regimes (Drake *et al.*, 2011, 2013; Blome *et al.*, 2012; Kageyama *et al.*, 2013; Scerri, 2017; Couvreur *et al.*, 2020; Terray et al. *under revision*) without exhibiting important turnovers of micro-faunal assemblages (Stoetzel *et al.*, 2011, 2012b). Because species that were present on this site are for the majority still present today in Morocco, our study adopts an actualist approach, allowing us to contrast the past phenotypic response of those organisms with their response to present climate change.

In archeological context, studies often do not distinguish the climate from the environment. To infer past external conditions, they rely on archives such as pollen records (e.g., Ibrahim *et al.*, 2020; Bolaji *et al.*, 2020), isotopes (e.g., Bar-Matthews *et al.*, 2010 ; Jeffrey, 2016) or faunal assemblages (e.g., Matthews, Denys, & Parkington, 2005; Stoetzel, 2017). Those proxies describe very local conditions, depict environments more than climate and can present important discrepancies with each other (Stoetzel *et al.*, 2011; Jeffrey, 2016;

Stoetzel, 2017). Yet, global climate variations are efficiently described by climate simulations. Those simulations rely on physically based models that describe the dynamics and thermodynamics of the atmosphere, ocean, and continental and frozen surfaces coupled with water and carbon cycles. Those models depict the directions and large scale patterns of past climate changes based on their consistency with past changes in the ice-sheet, Earth's orbit and trace gases (Braconnot *et al.*, 2012), and have long been used to investigate past climate changes (Kutzbach & Otto-Bliesner, 1982; Braconnot *et al.*, 2012; Duplessy & Ramstein, 2013; Schmidt *et al.*, 2014; Harrison *et al.*, 2015). In chapter 3 (Terray *et al.*, *under revision*), we produced a set of paleoclimate simulations covering periods corresponding to the stratigraphic layers of EH2. They allowed us to discuss inconsistencies between the different datations and to investigate large scale climate variations over the region of the EH2 site.

Several aspects of the phenotype are known to be closely related to environmental conditions, and they may not display the same response to climate changes. Morphological traits such as shape and size are related to the environment through diet for both the teeth (Wolf *et al.*, 2009; McGuire, 2010; Coillot *et al.*, 2013; Gómez Cano *et al.*, 2013; Gomes Rodrigues, 2015b) and the mandible (Caumul & Polly, 2005; Kouvari, Herrel, & Cornette, 2021). Because size and shape have different developmental pathways, size may be more sensible to climate than shape (Nevo, 1989; Whiting & Wheeler, 1994; Renaud *et al.*, 1999; Selig *et al.*, 2021). Size has even been hypothesized to be a line of least resistance to evolution (Marroig & Cheverud, 2005). A line of least evolutionary resistance is a morphological trait that constitutes the first axis of response to disturbances, because its evolution is facilitated by its genetic and developmental determinants (Schluter, 1996; Marroig & Cheverud, 2005). The more common trend of size response to climate gradient in endotherms is Bergmann's rule (Bergmann, 1848; Meiri & Dayan, 2003), which predicts an increase in body size under colder conditions. However, results about the validity of this trend in rodents and shrews are mitigated (Zeveloff & Boyce, 1988; Ochocińska & Taylor, 2003; Alhajeri & Steppan, 2016; Kouvari *et al.*, 2021). Patterns of developmental modularity of shape variation are also known to be related to environmental stress (Badyaev & Foresman, 2004). Our results in chapter 2 (Terray *et al.*, 2021) seem also to support that modularity is linked to local environmental changes. An alternative hypothesis suggests that conserved modularity patterns may allow faster shape changes and thus may facilitate repeated transitions between habitats (Conith *et al.*, 2020). This would be in line

with Kouvari *et al.* (2021), who did not find any relationship between environmental changes and modularity in the shrew's mandible. Finally, shape disparity indicates changes in the amount of variation in a group (Gould, 1989, 1991; Wills *et al.*, 1994; Foote, 1997). A decrease in disparity may reflect morphological selection due to more stringent environments (Erwin, 2007). The lower the disparity, the more we expect remaining morphologies to be fit to their environment.

Functional traits might display a different response to climate changes than morphological traits, because morphological and functional traits can be partially decoupled (Bergmann & McElroy, 2014). Bite force is a functional trait implicated in feeding, the function related to dietary ecology (Schwenk, 2000). Bite force is related to diet in many animals (Aguirre *et al.*, 2003; Anderson *et al.*, 2008), thus shifts in bite force may reflect shifts in the type of consumed preys, which depends on the habitat. Consequently, we hypothesized that the functional trait may be more sensible to climate than the morphological traits.

Splitting specimens according to shape is a promising way to characterize the main shape variation within populations. The morphological groups (MGs) obtained display different morphological and functional characteristics (Murray, 1973; Terray *et al.*, 2021; Terray *et al., under revision*). Morphology and functional abilities grealy reflect the ecology of organisms. Therefore, they are hypothesized to be tran-specific ecological groups (Terray *et al.*, 2021; Terray *et al., under revision*). The relative abundance of taxa is informative to assess organisms response to climate changes (i.e., Lyman, 2014; Schap, Meachen, & McGuire, 2021). As MGs do not split diversity by taxonomy, but by the main morpho-functional profiles in a population, we expect the relative abundance in MGs (i.e. the relative proportion of representatives of each MG) to be highly impacted by changes in climate (assuming taphonomic biases do not interfere).

In this study, we explored the impact of global climate changes on several morphological and functional aspects of the phenotype of rodents and shrews from the archeological site El Harhoura 2 (EH2). Climate variations were quantified using paleoclimate simulations. As indicators of the phenotypic diversity of small mammals we choose shape, size, relative abundance in MGs, modularity and disparity of rodent's teeth and shrew's mandibles, and shrew's estimated bite force. We assessed the impact of climate on each of these morphological and functional traits through covariation analyses. Then, we compared the strength of covariation between structures (teeth and mandibles) to assess if they display different sensibility to climate changes. We also compared the strength of covariation of

each indicator within each structure to assess if one indicator is more sensible to climate than the others. Finally, we assess if there are changes in the phenotypic response of rodents and shrews since the entry into the Anthropocene. Because recent climate changes are particularly fast (Foster, Royer, & Lunt, 2017), we could expect the phenotypic response to be intensified.

Material and methods

EH2 cave and sample

EH2 cave is a Late Pleistocene to mid-Holocene archeological site located in the Rabat-Témara region (33°57'08.9" N / 6°55'32.5" W), on the Atlantic coast. Its stratigraphy is divided into 11 layers among which the first eight are well studied and considered in this paper. The archeological material was sampled during the 2005–2009 excavation campaigns of the El Harhoura-Témara Archaeological Team (directors R. Nespoulet and M.A. El Hajraoui). The site revealed an exceptional taxonomic richness and delivered an important amount of large and small vertebrate remains (Michel *et al.*, 2009b; Stoetzel *et al.*, 2011, 2012b). Paleoenvironments along the EH2 sequence have been explored using a lot of proxies, including isotopes, faunal assemblages and species occurrences (Stoetzel, 2009; Stoetzel *et al.*, 2011, 2012a,b; Jeffrey, 2016). In the following, to ease the reading, each layer is abbreviated in "L" followed by the layer number, as in "L1" for layer 1. For period name's consistency, current days are referred to as "L0" (L0 is equivalent to Act in chapter 3).

As proxies for micromammals phenotype we used rodent's first lower (m1) and upper molars (M1) and shrew's mandibles. The rodent's teeth dataset is composed of 1133 m1 and 990 M1 sampled along the stratigraphic sequence of EH2. This material is housed at the Musée de l'Homme, Paris, France and the Institut National des Sciences de l'Archéologie et du Patrimoine, Rabat, Morocco. To extend the timeline to present days, the dataset was completed with current material from the collections of the Muséum National d'Histoire Naturelle. We choose exclusively Moroccan rodent specimens and excluded specimens from remote regions from Rabat with atypical environments such as the Atlas Mountains. In total, we added 77 m1 and 106 M1. The complete dataset is composed of 11 species: *Meriones grandis, Meriones shawii, Mus spretus* and *Dipodillus campestris, Meriones libycus*, *Mus musculus, Dipodillus maghrebi, Lemniscorys barbarus,*

Apodemus sylvaticus, Mastomys erythroleucus and *Rattus rattus*. Data acquisition regarding the archeological material is detailed in chapter 1 and the same methodology was applied to current material.

The shrew's mandibles dataset is composed of 93 remains temporarily housed at the Muséum National d'Histoire Naturelle, Paris, France. Four species of white-toothed shrews are represented: *Crocidura russula, Crocidura lusitania*, *Crocidura tarfayensis* and *Crocidura whitakeri* (Cornette *et al.*, 2015a,c). Complete mandibles are rare among archeological remains and most of the material is fragmented. However, mandibles fragments can also be informative (Cornette *et al.*, 2015a,c; Terray *et al.*, 2021). We selected complete mandibles and one type of fragments, the only one that carries information about both the mandible branch and body (referred as the C fragment in chapter 2 (Terray *et al.*, 2021)). Data acquisition is detailed in chapter 2 (Terray *et al.*, 2021). The abundance of teeth and mandibles per layer is indicated in **Table 1**.

Table 1. Summary of the sample

Layers	Rodent's teeth		Shrew's mandibles
	m1	M1	
L0	77	106	16
L1	74	69	4
L2	45	43	4
L3	64	65	4
L4a	57	50	3
L5	157	118	13
L6	189	181	19
L7	314	227	19
L8	233	237	11
TOTAL	**1210**	**1096**	**93**

Geometric morphometric analyses

Shape variation was investigated through 2D geometric morphometric analyses. All analyses and visualizations in this article were carried out under the free software R (R Development Core Team, 2018) using the libraries *geomorph* (Adams & Otárola-Castillo, 2013), *Morpho* (Schlager, 2017)*, clues* (Wang *et al.*, 2007), *pls* (Liland *et al.*, 2021), *ape* (Paradis *et al.*, 2004), *dispRity* (Guillerme, 2018), *MASS* (Venables & Ripley, 2002), *ggplot2* (Wickham, 2015) and *corrplot* (Wei & Simko, 2021).

Rodent's teeth shape was approximated using the outline of the molar crown in occlusal view. Wear related to age is an important bias of teeth shape and molar crowns are less affected by it, especially in the case of *Meriones,* which have semi-hypsodont teeth characteristics. Outline location is presented in **Fig 1A**. Teeth were converted to masks and outlines were extracted using the *Momocs* library (Bonhomme *et al.*, 2014). We performed Fourier analyses, an efficient method to describe teeth morphology (Renaud, 1999) that is less sensitive to wear than the landmarks-based approach (Renaud *et al.*, 1999). The registration process proposed here is an extension of the GPA algorithm that can be found in Dryden & Mardia (1998) (p. 90), but adapted in the case where the outline of an object is considered as a continuous closed curve. It relies on an algorithm of Functional Generalized Procrustes Analysis (FGPA). The idea behind this landmark free method is to avoid the delicate choice of the number and the position of landmarks. This method is further detailed in chapitre 1 (Terray *et al.*, *under review*). Once the contour lines have been registered, classical shape analyses can be achieved on the registered Fourier coefficients. Mask surface area was used as an estimate of size.

Shrew's mandibles shape could not be reliably captured using the same method as for teeth (outlines) as they are fragmented. Thus, they were analyzed through a landmark- and sliding semi-landmark-based approach. Anatomical landmarks represent biological homologies while semilandmarks represent geometric homologies, allowing the description of the shape of biological relevant areas without anatomical landmarks (Bookstein, 1996; Zelditch, 2004; Gunz *et al.*, 2005; Cornette *et al.*, 2013). Landmark locations are presented in **Fig 1B**. Semi-landmarks were slided to minimize the bending energy. To remove effects of translation, rotation and scale and make objects comparable we performed a Generalized Procrustes Analysis (GPA) (Rohlf & Slice, 1990) using the *gpagen* function of the library *geomorph* (Adams & Otárola-Castillo, 2013). Resulting shape coordinates are the Procrustes residuals, on which further statistical analyses have been performed. Size was estimated using the centroid size. The centroid size was $\log_{10}$-transformed in all further analyses.

Shape variability was quantified and visualized using principal component analysis performed with the *PCA* function of the *FactoMineR* library (Lê *et al.*, 2008). Only the two first principal components are used for visualizations, but analyses are performed on the overall shape variability.

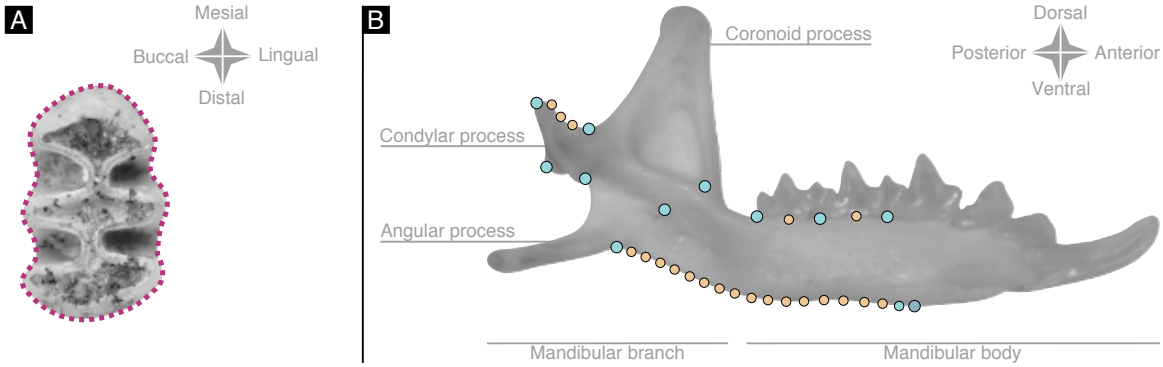

Fig. 1 Outline location on rodent's teeth presented on a M1 of *Meriones shawii/grandis* (A) and locations of anatomical landmarks (blue) and sliding semi-landmarks (yellow) on shrew's mandibles presented on a complete mandible of *Crocidura russula* (B).

MGs identification

To evaluate phenotypic diversity within each dataset (m1, M1, mandibles) and identify MGs, we partitioned the global variability by performing unsupervised clustering analyses. We used the K-nearest neighbors method (KNN), a non-parametric classification in which each shape object is attributed to the group of its K nearest neighbors. The *clues* function of the *clues* library (Wang *et al.*, 2007) proposes an unsupervised KNN algorithm. To assess dissimilarity between shape objects it computes euclidean distance. The K number of neighbors to consider is determined by the algorithm. First, a partition procedure is performed through a local shrinking procedure (data points are "shrinked" toward a cluster center) to obtain the number of clusters (Wang *et al.*, 2007). Then K is selected between 1 to n-1 (n being the number of objects) based on the more robust clustering result (Wang *et al.*, 2007). Partition robustness is assessed by the Silhouette index (SI) (Kaufman & Rousseeuw, 1990), which measures the strength of clusters. SI is determined for each data point. It is bounded by -1 and 1. If SI>0 the data point is closer to its assigned cluster than to other clusters. If SI<0 the data point is misassigned to its cluster. If SI=0 the data point is at equal distance from its assigned cluster and neighboring clusters. To ensure that points are correctly allocated to clusters the average SI is calculated and must be strictly positive (Wang *et al.*, 2007). For each dataset (m1, M1, mandibles), we examined the variation in relative abundance in MGs on each layer.

Allometry

Allometry is the part of shape due to the influence of size (Gould, 1966; Klingenberg, 1996, 2016; Klingenberg & Marugán-Lobón, 2013). Size variation is an important determinant of morphological changes, and consequently plays a critical role in the evolution of shape (Klingenberg, 2016). If the GPA procedure separates shape from size, it does not remove allometry. The presence of allometry was tested by performing the multivariate regression of shape on size using the function *procD.lm* from the library *geomorph* (Adams & Otárola-Castillo, 2013). We also explored if the MGs of each structure (m1, M1, mandible) display different allometric slopes (i.e. different relationship between shape and size). To test it, we performed a regression using the formula: shape ~ size + MG + size:MG. The interaction term between MGs and size was examined to assess homogeneity of allometric slopes between MGs.

Modularity

The degree of modularity within teeth and mandible was explored based on developmental modules defined *a priori*. Regarding teeth, we defined two modules: the distal part and the mesial part (**Fig 2A** and **2B**). In the molar row of rodents, the first molar is in contact with the second molar. The ‘‘neighboring rule’’proposed by Van Valen (1970) predicts strong spatial interactions between contiguous structures during development. This rule was verified in rodents molars of *Apodemus sylvaticus* and *Mus musculus* by Renaud *et al.* (2009). Thus, the second molar might induce a physical constraint on the distal part of the first molar during development. The mesial part, on the contrary, is free from that kind of constraints and can vary greatly. That may be why the first and third molars are the more variable in rodents (Labonne *et al.*, 2012). Thus, we hypothesized that the mesial and distal parts of the first molars could behave as modules as they are not subjected to the same constraints during development. To standardize our module definition between m1 and M1, we splitted teeth horizontally at their maximum width.

To quantify the modular structure of the mandible, we divided it according to the two primary developmental modules defined in the literature: the mandibular branch and the mandibular body (**Fig 2C**; Cheverud *et al.*, 1997; Mezey *et al.*, 2000; Klingenberg *et al.*, 2003; Klingenberg, 2004). Modularity is classically investigated based on the global Procrustes alignment of the biological object studied. However, to use modules splitted

after a common Procrustes superimposition is against the assumption that one should not interpret separately subsets of landmarks, as the superimposition is based on statistical convenience only (Cardini, 2019). So, prior modularity analyses, modules were subdivided and separate Procruste alignment were performed.

To quantify the degree of modularity we used the Covariance Ratio (CR) (Adams, 2016) using the *modularity.test* function from the *geomorph* library (Adams & Otárola-Castillo, 2013). This method compares the degree of modularity between the modules to what is expected under the null hypothesis (random association of variables). The independence of hypothesized modules (i.e. the modularity hypothesis) is verified when CR < 1 and is statistically significant. This measure is not affected by sample size (Adams, 2016). To assess if the degree of modularity between structures is significantly different, we used the function *compare.CR* from the *geomorph* library (Adams & Otárola-Castillo, 2013).

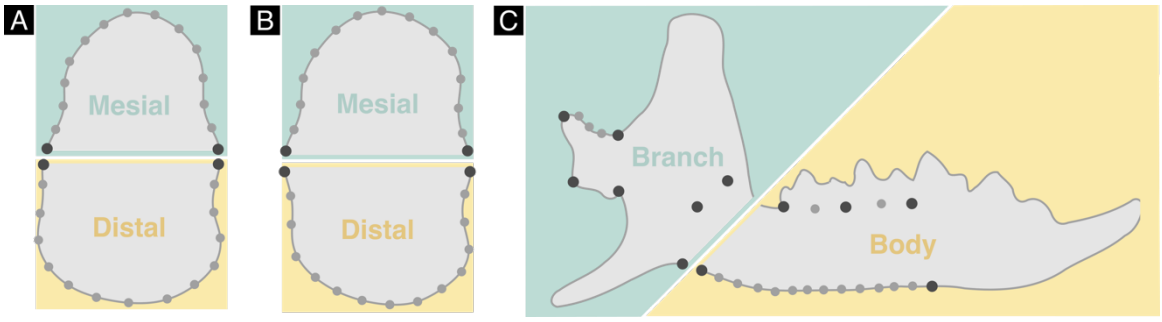

Fig. 2 Hypothesized developmental modules in the m1 (A), the M1 (B) and the mandible (C). Landmarks protocols used to independently align each module are also presented: black dots represent anatomical landmarks and grey dots sliding semi-landmarks.

Disparity

When considered outside of the phylogenetic framework, the amount of occupied morphospace is a good estimate of disparity (Wills *et al.*, 1994). Disparity was computed separately on each layer using the function *dispRity.per.group* from the *dispRity* library (Guillerme, 2018). As an estimator of disparity, we used the median of the distances from the centroid of the group, a variance measure relatively insensitive to outliers (Guillerme, 2018). A common issue when studying disparity is the effect of sample composition (Butler *et al.*, 2012). To prevent it, a bootstrap procedure (a resampling method based on random sampling with replacement) is included in the function *dispRity.per.group*. Variance is

generally not biased by sample size (Foote, 1997) and, thus, we did not apply any sample size correction.

Estimated bite force

As a proxy to estimate bite force from the shrew's mandible, we computed the mechanical potential of the temporalis muscle. The temporalis is one of the main muscles involved in bite force generation in mammals (Herrel *et al.*, 2008a; Santana *et al.*, 2010; Cornette *et al.*, 2015d,b; Brassard *et al.*, 2020b). The mechanical potential was computed using a biomechanical model based on mandible shape and then corrected to take size into account. The complete protocol is detailed in chapter 2 (Terray *et al.*, 2021). We considered this size-corrected mechanical potential as an estimate of bite force in nature.

Climate variation

In order to obtain a quantified characterisation of climate states, we produced in chapter 3 paleoclimate simulations for each stratigraphic layer studied. Climate simulations allow one to reconstruct the climate state corresponding to a defined period. Thus, the resulting climate sequence relies on datation estimations associated with each stratigraphic layer. However, dating a stratigraphic layer is not an obvious task. Fortunately, the chronological framework of EH2 has been extensively studied in the last decade. Three different methods were used to date layers: OSL (Optical Stimulated Luminescence) (Jacobs & Roberts, 2012; Jacobs *et al.*, 2012), combined US-ESR (combination of uranium series and electron spin resonance methods) (Janati-Idrissi *et al.*, 2012; Ben Arous *et al.*, 2020b) and AMS-14C (radiocarbon dating) (Nespoulet & El Hajraoui, 2012; Marquer *et al.*, *in press*). Those dating estimations present some discrepancies, mainly between combined US-ESR and OSL dating. In the light of the results of chapter 3, we choose to rely here on AMS-14C and combined US-ESR datings and to use the corresponding climate sequence (referred as DH1 in chapter 3).

The simulations used here were performed using the LMDZOR6A model, which is the atmosphere-land surface component of the coupled model IPSL-CM6v1.11-LR already described in chapter 3. Climate states were simulated for six periods: MIS5d (~115ka, corresponding to L8), late MIS4 (~60ka, corresponding to L5), mid-MIS3 (~40ka, corresponding to L4a and L3), early Holocene (~9ka, corresponding to L2), mid-Holocene

(~6ka, corresponding to L1) and current days. The output of each simulation consists of a mean seasonal cycle (12 months) averaged over the last 30 years of the simulation. They enabled us to study the main climate contrasts between these periods. However, they neglect the interannual variability within each period, which may also have a significant impact on ecosystems. Overall, they described an increasingly wetter climate from L8 to L3, and then a severe dry climate in L2, followed by a less and less dry climate in L1 and L0.

Nine output variables that are likely to directly or indirectly (through available resources) influence organisms morphology and performances were selected to represent climate state. They are listed and described in chapter 3, Table 2. For each variable, we considered two parameters, as in chapter 3. The annual mean, that represents global conditions and was computed as the mean value of the variable over the mean annual cycle, and the amplitude of seasonal variation, as a proxy for seasonality, which was calculated as the standard deviation of the variable over the mean annual cycle. All variables were centered and reduced.

Covariation between phenotype and climate

Climate data were not available for L6 and L7 because those layers have been dated only using the OSL method. Consequently phenotypic data from these layers were removed from covariance analyses. Not including those layers might deprive us of interesting information. However, according to OSL datations (Ben Arous *et al.*, 2020a) and the stratigraphy of EH2 (Stoetzel, 2009) L6, L7 and L8 are closed in date. Thus, maybe the simulated climate of L6 and L7 would not have been so different from that of L8. Therefore the removal of these layers may not greatly impact our results.

Regarding shape, size and estimated bite force covariation with climate were explored per individuals. As for relative abundance in MGs, modularity and disparity, they were explored per layer, as only one value per layer is computed. To investigate the covariation between climate variables and phenotypic indicators, we performed 2B-pls, which explore covariation patterns between two sets of variables (Sampson *et al.*, 1989; Streissguth *et al.*, 1993) and has been adapted to shape data (Rohlf & Corti, 2000). To perform 2B-pls we used the *two.b.pls* function from the *geomorph* library (Adams & Otárola-Castillo, 2013). Shapes at the extreme of axes and predicted shapes under arid and humid climates were

produced using the function *plotRefToTarget* from the *geomorph* library (Adams & Otárola-Castillo, 2013).

2B-pls analyses were performed both with and without L0 and the results of the two were compared. We assumed that if the covariation without L0 is significantly different than with L0, it would mean that (a) new selective pressure(s) may have appeared in present days, interfering with/exacerbating the influence of climate, as anthropic disturbances. When statistical differences are found, to confirm whether this is an atypical model or not, we recalculated the 2B-pls by removing each layer one after the other (and not only L0). If the removal of L0 was the only case where the significance changes, we considered our hypothesis is confirmed.

When comparing the strength of covariation of two 2B-pls analyses, the r-PLS is not appropriate as it is dependent on both the number of specimens and the number of variables (Adams & Collyer, 2016). Instead, we used the multivariate effect size (Z-score) of the r-PLS provided by Adams & Collyer (2016). The function *compare.pls* from the *geomorph* library (Adams & Otárola-Castillo, 2013) allows one to test if the Z-scores of two 2B-pls are significantly different. It calculates effect sizes as standard deviations and performs two-sample z-tests, using the pooled standard error from the sampling distributions of the 2B-pls analyses (Adams & Otárola-Castillo, 2013).

Results

Shape variation and MGs identification

Clustering analyses reveal three MGs among rodent's m1 (SI means = 0.13), five among rodent's M1 (SI means = 0.10) and three among shrew's mandibles (SI means = 0.15). For the three datasets (rodent's m1, rodent's M1 and shrew's mandible) SI means are strictly positive, which ensures the reliability of the associated partitions. Variations in shape and size between MGs are presented in **Fig 3**.

Regarding rodent's teeth, the morphological partitions isolate stephanodont-like teeth from lophodont-like teeth. Stephanodont-like teeth are regrouped in MG1 for m1 (**Fig 3A**) and in MG1 for M1 (**Fig 3B**), while lophodont-like teeth are regrouped in MG2 and MG3 for m1 (**Fig 3A**) and in MG2, MG3, MG4 and MG5 for M1 (**Fig 3B**). MGs split the variability of lophodont-like molars along a shape gradient from elongated and slender teeth to short and thick teeth. Extremes are, respectively, represented by MG3 for m1 (**Fig 3A**) and MG2

for M1 (**Fig 3B**)) and by MG2 for m1 (**Fig 3A**) and MG4 for M1 (**Fig 3B**)). Significant size differences were found between all MGs for m1 and M1, in agreement with the shape gradient. In both cases, the size difference between MG1 (stephanodont-like teeth) and other MGs (lophodont-like teeth) was much greater than between other MGs, only composed of lophodont-like teeth.

Concerning shrew's mandibles (**Fig 3C**), the morphological partition splits variability along a shape gradient from proportionally elongated and gracile to short and robust mandibles. MG1 is composed of mandibles with a proportionally thin and elongated mandibular body and a slightly dorsally-oriented condylar process. MG2 regroups mandibles with intermediate mandibular body in length and width with a short condylar process. Finally, mandibles of MG3 display a short and thick mandibular body and a ventrally-oriented condylar process. No significant size differences were found between MGs.

Significant allometry was found in rodent's m1 (R2 = 0.09; p-value = 0.001**), rodent's M1 (R2 = 0.10; p-value = 0.001**) and shrew's mandibles (R2 = 0.05; p-value = 0.001**). Regarding rodent's teeth, MGs display statistically different allometric slopes for m1 (interaction term: R2 = 0.009; p-value = 0.001**) and M1 (interaction term: R2 = 0.02; p-value = 0.001**), while MGs of shrew's mandibles do not (interaction term: R2 = 0.02; p-value = 0.2 NS).

A significant modular signal was found in teeth, in both m1 (CR = 0.49, p-value = 0.001**) and M1 (CR = 0.50, p-value = 0.001**), and in the mandible (CR = 0.41, p-value = 0.001**). The degree of modularity is not significantly different between M1 and m1 (Z = 0.15; p-value = 0.88), m1 and mandible (Z = 0.72; p-value = 0.47) nor between M1 and mandible (Z = 0.74; p-value = 0.46).

Covariation between phenotype and climate with and without L0

Results of all 2B-pls are presented in **Table 2**. To assess if there are changes in the phenotypic response of rodents and shrews since the entry into the Anthropocene, we computed 2B-pls between phenotypic traits and climate with and without L0. Regarding rodent's teeth (m1 and M1), the covariation between shape/relative abundance in MGs/size and climate are all statistically significant (p-value < 0.05). The strength of these covariation is not significantly different depending on whether L0 was included or not. The covariation between modularity/disparity and climate are not significant.

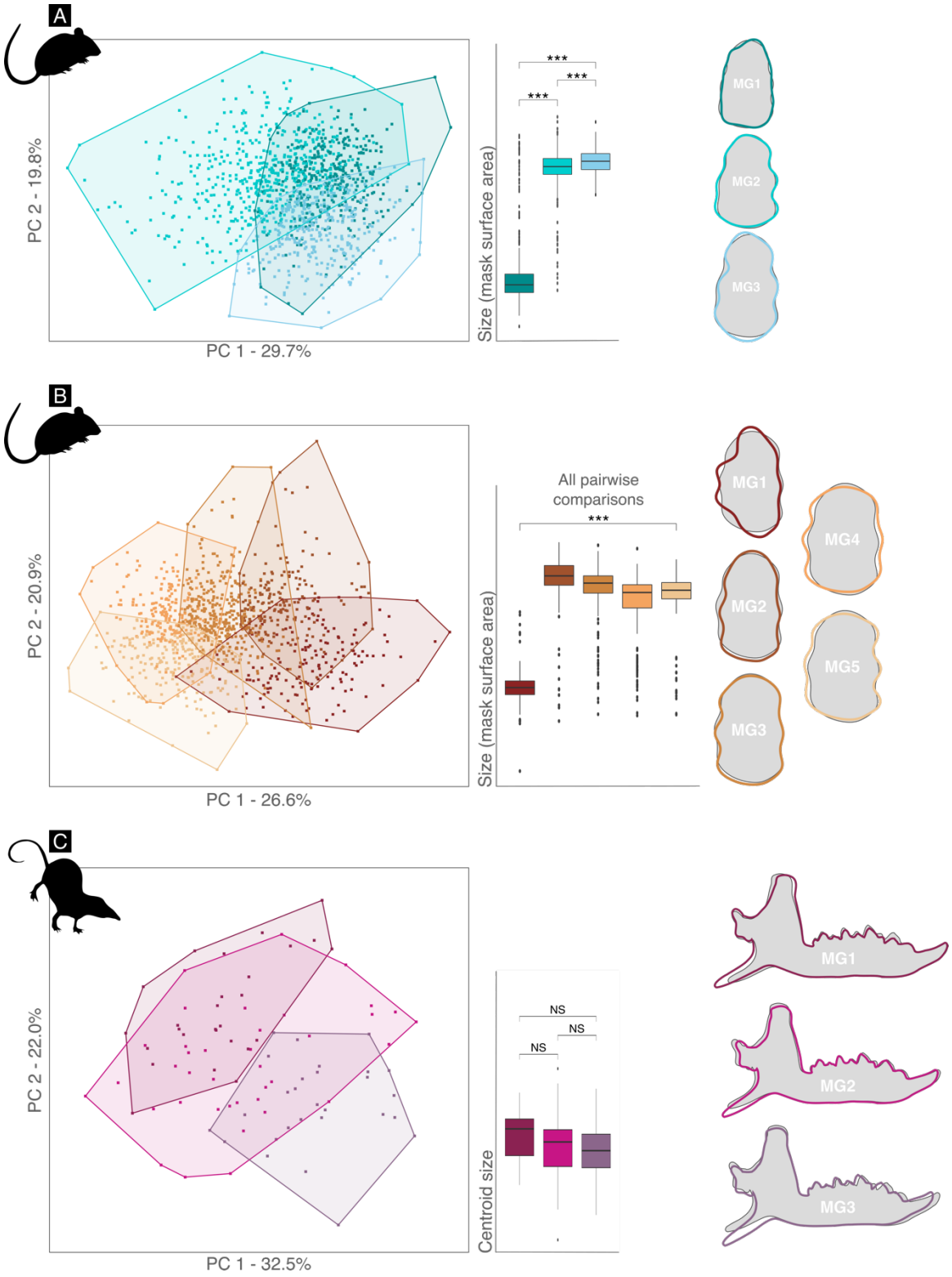

Fig. 3 Shape and size variation within rodent's teeth and shrew's mandibles. For each model, principal component analysis, size differences between morphological groups and groups mean shapes are presented. Size differences between morphological groups were tested using pairwise t-tests, NS indicates no significant differences between groups, (***) indicates significant differences between groups. A: rodent's m1; B: rodent's M1; C: shrew's mandible.

For mandibles, the covariation between shape/estimated bite force and climate are significant with L0, but not without L0. Conversely, the covariation between relative abundance in MGs and climate is significant without L0, but not with L0. To confirm whether shrew's mandible shape, relative abundance in MGs and estimated bite force display atypical patterns on L0 only or not, we computed again the 2B-pls by removing each layer one by one (and not only L0). Those results are available in supplementary material (**Table S1**). All cases of layer removal, except for L0, show no differences in significance with the 2B-pls performed on all layers. The covariation between size and climate is statistically significant in both cases, and the strength of covariation is not significantly different depending on whether L0 is included or not. No significant covariation was found between the degree of modularity or disparity and climate variables for either the teeth or the mandible.

Table. 2 Results of the 2B-pls performed on shape, relative abundance in MGs, size, modularity and disparity of m1, M1 and mandibles, and on shrew's estimated bite force with and without L0. Grey cells indicate not statistically significant results.

	m1	**M1**	**Mandible**
Shape			
With L0	r-PLS = 0.39 Z-score = 7.76 p-value = 0.001	r-PLS = 0.33 Z-score = 6.43 p-value = 0.001	r-PLS = 0.68 Z-score = 3.54 p-value = 0.001
Without L0	r-PLS = 0.34 Z-score = 5.8379 p-value = 0.001	r-PLS = 0.27 Z-score = 4.39 p-value = 0.001	r-PLS = 0.62 Z-score = 1.4081 p-value = 0.081
Compare.pls	p-value = 0.76	p-value = 0.45	NA
MGs abundances			
With L0	r-PLS = 0.87 Z-score = 1.69 p-value = 0.043	r-PLS: 0.87 Z-score = 1.99 p-value = 0.008	r-PLS = 0.64 Z-score = -0.41 p-value = 0.64
Without L0	r-PLS = 0.98 Z-score = 1.98 p-value = 0.0065	r-PLS = 0.97 Z-score = 1.99 p-value = 0.006	r-PLS: 0.96 Z-score = 1.56 p-value = 0.018
Compare.pls	p-value. 0.70	p-value. 0.85	NA

Table. 2 Continued.

Size			
With L0	r-PLS = 0.29 Z-score = 5.23 p-value = 0.001	r-PLS = 0.28 Z-score = 5.36 p-value = 0.001	r-PLS = 0.45 Z-score = 2.68 p-value = 0.002
Without L0	r-PLS = 0.25 Z-score = 5.16 p-value = 0.001	r-PLS = 0.22 Z-score = 4.1482 p-value = 0.001	r-PLS = 0.49 Z-score = 2.20 p-value = 0.009
Compare.pls	p-value = 0.082	p-value = 0.36	p-value = 0.86
Modularity			
With L0	r-PLS = 0.44 Z-score = -0.61 p-value = 0.72	r-PLS = 0.39 Z-score = -0.93 p-value = 0.80	r-PLS = 0.74 Z-score = 1.02 p-value = 0.18
Without L0	r-PLS = 0.40 Z-score = -0.95 p-value = 0.78	r-PLS = 0.72 Z-score = 0.62 p-value = 0.30	r-PLS = 0.75 Z-score = 0.77 p-value = 0.26
Compare.pls	NA	NA	NA
Disparity			
With L0	r-PLS = 0.69 Z-score = 0.77 p-value = 0.26	r-PLS = 0.48 Z-score = -0.40 p-value = 0.64	r-PLS = 0.674 Z-score = 0.7015 p-value = 0.27
Without L0	r-PLS = 0.60 Z-score = -0.045 p-value = 0.56	r-PLS = 0.35 Z-score = -1.38 p-value = 0.89	r-PLS = 0.72 Z-score = 0.63 p-value = 0.30
Compare.pls	NA	NA	NA
Estimated bite force			
With L0	-	-	r-PLS = 0.51 Z-score = 3.06 p-value = 0.001
Without L0	-	-	r-PLS = 0.284 Z-score = 0.8084 p-value = 0.225
Compare.pls	-	-	NA

Covariation between global climate and rodents teeth morphology

Results and visualizations of significant covariation between the phenotypic indicators of molars (shape, relative abundance in MGs and size) and climate variables are available in **Fig 4** for m1 and in **Fig 5** for M1. We present only visualizations and detailed results for covariation based on all layers (and not without L0), as they are all statistically significant.

Regarding m1 (**Fig 4**), covariation between phenotypic indicators and climate variables (2B-pls) are all statistically significant. The main climate variables implicated in the covariation between climate and m1 shape (**Fig 4A**) seem to be the means and seasonal variations of hydric stress, specific humidity, solar radiation, temperature, diurnal range of temperature and wind speed. As shown by the predicted shapes, under colder and wetter environments, m1 is expected to display a slight elongation, to have a rounder and narrower mesial part and to have a slightly broader distal part. The relative abundance in MGs (**Fig 4B**) seems to covary more with the seasonal variation of hydric stress, solar radiation, temperature and the diurnal temperature range. Also, it is interesting to note that, in the 2B-pls plot, all layers are well aligned on the covariation axis, excepted L0. The variation of relative abundance in MGs over EH2 layers informs us that, under more humid environments, MG2 and MG3 (which regroup lophodont-like teeth) are predominant (>50%), while under drier environments, MG1 (which is mainly composed of stephanodont-like teeth), is more abundant (>50%). The size of m1 (**Fig 4C**) seems to covary more with the mean variation of dry soil fraction, hydric stress, solar insolation, temperature and wind speed. Size variation over EH2 layers shows that teeth are smaller under hot and dry climates than under cold and wet conditions. Interestingly, the trend seems to be shifted by one layer on the most important climate transition (on L2).

Concerning M1 (**Fig 5**), covariation between phenotypic indicators and climate variables (2B-pls) are also all statistically significant. The mean and seasonal variation of all climate variables seem to be implicated in the covariation between climate and teeth shape (**Fig 5A**). The M1 is expected to display more marked lophs/cups, more angular mesial and distal parts and a slight buccolingual compression under warmer and drier environments. The relative abundance in MGs (**Fig 5B**) seem to covary more with the seasonal variation of water stress, precipitation, solar radiation, temperature, diurnal temperature range and wind speed. As for m1, all layers are well aligned on the main covariation axis of the 2B-pls, except for L0. The size of M1 (**Fig 5C**) seems to covary less with the seasonal variations of climate variables and more with mean conditions. As observed in m1, the M1s are smaller under warmer and drier climate conditions, and, as previously, this trend seems to be shifted by one layer on L2.

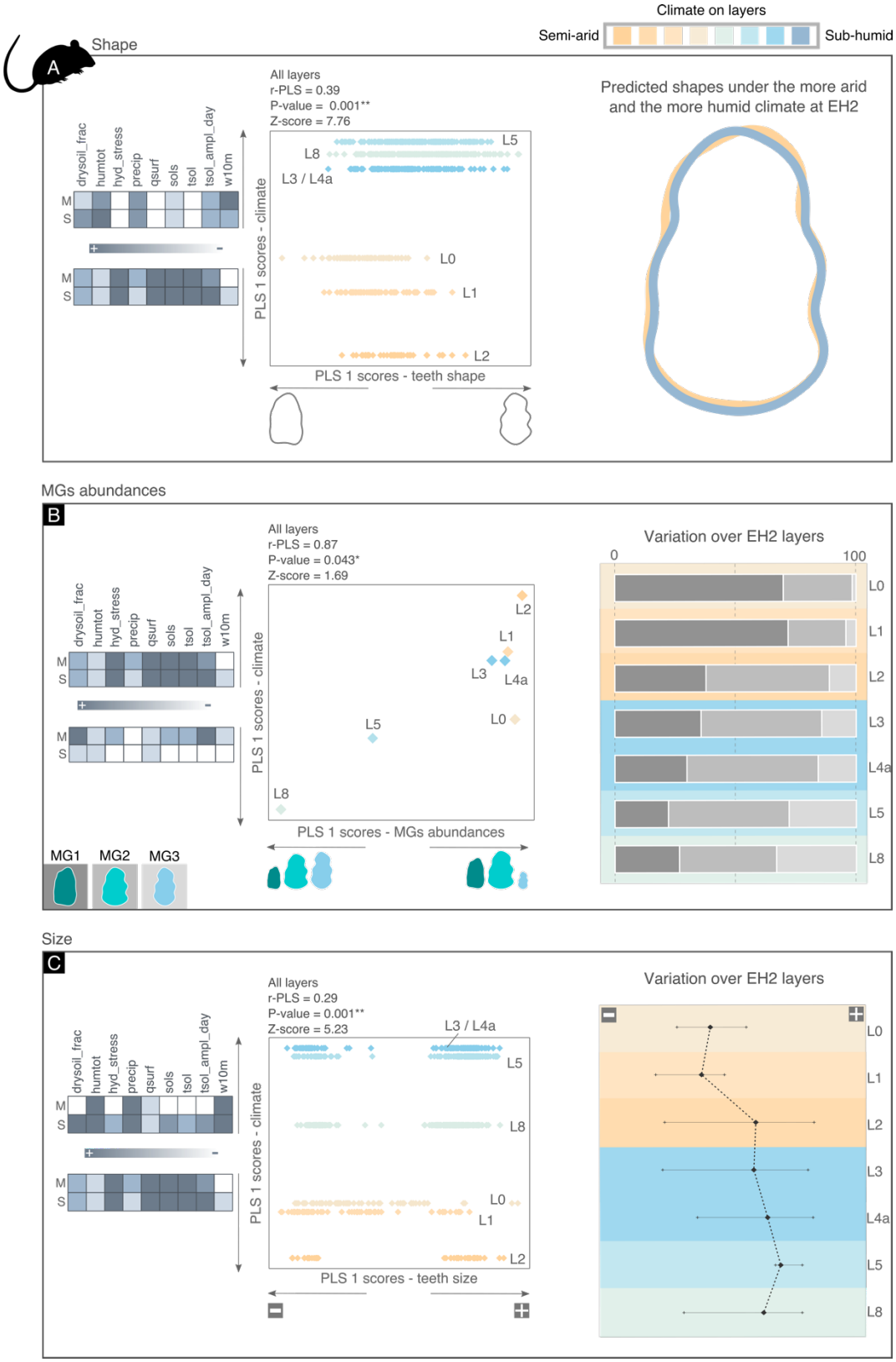

Fig. 4 Visualizations of the significant covariation between morphological indicators of the m1 (shape, relative abundance in MGs and size) and climate variables. In all panels, more arid layers are in orange and more humid are in blue (the order of the layers on the color scale was determined based on the Euclidean distances between the climate of the layers). A: 2B-pls between shape and climate. Extreme shape changes along the 2B-pls axis are

represented by teeth outlines. Extreme climates along the 2B-pls axes are presented *via* a grey gradient (the darker the grey color, the higher the value of the climate variable). M refers to the annual mean and S to the amplitude of seasonal variation. On the right side, we present predicted shapes under the more arid and the more humid climate encountered at EH2. B: 2B-pls between relative abundance in MGs and climate. Extreme changes in relative abundance along the 2B-pls axis are represented by the proportional size of the MGs mean shapes. On the right side, we present variation of relative abundance in MGs over the EH2 sequence (%). C: 2B-pls between teeth size and climate. Extreme changes in size along the 2B-pls axis are represented by (-) for smaller teeth and (+) for larger teeth. On the right side, we present variation of size over the EH2 sequence.

Covariation between climate and shrews mandible morphology

Results and visualizations of the statistically significant covariation between phenotypic indicators (shape, relative abundance in MGs and size) of the mandible and climate variables are available in **Fig 6**. Regarding shape and size, we present visualizations and detailed results for covariation based on all layers, as they are all statistically significant. For the relative abundance in MGs, we present results without L0, as the 2B-pls with all layers is not significant.

Mandible shape (**Fig 6A**) seems to covary with almost all climate variables except specific humidity and wind speed. Under warmer and drier conditions, mandibles are predicted to display a thinner and longer mandibular body and a shorter and more dorsally oriented condylar process. The relative abundance in MGs (**Fig 6B**) covaries more with seasonal variation in water stress, insolation, temperature and wind. MG3, which regroups hard biter shrews (chapter 2, Terray *et al*., 2021), seems predominant under colder and wetter climates, while MG2, which is composed of generalists shrews (chapter 2, Terray *et al*., 2021), seems to be the more abundant under warmer and drier climates. The MG1, the group of soft biter shrews (chapter 2, Terray *et al.,* 2021), is predominant on current days. Mandible size (**Fig 6C**) seems to covary equally with both mean and seasonal variations of almost all climate variables, except specific humidity and wind speed. Mandible size decreases under more humid and cold climates and increases under warmer and drier conditions.

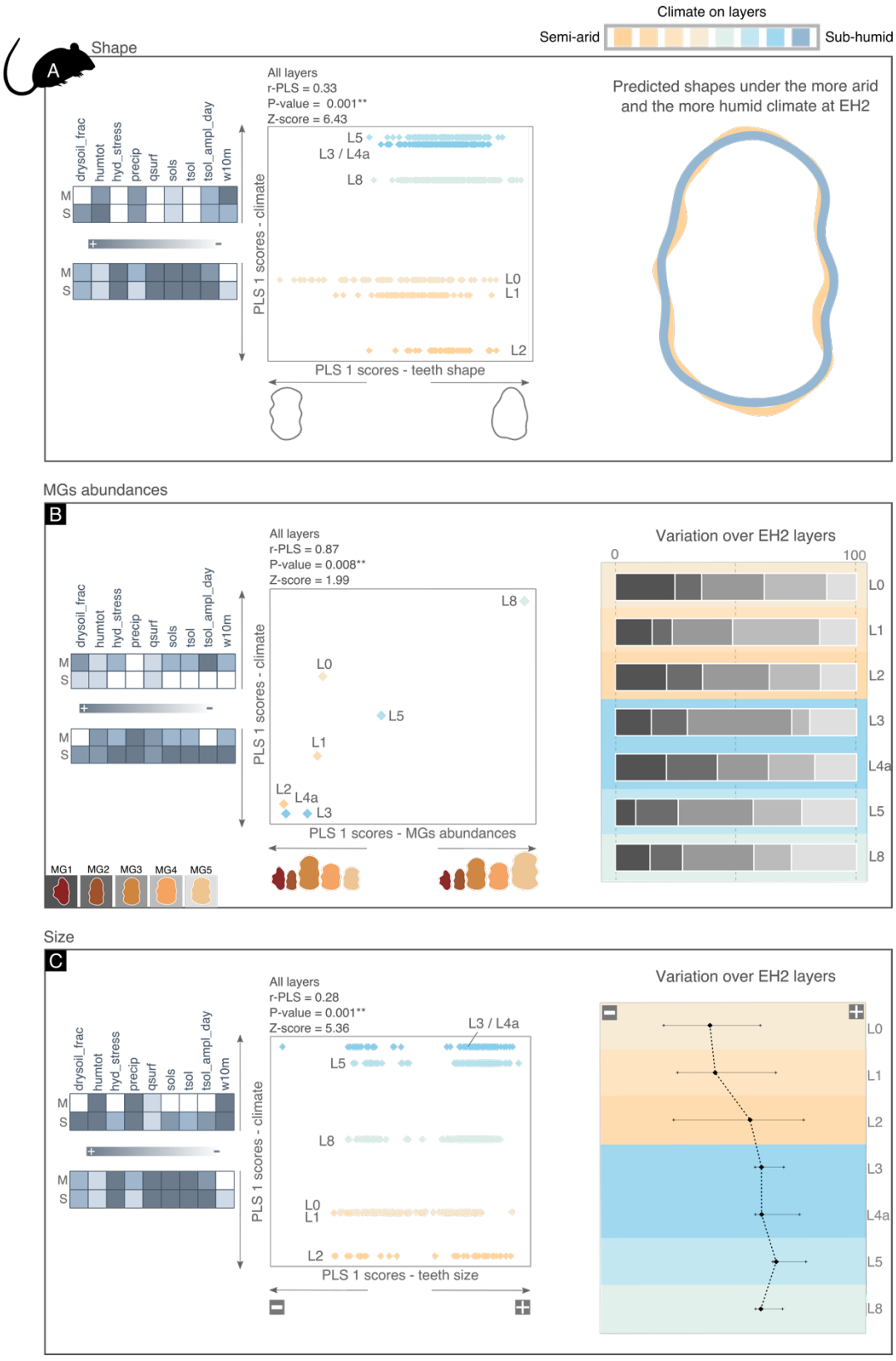

Fig. 5 Visualizations of the significant covariation between morphological indicators of the M1 (shape, relative abundance in MGs and size) and climate variables. In all panels, more arid layers are in orange and more humid are in blue (the order of the layers on the color scale was determined based on the Euclidean distances between the climates of the layers). A: 2B-pls between shape and climate. Extreme shape changes along the 2B-pls axis are

represented by teeth outlines. Extreme climates along the 2B-pls axes are presented *via* a gradient in grey's shading (the darker the grey color, the higher the value of the climate variable). M refers to the annual mean and S to the amplitude of seasonal variation. On the right side, we present predicted shapes under the more arid and humid climates encountered at EH2. B: 2B-pls between relative abundance in MGs and climate. Extreme changes in relative abundance along the 2B-pls axis are represented by the proportional size of the MGs mean shapes. On the right side, we present variation of relative abundance in MGs over the EH2 sequence (%). C: 2B-pls between teeth size and climate. Extreme changes in size along the 2B-pls axis are represented by (-) for smaller teeth and (+) for larger teeth. On the right side, we present variation of size over the EH2 sequence.

Covariation between climate and shrews estimated bite force

Results and visualizations of the significant covariation between shrew's estimated bite force and climate variables are available in **Fig 7**. Estimated bite force covaries equally with both mean and seasonal variations of almost all climate variables, except specific humidity and wind speed. Shrews seem to display stronger estimated bite force under cold and humid climates than under warm and dry climates. On current days, shrew's estimated bite force decreases greatly.

Differences in covariation strength between biological structures (m1, M1 and mandibles)

We compared the strength of covariation between structures (m1, M1 and mandibles) to assess if they display different sensibility to climate changes. For each phenotypic indicator, explored in the three structures, that covaries significantly with climate (shape, relative abundance in MGs and size), we present results of pairwise tests (compare.pls) between structures in **Table 3**. Only one case of comparison is statistically significant: the one that compares mandible and m1 shapes. The mandible shape covaries more significantly with climate than the m1 shape.

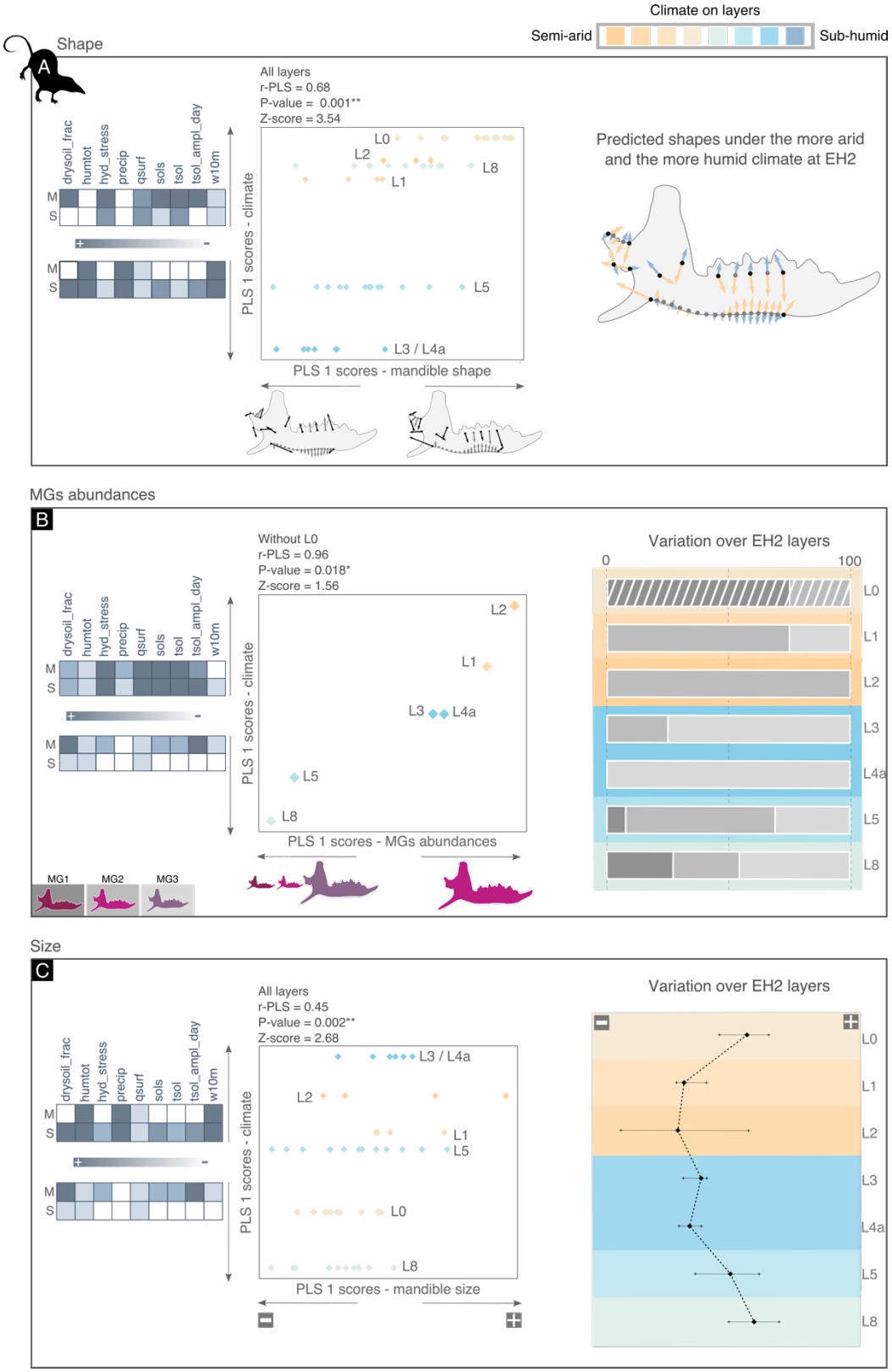

Fig. 6 Visualizations of the significant covariation between morphological indicators of the mandible (shape, relative abundance in MGs and size) and climate variables. In all panels, more arid layers are in orange and more humid are in blue (the order of the layers on the color scale was determined based on the Euclidean distances between the climates of the layers). A: 2B-pls between shape and climate. Extreme shape changes along the 2B-pls

axis are represented by vectors on the mandible. Extreme climates along the 2B-pls axes are presented *via* a gradient in grey's shading (the darker the grey, the higher the value of the climate variable). M refers to the annual mean and S to the amplitude of seasonal variation. On the right side, we present predicted shapes under the more arid and the more humid climate encountered at EH2. B: 2B-pls between relative abundance in MGs and climate. Extreme changes in relative abundance along the 2B-pls axis are represented by the proportional size of the MGs mean shapes. On the right side, we present variation of relative abundance in MGs over the EH2 sequence (%). C: 2B-pls between mandible size and climate. Extreme changes in size along the 2B-pls axis are represented by (-) for smaller mandibles and (+) for larger mandibles. On the right side, we present variation of size over the EH2 sequence.

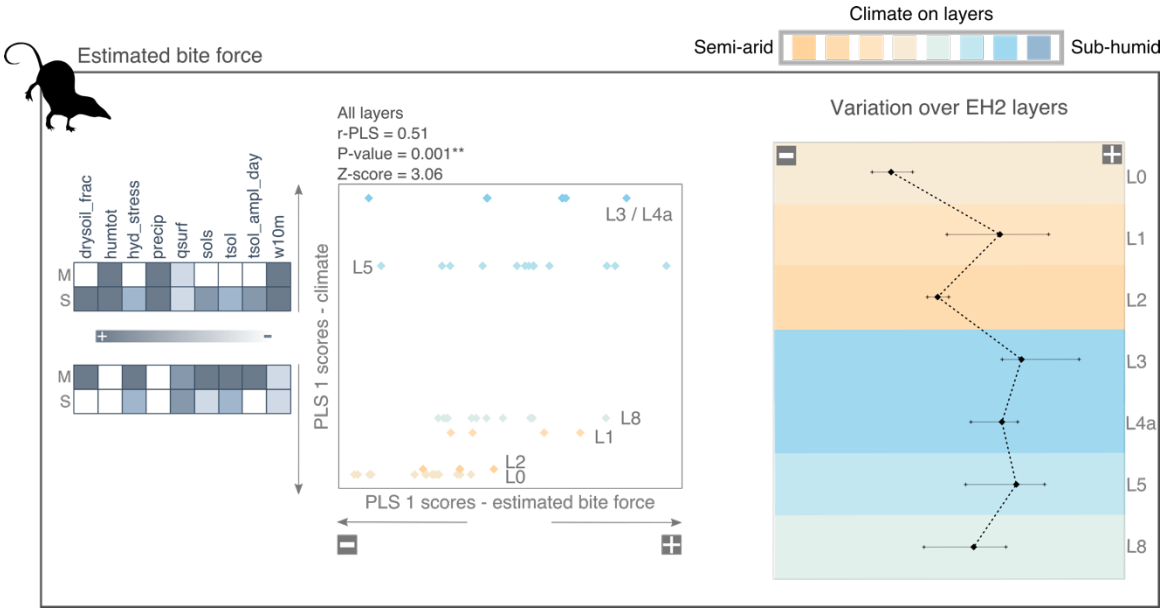

Fig. 7 Visualizations of the significant covariation between shrew's estimated bite force and climate variables. More arid layers are in orange and more humid are in blue (the order of the layers on the color scale was determined based on the Euclidean distances between the climates of the layers). Extreme changes in estimated bite force along the 2B-pls axis are represented by (-) for lower estimated bite force and (+) for higher estimated bite force. Extreme climates along the 2B-pls axes are presented *via* a gradient in grey's shading (the darker the grey, the higher the value of the climate variable). M refers to the annual mean and S to the amplitude of seasonal variation. On the right side, we present variation in estimated bite force over the EH2 sequence.

Table. 3 Results of pairwise tests of covariation with climate (compare.pls) between structures (m1, M1, mandible) for each phenotypic indicator (shape, relative abundance in MGs, size). Grey cells indicate not statistically significant results.

	M1	Mandible
Shape		
m1	Z = 1.24 p-value = 0.21	Z = 2.76 p-value = 0.0057
M1	-	Z = 1.63 p-value = 0.10
MGs abundances		
m1	Z = 0.33 p-value = 0.74	Z = 0.62 p-value = 0.53
M1	-	Z = 0.97 p-value = 0.33
Size		
m1	Z = 0.42 p-value = 0.67	Z = 0.94 p-value = 0.35
M1	-	Z = 0.63 p-value = 0.53

Differences in covariation strength between phenotypic indicators (shape, size, estimated bite force and relative abundance in MGs)

To identify if one of the phenotypic indicators is more closely related to climate than the others, we compared the strength of covariation of each indicator within each structure. Regarding shrews, we also compared the strength of covariation between indicators to assess if the functional trait, estimated bite force, is more sensible to climate than the morphological traits. In **Table 4**, we present the results of pairwise tests performed on each biological structure (m1, M1 and mandible) between phenotypic indicators. The relative abundance in MGs covaries differently with climate than shape and size. They also covary more tightly with climate than shape and size. Regarding shrews, the functional trait estimated bite force does not covary more with climate than the morphological traits.

Table. 4 Results of pairwise tests of covariation with climate (compare.pls) between phenotypic indicators (shape, relative abundance in MGs, size, estimated bite force) for each structure (m1, M1, mandible). Grey cells indicate not statistically significant results.

	MGs abundances	Size	Estimated bite force
m1			
Shape	Z = 3.99 p-value = 6.34e-5	Z = 0.69 p-value = 0.49	
MGs abundances	-	Z = 2.87 p-value = 4.1e-3	
M1			
Shape	Z = 2.43 p-value = 0.015	Z = 0.083 p-value = 0.93	
MGs abundances	-	Z = 2.20 p-value = 0.028	
Mandible			
Shape	Z = 2.15 p-value = 0.031	Z = 0.44 p-value = 0.66	Z = 0.48 p-value = 0.50
MGs abundances	-	Z = 1.94 p-value = 0.053	Z = 2.25 p-value = 0.024
Size	-	-	Z = 0.18 p-value = 0.85

Discussion

Methodological biases

While interpreting and discussing our results, it is important to keep in mind some limitations inherent to the archeological and paleontological records. The study of those common biases and their underlying geological and biological processes is the field of taphonomy (Behrensmeyer, Kidwell, & Gastaldo, 2000). Our sample, as usual in archeology or paleontology, is limited and determined by many factors other than the natural pressures that have affected organisms over their lifetime. Firstly, sample composition is largely defined by the accumulator agent of the deposit. Regarding EH2, the remains of different layers are suspected to have been accumulated by different agents: L1, L7 and L8 would result from the activity of a nocturnal raptor, L3 and L6 of a diurnal raptor and/or a carnivore and L2, L4a and L5 of several predators such as felids, canids, hyenas or small mustelids (Stoetzel, 2009; Campmas *et al.*, 2015, 2017). All those

accumulators do not have the same prey preferences, which may affect our sample composition. Fortunately, the impact of this potential bias on diversity indices was tested on EH2 microfauna and found not to be statistically significant (Stoetzel, 2009). The unevenness of our sample could also be directly impacted by the surface excavated, which can vary from a layer to another (at EH2, the deeper levels are excavated on a much reduced surface than the more recent ones). However, the surface to be excavated is usually adjusted to the richness in remains of the layers, in order to compensate for taphonomic biases. In addition, climate simulations present their own biases. For example, regarding vegetation, current vegetation was imposed in all simulations. The retroaction of the vegetation on climate is therefore not taken into account, which can potentially impact our output climate variables. All of these factors constitute potential biases that lead us to temper our conclusions.

Impact of climate on shape

Climate significantly impacts both m1 and M1 rodent's molars shape (**Fig 4A** and **5A**). Under wetter and less stressful environments as in L3 and L4a, where vegetation is expected to thrive, we observed broader molars, a characteristic of taxa that include plants in their diet (Casanovas-Vilar *et al.*, 2011). On the opposite, under drier and warmer conditions as in L2, when vegetation is supposed to be scarcer, molars display a slight buccolingual compression and elongation. In rodents, teeth morphology is highly related to dietary habits (Gómez Cano *et al.*, 2013; Verde Arregoitia *et al.*, 2017), and most rodents are known for being opportunistic feeders (Nowak, 1999; Cox & Hautier, 2015). It means that their diet can vary greatly according to available resources, ranging from faunivory to herbivory. Our results support that water stress, temperature and insolation impact more teeth shape parameters than other climate variables. Being three major factors of plant community composition, we assume that climate indirectly influences tooth shape *via* available resources through selection. Depending on the resources available, and thus climatic conditions, our results suggest that rodents adjust their diet towards more faunivorous or more herbivorous habits. This is consistent with what we know of the current diet of some species in our sample: *Meriones shawii* (which is highly abundant in our sample) seems to have a preference for plants, especially grasses, but adds a few arthropods to its meal in summer when vegetation is less abundant (Zaime & Gautier, 1989;

Adamou-Djerbaoui *et al.*, 2013), and *Mus spretus*'s diet reflects more available resources rather than any dietary preference (Palomo, Justo, & Vargas, 2009).

MGs also split rodent's teeth variability over this shape gradient ranging from large and slender molars to small and broad molars (**Fig 3**). This pattern of intra-population variation was also evidenced in the house mice *Mus musculus* (Renaud, Pantalacci, & Auffray, 2011; Ledevin *et al.*, 2016) and the wood mouse *Apodemus sylvaticus* (Renaud *et al.*, 2009), and it characterizes the main direction of dental variation in fossil rodents (Renaud, Auffray, & Michaux, 2006). This pattern seems then to be shared among Muridae, and Renaud *et al.* (2011) suggested that its conservation over millions of years supports that it may result from intrinsic developmental properties. This conserved pattern may constitute a potential to repeatedly evolve broad molars (Renaud & Michaux, 2004).

This pattern of teeth's shape variation is shared with Carnivora, a group that also exhibits a broad range of diets. Slender teeth seem to be a specialization for shearing or slicing in both carnivorans (Ungar, 2010) and murine rodents having a more faunivorous diet (Gómez Cano *et al.*, 2013). Such a diet-related similarity between those two groups has also been evidenced by Evans *et al.* (2007) who showed that, despite the lack of proximity between their tooth morphology, their tooth crowns complexity reflects the food consumed more than taxonomy.

Shrew's mandible shape is also statistically significantly impacted by climate (**Fig 6B**). But, surprisingly, the mandible body is thinner and longer under more arid climates, and thicker and shorter under more humid climates. This trend is opposite to what we expected. Under drier climate, insects are known to display a harder cuticle to better retain water (Klocke & Schmitz, 2011), and Young *et al.* (2007) supports that the harder the food, the greater the biting force and the shorter and thicker the mandible. A plausible explanation might reside in that under wetter and colder conditions, we found smaller shrews (this result is discussed further below). Size is one of the main drivers of bite force, resulting in larger individuals biting harder (Herrel *et al.*, 2008a; Chazeau *et al.*, 2013; Manhães *et al.*, 2017; Ginot *et al.*, 2018). Then, smaller individuals may be selected on shapes associated with stronger bite force to eventually compensate for their small size (Herrel & Gibb, 2006).

Mandible shape was found to be more sensitive to climate than the m1 (**Table 4**), which is not really surprising. Climate may indirectly impact mandibles more deeply than teeth because the functional constraints related to feeding result in mechanical constraints on the

bone. However, bones are known for being a highly plastic material in constant remodeling in response to physical constraints in their environments (Wolff, 1892; West-Eberhard, 1989; Currey, 2003), and muscular constraints have been evidenced to induce bone remodeling (Weijs & Hillen, 1986; Raadsheer *et al.*, 1999; Mavropoulos, Bresin, & Kiliaridis, 2004). This phenomenon has been evidenced on shrew's skulls *via* muscle insertions (Cornette *et al.*, 2015d), and it is highly likely that it also applies on the mandible. Conversely, the mandible and the M1 do not display a statistically significant difference in sensibility to climate, likely because both structures carry an important ecomorphological signal (Renaud & van Dam, 2002; Renaud *et al.*, 2011).

Impact of climate on size

Both m1 and M1 are larger under cooler and wetter climates (**Fig 4C** and **5C**). Teeth enlargement can mean two things: it could indicate larger individuals, but it also can be the result of a compromise between the sizes of the first, the second and the third molars. Indeed, the relative importance of each tooth, in particular the first and the third, is related to ecological parameters (Gomes Rodrigues, 2015b). However, in our results, m1 and M1 size are equally impacted by climate. The fact that teeth size varies in the same way may result from their common relationship with body size, as suggested by Kurtén (1967). Thus, molars size is thought to be a good proxy for animal size. We therefore chose to interpret our results by considering molar size as an indicator of body size, although the second hypothesis cannot be completely discarded and remains to be tested. Hence, we observe that rodents are larger during cooler and wetter periods. This result is consistent with Bergmann's rule (Bergmann, 1848; Ashton, Tracy, & Queiroz, 2000; Meiri & Dayan, 2003). However, even if our results do not contradict Bergmann's rule, it has been suggested that food availability may drive rodent body size more than temperature (Alhajeri & Steppan, 2016). We found that size is related to several climate variables susceptible to have an impact on food resources and not only to temperature, suggesting that the hypothesis of Alhajeri & Steppan (2016) might be more relevant than Bergmann's rule.

Regarding shrews, we found individuals with larger mandibles under warmer and drier climates than under cooler and wetter climates (**Fig 6C**). If we consider mandible size as a proxy for body size, those results are opposite to Bergmann's rule (Bergmann, 1848; Ashton *et al.*, 2000; Meiri & Dayan, 2003). However, to our knowledge, evidences for

Bergmann's rule in *Crocidura* rely on observations more than statistical testings (Piper, 2008; van der Geer *et al.*, 2013), and other shrews species were not found to follow it (Ochocińska & Taylor, 2003; Kouvari *et al.*, 2021). If shrews are mainly insectivorous, they are also generalists faunivorous and are known to sometimes add larger preys as lizards to their ration (Brahmi *et al.*, 2012). Under drier climate, the diversity of prey must be considerably reduced and a larger mandible may provide an advantage to capture and eat larger preys as it is the case for bats (Santana & Cheung, 2016).

Some studies supported that size could be a line of least resistance to evolution (Marroig & Cheverud, 2005; Renaud *et al.*, 2011). Our results do not support this hypothesis, as climate does not impact size more than all other shape parameters (**Table 4**). Moreover, size of both rodents and shrews covary with climate with a time lag of at least one stratigraphic layer. We could interpret this lag as the time needed for populations to adjust to new environmental conditions, suggesting a delay in the size response.

Allometry

After examining shape and size separatly, we explored allometry, the study of the consequences of size on shape (Gould, 1966). A significant but weak allometric signal was found in the three structures. In rodent's teeth size explains ~10 % of shape variation in both m1 and M1, which is quite low but within the range of allometry usually found in rodent's teeth (e.g., ~3% in the insular mice as found by Ledevin *et al.* (2016) and ~ 20% in the Orkney vole as found by Cucchi *et al.* (2014)). In shrew's mandible size explains ~5 % of shape variation, which is, once aigain, quite low but within the range of allometry usually found in shrew mandibles (e.g., ~ 2% in *Suncus estrucus* as found by Kouvari *et al.* (2021) and ~ 26% in the greater white-toothed shrew as found by Cornette *et al.* (2012))

We also found that MGs of rodent's teeth display statistically significant different allometric patterns. This is not the case for shrew's mandibles, which is consistent with the fact that shrew's mandibles MGs do not differ significantly in size.

Impact of climate on the relative abundance in MGs

The relative abundance in MGs is significantly related to climate (**Fig 4B** and **5B**) and seems linked to a particular change in climate: the seasonal variation in insolation, water

stress and temperature, which therefore conditions the seasonal variation of vegetation. As the MGs range from slender to broad teeth, this corroborates the conclusions of Ledevin *et al.* (2016) that the slender versus broad pattern is involved in differences in seasonality. As discussed above, slender versus broad teeth morphologies can result from shifts between more faunivorous and more herbivorous habits. Rapid morphological variation can occur at intraspecific level over a few decades (Cornette *et al.*, 2012; Karagic, Meyer, & Hulsey, 2020; Kouvari *et al.*, 2021). Thus, changes in the amplitude of seasonal variation might impact the proportions of relatively more faunivorous and herbivorous morphs (**Fig 8**).

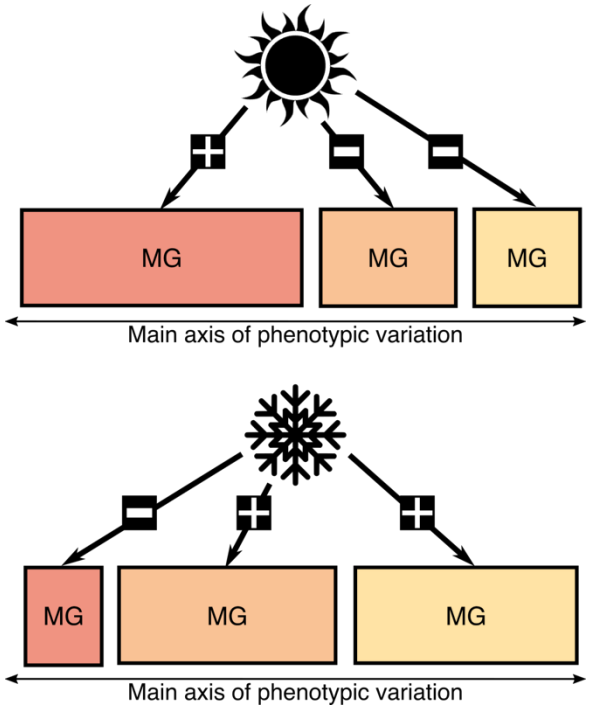

Fig 8. Diagram showing how a change in climate can impact the relative abundance in MGs.

Regarding shrews (**Fig 6B**), MGs split the mandible variability between thin and elongated mandibles associated to soft eater shrews, short and thick mandibles associated to hard eater shrews and intermediate mandibles associated to generalist shrews (Young *et al.*, 2007; Cornette *et al.*, 2012, 2015b) as in chapter 2 (Terray *et al.*, 2021). The relative abundance in MGs is also mainly related to climate seasonal variations. The generalist group is predominant under more stressful and warmer conditions, which makes sense given that the possible reduction of the number of prey may not allow specialist eaters to find enough resources to survive.

Impact of climate on modularity

We found no relationship between climate and the modularity of the teeth or the mandible (**Table 2**). Regarding shrews, these results echo those of Kouvari *et al.* (2021) who found the modularity between the mandibular branch and body to be not informative compared to environmental variation.

Both the teeth and the mandible are found to be highly modular structures. Conith *et al.* (2020) support that strong and conserved patterns of modularity may allow faster shape changes and may facilitate repeated transitions between habitats. Thus, modularity may not be impacted by climate, but a high degree of modularity might be selected under highly variable climate conditions because they facilitate the adjustment of organisms to their environment.

The next step would be to study modularity according to a more functional modularity pattern that relies on muscle insertions (e.g., Anderson *et al.*, 2008; Cornette *et al.*, 2012) instead of the developmental pattern (Cheverud *et al.*, 1997; Mezey *et al.*, 2000; Klingenberg *et al.*, 2003; Klingenberg, 2004). Indeed, functional modularity is thought to increase under environmental stress (Badyaev, Foresman, & Young, 2005), thus facilitating functional changes (Young *et al.*, 2007, 2010).

Impact of climate on disparity

We did not detect any impact of climate on disparity (**Table 2**) (nor of the local environment, as found in chapter 1). Maybe the time scale at which we examine the phenotypic response is too short to evidence responses in disparity, or disparity might be influenced by another factor than climate. Ledevin *et al.* (2016) evidence that climate is not the main factor driving the molar shape of the insular mice, and that competition has a greater impact on it. (Cornette *et al.*, 2015c) also suggested that competition more than climate might be driving the relative abundance of *Crocidura* species on EH2. Then, competition, as well as other ecological factors, may be the main determinant of disparity patterns.

Difference(s) in responsiveness to climate changes between morphological and functional traits

We found no significant differences between the impact of climate on morphological and functional traits (**Table 4**). We hypothesized that functional and morphological traits could participate in a decoupled way and with different intensities to phenotypic evolution. Contrary to our hypothesis, functional and morphological traits do not display different sensibility to climate changes. However, our results do not allow us to completely reject the hypothesis that functional traits may be more sensible to climate changes than morphological traits. The trait used here is an estimate of bite force, and not the bite force itself. For example, it neglects the part of bite force modulated by soft tissues, as muscles, which are an essential component of bite force strength. Moreover, the biomechanical model used here is based only on the temporalis muscle, which is not the only muscle involved in bite force (Herrel *et al.*, 2008a,a; Santana *et al.*, 2010; Brassard *et al.*, 2021), even though it is the main one in shrews (Cornette *et al.*, 2015d). Consequently, this hypothesis deserves to be tested in a more controlled context.

Difference(s) in the phenotypic response in the Anthropocene

Several results point towards a significant change in the phenotypic response since the entry into the Anthropocene. Regarding rodent's teeth, the relative abundance in MGs on L0 is less correlated to climate than on other layers (**Fig 4B** and **5B**). For shrew's mandible, it is not at all related to climate when L0 is taken into account (**Table 2**). Human-induced changes caused important variations in the composition of communities, both through the extinctions of somes species and populations (Ceballos *et al.*, 2017) and through the introduction of invasive species (Hill & Hadly, 2018). It is then consistent that it impacts the abundance of morphs, resulting in that the relative abundance in MGs may currently be more driven by human-induced changes than by climate changes. Moreover, there is a clear drop in the shrew's estimated bite force on L0 (**Fig 7**). Maybe new selective pressure(s) might currently interfere with climate, as anthropic disturbances. As shown by Renaud *et al.* (2015) in the house mouse and Kouvari *et al.* (2021) in *Suncus* shrews, recent anthropogenic disturbances may have induced important non functionally relevant changes in the feeding apparatus (i.e. functional changes without increase of performance).

According to climate simulations from chapter 3, current climate conditions on EH2 do not exceed the range of climate conditions encountered in the past. This is supported by the fact that L0 is not on an extremity of the climate gradient computed based on Euclidean distances between the climates of the layers (**Fig 4, 5, 6** and **7**). Except regarding shrews estimated bite force, that would require further investigations, the phenotypes present on current days are not that different from the phenotypes found in the fossil record of EH2. Thus, Anthropocene changes do not appear to have a huge impact on the climate and the fauna at EH2 yet. Maybe the time scale at which we examine the Anthropocene is too recent to evidence drastic changes in climate and phenotypes. Predictions support that future climate changes will be more radical than those observed in the past (Foster *et al.*, 2017), and by 2050 temperatures in Morocco are expected to rise between 2 and 3°C (Schilling *et al.*, 2012). It is therefore not impossible in the future to observe much more different phenotypes than those present in the past in response to these drastic climate changes. This point will be discuss in the perspectives section.

Conclusion

In this chapter, we explored the impact of global climate changes on the phenotype of small mammals. We found that climate has an important impact on the phenotype of both rodents and shrews. Water stress, temperature and insolation have a greater impact on phenotypic parameters, more than other climate variables. Being three major factors of plant community composition, we assume that they indirectly influence the phenotype *via* available resources. Regarding rodents, climate induced changes in teeth shape related to shifts in their feeding habits between predominantly faunivorous and herbivorous diets. For shrews, the mandible shape associated with a more generalist diet is favored under drier and more stressful conditions. Mandible shape was found to be more impacted by climate than teeth shape, which was expected considering its greater plastic potential due to bone remodeling (*via* rapid selection or phenotypic plasticity). Morphological groups revealed patterns of intra-specific variation that reflect morphological adjustments to climate seasonal variations. Both teeth and the mandible were found to be highly modular structures. Those strong and conserved patterns of modularity may have been selected because they allow for faster shape changes and, thus, may facilitate repeated transitions between habitats. Conversely, disparity does not seem to be impacted at all by climate variations. The impact of climate on the morpho-functional aspects of the shrew mandible

is not the same in present days as in the past. This suggests the presence of another selective pressure, as anthropogenic disturbances. This new pressure might have induced non functionally relevant changes in the feeding apparatus since the entry into the Anthropocene.

Supplementary material

Table. S1 Results of the 2B-pls performed on shrew's mandible shape, relative abundance in MGs and estimated bite force with all layers and without each layer one by one. Grey cells indicate not statistically significant results.

Layers	Shape	MGs abundances	Estimated bite force
All layers	r-PLS = 0.68 Z = 3.54 p-value = 0.001	r-PLS = 0.64 Z = -0.41 p-value = 0.64	r-PLS = 0.51 Z = 3.06 p-value = 0.001
Without… L0	r-PLS = 0.62 Z = 1.41 p-value = 0.081	r-PLS = 0.96 Z = 1.56 p-value = 0.018	r-PLS = 0.28 Z = 0.81 p-value = 0.23
L1	r-PLS = 0.73 Z = 4.22 p-value = 0.001	r-PLS = 0.69 Z = -0.43 p-value = 0.614	r-PLS = 0.56 Z = 3.18 p-value = 0.001
L2	r-PLS = 0.69 Z = 3.46 p-value = 0.001	r-PLS = 0.69 Z = 0.044 p-value = 0.51	r-PLS = 0.51 Z = 2.97 p-value = 0.001
L3	r-PLS = 0.66 Z = 3.23 p-value = 0.001	r-PLS = 0.62 Z = -1.26 p-value = 0.85	r-PLS = 0.53 Z = 3.038 p-value = 0.001
L4a	r-PLS = 0.64 Z = 3.15 p-value = 0.001	r-PLS = 0.61 Z = -1.17 p-value = 0.84	r-PLS = 0.52 Z = 3.057 p-value = 0.001
L5	r-PLS = 0.72 Z = 3.43 p-value = 0.001	r-PLS = 0.68 Z = 0.0075 p-value = 0.49	r-PLS = 0.49 Z = 2.40 p-value = 0.005
L8	r-PLS = 0.75 Z = 3.68 p-value = 0.001	r-PLS = 0.64 Z = -0.41 p-value = 0.64	r-PLS = 0.57 Z = 3.061 p-value = 0.002

Conclusions & Perspectives

In this thesis, we explored the impact of environmental and climate variations on the phenotype of Moroccan rodents and shrews over the last 100 ka through a bi-disciplinary approach combining evolutionary biology and paleoclimatology. In this conclusion, we first summarize our main results regarding the complex relationship between the environment/climate and the phenotype of rodents and shrews. Then, we deepen the evolutionary and ecological meaning of MGs in the context of our phenotypic approach. For each, we discuss potential implications for future studies. Finally, we propose some directions to further exploit the potential of the bi-disciplinary approach.

The impact of local environment and global climate on the phenotype

Our results support that teeth and mandibles, even fragmented and unidentified ones, carry a significant and interpretable ecomorphological signal, in agreement with the conclusions of Paine *et al.* (2019) and (Cornette *et al.*, 2015a,c) who praised the interest of isolated and unidentified remains. We found that both morphological and functional traits are equally impacted by external variations (environmental and climate variations), and that responses at different phenotypic scales seem to correspond to external variations at different scales. In chapter 1 and 2, we highlighted that local environmental changes mainly impact morphological and functional variation within MGs. In chapter 4, we showed that global climate variations over the region influence the between MGs variation. Thus, global climate changes seem to mainly impact global patterns of phenotypic variation, while local environmental changes seem to mostly affect more minor patterns of phenotypic variation. The environment/climate appears to impact the phenotype of organisms following a scale-dependent pattern (**Fig 1**). Few other studies also found such a scale-dependent relationship between external variations and phenotypic diversity. For example, Reum *et al.* (2011) demonstrated that local- and regional-scale environmental changes differently affect the abundance and distribution of forage fishes; and Garcia *et al.* (2014) evidenced a scale-dependent impact of current climate change on the demography and phenology of extant biodiversity. They showed that local changes mainly affect populations, while regional changes impact species and species assemblages.

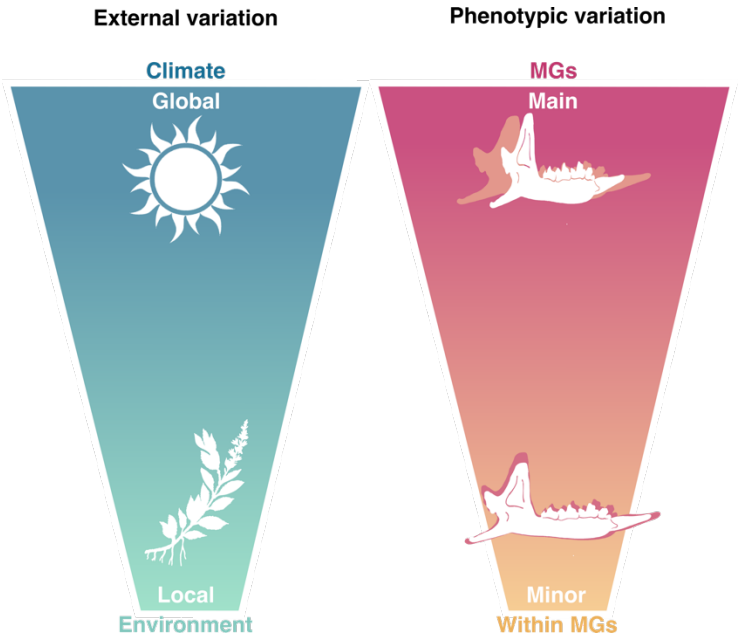

Fig. 1 Summary of the scale-dependent impact of external variations on the phenotype. Global climate changes mostly impact the main pattern of phenotypic variations, while local environmental changes mainly affect minor patterns of phenotypic variation.

The scale-dependent relationship we found between external and phenotypic variations may seem counterintuitive. Since the environment determines the surroundings of organisms (Begon *et al.*, 2006; Bhargava *et al.*, 2019), one would expect it to drive the phenotype more than global climate and atmospheric conditions. A possible explanation is that variations in the environment may be tempered by behavioral adjustments (Gross, Pasinelli, & Kunc, 2010; Candolin & Wong, 2012; Abreu *et al.*, 2016). Behavioral adjustments are often the first response when conditions are altered (Wong & Candolin, 2015). In particular, behavioral plasticity appears to be vital in helping to mitigate the impacts of these changes (Wong & Candolin, 2015). Behavioral adjustments may allow an organism to cope with the conditions of its immediate environment, and thus increase its fitness, without altering other aspects of its phenotype such as its morphology, functional abilities or physiology (Van Buskirk, 2012). Some rodents have been observed to modify their foraging behavior to track food availability, such as the African striped mouse *Rhabdomys pumilio* (Schradin & Pillay, 2006) or the wood mouse *Apodemus sylvaticus* (Butet, 1994). The wood mouse forages in the open landscape during the summer, being territorial, and retreats to the forest during the winter, sharing common shelters (Butet,

1994). On the contrary, behavioral buffering might not be sufficient for animals to cope with climate and atmospheric variations at a larger geographic scale (Wong & Candolin, 2015). Consequently, the scale-dependent relationship we found between external changes and phenotypic variations could also suggest that the levels of phenotypic variation (i.e. morphological, functional and behavioral) might be differentially involved in the phenotypic response. Environmental changes could trigger prominent behavioral responses, possibly related to behavioral plasticity (Wong & Candolin, 2015), accompanied by more minor morphological and functional responses. While, on the opposite, climatic variations could induce more important morphological and functional responses. In both cases, the morphological and functional responses might result from both/either phenotypic plasticity or adaptation. Although, it is important to keep in mind that while the mandible can indeed be subject to phenotypic plasticity through bone remodeling (Weijs & Hillen, 1986; Raadsheer *et al.*, 1999; Mavropoulos *et al.*, 2004), this is not the case for teeth, which are subject to phenotypic plasticity mainly through developmental plasticity (Karagic *et al.*, 2020; Selig *et al.*, 2021).

This scale-dependent relationship between the phenotype and external variations raises the delicate question of the choice of the phenotypic proxies when investigating the relationship between the phenotype and the environment/climate. Whether the addressed question is to evaluate the impact of the environment/climate on the phenotype, or to provide paleoenvironmental reconstructions from the phenotype, the choice of the studied phenotypic trait(s) must be carefully considered depending on the objectives of the study. Indeed, all phenotypic traits do not reflect environmental/climate changes at the same scale, nor the same type of variation. For example, the relative abundances in MGs are mainly related to seasonal variations . Thus, focusing on one phenotypic trait can be misleading, as they reflect different aspects of the environment. One way for future studies to circumvent this issue is to consider several phenotypic traits. The interest of such a multi-proxy approach over a single-proxy approach has been demonstrated by Pineda-Munoz *et al.* (2017). They showed that combining different morphological proxies provided a much better discrimination between dietary categories in mammals than each proxy separately.

This idea of a multi-proxy approach is in line with the growing interest over the past 30 years for the concept of phenomic (Houle *et al.*, 2010). The phenomic is defined as “the acquisition of high-dimensional phenotypic data on an organism-wide scale”. It involves collecting a large number of phenotypic traits from a large number of individuals. To tend

towards phenomic, i.e. to an integrative consideration of the phenotype, may be the next step in our comprehension of complex interactions between organisms and external factors, such as their environment. So far, the main challenges in addressing this goal lie in technical limitations in acquiring and analyzing such datasets. The promises of artificial intelligence algorithms, and especially machine learning methods seem to fulfill this need (Camacho *et al.*, 2018). Machine learning is a set of data analysis techniques aiming at building predictive models from high-dimensional datasets. In the past decade, several studies showed the advantages in these methods for acquiring high-dimensional datasets or analyzing them (e.g., Nath *et al.*, 2018; Li *et al.*, 2019; Courtenay *et al.*, 2019; Miele *et al.*, 2020; Devine *et al.*, 2020; Abellán *et al.*, 2021). Given the advantages of the multi-proxy approach for studying the relationship between phenotype and environment/climate demonstrated by our results, a phenomic approach could provide a deeper insight into this complex question. However, by the time such protocol is routine, understanding the complex relationship between the phenotype and the environment/climate can provide directions to select a subset of traits relevant to the question.

The evolutionary and ecological meaning of morphological groups

The MGs represent trans-specific groups of individuals which differ in shape and functional abilities (chapters 1, 2 and 4). They are distributed along the main axis of phenotypic variation, which is shared between several species and seems related to dietary ecology (chapter 4). Indeed, MGs partition individuals on the basis of morphological traits involved in the ability to consume certain resources. Regarding rodents, it distinguishes individuals who consume mainly plants from those who add animals to their diet. Concerning shrews, it separates soft eaters from hard eaters. This suggests that dietary niches are distributed at the populational level and not at the species level in our studied species. Individuals from different species can share a dietary niche because they consume the same ressources. On the contrary, conspecifics may occupy different dietary niches and consume different resources (**Fig 2**).

This perpendicular relationship between species and MGs may be explained by the fact that the groups studied here, rodents and shrews, are opportunistic feeders (Churchfield, 1990; Nowak, 1999; Cox & Hautier, 2015). Opportunism can sometimes be the result of within species pluri-specialization. It means that individuals of the same generalist species may

differ in such a way that the species is actually composed of many specialist individuals that feed differently from the species typical diet (Vander Zanden *et al.*, 2010; Pagani-Núñez, Valls, & Senar, 2015). Within species dietary variations in rodents have also been evidenced by microwears on teeth (Gomes Rodrigues, Merceron, & Viriot, 2009; Ungar *et al.*, 2021b). Here, this pluri-specialization seems to be shared between species, as illustrated by the fact that the same axis of main phenotypic variation is shared by many rodent species (Renaud *et al.*, 2006, 2009, 2011; Ledevin *et al.*, 2016). Such individual specialization is supported to be mainly determined by ecological opportunities and intra-specific competition (Araújo, Bolnick, & Layman, 2011), as individuals tend to avoid competition by searching for alternative food ressources (Roughgarden, 1972; Bolnick *et al.*, 2003; Araújo *et al.*, 2011). Both depend on the type and the amount of available resources, which are related to climate conditions.

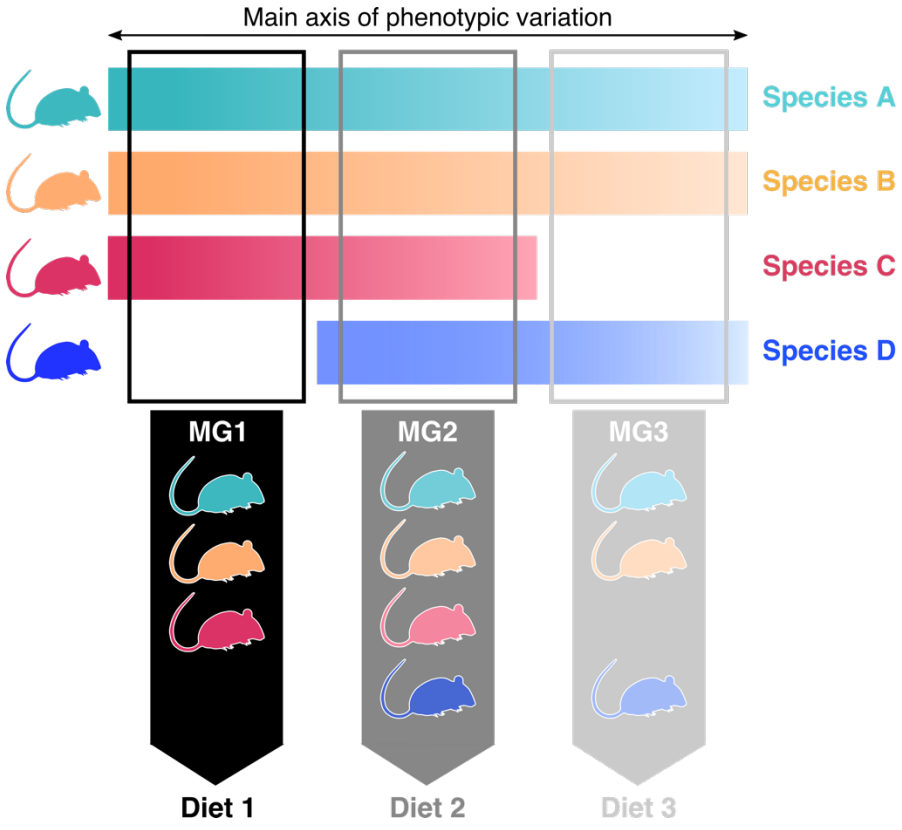

Fig. 2 Diagram of the relationship between species, morphological groups (MG) and dietary ecology.

In ecology, groups of individuals that display correlations among morphology and ecology but not lineage are referred to as ecomorphs (Williams, 1983). The most emblematic group

of ecomorphs is undeniably *Anolis* lizards. They colonized several Caribbean islands, and independently and repeatedly evolved six ecomorphs adapted to different microhabitats (Losos, 1990a,b; Herrel *et al.*, 2008b; Feiner *et al.*, 2020). Ecomorphs have also been evidenced in several other groups, such as birds (Karr & James, 1975) and spiders (Gillespie *et al.*, 2018). In rodents, ecomorphs related to dietary ecology have been identified (e.g., Miljutin, 2011; Rowe, Achmadi, & Esselstyn, 2016). Consequently, the use of ecomorphs offers significant advantages in the case of species with poorly known ecology. This approach may be particularly useful in the context of archeological and paleontological studies. Microfaunal remains are extremely abundant and often difficult to identify, and most methods to evaluate past biodiversity rely on species occurrences and species abundances. Our results demonstrate that, first, even unidentified remains contain an informative ecomorphological signal, allowing one to greatly increase its dataset. Secondly, even when there is no apparent species turnover, as is the case at EH2, variations in morphotypes can be highly informative. Thus, future works addressing the relationship between phenotype and the environment/climate over time may reveal a more important ecological signal by examining ecomorphs in addition to species. This approach also has the potential to be a powerful ally in measuring the extent of the sixth mass extinction crisis. Indeed, because we mostly rely on extinctions to evaluate it, the contemporary biological annihilation might be underestimated (Skelly *et al.*, 2007; Ceballos *et al.*, 2017). Looking at ecomorphs could provide information about the within species response to climate changes before population or species extinctions occur. Moreover, it can easily provide an estimation of functional diversity in addition to taxonomic diversity, an aspect of biodiversity also greatly endangered by the ongoing climate change (Carmona *et al.*, 2021).

The benefits and limits of the bi-disciplinary approach

Couvreur *et al.* (2020) mentioned that one of the next challenges in the study of African biodiversity is to consider in a common framework Earth and life sciences. Here, we attempted to address this issue by conducting a study combining evolutionary biology and paleoclimate modeling in a common analytical framework. The potential of this bi-disciplinary approach opens a whole new range of possible advances for both fields.

First, paleoclimate simulations could be a powerful tool to refine the chronological context of archeological and paleontological sites. Depending on the average age of a stratigraphic

layer, all dating methods do not have the same reliability. For layers older than 20 000 years, it is possible to date biological material such as teeth using combined US-ESR methods (combination of uranium series and electron spin resonance) or to date the sediment using OSL methods (Optical Stimulated Luminescence), while for layers younger than 50 000 years dating based on AMS-^{14}C (radiocarbon dating) are more reliable. Dates estimated from different methods can display important discrepancies (e.g., Ben Arous *et al.*, 2020a). As we did in chapter 3, the consistency between the climate described by paleoclimate simulations and environmental proxies can provide arguments to discuss discrepancies between non-congruent dating.

Paleoclimate simulations could also contribute to refine the paleoenvironmental context of archeological and paleontological sites. Paleoclimate simulations can help decide between inconsistent paleoenvironmental proxies. To improve the accuracy of this approach, downscaling (statistical or dynamical) methods may be applied on paleoclimate simulations. Downscaling is a procedure which makes predictions at local scale from information at large scale. It corrects or interpolates simulation outputs to take regional characteristics into account (as topography, distance to the coastline, etc), thus producing more accurate regional climate estimations. The use of downscaling might reduce the differences between paleoclimate simulations and paleoenvironmental proxies that are due to the difference in scale between the quantified environmental features (Ekström, Grose, & Whetton, 2015).

Conversely, biological data may also be a useful asset to test the reliability of paleoclimate simulations. Biological indicators such as species and morphotype climate niches could be used to validate simulated paleoclimates on precise localities. In particular, the shape of the faunal remains as teeth and mandibles are tightly related to the vegetation. They could be useful to test the accuracy of dynamic vegetation schemes recently included in paleoclimate models.

The main limitation in crossing those two fields lies in their difference in dating resolution. To date a stratigraphic layer is complex. An archeological layer is a palimpsest. It is an accumulation of materials with composite dates, over an unknown time interval. We can date certain objects within this layer to place it approximately. However, several informations are not available, such as the interval that the layer covers. It depends on the thickness of the deposit, which is known, but also on the duration of the deposit, which is not known. To date objects belonging to the lower and upper ends of a layer would not be

sufficient either, because these objects could have been mixed when the deposit was not yet fixed. On the other hand, climate simulations characterize the climatic state at a specific date, determined notably by orbital parameters, gas concentrations and topographic configuration. Often, the uncertainty of a stratigraphic dating can cover very different climatic states, and an arbitrary choice must be made in the selection of the exact period for which the climate simulation is run.

Perspectives

Many aspects of the relationship between the phenotype and the environment and climate remain to be investigated. We present here some of the directions we are considering in pursuing this thesis work.

Firstly, a way to further investigate the scale-dependent relationship we found between the phenotype and external variations would be to explore the spatial variability of the phenotype in addition to the temporal variability. Adding the spatial dimension would allow us to explore variations in the distribution of MGs over time and, in the case other sites have undergone faster or slower changes, to assess whether the intensity of the phenotypic response varies with the speed and/or the intensity of environmental variations. This could be done by completing our dataset with material from other archeological sites, contemporary of EH2. Some of the other Rabat-Témara sites (Contrebandiers, El Mnasra and Dar es Soltan 1) and of the eastern Morocco sites (Ifri n'Ammar, Rhafas and Taforalt) are promising candidates as they are attributed to a period similar to that of EH2 (Ben Arous *et al.*, 2020a). They would allow us to cover all the north of Morocco, and to contrast littoral regions with more continental ones. In a second step, we could enlarge our geographical range to the African continent by including sites from South Africa and East Africa. Those regions present different environmental constraints and different climate conditions, and some archeological sites (e.g. Elandsfontein for South Africa (Braun *et al.*, 2013) and Goda Buticha for East Africa (Tribolo *et al.*, 2017)) could provide material contemporary of EH2.

A second direction concerns a deepening of the biological meaning of the MGs. An inconvenience of the MG approach is that the number of groups identified can vary between biological structures from the same individuals. It is illustrated by the difference in the number of MGs obtained for M1 (five in chapter 4) and m1 (three in chapter 4). Several sources of variability contribute to the phenotypic diversity, such as diet, microhabitat and

other ecological factors, but also phylogenetic history or sexual dimorphism for example. It implies that from one structure to another, MGs might not be related to the same source(s) of variability. To further explore the potential of the MG approach, and the relationship between MGs and ecomorphs, a lead may be to investigate the relationship between the biological structures and the potential sources of variability. It could be done by conducting a MG study on several structures (e.g., the teeth, the mandible, the tympanic bullae, and other morphological features) on species whose ecology and phylogenetic history are well known, to highlight the link between the MGs of the different structures and the different source(s) of variability. Results of such a study could allow one to better interpret MGs variations in fossil representatives.

A third perspective would be to turn to the future and use our results to quantify the potential consequences of the Anthropocene on the phenotype of small mammals. Considering the ongoing climate change, a major concern is how organisms will cope with future climate changes. The projections suggest more radical climate changes in the future than those observed in the past (Foster *et al.*, 2017), requiring species' rates of dispersal that are probably unprecedented in vertebrates (Quintero & Wiens, 2013). The IPCC (Intergovernmental Panel on Climate Change) produced an ensemble of climate projections under the different Shared Socioeconomic Pathways (SSPs), which are based on different socio-economic development assumptions (Riahi *et al.*, 2017), to predict future climates. These simulations have been used in ecological niche studies to predict the future distribution of some species (e.g., Ramasamy *et al.*, 2021; Gür, 2021; Meyer & Pie, 2021). However, ecological niche studies, by considering only distribution, often neglect the fact that organisms can evolve. To test if evolutionary processes could allow organisms to cope with future climate changes, we could predict what phenotypic changes would be required. We could use our covariation analyses to predict the morphology of rodents teeth and shrews mandible, as well as shrews estimated bite force, under these different climate scenarios. If predicted morphological and functional changes have an interpretable biological meaning, they could constitute potential directions of phenotypic responses to future climate changes.

This thesis as seen by Wombo Dream, creator of AI-powered paintings.

(https://app.wombo.art)

References

Abellán N, Jiménez-García B, Aznarte J, Baquedano E, Domínguez-Rodrigo M (2021) Deep learning classification of tooth scores made by different carnivores: achieving high accuracy when comparing African carnivore taxa and testing the hominin shift in the balance of power. Archaeol. Anthropol. Sci. 13: 31.

Abreu F, De la Fuente MFC, Schiel N, Souto A (2016) Feeding ecology and behavioral adjustments: flexibility of a small neotropical primate (Callithrix jacchus) to survive in a semiarid environment. Mammal Res. 61: 221–229.

Adamou-Djerbaoui M, Denys C, Chaba H, Seid MM, Djelaila Y, Labdelli F (2013) Etude du régime alimentaire d'un rongeur nuisible (*Meriones shawii* Duvernoy, 1842, Mammalia, Rodentia) en Algérie. Leban. Sci. J. 14: 18.

Adams DC (2016) Evaluating modularity in morphometric data: challenges with the RV coefficient and a new test measure (P Peres-Neto, Ed.). Methods Ecol. Evol. 7: 565–572.

Adams DC, Collyer ML (2016) On the comparison of the strength of morphological integration across morphometric datasets. Evolution 70: 2623–2631.

Adams DC, Otárola-Castillo E (2013) geomorph: an R package for the collection and analysis of geometric morphometric shape data (E Paradis, Ed.). Methods Ecol. Evol. 4: 393–399.

Adams DC, Rohlf FJ, Slice DE (2013) A field comes of age: geometric morphometrics in the 21st century. Hystrix Ital. J. Mammal.

Aguirre LF, Herrel A, Van Damme R, MatThysen E (2003) The implications of food hardness for diet in bats: *Ecomorphology of food partitioning in bats*. Funct. Ecol. 17: 201–212.

Alegret L, Thomas E, Lohmann KC (2012) End-Cretaceous marine mass extinction not caused by productivity collapse. Proc. Natl. Acad. Sci. 109: 728–732.

Alfaro ME, Bolnick DI, Wainwright PC (2005) Evolutionary Consequences of Many-to-One Mapping of Jaw Morphology to Mechanics in Labrid Fishes. Am. Nat. 165: E140–E154.

Alhajeri BH (2018) Craniomandibular variation in the taxonomically problematic gerbil genus Gerbillus (Gerbillinae, Rodentia): assessing the influence of climate, geography, phylogeny, and sangilettaize. J. Mamm. Evol. 25: 261–276.

Alhajeri BH, Hunt OJ, Steppan SJ (2015) Molecular systematics of gerbils and deomyines (Rodentia: Gerbillinae, Deomyinae) and a test of desert adaptation in the tympanic bulla. J. Zool. Syst. Evol. Res. 53: 312–330.

Alhajeri BH, Steppan SJ (2016) Association between climate and body size in rodents: A phylogenetic test of Bergmann's rule. Mamm. Biol. 81: 219–225.

Alhajeri BH, Steppan SJ (2018) Ecological and Ecomorphological Specialization Are Not Associated with Diversification Rates in Muroid Rodents (Rodentia: Muroidea). Evol. Biol. 45: 268–286.

Alperin MI, Cusminsky GC, Bernasconi E (2011) Benthic foraminiferal morphogroups on the argentine continental shelf. J. Foraminifer. Res. 41: 155–166.

Anderson TF, Arthur MA (1983) Stable isotopes of oxygen and carbon and their application to sedimentological and palaeoenvironmental problems. In: Arthur MA, Anderson TF, Kaplan IR, Veizer J, Land LS (eds.) Stable Isot. Sediment. Geochem. Soc. Econ. Palaeontol. Mineral. Short Course Vol 10., 1.1-1–151.

Anderson RA, Mcbrayer LD, Herrel A (2008) Bite force in vertebrates: opportunities and caveats for use of a nonpareil whole-animal performance measure: bite force in vertebrates. Biol. J. Linn. Soc. 93: 709–720.

Angilletta, Jr MJ, Dunham AE (2003) The temperature-size rule in ectotherms: simple evolutionary explanations may not be general. Am. Nat. 162: 332–342.

Araújo MS, Bolnick DI, Layman CA (2011) The ecological causes of individual specialisation: The causes of individual specialisation. Ecol. Lett. 14: 948–958.

Arnold SJ (1983) Morphology, Performance and Fitness. Am. Zool. 23: 347–361.

Arnold SJ, Pfrender ME, Jones AG (2001) The adaptive landscape as a conceptual bridge between micro- and macroevolution. In: Hendry AP, Kinnison MT (eds.) Microevolution Rate Pattern Process. Dordrecht, Springer Netherlands, 9–32.

Ashton KG, Tracy MC, Queiroz A de (2000) Is Bergmann's Rule Valid for Mammals? Am. Nat. 156: 390–415.

Aubret F, Shine R (2009) Genetic Assimilation and the Postcolonization Erosion of Phenotypic Plasticity in Island Tiger Snakes. Curr. Biol. 19: 1932–1936.

Avery DM (1982) Micromammals as paleoenvironmental indicators and an interpretation of the late Quaternary in the Southern Cape Province. Ann. South Afr. Mus. 85: 183–374.

Avery DM (2007) Pleistocene micromammals from Wonderwerk Cave, South Africa: practical issues. J. Archaeol. Sci. 34: 613–625.

Badyaev AV, Foresman KR (2000) Extreme environmental change and evolution: stress-induced morphological variation is strongly concordant with patterns of evolutionary divergence in shrew mandibles. Proc. R. Soc. Lond. B Biol. Sci. 267: 371–377.

Badyaev AV, Foresman KR (2004) Evolution of Morphological Integration. I. Functional Units Channel Stress-Induced Variation in Shrew Mandibles. Am. Nat. 163: 868–879.

Badyaev AV, Foresman KR, Young RL (2005) Evolution of Morphological Integration: Developmental Accommodation of Stress-Induced Variation. : 14.

Baker RJ, Bradley RD (2006) Speciation in mammals and the genetic species concept. J. Mammal. 87: 643–662.

Bar-Matthews M, Marean CW, Jacobs Z, Karkanas P, Fisher EC, Herries AIR, Brown K,

Williams HM, Bernatchez J, Ayalon A, Nilssen PJ (2010) A high resolution and continuous isotopic speleothem record of paleoclimate and paleoenvironment from 90 to 53 ka from Pinnacle Point on the south coast of South Africa. Quat. Sci. Rev. 29: 2131–2145.

Baylac M, Frieß M (2005) Fourier Descriptors, Procrustes Superimposition, and Data Dimensionality: An Example of Cranial Shape Analysis in Modern Human Populations. In: Slice DE (ed.) Mod. Morphometrics Phys. Anthropol. New York, Kluwer Academic Publishers-Plenum Publishers, 145–165.

Begon M, Townsend CR, Harper JL (2006) *Ecology: from individuals to ecosystems*. Malden, MA, Blackwell Pub.

Behrensmeyer AK, Kidwell SM, Gastaldo RA (2000) Taphonomy and paleobiology. Paleobiology 26: 103–147.

Belmaker M, Hovers E (2011a) Ecological change and the extinction of the Levantine Neanderthals: implications from a diachronic study of micromammals from Amud Cave, Israel. Quat. Sci. Rev. 30: 3196–3209.

Belmaker M, Hovers E (2011b) Ecological change and the extinction of the Levantine Neanderthals: implications from a diachronic study of micromammals from Amud Cave, Israel. Quat. Sci. Rev. 30: 3196–3209.

Ben Arous E, Falguères C, Tombret O, El Hajraoui MA, Nespoulet R (2019) Combined US-ESR dating of fossil teeth from El Harhoura 2 cave (Morocco): New data about the end of the MSA in Temara region. Quat. Int.: S1040618218310668.

Ben Arous E, Falguères C, Nespoulet R, El Hajraoui MA (2020a) Review of chronological data from the Rabat-Temara caves (Morocco): Implications for understanding human occupation in north-west Africa during the Late Pleistocene. In: Leplongeon A, Goder-Goldberger M, Pleurdeau D (eds.) Just Corridor Hum. Occup. Nile Val. Neighb. Reg. 75000 15000 Years Ago. Paris, 177–201.

Ben Arous E, Falguères C, Tombret O, El Hajraoui MA, Nespoulet R (2020b) Combined US-ESR dating of fossil teeth from El Harhoura 2 cave (Morocco): New data about the end of the MSA in Temara region. Quat. Int. 556: 88–95.

Bergmann C (1848) Über die Verhältnisse der Wärmeökonomie der Thiere zu ihrer Grösse. Gött. Stud. 3: 595–708.

Bergmann PJ, McElroy EJ (2014) Many-to-Many Mapping of Phenotype to Performance: An Extension of the F-Matrix for Studying Functional Complexity. Evol. Biol. 41: 546–560.

Bernal R, Bacon CD, Balslev H, Hoorn C, Bourlat SJ, Tuomisto H, Salamanca S, Manen MT, Romero I, Sepulchre P, Antonelli A (2019) Could coastal plants in western Amazonia be relicts of past marine incursions? J. Biogeogr. 46: 1749–1759.

Bhargava RN, Rajaram V, Olson K, Tiede L (2019) *Ecology and Environment*.

Bickford D, Howard SD, Ng DJJ, Sheridan JA (2010) Impacts of climate change on the amphibians and reptiles of Southeast Asia. Biodivers. Conserv. 19: 1043–1062.

Blois JL, McGuire JL, Hadly EA (2010) Small mammal diversity loss in response to late-

Pleistocene climatic change. Nature 465: 771–774.

Blome MW, Cohen AS, Tryon CA, Brooks AS, Russell J (2012) The environmental context for the origins of modern human diversity: A synthesis of regional variability in African climate 150,000–30,000 years ago. J. Hum. Evol. 62: 563–592.

Blondel J, Ferry C, Frochot B (1973) Avifaune et végétation. Essai d'analyse de la diversité. Cent Ecol Camargue 13- Sambuc.

Bocxlaer BV, Schultheiß R (2010) Comparison of morphometric techniques for shapes with few homologous landmarks based on machine-learning approaches to biological discrimination. Paleobiology 36: 497–515.

Bolaji TA, Ndukwe OS, Oyebamiji AR, Ikegwuonu ON (2020) Palynological Age Control and Paleoenvironments of the Paleogene Strata in Eastern Dahomey Basin, Southwestern Nigeria. Sci. Rep. 10: 8991.

Bolnick DI, Svanbäck R, Fordyce JA, Yang LH, Davis JM, Hulsey CD, Forister ML (2003) The Ecology of Individuals: Incidence and Implications of Individual Specialization. Am. Nat. 161.

Bonhomme V, Picq S, Gaucherel C, Claude J (2014) Momocs: outline Analysis Using R. J. Stat. Softw. 56.

Bookstein FL (1996) Landmark Methods for Forms Without Landmarks: Localizing Group Differences in Outline Shape. Univ. Mich. Ann Arbor Mich.: 11.

Boucher O, Servonnat J, Albright AL, Aumont O, Balkanski Y, Bastrikov V, Bekki S, Bonnet R, Bony S, Bopp L, Braconnot P, Brockmann P, Cadule P, Caubel A, Cheruy F, Codron F, Cozic A, Cugnet D, D'Andrea F, Davini P, Lavergne C, Denvil S, Deshayes J, Devilliers M, Ducharne A, Dufresne J, Dupont E, Éthé C, Fairhead L, Falletti L, Flavoni S, Foujols M, Gardoll S, Gastineau G, Ghattas J, Grandpeix J, Guenet B, Guez L E, Guilyardi E, Guimberteau M, Hauglustaine D, Hourdin F, Idelkadi A, Joussaume S, Kageyama M, Khodri M, Krinner G, Lebas N, Levavasseur G, Lévy C, Li L, Lott F, Lurton T, Luyssaert S, Madec G, Madeleine J, Maignan F, Marchand M, Marti O, Mellul L, Meurdesoif Y, Mignot J, Musat I, Ottlé C, Peylin P, Planton Y, Polcher J, Rio C, Rochetin N, Rousset C, Sepulchre P, Sima A, Swingedouw D, Thiéblemont R, Traore AK, Vancoppenolle M, Vial J, Vialard J, Viovy N, Vuichard N (2020) Presentation and Evaluation of the IPSL-CM6A-LR Climate Model. J. Adv. Model. Earth Syst. 12.

Boutin S, Lane JE (2014) Climate change and mammals: evolutionary versus plastic responses. Evol. Appl. 7: 29–41.

Bown TM, Holroyd PA, Rose KD (1994) Mammal extinctions, body size, and paleotemperature. Proc. Natl. Acad. Sci. 91: 10403–10406.

Braconnot P, Harrison SP, Kageyama M, Bartlein PJ, Masson-Delmotte V, Abe-Ouchi A, Otto-Bliesner B, Zhao Y (2012) Evaluation of climate models using palaeoclimatic data. Nat. Clim. Change 417–424: 8.

Braconnot P, Albani S, Balkanski Y, Cozic A, Kageyama M, Sima A, Marti O, Peterschmitt JY (2021) Impact of dust in PMIP-CMIP6 mid-Holocene simulations with the IPSL model. Clim. Past 17: 1091–1117.

Brahmi K, Aulagnier S, Slimani S, Mann CS, Doumandji S, Baziz B (2012) Diet of the Greater white-toothed shrew *Crocidura russula* (Mammalia: Soricidae) in Grande Kabylie (Algeria). Ital. J. Zool. 79: 239–245.

Brassard C, Merlin M, Guintard C, Monchâtre-Leroy E, Barrat J, Bausmayer N, Bausmayer S, Bausmayer A, Beyer M, Varlet A, Houssin C, Callou C, Cornette R, Herrel A (2020a) Bite force and its relation to jaw shape in domestic dogs. J. Exp. Biol. 223: jeb224352.

Brassard C, Merlin M, Guintard C, Monchâtre-Leroy E, Barrat J, Callou C, Cornette R, Herrel A (2020b) Interrelations Between the Cranium, the Mandible and Muscle Architecture in Modern Domestic Dogs. Evol. Biol.: 17.

Brassard C, Merlin M, Monchâtre-Leroy E, Guintard C, Barrat J, Callou C, Cornette R, Herrel A (2020c) How Does Masticatory Muscle Architecture Covary with Mandibular Shape in Domestic Dogs? Evol. Biol. 47: 133–151.

Brassard C, Merlin M, Monchâtre-Leroy E, Guintard C, Barrat J, Garès H, Larralle A, Triquet R, Houssin C, Callou C, Cornette R, Herrel A (2021) Masticatory system integration in a commensal canid: interrelationships between bones, muscles and bite force in the red fox. J. Exp. Biol. 224: jeb224394.

Braun DR, Levin NE, Stynder D, Herries AIR, Archer W, Forrest F, Roberts DL, Bishop LC, Matthews T, Lehmann SB, Pickering R, Fitzsimmons KE (2013) Mid-Pleistocene Hominin occupation at Elandsfontein, Western Cape, South Africa. Quat. Sci. Rev. 82: 145–166.

Brocklehurst N, Benevento GL (2020) Dental characters used in phylogenetic analyses of mammals show higher rates of evolution, but not reduced independence. PeerJ 8: e8744.

Butet A (1994) Nutritional conditions and annualfluctuations in Apodemus sylvaticuspopulations. Russ. J. Ecol. 25: 111–119.

Butler RJ, Brusatte SL, Andres B, Benson RBJ (2012) How do geological sampling biases affect studies of morphological evolution in deep time? A case study of Pterosaur (Reptilia: Archosauria) disparity: geological sampling biases and disparity. Evolution 66: 147–162.

Camacho DM, Collins KM, Powers RK, Costello JC, Collins JJ (2018) Next-Generation Machine Learning for Biological Networks. Cell 173: 1581–1592.

Campmas E, Michel P, Costamagno S, Amani F, Stoetzel E, Nespoulet R, El Hajraoui MA (2015) Were Upper Pleistocene human/non-human predator occupations at the Témara caves (El Harhoura 2 and El Mnasra, Morocco) influenced by climate change? J. Hum. Evol. 78: 122–143.

Campmas É, Michel P, Costamagno S, Abdeljalil El Hajraoui M, Nespoulet R (2017) Which predators are responsible for faunal accumulations at the Late Pleistocene layers of El Harhoura 2 Cave (Témara, Morocco)? Comptes Rendus Palevol 16: 333–350.

Candolin U, Wong BBM **(Eds.)** (2012) *Behavioural responses to a changing world: mechanisms and consequences*. Oxford, Oxford University Press.

Cardini A (2019) Integration and Modularity in Procrustes Shape Data: Is There a Risk of Spurious Results? Evol. Biol. 46: 90–105.

Carleton MD, Musser GG (2005) Order Rodentia. In: Mammal Species World Taxon. Geogr. Ref. Eds Wilson DM Reeder., 745–753.

Carmona CP, Tamme R, Pärtel M, de Bello F, Brosse S, Capdevila P, González-M. R, González-Suárez M, Salguero-Gómez R, Vásquez-Valderrama M, Toussaint A (2021) Erosion of global functional diversity across the tree of life. Sci. Adv. 7: eabf2675.

Carto SL, Weaver AJ, Hetherington R, Lam Y, Wiebe EC (2009) Out of Africa and into an ice age: on the role of global climate change in the late Pleistocene migration of early modern humans out of Africa. J. Hum. Evol. 56: 139–151.

Casanovas-Vilar I, van Dam JA, Moyà-Solà S, Rook L (2011) Late Miocene insular mice from the Tusco-Sardinian palaeobioprovince provide new insights on the palaeoecology of the Oreopithecus faunas. J. Hum. Evol. 61: 42–49.

Casanovas-Vilar I, van Dam J (2013) Conservatism and Adaptability during Squirrel Radiation: What Is Mandible Shape Telling Us? (A Goswami, Ed.). PLoS ONE 8: e61298.

Caumul R, Polly D (2005) Phylogenetic and environmental components of morphological variation: skull, mandible and molar shape in marmots (Marmota, Rodentia). Evolution 59: 2460–2472.

Ceballos G, Ehrlich PR, Dirzo R (2017) Biological annihilation via the ongoing sixth mass extinction signaled by vertebrate population losses and declines. Proc. Natl. Acad. Sci. 114: E6089–E6096.

Chapman JW, Klaassen RHG, Drake VA, Fossette S, Hays GC, Metcalfe JD, Reynolds AM, Reynolds DR, Alerstam T (2011) Animal Orientation Strategies for Movement in Flows. Curr. Biol. 21: R861–R870.

Chazeau C, Marchal J, Hackert R, Perret M, Herrel A (2013) Proximate determinants of bite force capacity in the mouse lemur: Bite force in mouse lemurs. J. Zool. 290: 42–48.

Cheverud JM, Routman EJ, Irschick DJ (1997) Pleiotropic effects of individual gene loci on mandibular morphology. Evolution 51: 2006–2016.

Chevin LM, Collins S, Lefèvre F (2013) Phenotypic plasticity and evolutionary demographic responses to climate change: taking theory out to the field (A Hoffmann, Ed.). Funct. Ecol. 27: 967–979.

Christiansen P, Wroe S (2007) Bite forces and evolutionary adaptations to feeding ecology in Carnivores. Ecology 88: 347–358.

Churchfield S (1990) *The Natural History of Shrews*. Ithaca, United States.

Clavel J, Morlon H (2017) Accelerated body size evolution during cold climatic periods in the Cenozoic. Proc. Natl. Acad. Sci. 114: 4183–4188.

Coillot T, Chaimanee Y, Charles C, Gomes-Rodrigues H, Michaux J, Tafforeau P, Vianey-Liaud M, Viriot L, Lazzari V (2013) Correlated changes in occlusal pattern and diet in stem murinae during the onset of the radiation of old world rats and mice. Evolution 67: 3323–3338.

Comay O, Dayan T (2018) From micromammals to paleoenvironments. Archaeol.

Anthropol. Sci. 10: 2159–2171.

Comay O, Weissbrod L, Dayan T (2019) Predictive modelling in paleoenvironmental reconstruction: The micromammals of Manot Cave, Israel. J. Hum. Evol.: 102652.

Condamine FL, Rolland J, Morlon H (2013) Macroevolutionary perspectives to environmental change (H Maherali, Ed.). Ecol. Lett. 16: 72–85.

Conenna I, Santini L, Rocha R, Monadjem A, Cabeza M, Russo D (2021) Global patterns of functional trait variation along aridity gradients in bats (S Meiri, Ed.). Glob. Ecol. Biogeogr.: geb.13278.

Conith AJ, Kidd MR, Kocher TD, Albertson RC (2020) Ecomorphological divergence and habitat lability in the context of robust patterns of modularity in the cichlid feeding apparatus. BMC Evol. Biol. 20: 95.

Cornette R, Herrel A, Cosson JF, Poitevin F, Baylac M (2012) Rapid morpho-functional changes among insular populations of the greater white-toothed shrew: MORPHOLOGY AND FUNCTION IN INSULAR SHREWS. Biol. J. Linn. Soc. 107: 322–331.

Cornette R, Baylac M, Souter T, Herrel A (2013) Does shape co-variation between the skull and the mandible have functional consequences? A 3D approach for a 3D problem. J. Anat. 223: 329–336.

Cornette R, Herrel A, Stoetzel E, Moulin S, Hutterer R, Denys C, Baylac M (2015a) Specific information levels in relation to fragmentation patterns of shrew mandibles: do fragments tell the same story? J. Archaeol. Sci. 53: 323–330.

Cornette R, Tresset A, Houssin C, Pascal M, Herrel A (2015b) Does bite force provide a competitive advantage in shrews? The case of the greater white-toothed shrew. Biol. J. Linn. Soc. 114: 795–807.

Cornette R, Stoetzel E, Baylac M, Moulin S, Hutterer R, Nespoulet R, El Hajraoui MA, Denys C, Herrel A (2015c) Shrews of the genus Crocidura from El Harhoura 2 (Témara, Morocco): The contribution of broken specimens to the understanding of Late Pleistocene–Holocene palaeoenvironments in North Africa. Palaeogeogr. Palaeoclimatol. Palaeoecol. 436: 1–8.

Cornette R, Tresset A, Herrel A (2015d) The shrew tamed by Wolff's law: Do functional constraints shape the skull through muscle and bone covariation? J. Morphol. 276: 301–309.

Courtenay LA, Yravedra J, Huguet R, Aramendi J, Maté-González MÁ, González-Aguilera D, Arriaza MC (2019) Combining machine learning algorithms and geometric morphometrics: A study of carnivore tooth marks. Palaeogeogr. Palaeoclimatol. Palaeoecol. 522: 28–39.

Couvreur TLP, Dauby G, Blach-Overgaard A, Deblauwe V, Dessein S, Droissart V, Hardy OJ, Harris DJ, Janssens SB, Ley AC, Mackinder BA, Sonké B, Sosef MSM, Stévart T, Svenning J, Wieringa JJ, Faye A, Missoup AD, Tolley KA, Nicolas V, Ntie S, Fluteau F, Robin C, Guillocheau F, Barboni D, Sepulchre P (2020) Tectonics, climate and the diversification of the tropical African terrestrial flora and fauna. Biol. Rev. 96: 16–51.

Cox PG, Hautier L **(Eds.)** (2015) *Evolution of the Rodents: Advances in Phylogeny,*

Functional Morphology and Development. Cambridge, Cambridge University Press.

Cramer BS, Miller KG, Barrett PJ, Wright JD (2011) Late Cretaceous–Neogene trends in deep ocean temperature and continental ice volume: Reconciling records of benthic foraminiferal geochemistry (δ^{18} O and Mg/Ca) with sea level history. J. Geophys. Res. 116: C12023.

Crispo E (2007) The Baldwin effect and genetic assimilation: revisiting two mechanisms of evolutionary change mediated by phenotypic plasticity. Evolution 61: 2469–2479.

Cruz FB, Moreno Azocar DL, Vanhooydonck B, Schulte JA, Abdala CS, Herrel A (2021) Drivers and patterns of bite force evolution in liolaemid lizards. Biol. J. Linn. Soc. 134: 126–140.

Cruz-Uribe K (1988) The use and meaning of species diversity and richness in archaeological faunas. J. Archaeol. Sci. 15: 179–196.

Cucchi T, Barnett R, Martínková N, Renaud S, Renvoisé E, Evin A, Sheridan A, Mainland I, Wickham-Jones C, Tougard C, Quéré JP, Pascal M, Pascal M, Heckel G, O'Higgins P, Searle JB, Dobney KM (2014) The changing pace of insular life: 5000 years of microevolution in the orkney vole (<i>Microtus arvalis orcadensis)<i>): 5000 years of microevolution in the orkney vole. Evolution 68: 2804–2820.

Curran J (2017) Package 'Hotelling'.

Currey JD (2003) The many adaptations of bone. J. Biomech. 36: 1487–1495.

Cyriac VP, Kodandaramaiah U (2017) Paleoclimate determines diversification patterns in the fossorial snake family Uropeltidae Cuvier, 1829. Mol. Phylogenet. Evol. 116: 97–107.

Darvish J (2011) Morphological comparison of fourteen species of the genus Meriones Illiger, 1811 (Rodentia: Gerbillinae) from Asia and North Africa. Iran. J. Anim. Biosyst. 7: 49–74.

Davis M, Pineda-Munoz S (2016) The temporal scale of diet and dietary proxies. Ecol. Evol. 6: 1883–1897.

deMenocal PB (1995) Plio-Pleistocene African Climate. Science 270: 53–59.

deMenocal PB (2004) African climate change and faunal evolution during the Pliocene–Pleistocene. Earth Planet. Sci. Lett. 220: 3–24.

Denys C, Stoetzel E, Andrews P, Bailon S, Rihane A, Huchet JB, Fernandez-Jalvo Y, Laroulandie V (2018) Taphonomy of Small Predators multi-taxa accumulations: palaeoecological implications. Hist. Biol. 30: 868–881.

Devine J, Aponte JD, Katz DC, Liu W, Vercio LDL, Forkert ND, Marcucio R, Percival CJ, Hallgrímsson B (2020) A Registration and Deep Learning Approach to Automated Landmark Detection for Geometric Morphometrics. Evol. Biol. 47: 246–259.

Douady CJ, Catzeflis F, Raman J, Springer MS, Stanhope MJ (2003) The Sahara as a vicariant agent, and the role of Miocene climatic events, in the diversification of the mammalian order Macroscelidea (elephant shrews). Proc. Natl. Acad. Sci. 100: 8325–8330.

Drake NA, Blench RM, Armitage SJ, Bristow CS, White KH (2011) Ancient watercourses and biogeography of the Sahara explain the peopling of the desert. Proc. Natl. Acad. Sci. 108: 458–462.

Drake NA, Breeze P, Parker A (2013) Palaeoclimate in the Saharan and Arabian Deserts during the Middle Palaeolithic and the potential for hominin dispersals. Quat. Int. 300: 48–61.

Dryden I, Mardia K (1998) *Statistical shape analysis*. Chichester., Wiley.

Dubey BP, Bhagwat SG, Shouche SP, Sainis JK (2006) Potential of Artificial Neural Networks in Varietal Identification using Morphometry of Wheat Grains. Biosyst. Eng. 95: 61–67.

Dufresne JL, Foujols MA, Denvil S, Caubel A, Marti O, Aumont O, Balkanski Y, Bekki S, Bellenger H, Benshila R, Bony S, Bopp L, Braconnot P, Brockmann P, Cadule P, Cheruy F, Codron F, Cozic A, Cugnet D, de Noblet N, Duvel JP, Ethé C, Fairhead L, Fichefet T, Flavoni S, Friedlingstein P, Grandpeix JY, Guez L, Guilyardi E, Hauglustaine D, Hourdin F, Idelkadi A, Ghattas J, Joussaume S, Kageyama M, Krinner G, Labetoulle S, Lahellec A, Lefebvre MP, Lefevre F, Levy C, Li ZX, Lloyd J, Lott F, Madec G, Mancip M, Marchand M, Masson S, Meurdesoif Y, Mignot J, Musat I, Parouty S, Polcher J, Rio C, Schulz M, Swingedouw D, Szopa S, Talandier C, Terray P, Viovy N, Vuichard N (2013) Climate change projections using the IPSL-CM5 Earth System Model: from CMIP3 to CMIP5. Clim. Dyn. 40: 2123–2165.

Dumont ER, Herrel A, MedellÃ-n RA, Vargas-Contreras JA, Santana SE (2009) Built to bite: cranial design and function in the wrinkle-faced bat. J. Zool. 279: 329–337.

Duplessy JC, Ramstein G (2013) *Paléonclimatologie, tome II : enquêter sur les climats anciens.*

Ebrahimi-Khusfi Z, Mirakbari M, Khosroshahi M (2020) Vegetation response to changes in temperature, rainfall, and dust in arid environments. Environ. Monit. Assess. 192: 691.

Ehrenreich IM, Pfennig DW (2016) Genetic assimilation: a review of its potential proximate causes and evolutionary consequences. Ann. Bot. 117: 769–779.

Ekström M, Grose MR, Whetton PH (2015) An appraisal of downscaling methods used in climate change research. WIREs Clim. Change 6: 301–319.

El Hajraoui MA, Nespoulet R, Debénath A, Dibble HL (2012) *Préhistoire de la région de Rabat-Témara.* Rabat.

Elewa AMT (2008) Mass Extinction - a general view. In: Mass Extinction. Berlin, Heidelberg, Springer Berlin Heidelberg, 1–4.

Erickson GM, Kirk SDV, Su J, Levenston ME, Caler WE, Carter DR (1996) Bite-force estimation for Tyrannosaurus rex from tooth-marked bones. Nature 382: 706–708.

Erwin DH (2000) Macroevolution is more than repeated rounds of microevolution. Evol. Dev. 2: 78–84.

Erwin DH (2007) Disparity: morphological pattern and developmental context. Palaeontology 50: 57–73.

Escudé É, Renvoisé É, Lhomme V, Montuire S (2013) Why all vole molars (Arvicolinae, Rodentia) are informative to be considered as proxy for Quaternary paleoenvironmental reconstructions. J. Archaeol. Sci. 40: 11–23.

Evans AR, Wilson GP, Fortelius M, Jernvall J (2007) High-level similarity of dentitions in carnivorans and rodents. Nature 445: 78–81.

Ezard THG, Aze T, Pearson PN, Purvis A (2011) Interplay Between Changing Climate and Species' Ecology Drives Macroevolutionary Dynamics. Science 332: 349–351.

Fabre PH, Hautier L, Dimitrov D, P Douzery EJ (2012) A glimpse on the pattern of rodent diversification: a phylogenetic approach. BMC Evol. Biol. 12: 88.

Faith JT, Du A (2018) The measurement of taxonomic evenness in zooarchaeology. Archaeol. Anthropol. Sci. 10: 1419–1428.

Fang Z, Fan J, Chen X, Chen Y (2018) Beak identification of four dominant octopus species in the East China Sea based on traditional measurements and geometric morphometrics. Fish. Sci. 84: 975–985.

Feiner N, Jackson IS, Munch KL, Radersma R, Uller T (2020) Plasticity and evolutionary convergence in the locomotor skeleton of Greater Antillean Anolis lizards. eLife 9: e57468.

Fernandez-Jalvo Y, Denys C, Andrews P, Williams T, Dauphin Y, Humphrey L (1998) Taphonomy and palaeoecology of Olduvai Bed-I (Pleistocene, Tanzania). J. Hum. Evol. 34: 137–172.

Finarelli JA, Badgley C (2010) Diversity dynamics of Miocene mammals in relation to the history of tectonism and climate. Proc. R. Soc. B Biol. Sci. 277: 2721–2726.

Foote M (1997) The evolution of morphological diversity. Annu. Rev. Ecol. Syst. 28: 129–152.

Foster GL, Royer DL, Lunt DJ (2017) Future climate forcing potentially without precedent in the last 420 million years. Nat. Commun. 8: 14845.

Freeman PW (1979) Specialized Insectivory: Beetle-Eating and Moth-Eating Molossid Bats. J. Mammal. 60: 467–479.

Freeman PW, Lemen CA (2008) A simple morphological predictor of bite force in rodents. J. Zool. 275: 418–422.

Furió M, Agustí J, Mouskhelishvili A, Sanisidro Ó, Santos-Cubedo A (2010) The paleobiology of the extinct venomous shrew *Beremendia* (Soricidae, Insectivora, Mammalia) in relation to the geology and paleoenvironment of Dmanisi (Early Pleistocene, Georgia). J. Vertebr. Paleontol. 30: 928–942.

Fusco G (2001) How many processes are responsible for phenotypic evolution? Evol. Dev. 3: 279–286.

Fyllas NM, Bentley LP, Shenkin A, Asner GP, Atkin OK, Díaz S, Enquist BJ, Farfan-Rios W, Gloor E, Guerrieri R, Huasco WH, Ishida Y, Martin RE, Meir P, Phillips O, Salinas N, Silman M, Weerasinghe LK, Zaragoza-Castells J, Malhi Y (2017) Solar radiation and functional traits explain the decline of forest primary productivity along a tropical elevation

gradient (DrN Swenson, Ed.). Ecol. Lett. 20: 730–740.

Garcia RA, Cabeza M, Rahbek C, Araujo MB (2014) Multiple Dimensions of Climate Change and Their Implications for Biodiversity. Science 344: 1247579–1247579.

Garcia-Ibaibarriaga N, Suárez-Bilbao A, Bailon S, Arrizabalaga A, Iriarte-Chiapusso MJ, Arnold L, Demuro M, Murelaga X (2018) Paleoenvironmental and paleoclimatic interpretation of the stratigraphic sequence of Lezetxiki II Cave (Basque Country, Iberian Peninsula) inferred from small vertebrate assemblages. Quat. Res. 90: 164–179.

Gardner JL, Peters A, Kearney MR, Joseph L, Heinsohn R (2011) Declining body size: a third universal response to warming? Trends Ecol. Evol. 26: 285–291.

Garland T, Losos JB (1994) Ecological morphology of locomotor performance in squamate reptiles. In: Wainwright PC, Reilly SM (eds.) Ecol. Morphol. Integr. Org. Biol. Chicago, USA, 240–302.

van der Geer AA, Lyras GA, Lomolino MV, Palombo MR, Sax DF (2013) Body size evolution of palaeo-insular mammals: temporal variations and interspecific interactions (J Masters, Ed.). J. Biogeogr. 40: 1440–1450.

Geraads D, Amani F, Ben-Ncer A, McPherron SP, Raynal JP, Hublin JJ (2013) The rodents from the late middle Pleistocene hominid-bearing site of J'bel Irhoud, Morocco, and their chronological and paleoenvironmental implications. Quat. Res. 80: 552–561.

Ghawar W, Zaätour W, Chlif S, Bettaieb J, Chelghaf B, Snoussi MA, Salah AB (2015) Spatiotemporal dispersal of Meriones shawi estimated by radio-telemetry. Int. J. Multidiscip. Res. Dev. 2: 211–216.

Gillespie RG, Benjamin SP, Brewer MS, Rivera MAJ, Roderick GK (2018) Repeated Diversification of Ecomorphs in Hawaiian Stick Spiders. Curr. Biol. 28: 941-947.e3.

Gillooly JF, Brown JH, West GB, Savage VM, Charnov EL (2001) Effects of Size and Temperature on Metabolic Rate. Science 293: 2248–2251.

Ginot S, Herrel A, Claude J, Hautier L (2018) Skull Size and Biomechanics are Good Estimators of *In Vivo* Bite Force in Murid Rodents: *in vivo* bite force estimation in murid rodents. Anat. Rec. 301: 256–266.

Ginot S, Herrel A, Claude J, Hautier L (2019) Morphometric models for estimating bite force in *Mus* and *Rattus* : mandible shape and size perform better than lever-arm ratios. J. Exp. Biol. 222: jeb204867.

Girard C, Renaud S, Korn D (2004) Step-wise morphological trends in fluctuating environments: Evidence in the Late Devonian conodont genus Palmatolepis. Geobios 37: 404–415.

Gomes Rodrigues H (2015a) The great variety of dental structures and dynamics in rodents: new insights into their ecological diversity. In: Cox P, Hautier L (eds.) Evol. Rodents Adv. Phylogeny Funct. Morphol. Dev., 424–447.

Gomes Rodrigues H (2015b) The great variety of dental structures and dynamics in rodents: new insights into their ecological diversity. In: Cox PG, Hautier L (eds.) Evol. Rodents. Cambridge, Cambridge University Press, 448–477.

Gomes Rodrigues H, Merceron G, Viriot L (2009) Dental microwear patterns of extant and extinct Muridae (Rodentia, Mammalia): ecological implications. Naturwissenschaften 96: 537–542.

Gómez Cano AR, Hernández Fernández M, Álvarez-Sierra MÁ (2013) Dietary ecology of murinae (Muridae, Rodentia): a geometric morphometric approach (L Viriot, Ed.). PLoS ONE 8: e79080.

Goswami A, Smaers JB, Soligo C, Polly PD (2014) The macroevolutionary consequences of phenotypic integration: from development to deep time. Philos. Trans. R. Soc. B Biol. Sci. 369: 20130254–20130254.

Gould SJ (1966) Allometry and size in ontogeny and phylogeny. Biol. Rev. 41: 587–638.

Gould SJ (1989) *Wonderful life: the Burgess Shale and the nature of history*.

Gould SJ (1991) The disparity of the Burgess Shale arthropod fauna and the limits of cladistic analysis: why we must strive to quantify morphospace. Paleobiology 17: 411–423.

Gross K, Pasinelli G, Kunc HP (2010) Behavioral Plasticity Allows Short-Term Adjustment to a Novel Environment. Am. Nat. 176: 456–464.

Guillaud E, Cornette R, Béarez P (2016) Is vertebral form a valid species-specific indicator for salmonids? The discrimination rate of trout and Atlantic salmon from archaeological to modern times. J. Archaeol. Sci. 65: 84–92.

Guillerme T (2018) dispRity : a modular R package for measuring disparity (T Poisot, Ed.). Methods Ecol. Evol. 9: 1755–1763.

Guillerme T, Cooper N, Brusatte SL, Davis KE, Jackson AL, Gerber S, Goswami A, Healy K, Hopkins MJ, Jones MEH, Lloyd GT, O'Reilly JE, Pate A, Puttick MN, Rayfield EJ, Saupe EE, Sherratt E, Slater GJ, Weisbecker V, Thomas GH, Donoghue PCJ (2020) Disparities in the analysis of morphological disparity. Biol. Lett. 16: 20200199.

Guillermot H (2011) 2. Bref historique de la modélisation du climat en France. In: Clim. À Découvert. Paris, 148–149.

Gunz P, Mitteroecker P, Bookstein FL (2005) Semilandmarks in Three Dimensions. In: Slice DE (ed.) Mod. Morphometrics Phys. Anthropol. New York, Kluwer Academic Publishers-Plenum Publishers, 73–98.

Gür H (2021) *The future impact of climate and land-use changes on Anatolian ground squirrels under different scenarios*. Ecology.

Hansen TF, Martins EP (1996) Translating between microevolutionary process and macroevolutionary patterns: the correlation structure of interspecific data. Evolution 50: 1404–1417.

Harrison SP, Bartlein PJ, Izumi K, Li G, Annan J, Hargreaves J, Braconnot P, Kageyama M (2015) Evaluation of CMIP5 palaeo-simulations to improve climate projections. Nat. Clim. Change 5: 735–743.

Hastie T, Tibshirani R, Friedman J (2009) *The elements of statistical learning: data mining, inference, and prediction.* New York, Springer.

Hautier L, Lebrun R, Cox PG (2012) Patterns of covariation in the masticatory apparatus of hystricognathous rodents: Implications for evolution and diversification. J. Morphol. 273: 1319–1337.

Hautmann M (2020) What is macroevolution? (A Smith, Ed.). Palaeontology 63: 1–11.

Hendry AP, Farrugia TJ, Kinnison MT (2008) Human influences on rates of phenotypic change in wild animal populations. Mol. Ecol. 17: 20–29.

Hendry AP, Kinnison MT (2001) An introduction to microevolution: Rate, pattern, process. In: Hendry AP, Kinnison MT (eds.) Microevolution Rate Pattern Process. Dordrecht, Springer Netherlands, 1–8.

Herrel A, De Smet A, Aguirre LF, Aerts P (2008a) Morphological and mechanical determinants of bite force in bats: do muscles matter? J. Exp. Biol. 211: 86–91.

Herrel A, Vanhooydonck B, Porck J, Irschick DJ (2008b) Anatomical Basis of Differences in Locomotor Behavior in Anolis Lizards: A Comparison Between Two Ecomorphs. Bull. Mus. Comp. Zool. 159: 213–238.

Herrel A, Gibb AC (2006) Ontogeny of Performance in Vertebrates. Physiol. Biochem. Zool. 79: 1–6.

Herrel A, O'Reilly JC, Richmond AM (2002) Evolution of bite performance in turtles: Evolution of bite force in turtles. J. Evol. Biol. 15: 1083–1094.

Hijmans RJ, van Etten J (2012) raster: Geographic analysis and modeling with raster data. R package version 2.0-12.

Hill MO (1973) Diversity and Evenness: A Unifying Notation and Its Consequences. Ecology 54: 427–432.

Hill AP, Hadly EA (2018) Rethinking "Native" in the Anthropocene. Front. Earth Sci. 6: 96.

Hoffmann AA, Sgrò CM (2011) Climate change and evolutionary adaptation. Nature 470: 479–485.

Holt RD (1990) The microevolutionary consequences of climate change. Trends Ecol. Evol. 5: 311–315.

Holzman R, Collar DC, Mehta RS, Wainwright PC (2011) Functional Complexity Can Mitigate Performance Trade-Offs. Am. Nat. 177: 15.

Hooghiemstra H, Stalling H, Agwu COC, Dupont LM (1992) Vegetational and climatic changes at the northern fringe of the sahara 250,000–5000 years BP: evidence from 4 marine pollen records located between Portugal and the Canary Islands. Rev. Palaeobot. Palynol. 74: 1–53.

Houle D, Govindaraju DR, Omholt S (2010) Phenomics: the next challenge. Nat. Rev. Genet. 11: 855–866.

Hovenden MJ, Vander Schoor JK, Osanai Y (2012) Relative humidity has dramatic impacts on leaf morphology but little effect on stomatal index or density in Nothofagus

cunninghamii (Nothofagaceae). Aust. J. Bot. 60: 700.

Huang G, Rosowski J, Ravicz M, Peake W (2002) Mammalian ear specializations in arid habitats: structural and functional evidence from sand cat (Felis margarita). J. Comp. Physiol. [A] 188: 663–681.

Huber DR (2005) Analysis of the bite force and mechanical design of the feeding mechanism of the durophagous horn shark Heterodontus francisci. J. Exp. Biol. 208: 3553–3571.

Ibrahim MIA, Tahoun SS, Zobaa MK, Oboh-Ikuenobe FE, Kholeif SE (2020) Late Cretaceous palynology and paleoenvironment of the Razzak-3 well, North Western Desert, Egypt. Arab. J. Geosci. 13: 870.

Ilieș IA, Oltean G, Bindiu Haitonic R, Filipescu S, Miclea A, Jipa C (2020) Early middle Miocene paleoenvironmental evolution in southwest Transylvania (Romania): Interpretation based on foraminifera. Geol. Carpathica 71: 444–461.

Irschick DJ, Meyers JJ, Husak JF, Galliard JFL (2008) How does selection operate on whole-organism functional performance capacities? A review and synthesis. Evol. Ecol. Res. 10: 177–196.

Jacobs Z, Roberts RG, Nespoulet R, El Hajraoui MA, Debénath A (2012) Single-grain OSL chronologies for Middle Palaeolithic deposits at El Mnasra and El Harhoura 2, Morocco: Implications for Late Pleistocene human–environment interactions along the Atlantic coast of northwest Africa. J. Hum. Evol. 62: 377–394.

Jacobs Z, Roberts RG (2012) Chapitre III. Datations par OSL avec la technique du grain unique. In: Préhistoire Région Rabat-Témara. Rabat, 52–54.

Janati-Idrissi N, Falgueres C, Nespoulet R, El Hajraoui MA, Debénath A, Bejjit L, Bahain JJ, Michel P, Garcia T, Boudad L, El Hammouti K, Oujaa A (2012) Datation par ESR-U/th combinées de dents fossiles des grottes d'El Mnasra et d'El Harhoura 2, région de Rabat-Temara. Implications chronologiques sur le peuplement du Maroc atlantique au Pléistocène supérieur et son. Quaternaire 23: 25–35.

Jaramillo C, Sepulchre P, Cardenas D, Correa-Metrio A, Moreno JE, Trejos R, Vallejos D, Hoyos N, Martínez C, Carvalho D, Escobar J, Oboh-Ikuenobe F, Prámparo MB, Pinzón D (2020) Drastic Vegetation Change in the Guajira Peninsula (Colombia) During the Neogene. Paleoceanogr. Paleoclimatology 35.

Jeffrey A (2016) Exploring palaeoaridity using stable oxygen and carbon isotopes in small mammal teeth: a case study from two Late Pleistocene archaeological cave sites in Morocco, North Africa.

Jolliffe IT, Cadima J (2016) Principal component analysis: a review and recent developments. Philos. Trans. R. Soc. Math. Phys. Eng. Sci. 374: 20150202.

Jones CG (2012) Ecosystem engineers and geomorphological signatures in landscapes. Geomorphology 157–158: 75–87.

de Jong G (1995) Phenotypic Plasticity as a Product of Selection in a Variable Environment. Am. Nat. 145: 493–512.

Kageyama M, Braconnot P, Bopp L, Caubel A, Foujols MA, Guilyardi E, Khodri M, Lloyd J, Lombard F, Mariotti V, Marti O, Roy T, Woillez MN (2013) Mid-Holocene and Last Glacial Maximum climate simulations with the IPSL model—part I: comparing IPSL_CM5A to IPSL_CM4. Clim. Dyn. 40: 2447–2468.

Kageyama M, Albani S, Braconnot P, Harrison SP, Hopcroft PO, Ivanovic RF, Lambert F, Marti O, Peltier WR, Peterschmitt JY, Roche DM, Tarasov L, Zhang X, Brady EC, Haywood AM, LeGrande AN, Lunt DJ, Mahowald NM, Mikolajewicz U, Nisancioglu KH, Otto-Bliesner BL, Renssen H, Tomas RA, Zhang Q, Abe-Ouchi A, Bartlein PJ, Cao J, Li Q, Lohmann G, Ohgaito R, Shi X, Volodin E, Yoshida K, Zhang X, Zheng W (2017) The PMIP4 contribution to CMIP6 – Part 4: Scientific objectives and experimental design of the PMIP4-CMIP6 Last Glacial Maximum experiments and PMIP4 sensitivity experiments. : 23.

Kaňuščák P, Hromada M, Tryjanowski P, Sparks T (2004) Does climate at different scales inlfuence the phenology and phenotype of the River Warbler Locustella fluviatilis? Oecologia: 158–163.

Karagic N, Meyer A, Hulsey CD (2020) Phenotypic Plasticity in Vertebrate Dentitions. Integr. Comp. Biol. 60: 608–618.

Karell P, Ahola K, Karstinen T, Valkama J, Brommer JE (2011) Climate change drives microevolution in a wild bird. Nat. Commun. 2: 208.

Karr J, James F (1975) Ecomorphological configurations and convergent evolution in species and communities. In: Cody M, Diamond J (eds.) Ecol. Evol. Communities., 258–291.

Kaufman L, Rousseeuw PJ (1990) *Finding groups in data. an introduction to cluster analysis.*

Kerr E, Cornette R, Rodrigues HG, Renaud S, Chevret P, Tresset A, Herrel A (2017) Can functional traits help explain the coexistence of two species of Apodemus? Biol. J. Linn. Soc. 122: 883–896.

Khare N, Nigam R, Mayenkar DN, Saraswat R (2017) Cluster analysis of benthic foraminiferal morpho-groups from the western margin of India reflects its depth preference. Cont. Shelf Res. 151: 72–83.

Klingenberg CP (1996) Multivariate Allometry. In: Marcus LF, Corti M, Loy A, Naylor GJP, Slice DE (eds.) Adv. Morphometrics. Boston, MA, Springer US, 23–49.

Klingenberg CP (2004) Integration and Modularity of Quantitative Trait Locus Effects on Geometric Shape in the Mouse Mandible. Genetics 166: 1909–1921.

Klingenberg CP (2008) Morphological Integration and Developmental Modularity. Annu. Rev. Ecol. Evol. Syst. 39: 115–132.

Klingenberg CP (2016) Size, shape, and form: concepts of allometry in geometric morphometrics. Dev. Genes Evol. 226: 113–137.

Klingenberg CP, Marugán-Lobón J (2013) Evolutionary Covariation in Geometric Morphometric Data: Analyzing Integration, Modularity, and Allometry in a Phylogenetic Context. Syst. Biol. 62: 591–610.

Klingenberg CP, Mebus K, Auffray JC (2003) Developmental integration in a complex morphological structure: how distinct are the modules in the mouse mandible? Evol. Dev. 5: 522–531.

Klocke D, Schmitz H (2011) Water as a major modulator of the mechanical properties of insect cuticle. Acta Biomater. 7: 2935–2942.

Kouvari M, Herrel A, Cornette R (2021) Humans and climate as possible drivers of the morphology and function of the mandible of Suncus etruscus in Corsica. J. Archaeol. Sci. 132: 105434.

Ksepka DT (2020) Feathered dinosaurs. Curr. Biol. 30: R1347–R1353.

Kurtén B (1967) Some Quantitative Approaches to Dental Microevolution. J. Dent. Res. 46: 817–828.

Kutzbach JE, Otto-Bliesner BL (1982) The Sensitivity of the African-Asian Monsoonal Climate to Orbital Parameter Changes for 9000 Years B.P. in a Low-Resolution General Circulation Model. J. Atmospheric Sci. 39.

Labonne G, Laffont R, Renvoise E, Jebrane A, Labruere C, Chateau-Smith C, Navarro N, Montuire S (2012) When less means more: evolutionary and developmental hypotheses in rodent molars. J. Evol. Biol. 25: 2102–2111.

Lalis A, Leblois R, Stoetzel E, Benazzou T, Souttou K, Denys C, Nicolas V (2016) Phylogeography and demographic history of Shaw's Jird (*Meriones shawii* complex) in North Africa. Biol. J. Linn. Soc. 118: 262–279.

Lalis A, Mona S, Stoetzel E, Bonhomme F, Souttou K, Ouarour A, Aulagnier S, Denys C, Nicolas V (2019) Out of Africa: demographic and colonization history of the Algerian mouse (Mus spretus Lataste). Heredity 122: 150–171.

Lande R (2009) Adaptation to an extraordinary environment by evolution of phenotypic plasticity and genetic assimilation. J. Evol. Biol. 22: 1435–1446.

Langerhans RB (2009) Trade-off between steady and unsteady swimming underlies predator-driven divergence in *Gambusia affinis*. J. Evol. Biol. 22: 1057–1075.

Langerhans, RB, Reznick DN (2010) Ecology and evolution of swimming performance in fishes: Predicting evolution with biomechanics. In: Domenici P, Kapoor BG (eds.) Fish Locomot. Etho-Ecol. Perspect. Enfield, USA, CRC Press, 200–248.

Lappin AK, Wilcox SC, Moriarty DJ, Stoeppler SAR, Evans SE, Jones MEH (2017) Bite force in the horned frog (Ceratophrys cranwelli) with implications for extinct giant frogs. Sci. Rep. 7: 11963.

Le Houérou HN (1997) Climate, flora and fauna changes in the Sahara over the past 500 million years. J. Arid Environ. 37: 619–647.

Lê S, Josse J, Husson F (2008) FactoMineR: an R Package for multivariate analysis. J. Stat. Softw. 25.

Le Mézo P, Beaufort L, Bopp L, Braconnot P, Kageyama M (2017) From monsoon to marine productivity in the Arabian Sea: insights from glacial and interglacial climates.

Clim. Past 13: 759–778.

Ledevin R, Chevret P, Ganem G, Britton-Davidian J, Hardouin EA, Chapuis JL, Pisanu B, da Luz Mathias M, Schlager S, Auffray JC, Renaud S (2016) Phylogeny and adaptation shape the teeth of insular mice. Proc. R. Soc. B Biol. Sci. 283: 20152820.

Legland D, Arganda-Carreras I, Andrey P (2016) MorphoLibJ: integrated library and plugins for mathematical morphology with ImageJ. Bioinformatics: btw413.

Levin NE, Cerling TE, Passey BH, Harris JM, Ehleringer JR (2006) A stable isotope aridity index for terrestrial environments. Proc. Natl. Acad. Sci. 103: 11201–11205.

Lewis SL, Maslin MA (2015) Defining the Anthropocene. Nature 519: 171–180.

Lewitus E, Morlon H (2018) Detecting Environment-Dependent Diversification From Phylogenies: A Simulation Study and Some Empirical Illustrations. Syst. Biol.: 18.

Li Y, Huang C, Ding L, Li Z, Pan Y, Gao X (2019) *Deep learning in bioinformatics: introduction, application, and perspective in big data era*. Bioinformatics.

Liland KH, Mevik BH, Wehrens R, Hiemstra P (2021) pls: Partial Least Squares and Principal Component regression, R package.

Lin G (2013) Chapter 4: Research on stable isotope and carbon cycle (1st ed.). In: Stable Isot. Ecol. Beijing, 89–123.

Lionello P, Malanotte P, Boscolo R **(Eds.)** (2006) *Mediterranean Climate Variability*. Amsterdam, Elsevier.

Longinelli A, Selmo E (2003) Isotopic composition of precipitation in Italy: a first overall map. J. Hydrol. 270: 75–88.

López-García JM, Cuenca-Bescós G, Galindo-Pellicena MÁ, Luzi E, Berto C, Lebreton L, Desclaux E (2021) Rodents as indicators of the climatic conditions during the Middle Pleistocene in the southwestern Mediterranean region: implications for the environment in which hominins lived. J. Hum. Evol. 150: 102911.

Losos JB (1990a) The evolution of form and function: morphology and locomotor performance in west indian *Anolis* lizards. Evolution 44: 1189–1203.

Losos JB (1990b) Ecomorphology, Performance Capability, and Scaling of West Indian Anolis Lizards: An Evolutionary Analysis. Ecol. Monogr. 60: 369–388.

Losos JB (1992) The evolution of convergent structure in caribbean anolis communities. Syst. Biol. 41: 18.

Lyman RL (2014) Paleoenvironmental implications of two relative indicator rodent taxa during the Pleistocene to Holocene transition in south-eastern Washington state, USA: paleoenvironmental implications of two rodents taxa. J. Quat. Sci. 29: 691–697.

Maestri R, Patterson BD, Fornel R, Monteiro LR, de Freitas TRO (2016) Diet, bite force and skull morphology in the generalist rodent morphotype. J. Evol. Biol. 29: 2191–2204.

Mallet J (1995) A species definition for the Modern Synthesis. Trends Ecol. Evol. 10: 294–299.

Manhães IA, Nogueira MR, Monteiro LR (2017) Bite force and evolutionary studies in phyllostomid bats: a meta-analysis and validation. J. Zool. 302: 288–297.

Mapp J, Hunter E, Van Der Kooij J, Songer S, Fisher M (2017) Otolith shape and size: The importance of age when determining indices for fish-stock separation. Fish. Res. 190: 43–52.

Marquer L, Otto T, Ben Arous E, Stoetzel E, Campmas E, Zazzo A, Tombret O, Falgueres C, El Hajraoui MA, Nespoulet R (*in press*) Early human use of wild olive during the Aterian Middle Stone Age in North Africa.

Marroig G, Cheverud JM (2005) Size as a line of least resistance: diet and adaptative morphological radiation in new world monkeys. Evolution 59: 1128–1142.

Marti O, Braconnot P, Dufresne JL, Bellier J, Benshila R, Bony S, Brockmann P, Cadule P, Caubel A, Codron F, de Noblet N, Denvil S, Fairhead L, Fichefet T, Foujols MA, Friedlingstein P, Goosse H, Grandpeix JY, Guilyardi E, Hourdin F, Idelkadi A, Kageyama M, Krinner G, Lévy C, Madec G, Mignot J, Musat I, Swingedouw D, Talandier C (2010) Key features of the IPSL ocean atmosphere model and its sensitivity to atmospheric resolution. Clim. Dyn. 34: 1–26.

Martínez-Blancas A, Martorell C (2020) Changes in niche differentiation and environmental filtering over a hydric stress gradient (S Wang, Ed.). J. Plant Ecol. 13: 185–194.

Masson-Delmotte V, Zhai P, Pirani A, Connors S, Péan C, Berger S, Caud N, Chen Y, Goldfarb L, Gomis M, Huang M, Leitzell K, Lonnoy E, Matthews J, Maycock T, Waterfield T, Yelekçi O, Yu R, Zhou B **(Eds.)** (In Press) IPCC, 2021: Climate Change 2021: The Physical Science Basis. Contribution of Working Group I to the Sixth Assessment Report of the Intergovernmental Panel on Climate Change. Camb. Univ. Press.

Matthews T (2000) Predators, prey and the palaeoenvironment. South Afr. J. Sci. 95: 22–24.

Matthews T, Denys C, Parkington JE (2005) The palaeoecology of the micromammals from the late middle Pleistocene site of Hoedjiespunt 1 (Cape Province, South Africa). J. Hum. Evol. 49: 432–451.

Mavropoulos A, Bresin A, Kiliaridis S (2004) Morphometric analysis of the mandible in growing rats with different masticatory functional demands: adaptation to an upper posterior bite block. Eur. J. Oral Sci. 112: 259–266.

Mayr E (1942) *Systematics And The Origin Of Species*.

McGuire JL (2010) Geometric morphometrics of vole (Microtus californicus) dentition as a new paleoclimate proxy: Shape change along geographic and climatic clines. Quat. Int. 212: 198–205.

McNeil JN (1991) Behavioral Ecology of Pheromone-Mediated Communication in Moths and Its Importance in the Use of Pheromone Traps. Annu. Rev. Enthomology 36: 407–30.

Meiri S, Dayan T (2003) On the validity of Bergmann's rule. J. Biogeogr. 30: 331–351.

Merilä J, Hendry AP (2014) Climate change, adaptation, and phenotypic plasticity: the

problem and the evidence. Evol. Appl. 7: 1–14.

Merilä J, Sheldon BC, Kruuk LEB (2001) Explaining stasis: Microevolutionary studies in natural populations. In: Hendry AP, Kinnison MT (eds.) Microevolution Rate Pattern Process. Dordrecht, Springer Netherlands, 199–222.

Meunier M, Stoetzel E, Souttou K, Sekour M, Moussa H, Boukhemza M, Doumandji S, Denys C (2020) Mise à jour de la liste des rongeurs d'Algérie, biogéographie et implications paléoécologiques. Bull. Société Zool. Fr. 145: 413–474.

Mevik BH, Wehrens R (2007) The **pls** Package: Principal Component and Partial Least Squares Regression in *R*. J. Stat. Softw. 18.

Meyer ALS, Pie MR (2021) Climate Change Estimates Surpass Rates of Climatic Niche Evolution in Primates. Int. J. Primatol.

Mezey JG, Cheverud JM, Wagner GP (2000) Is the Genotype-Phenotype Map Modular?: A Statistical Approach Using Mouse Quantitative Trait Loci Data. Genet. Soc. Am. 156: 305–311.

Michel P, Campmas É, Stoetzel E, Nespoulet R, Abdeljalil El Hajraoui M, Amani F (2009a) La macrofaune du Pléistocène supérieur d'El Harhoura 2 (Témara, Maroc) : données préliminaires. L'Anthropologie 113: 283–312.

Michel P, Campmas É, Stoetzel E, Nespoulet R, Abdeljalil El Hajraoui M, Amani F (2009b) La macrofaune du Pléistocène supérieur d'El Harhoura 2 (Témara, Maroc) : données préliminaires. L'Anthropologie 113: 283–312.

Miele V, Dussert G, Cucchi T, Renaud S (2020) *Deep learning for species identification of modern and fossil rodent molars*. Zoology.

Miljutin A (2011) Trends of specialisation in rodents: the hamsters, subfamily Cricetinae (Cricetidae, Rodentia, Mammalia). Acta Zool. Litu. 21: 192–206.

Mitteroecker P, Gunz P (2009) Advances in Geometric Morphometrics. Evol. Biol. 36: 235–247.

Monteiro LR, Nogueira MR (2011) Evolutionary patterns and processes in the radiation of phyllostomid bats. BMC Evol. Biol. 11: 137.

Monteith JL (1972) Solar Radiation and Productivity in Tropical Ecosystems. J. Appl. Ecol. 9: 747.

Murray W (1973) *Distribution and Ecology of Living Benthic Foraminiferids.*

Murray W (2006) *Ecology and Applications of Benthic Foraminifera.*

Nagy J (1992) Environmental significance of foraminiferal morphogroups in Jurassic North sea deltas. Palaeogeogr. Palaeoclimatol. Palaeoecol. 95: 111–134.

Nancy A. N (1982) *The Big Cats: The Paintings of Guy Coheleach.*

Nath T, Mathis A, Chen AC, Patel A, Bethge M, Mathis MW (2018) Using DeepLabCut for 3D markerless pose estimation across species and behaviors. bioRxiv.

Navarro N, Lécuyer C, Montuire S, Langlois C, Martineau F (2004) Oxygen isotope compositions of phosphate from arvicoline teeth and Quaternary climatic changes, Gigny, French Jura. Quat. Res. 62: 172–182.

Nespoulet R, El Hajraoui MA, Amani F, Ben Ncer A, Debénath A, El Idrissi A, Lacombe JP, Michel P, Oujaa A, Stoetzel E (2008) Palaeolithic and Neolithic Occupations in the Témara Region (Rabat, Morocco): Recent Data on Hominin Contexts and Behavior. Afr. Archaeol. Rev. 25: 21–39.

Nespoulet R, El Hajraoui MA (2012) Excavation report.

Nevo E (1989) Natural selection of body size differentiation in the spiny mice, Acomys. Z. Saugetierkunde 99: 54–81.

Nogueira MR, Peracchi AL, Monteiro LR (2009) Morphological correlates of bite force and diet in the skull and mandible of phyllostomid bats. Funct. Ecol. 23: 715–723.

Nogués-Bravo D, Rodríguez-Sánchez F, Orsini L, de Boer E, Jansson R, Morlon H, Fordham DA, Jackson ST (2018) Cracking the Code of Biodiversity Responses to Past Climate Change. Trends Ecol. Evol. 33: 765–776.

Nowak RM (1999) *Walker's mammals of the world (Vols. 1 and 2, 6th ed.)*. Baltimore.

Ochocińska D, Taylor JRE (2003) Bergmann's rule in shrews: geographical variation of body size in Palearctic Sorex species. Biol. J. Linn. Soc. 78: 365–381.

O'Leary MH (1988) Carbon Isotopes in Photosynthesis. BioScience 38: 328–336.

Pagani-Núñez E, Valls M, Senar JC (2015) Diet specialization in a generalist population: the case of breeding great tits Parus major in the Mediterranean area. Oecologia 179: 629–640.

Paillard D (2001) Glacial cycles: Toward a new paradigm. Rev. Geophys. 39: 325–346.

Paine OCC, Leichliter JN, Avenant N, Codron D, Lawrence A, Sponheimer M (2019) The ecomorphology of southern African rodent incisors: Potential applications to the hominin fossil record (C Charles, Ed.). PLOS ONE 14: e0205476.

Palomo LJ, Justo ER, Vargas JM (2009) Mus spretus (Rodentia: Muridae). Mamm. Species 840: 1–10.

Paradis E, Claude J, Strimmer K (2004) APE: Analyses of Phylogenetics and Evolution in R language. Bioinformatics 20: 289–290.

Parmesan C (2006) Ecological and Evolutionary Responses to Recent Climate Change. Annu. Rev. Ecol. Evol. Syst. 37: 637–669.

Parmesan C, Matthews J (2005) Biological Impacts of Climate Change. : 42.

Paz H, Pineda-García F, Pinzón-Pérez LF (2015) Root depth and morphology in response to soil drought: comparing ecological groups along the secondary succession in a tropical dry forest. Oecologia 179: 551–561.

Peet RK (1974) The Measurement of Species Diversity. Annu. Rev. Ecol. Syst. 5: 285–307.

Pellegrino AC, Peñaflor MFGV, Nardi C, Bezner-Kerr W, Guglielmo CG, Bento JMS, McNeil JN (2013) Weather Forecasting by Insects: Modified Sexual Behaviour in Response to Atmospheric Pressure Changes (CR Lazzari, Ed.). PLoS ONE 8: e75004.

Peters SE, Bork KB (1999) Species-Abundance Models: An Ecological Approach to Inferring Paleoenvironment and Resolving Paleoecological Change in the Waldron Shale (Silurian). PALAIOS 14: 234.

Pielou EC (1969) *An introduction to mathematical ecology.* New York, USA, Wiley-Interscience.

Pineda-Munoz S, Lazagabaster IA, Alroy J, Evans AR (2017) Inferring diet from dental morphology in terrestrial mammals (N Cooper, Ed.). Methods Ecol. Evol. 8: 481–491.

Piper PJ (2008) Post-Pleistocene evolution of Bornean shrews Crocidura foetida (Mammalia, Soricidae): POST-PLEISTOCENE EVOLUTION OF C. FOETIDA. Biol. J. Linn. Soc. 94: 413–419.

Pohl A, Harper DAT, Donnadieu Y, Le Hir G, Nardin E, Servais T (2018) Possible patterns of marine primary productivity during the Great Ordovician Biodiversification Event. Lethaia 51: 187–197.

Porada P, Lenton TM, Pohl A, Weber B, Mander L, Donnadieu Y, Beer C, Pöschl U, Kleidon A (2016) High potential for weathering and climate effects of non-vascular vegetation in the Late Ordovician. Nat. Commun. 7: 12113.

Quenu M, Trewick SA, Brescia F, Morgan-Richards M (2020) Geometric morphometrics and machine learning challenge currently accepted species limits of the land snail Placostylus (Pulmonata: Bothriembryontidae) on the Isle of Pines, New Caledonia. J. Molluscan Stud.: eyz031.

Quintero I, Wiens JJ (2013) Rates of projected climate change dramatically exceed past rates of climatic niche evolution among vertebrate species (L Harmon, Ed.). Ecol. Lett. 16: 1095–1103.

R Development Core Team (2018) *R: A language and environment for statistical computing. R Foundation for Statistical Computing, Vienna, Austria. ISBN 3-900051-07-0, URL: http://www.R-project.org.*

Raadsheer MC, van Eijden TMGJ, van Ginkel FC, Prahl-Andersen B (1999) Contribution of Jaw Muscle Size and Craniofacial Morphology to Human Bite Force Magnitude. J. Dent. Res. 78: 31–42.

Radchuk V, Reed T, Teplitsky C, van de Pol M, Charmantier A, Hassall C, Adamík P, Adriaensen F, Ahola MP, Arcese P, Miguel Avilés J, Balbontin J, Berg KS, Borras A, Burthe S, Clobert J, Dehnhard N, de Lope F, Dhondt AA, Dingemanse NJ, Doi H, Eeva T, Fickel J, Filella I, Fossøy F, Goodenough AE, Hall SJG, Hansson B, Harris M, Hasselquist D, Hickler T, Joshi J, Kharouba H, Martínez JG, Mihoub JB, Mills JA, Molina-Morales M, Moksnes A, Ozgul A, Parejo D, Pilard P, Poisbleau M, Rousset F, Rödel MO, Scott D, Senar JC, Stefanescu C, Stokke BG, Kusano T, Tarka M, Tarwater CE, Thonicke K, Thorley J, Wilting A, Tryjanowski P, Merilä J, Sheldon BC, Pape Møller A, Matthysen E, Janzen F, Dobson FS, Visser ME, Beissinger SR, Courtiol A, Kramer-Schadt S (2019) Adaptive responses of animals to climate change are most likely insufficient. Nat.

Commun. 10: 3109.

Ramasamy M, Das B, Ramesh R (2021) Predicting climate change impacts on potential worldwide distribution of fall armyworm based on CMIP6 projections. J. Pest Sci.

Ramsay J, Silverman B (2005) Modelling functional responses with multivariate covariates. In: Funct. Data Anal. New York, Springer-Verlag, 223–245.

Read CF, Duncan DH, Vesk PA, Elith J (2014) Biocrust morphogroups provide an effective and rapid assessment tool for drylands (S Wan, Ed.). J. Appl. Ecol. 51: 1740–1749.

Reed TE, Schindler DE, Waples RS (2011) Interacting effects of phenotypic plasticity and evolution on population persistence in a changing climate: evolution, plasticity, and climate change. Conserv. Biol. 25: 56–63.

Renaud S (1999) Size and shape variability in relation to species differences and climatic gradients in the African rodent Oenomys. J. Biogeogr. 26: 857–865.

Renaud S (2005) First upper molar and mandible shape of wood mice (*Apodemus sylvaticus*) from northern Germany: ageing, habitat and insularity. Mamm. Biol. 70: 157–170.

Renaud S, Pantalacci S, Quéré JP, Laudet V, Auffray JC (2009) Developmental constraints revealed by co-variation within and among molar rows in two murine rodents. Evol. Dev. 11: 590–602.

Renaud S, Gomes Rodrigues H, Ledevin R, Pisanu B, Chapuis JL, Hardouin EA (2015) Fast evolutionary response of house mice to anthropogenic disturbance on a Sub-Antarctic island. Biol. J. Linn. Soc. 114: 513–526.

Renaud S, Auffray JC, Michaux J (2006) Conserved phenotypic variation patterns, evolution along lines of least resistance, and departure due to selection in fossil rodents. Evolution 60: 1701.

Renaud S, Benammi M, Jaeger JJ (1999) Morphological evolution of the murine rodent *Paraethomys* in response to climatic variations (Mio-Pleistocene of North Africa). Paleobiology 25: 369–382.

Renaud S, van Dam J (2002) Influence of biotic and abiotic environment on dental size and shape evolution in a Late Miocene lineage of murine rodents (Teruel Basin, Spain). Palaeogeogr. Palaeoclimatol. Palaeoecol. 184: 163–175.

Renaud S, Ledevin R (2017) Impact of wear and diet on molar row geometry and topography in the house mouse. Arch. Oral Biol. 81: 31–40.

Renaud S, Michaux J (2004) Parallel evolution in molar outline of murine rodents: the case of the extinct Malpaisomys insularis (Eastern Canary Islands). Zool. J. Linn. Soc. 142: 555–572.

Renaud S, Pantalacci S, Auffray JC (2011) Differential Evolvability Along Lines of Least Resistance of Upper and Lower Molars in Island House Mice (A Goswami, Ed.). PLoS ONE 6: e18951.

Reum J, Essington T, Greene C, Rice C, Fresh K (2011) Multiscale influence of climate on

estuarine populations of forage fish: the role of coastal upwelling, freshwater flow and temperature. Mar. Ecol. Prog. Ser. 425: 203–215.

Reznick DN, Ricklefs RE (2009) Darwin's bridge between microevolution and macroevolution. Nature 457: 837–842.

Riahi K, van Vuuren DP, Kriegler E, Edmonds J, O'Neill BC, Fujimori S, Bauer N, Calvin K, Dellink R, Fricko O, Lutz W, Popp A, Cuaresma JC, Kc S, Leimbach M, Jiang L, Kram T, Rao S, Emmerling J, Ebi K, Hasegawa T, Havlik P, Humpenöder F, Da Silva LA, Smith S, Stehfest E, Bosetti V, Eom J, Gernaat D, Masui T, Rogelj J, Strefler J, Drouet L, Krey V, Luderer G, Harmsen M, Takahashi K, Baumstark L, Doelman JC, Kainuma M, Klimont Z, Marangoni G, Lotze-Campen H, Obersteiner M, Tabeau A, Tavoni M (2017) The Shared Socioeconomic Pathways and their energy, land use, and greenhouse gas emissions implications: An overview. Glob. Environ. Change 42: 153–168.

Ricklefs RE, Miles DB (1994) Ecological and evolutionary inferences from morphology: an ecological perspective. In: Ecol. Morphol. Integr. Org. Biol., 166, pp. 13–41.

Rieder JP, Newbold TAS, Ostoja SM (2010) Structural changes in vegetation coincident with annual grass invasion negatively impacts sprint velocity of small vertebrates. Biol. Invasions 12: 2429–2439.

Rinderknecht A, Jones WW, Araújo N, Grinspan G, Blanco RE (2019) Bite force and body mass of the fossil rodent *Telicomys giganteus* (Caviomorpha, Dinomyidae). Hist. Biol. 31: 644–652.

Rohlf FJ, Corti M (2000) Use of Two-Block Partial Least-Squares to Study Covariation in Shape (R Olmstead, Ed.). Syst. Biol. 49: 740–753.

Rohlf FJ, Slice D (1990) Extensions of the Procrustes Method for the Optimal Superimposition of Landmarks. Syst. Zool. 39: 40.

Rolland J, Condamine FL, Jiguet F, Morlon H (2014) Faster Speciation and Reduced Extinction in the Tropics Contribute to the Mammalian Latitudinal Diversity Gradient (C Moritz, Ed.). PLoS Biol. 12: e1001775.

Roughgarden J (1972) Evolution of Niche Width. Am. Nat. 106.

Rowe KC, Achmadi AS, Esselstyn JA (2016) Repeated evolution of carnivory among Indo-Australian rodents: CARNIVOROUS RODENTS OF INDO-AUSTRALIA. Evolution 70: 653–665.

Royer A, Lécuyer C, Montuire S, Amiot R, Legendre S, Cuenca-Bescós G, Jeannet M, Martineau F (2013) What does the oxygen isotope composition of rodent teeth record? Earth Planet. Sci. Lett. 361: 258–271.

Royer A, Garcia Yelo BA, Laffont R, Hernandez Fernandez M (2020) New bioclimatic models for the quaternary palaearctic based on insectivore and rodent communities. Palaeogeogr. Palaeoclimatol. Palaeoecol. 560: 18.

Salles T, Mallard C, Husson L, Zahirovic S, Sarr AC, Sepulchre P (2021) Quaternary landscape dynamics boosted species dispersal across Southeast Asia. Commun. Earth Environ. 2: 240.

Sampson PD, Streissguth AP, Bookstein FL (1989) Neurobehavioral Effects of Prenatal Alcohol: Part II. Partial Least Squares Analysis I. Neurotoxicol. Teratol. 11: 477–491.

Santana SE, Cheung E (2016) Go big or go fish: morphological specializations in carnivorous bats. Proc. R. Soc. B Biol. Sci. 283: 20160615.

Santana SE, Dumont ER, Davis JL (2010) Mechanics of bite force production and its relationship to diet in bats: Bite force and diet in bats. Funct. Ecol. 24: 776–784.

Scerri EML (2017) The North African Middle Stone Age and its place in recent human evolution. Evol. Anthropol. Issues News Rev. 26: 119–135.

Schap JA, Meachen JA, McGuire JL (2021) Microfauna relative abundance since the Late Pleistocene at Natural Trap Cave, Wyoming, U.S.A. Quat. Int.

Schilling J, Freier KP, Hertig E, Scheffran J (2012) Climate change, vulnerability and adaptation in North Africa with focus on Morocco. Agric. Ecosyst. Environ. 156: 12–26.

Schlager S (2017) Morpho and Rvcg – Shape Analysis in R. In: Stat. Shape Deform. Anal. Elsevier, 217–256.

Schluter D (1996) Adaptative radiation along genetic lines of least resistance. Evolution 50: 1766–1774.

Schmidt GA, Annan JD, Bartlein PJ, Cook BI, Guilyardi E, Hargreaves JC, Harrison SP, Kageyama M, LeGrande AN, Konecky B, Lovejoy S, Mann ME, Masson-Delmotte V, Risi C, Thompson D, Timmermann A, Tremblay LB, Yiou P (2014) Using palaeo-climate comparisons to constrain future projections in CMIP5. Clim. Past 10: 221–250.

Schneider CA, Rasband WS, Eliceiri KW (2012) NIH Image to ImageJ: 25 years of image analysis. Nat. Methods 9: 671–675.

Schradin C, Pillay N (2006) Female striped mice (Rhabdomys pumilio) change their home ranges in response to seasonal variation in food availability. Behav. Ecol. 17: 452–458.

Schulzweida U (2019) CDO User Guide (Version 1.9.8).

Schwenk K (2000) *Form, Function, and Evolution in Tetrapod Vertebrates*.

Selig KR, Khalid W, Silcox MT (2021) Mammalian molar complexity follows simple, predictable patterns. Proc. Natl. Acad. Sci. 118: e2008850118.

Sepulchre P (2016) Links between Solid Earth, Climate Changes, and Biodiversity through Time: Insights from the Cenozoic. In: Ambrosetti D, Boisserie JR, Ayenachew D, Guindeuil T (eds.) Clim. Environ. Chall. Learn. Horn Afr. Centre français des études éthiopiennes.

Sepulchre P, Caubel A, Ladant JB, Bopp L, Boucher O, Braconnot P, Brockmann P, Cozic A, Donnadieu Y, Dufresne JL, Estella-Perez V, Ethé C, Fluteau F, Foujols MA, Gastineau G, Ghattas J, Hauglustaine D, Hourdin F, Kageyama M, Khodri M, Marti O, Meurdesoif Y, Mignot J, Sarr AC, Servonnat J, Swingedouw D, Szopa S, Tardif D (2020) IPSL-CM5A2 – an Earth system model designed for multi-millennial climate simulations. Geosci Model Dev: 43.

Simpson GG (1944) *Tempo and Mode in Evolution.* New York, NY, Columbia University Press.

Simpson GG (1951) The species concept. Evolution 5: 285–298.

Skelly DK, Joseph LN, Possingham HP, Freidenburg LK, Farrugia TJ, Kinnison MT, Hendry AP (2007) Evolutionary Responses to Climate Change. Conserv. Biol. 21: 1353–1355.

Smiley TM, Cotton JM, Badgley C, Cerling TE (2016) Small-mammal isotope ecology tracks climate and vegetation gradients across western North America. Oikos 125: 1100–1109.

Smith HR, Remington CL (1996) Food Specificity in Interspecies Competition. BioScience 46: 436–447.

Sobrino JA, Raissouni N (2000) Toward remote sensing methods for land cover dynamic monitoring: Application to Morocco. Int. J. Remote Sens. 21: 353–366.

Soda KJ, Slice DE, Naylor GJP (2017) Artificial neural networks and geometric morphometric methods as a means for classification: A case-study using teeth from *Carcharhinus* sp. (Carcharhinidae). J. Morphol. 278: 131–141.

Souquet L, Chevret P, Ganem G, Auffray JC, Ledevin R, Agret S, Hautier L, Renaud S (2019) Back to the wild: does feralization affect the mandible of non-commensal house mice (*Mus musculus domesticus*)? Biol. J. Linn. Soc. 126: 471–486.

Stayton CT (2006) Testing hypotheses of convergence with multivariate data: morphological and functional convergence among herbivorous lizards. Evolution 60: 824–841.

Stoetzel E (2009) Les microvertébrés du site d'occupation humaine d'El Harhoura 2 (Pleistocene supérieur - Holocène, Maroc) : systématique, évolution, taphonomie et paléoécologie. : 437.

Stoetzel E, Bailon S, Nespoulet R, El Hajraoui MA, Denys C (2010) Pleistocene and holocene small vertebrates of El Harhoura 2 cave (Rabat–Témara, Morocco): an annotated preliminary taxonomic list. Hist. Biol. 22: 303–319.

Stoetzel E, Marion L, Nespoulet R, El Hajraoui MA, Denys C (2011) Taphonomy and palaeoecology of the late Pleistocene to middle Holocene small mammal succession of El Harhoura 2 cave (Rabat-Témara, Morocco). J. Hum. Evol. 60: 1–33.

Stoetzel E, Bougariane B, Campmas E, Ouchaou B, Michel P (2012a) Chapitre V. Faunes et paléoenvironnements. In: Préhistoire Région Rabat-Témara. Rabat, 35–51.

Stoetzel E, Denys C, Bailon S, El Hajraoui MA, Nespoulet R (2012b) Taphonomic Analysis of Amphibian and Squamate Remains from El Harhoura 2 (Rabat-Témara, Morocco): Contributions to Palaeoecological and Archaeological Interpretations: Taphonomic Study of Amphibian and Squamate Fossil Remains. Int. J. Osteoarchaeol. 22: 616–635.

Stoetzel E, Denys C, Michaux J, Renaud S (2013) *Mus* in Morocco: a Quaternary sequence of intraspecific evolution: Quaternary Evolution of *Mus* in Morocco. Biol. J. Linn. Soc.

109: 599–621.

Stoetzel E (2013) Late Cenozoic micromammal biochronology of northwestern Africa. Palaeogeogr. Palaeoclimatol. Palaeoecol. 392: 359–381.

Stoetzel E, Campmas E, Michel P, Bougariane B, Ouchaou B, Amani F, El Hajraoui MA, Nespoulet R (2014) Context of modern human occupations in North Africa: Contribution of the Témara caves data. Quat. Int. 320: 143–161.

Stoetzel E, Cornette R, Lalis A, Nicolas V, Cucchi T, Denys C (2017) Systematics and evolution of the Meriones shawii/grandis complex (Rodentia, Gerbillinae) during the Late Quaternary in northwestern Africa: Exploring the role of environmental and anthropogenic changes. Quat. Sci. Rev. 164: 199–216.

Stoetzel E (2017) Adaptations and dispersals of anatomically modern humans in the changing environments of North Africa: the contribution of microvertebrates. Afr. Archaeol. Rev. 34: 453–468.

Stoetzel E, Lalis A, Nicolas V, Aulagnier S, Benazzou T, Dauphin Y, El Hajraoui MA, El Hassani A, Fahd S, Fekhaoui M, Geigl EM, Lapointe FJ, Leblois R, Ohler A, Nespoulet R, Denys C (2019) Quaternary terrestrial microvertebrates from mediterranean northwestern Africa: State-of-the-art focused on recent multidisciplinary studies. Quat. Sci. Rev. 224: 105966.

Streissguth AP, Bookstein FL, Sampson PD, Barr HM (1993) *The enduring effects of prenatal alcohol exposure on child development: Birth through seven years, a partial least squares solution.*

Sultan SE, Spencer HG (2002) metapopulation structure favors plasticity over local adaptation. Am. Nat. 160: 13.

Tanner EVJ, Kapos V, Healey JR (1991) Hurricane Effects on Forest Ecosystems in the Caribbean. Biotropica 23: 513.

Tchernov E (2002) The Faunal Sequence of the Southwest Asian Middle Paleolithic in Relation to Hominid Dispersal Events. In: Akazawa T, Aoki K, Bar-Yosef O (eds.) Neandertals Mod. Hum. West. Asia. Boston, Kluwer Academic Publishers, 77–94.

Terray L, Stoetzel E, Herrel A, Cornette R (2021) The contribution of functional traits to the understanding of palaeoenvironmental changes. Biol. J. Linn. Soc.: blab057.

The GIMP Development Team (2018) *GIMP*.

Therrien F (2005) Feeding behaviour and bite force of sabretoothed predators. Zool. J. Linn. Soc. 145: 393–426.

Tieszen LL (1991) Natural variations in the carbon isotope values of plants: Implications for archaeology, ecology, and paleoecology. J. Archaeol. Sci. 18: 227–248.

Trauth MH, Larrasoaña JC, Mudelsee M (2009) Trends, rhythms and events in Plio-Pleistocene African climate. Quat. Sci. Rev. 28: 399–411.

Tribolo C, Asrat A, Bahain JJ, Chapon C, Douville E, Fragnol C, Hernandez M, Hovers E, Leplongeon A, Martin L, Pleurdeau D, Pearson O, Puaud S, Assefa Z (2017) Across the

Gap: Geochronological and Sedimentological Analyses from the Late Pleistocene-Holocene Sequence of Goda Buticha, Southeastern Ethiopia (N Bicho, Ed.). PLOS ONE 12: e0169418.

Tseng H -Y., Liao C -P., Hsu J -Y., Wang L -Y., Huang W -S. (2019) Parental behavior drives large bite force in an insular skink population. J. Zool. 307: 223–231.

Tyszka J (1994) Response of Middle Jurassic benthic foraminiferal morphogroups to dysoxic/anoxic conditions in the Pieniny Klippen Basim Polish Carpathians. Palaeogeogr. Palaeoclimatol. Palaeoecol. 110: 55–81.

Ungar P (2010) *Mammal teeth: origin, evolution and diversity*.

Ungar PS, Sokolova NA, Purifoy J, Fufachev IA, Sokolov AA (2021a) Assessing molar wear in narrow-headed voles as a proxy for diet and habitat in a changing Arctic. Mamm. Biol. 101: 137–151.

Ungar PS, Saylor L, Sokolov AA, Sokolova NA, Gilg O, Montuire S, Royer A (2021b) Incisor microwear of Arctic rodents as a proxy for microhabitat preference. Mamm. Biol. 101: 1033–1052.

Valenzuela S, Poitevin F, Cornette R, Bournery A, Nadal J, Vigne JD (2009) Evolving ecosystems: ecological data from an Iron Age small mammal accumulation at Alorda Park (Catalonia, Spain). J. Archaeol. Sci. 36: 1248–1255.

Van Buskirk J (2012) Behavioural plasticity and environmental change. In: Candolin U, Wong BBM (eds.) Behav. Responses Chang. World Mech. Consequences. Oxford, 145–158.

Van Damme R, Vanhooydonck B, Aerts P, De Vree F (2003) Evolution of lizard locomotion: Context and constraint. In: Vertebr. Biomech. Evol. Oxford, England, 267–282.

Van Valen L (1970) An analysis of developmental fields. Dev. Biol. 23: 456–477.

Van Valkenburgh B (1994) Ecomorphological analysis of fossil vertebrates and their paleocommunities. In: Ecol. Morphol. Integr. Org. Biol., 166, pp. 140–166.

Vander Zanden HB, Bjorndal KA, Reich KJ, Bolten AB (2010) Individual specialists in a generalist population: results from a long-term stable isotope series. Biol. Lett. 6: 711–714.

Vanhooydonck B, Boistel R, Fernandez V, Herrel A (2011) Push and bite: trade-offs between burrowing and biting in a burrowing skink (Acontias percivali). Biol. J. Linn. Soc. 102: 91–99.

Vedder O, Bouwhuis S, Sheldon BC (2013) Quantitative Assessment of the Importance of Phenotypic Plasticity in Adaptation to Climate Change in Wild Bird Populations (C Moritz, Ed.). PLoS Biol. 11: e1001605.

Venables WN, Ripley BD (2002) Modern Applied Statistics with S (Fourth Edition). Springer: 504.

Verde Arregoitia LD, Fisher DO, Schweizer M (2017) Morphology captures diet and locomotor types in rodents. R. Soc. Open Sci. 4: 160957.

Via S (1993) Adaptive Phenotypic Plasticity: Target or By-Product of Selection in a Variable Environment? Am. Nat. 142: 352–365.

Wainwright PC (1994) Functional morphology as a tool in ecological research. In: Ecol. Morphol. Eds PC Wainwright SM Reilly. Chicago, USA, 42–59.

Wainwright PC (2005) Many-to-One Mapping of Form to Function: A General Principle in Organismal Design? Integr. Comp. Biol. 45: 256–262.

Walker JA (2007) A General Model of Functional Constraints on Phenotypic Evolution. Am. Nat. 170: 681–689.

Walker JA (2010) An Integrative Model of Evolutionary Covariance: A Symposium on Body Shape in Fishes. Integr. Comp. Biol. 50: 1051–1056.

Wang X, Qiu W, Zamar RH (2007) CLUES: A non-parametric clustering method based on local shrinking. Comput. Stat. Data Anal. 52: 286–298.

Wei T, Simko V (2021) R package 'corrplot': Visualization of a Correlation Matrix. (Version 0.90).

Weijs WA, Hillen B (1986) Correlations between the cross-sectional area of the jaw muscles and craniofacial size and shape. Am. J. Phys. Anthropol. 70: 423–431.

Wengler L, Vernet JL, Ballouche A, Damblon F, Michel P (1992) Signification des paléomilieux et évolution du climat au Maghreb. Le Maroc oriental au Pléistocène récent. Bull. Société Bot. Fr. Actual. Bot. 139: 507–529.

West-Eberhard MJ (1989) Phenotypic Plasticity and the Origins of Diversity. Annu. Rev. Ecol. Syst. 20: 249–78.

Wheeler QD, Meier R **(Eds.)** (2000) *Species concepts and phylogenetic theory: a debate*. New York, Columbia University Press.

Whiting MR, Wheeler WC (1994) Insect homeotic transformation. Nature.

Wickham H (2015) *ggplot2: elegant graphics for data analysis.* Springer.

Williams EE (1983) Ecomorphs, faunas, island size, and diverse end points in island radiations of *Anolis*. In: Huey RB, Pianka ER, Schoener TW (eds.) Lizard Ecol. Harvard University Press, 326–370.

Wills MA, Briggs DEG, Fortey RA (1994) Disparity as an evolutionary index: a comparison of Cambrian and Recent arthropods. Paleobiology 20: 93–130.

Wolf M, Friggens M, Salazar-Bravo J (2009) Does weather shape rodents? Climate related changes in morphology of two heteromyid species. Naturwissenschaften 96: 93–101.

Wolff J (1892) *Das Gesetz der Transformation der Knochen*. Berlin.

Wong BBM, Candolin U (2015) Behavioral responses to changing environments. Behav. Ecol. 26: 665–673.

Wroe S, McHenry C, Thomason J (2005) Bite club: comparative bite force in big biting mammals and the prediction of predatory behaviour in fossil taxa. Proc. R. Soc. B Biol.

Sci. 272: 619–625.

Yazdi T, Adriaens D (2011) Patterns of skull shape variation in Meriones persicus (Rodentia: Muridae) in relation to geoclimatical conditions. 7: 129–142.

Yom-Tov Y, Geffen E (2006) Geographic variation in body size: the effects of ambient temperature and precipitation. Oecologia 148: 213–218.

Young HS, McCauley DJ, Galetti M, Dirzo R (2016) Patterns, Causes, and Consequences of Anthropocene Defaunation. Annu. Rev. Ecol. Evol. Syst. 47: 333–358.

Young RL, Badyaev AV (2006) Evolutionary persistence of phenotypic integration: influence of developmental and functional relationships on complex trait evolution. Evolution 60: 1291–1299.

Young RL, Badyaev AV (2010) Developmental plasticity links local adaptation and evolutionary diversification in foraging morphology. J. Exp. Zoolog. B Mol. Dev. Evol. 314B: 434–444.

Young RL, Haselkorn TS, Badyaev AV (2007) Functional equivalence of morphologies enables morphological and ecological diversity. Evolution 61: 2480–2492.

Young RL, Sweeney MJ, Badyaev AV (2010) Morphological diversity and ecological similarity: versatility of muscular and skeletal morphologies enables ecological convergence in shrews: *Morphological versatility and evolution*. Funct. Ecol. 24: 556–565.

Zachos J, Pagani M, Sloan L, Thomas E, Billups K (2001) Trends, Rhythms, and Aberrations in Global Climate 65 Ma to Present. Science 292: 686–693.

Zaime A, Gautier J (1989) Comparaison des régimes alimentaires de trois espèces sympatriques de Gerbillidae en milieu saharien au Maroc. Rev Ecol Terre Vie 4: 153–163.

Zalasiewicz J, Williams M, Smith A, Barry TL, Coe AL, Bown PR, Brenchley P, Cantrill D, Gale A, Gibbard P, Gregory FJ, Hounslow MW, Kerr AC, Pearson P, Knox R, Powell J, Waters C, Marshall J, Oates M, Rawson P, Stone P (2008) Are we now living in the Anthropocene. GSA Today 18: 4.

Zelditch M **(Ed.)** (2004) *Geometric morphometrics for biologists: a primer*. Amsterdam ; Boston, Elsevier Academic Press.

Zeveloff SI, Boyce MS (1988) Body size patterns in North American mammal faunas. In: Boyce MS (ed.) Evol. Life Hist. Mamm. Connecticut, United States, 123–146.

List of abbreviations

General

EH2	El Harhoura 2
L1	Stratigraphic layer number 1
Act, L0	Current days period
MG	Morphological group
m1	First lower molar
M1	First upper molar

Datation

ka	kiloannum (1000 years)
BP	Before present
ESR	Electron Spin Resonance
OSL	Optically Stimulated Luminescence
US	Uranium series
DH	Dating hypothesis

Paleoclimatology

CM	Climate model
LR	Low resolution
MR	Medium resolution
IPSL	Institut Pierre Simon Laplace

Statistics

2B-pls	Two blocks partial least square
MANOVA	Multivariate analysis of variance
ANOVA	Analysis of variance
CR	Covariance ratio
GPA	Generalized Procrustes Analysis

Appendix

This appendix gathers additionnal scientific productions published during the thesis, but that are not directly related to it.

Terray L, Plateau O, Abourachid A, Böhmer C, Delapré A, de la Bernardie X, Cornette R (2020) Modularity of the Neck in Birds (Aves). Evol Biol 47: 97–110.

Terray L, Denys C, Steven SM, Soarimalala V, Lalis A*, Cornette R* (*In press*) Skull morphological evolution in Malagasy endemic Nesomyinae rodents. PloS ONE.

Evolutionary Biology
https://doi.org/10.1007/s11692-020-09495-w

RESEARCH ARTICLE

Modularity of the Neck in Birds (Aves)

Léa Terray[1] · Olivia Plateau[2] · Anick Abourachid[3] · Christine Böhmer[3] · Arnaud Delapré[1] · Xavier de la Bernardie[4] · Raphaël Cornette[1]

Received: 9 December 2019 / Accepted: 10 March 2020

Abstract

The neck connects the head and the trunk and is the key structure allowing all movements of the head. The neck morphology of birds is the most variable among living tetrapods, including significant differences in the number and shape of the cervical vertebrae. Despite these differences, according to the literature, three morphofunctional regions (i.e., modules) have been identified along the neck. However, this regionalization has not been quantitatively tested through a geometric morphometric approach applied to the cervical vertebrae. Based on the examination of 187 cervical vertebrae belonging to 16 species with various ecologies, we revealed a common modular structure of the neck using 3D surface geometric morphometrics. We adopted an approach without a priori clustering to identify modules along the neck. The phylogenetic influence on each module was tested. Then, each module was digitally reconstructed as a 3D vertebral model, and postural characteristics were studied. We characterized 9 modules: 7 are transpecific, being shared by at least 2 and up to 15 species. Two modules are specific to species with particularly long necks. The modularity pattern appears to be tightly linked to morphofunctional aspects and partially to phylogeny. In contrast, feeding ecology seems to be more closely related to the chaining of modules (the neck) than to the modules themselves. A study of postural properties revealed that each modular unit exhibits a characteristic curvature. Overall, the modular structure of the neck corresponds to the three traditional functional regions. However, the results also revealed unexpected pattern complexity, including subdivisions within these regions. The study of the patterns of modularity is therefore a relevant approach for challenging the three-functional-region hypothesis and allowed us to identify the structure of the diversity of the necks of birds.

Keywords Functional biology · Modularity · Birds · Cervical vertebrae · Geometric morphometrics

Lea Terray and Olivia Plateau have Equal Authorship.

Electronic supplementary material The online version of this article (https://doi.org/10.1007/s11692-020-09495-w) contains supplementary material, which is available to authorized users.

✉ Léa Terray
lea.terray@mnhn.fr

✉ Olivia Plateau
olivia.plateau@unifr.ch

[1] UMR 7205 Institut de Systématique, Evolution, Biodiversité (ISYEB), Muséum National D'Histoire Naturelle, CNRS, Sorbonne Université, EPHE, Université des Antilles, CP 50, 57 rue Cuvier, 75005 Paris, France

[2] Faculté des sciences, Département de géosciences, Université de Fribourg, Chemin du musée 6, 1700 Fribourg, Switzerland

[3] UMR 7179 Mécanismes Adaptatifs Et Evolution (Mecadev), Muséum National d'Histoire Naturelle – CNRS., CP 55, 57 rue Cuvier, 75231 Paris, France

[4] UMR 6457, SUBATECH, IMT-Atlantique, Université de Nantes, CNRS/IN2P3, 4 rue Alfred Kastler, Nantes, France

Introduction

The neck, which is morphologically defined as an association of multiple cervical vertebrae (Romer 1950), is a key structure of tetrapods (limbed vertebrates) facilitating varied complex movements (Long et al. 1997; Johnson and Shapiro 1998; Daeschler et al. 2006; Ericsson et al. 2013; Pierce et al. 2013). In contrast to mammals, which almost exclusively exhibit seven cervical vertebrae, irrespective of neck length (Galis 1999), the number of vertebrae in the necks of birds varies greatly (Böhmer et al. 2019), ranging from ten cervical vertebrae in many parrots to 26 cervical vertebrae in the swan (Boas 1929; Böhmer et al. 2019). In addition to this numerical variability, birds display a high shape variability of the cervical vertebrae across species (Boas 1929). The differences in vertebral morphology and number appear to be linked to behavioral adaptations involving special feeding techniques (as observed in the darter bird *Anhinga anhinga*

Published online: 18 March 2020

Boas 1929) or peculiar locomotion modes (Dilger 2010; Müller et al. 2010; Wilkinson and Ruxton 2012). This high diversity of shape and associated functions is associated with a wide range of ecologies (Stevens and Parrish 1999; Graf et al. 1994; Alexander 1985); for example bassoon nuts are fishing birds, while woodpeckers are strongly specialized to extract insects directly from tree bark.

Despite the wide variation in the number and morphology of cervical vertebrae, the necks of birds have traditionally been divided into three main morphofunctional regions. Inspired by Virchow (1910), who investigated the mobility of the neck in the penguin, Boas (1929) compared neck mobility across a larger sample of bird species. According to differences in maximal dorsoventral mobility between successive vertebrae, the cervical vertebral column of birds can be divided into three main regions (Virchow 1910; Boas 1929). The cranial portion is characterized by prevalent ventral flexion, the intermediate region is prevalently flexible in the dorsal direction, and the caudal portion allows movements in both directions. Several studies have supported this regionalization of the avian neck (e.g., Zweers et al. 1987; Heidweiller et al. 1992; Bout 1997; van der Leeuw et al. 2001; Tambussi et al. 2012; Cobley et al. 2013; Krings et al. 2017; but see also Kambic et al. (2017), who challenged this three-region model).

The concept of modularity suggests the existence of modules, or sets of traits that show greater covariance within each set than compared with traits of other sets and, thus, evolve partially independently (Olson and Miller 1958; Riedl 1978; Cheverud 1996; Klingenberg 2008, 2010; Hallgrimsson et al. 2009). Three main types of modularity exist (West-Eberhart 2003; Klingenberg 2008; Hallgrimsson et al. 2009): developmental, functional and evolutionary modularity, which affect morphological variation at different scales. Modules are generally defined based on shape covariation (Klingenberg 2008). Here, because we worked on serially homologous structures (vertebrae), we assessed degree of shape covariation between them based on their morphological proximity. We define a module as a set of homologous structures that are the most similar. The patterning and regionalization of the vertebral column is a topic that has been well studied in a broad panel of tetrapods (e.g., Polly et al. 2001; Hautier et al. 2010; Asher et al. 2011; Arnold et al. 2016; Randau et al. 2017 among others); however, within birds, such studies have been quite limited (e.g., Guinard et al. 2010; Guinard and Marchand 2010; Guinard 2012; Azevedo et al. 2012; Böhmer et al. 2015). Diverse methods have been used to quantify these characteristics, such as traditional linear distance approaches (e.g., Guinard et al. 2010; Guinard and Marchand 2010), among which geometric morphometrics (GM) is the most widespread method for the study of morphological modularity (Klingenberg 2008; Klingenberg and Marugan-Lobon 2013; Klingenberg 2014; e.g., Böhmer et al. 2015; Head and Polly 2015; Randau et al. 2017). However, previous studies on the modularity of the neck of birds have focused only on a single taxon or a few taxa have often applied a developmental perspective to the structure. At present, a large-scale analysis of the modularity of the necks of birds using state-of-the-art statistical shape methods is lacking.

The aim of this study was to reveal how shape diversity is structured in bird necks by studying the patterns of modularity at the interspecific level. To this end, we investigated the complete cervical vertebral columns of 16 different bird species with varied ecologies using a three-dimensional surface GM (3D SGM) approach, allowing us to accurately quantify the entire shape of the cervical vertebrae. We chose an innovative approach to investigate modularity, and we defined a module as a set of vertebrae that share a common morphology and are more similar to each other compared to the vertebrae outside the module. This definition is applicable because vertebrae are serially homologous structures. To identify modules, vertebrae were grouped using an approach without a priori clustering. For each module, the phylogenetic signal was assessed, and postural properties in a relaxed posture were studied. We discuss the relative importance of three potential factors: feeding ecology, phylogeny, and morphofunctional aspects, at two different scales of shape variation: the modules and the neck, and we then challenge the three commonly established functional regions in light of our results.

Material and Methods

Sample

We sampled the cervical vertebral columns of 16 extant bird species (Table 1). The atlas (first cervical vertebra) was not included in the analysis due to its unique morphology and the lack of specific anatomical homologies with the postatlantal cervical vertebrae. In total, 3D models of 187 cervical vertebrae (CVs) were obtained. The taxa were chosen to be distributed within the phylogenetic tree and to provide a wide range of body sizes (from the 7.5 cm colibri to the 2.5 m ostrich) and feeding ecologies (piscivores, frugivores, granivores, nectarivores, scavengers) within the limits of the available specimens in the Muséum National d'Histoire Naturelle osteological collection.

3D scans

3D models of the specimens were generated using different scanning methods depending upon the size of the bones to achieve the best results. The CVs of the four largest specimens in the sample were digitized using Breuckmann

Table 1 Sampling

Genus	Species	Number of CVs	Collection number	Missing data	Feeding ecology
Crypturellus	*cinereus*	16	MNHN 2004–187	–	Insectivorous Frugivorous Granivorous
Apteryx	*sp.*	14	BMNH 17–01-72–1	–	Insectivorous
Struthio	*camelus*	18	MNHN 1908–160	–	Insectivorous Frugivorous Granivorous
Chlorostilbon	*mellisugus*	11	MNHN 2000–466	CV 6	Nectarivorous
Gallirallus	*gallirallus*	13	MNHN 1870–182	–	Insectivorous
Aptenodytes	*patagonicus*	12	Unumbered	–	Piscivorous
Anhinga	*anhinga*	18	MNHN 1885–543	CV 10	Piscivorous
Morus	*bassanus*	15	MNHN 1997–189	–	Piscivorous
Gyps	*fulvus*	15	MNHN 1996–43	–	Scavenger
Dryocopus	*martius*	11	MNHN 2013–344	CVs 3, 4, 8	Insectivorous
Cacatua	*moluccensis*	11	MNHN 2000–88	CV 2, 8	Frugivorous
Amazona	*dufresniana*	12	MNHN 2004–198	–	Frugivorous
Calyptomena	*viridis*	11	MNHN 1997–886	CV 2, 11	Frugivorous Granivorous
Oriolus	*oriolus*	12	MNHN 1993–131	–	Frugivorous Granivorous
Bombycilla	*garullus*	12	MNHN 2010–115	CV 9	Frugivorous Granivorous
Hirundo	*rustica*	13	MNHN 2000–733	CV 3	Granivorous

BMNH British Museum of Natural History, *MNHN* Muséum National d'Histoire Naturelle Paris

3D surface scanners at the Museum National d'Histoire Naturelle, Paris (UMS 2700): the taxa of intermediate size (*Aptenodytes, Morus, Gyps*) were digitized using a blue-light fringe 3D scanner (SmartScan 3D model) and the larger taxon *Struthio* using a white-light fringe 3D scanner (StereoScan 3D model with a camera resolution of 5 megapixels). Then, Geomagic (Geomagic Studio; Raindrop Geomagic, Research Triangle Park, North Carolina, USA) was used to prepare the scans as described by Botton-Divet et al. (2015). The other 12 specimens were scanned with an RX Solutions microtomograph (Easy Tom 4) with the following settings::U = 100 kV, I = [100–386] µA, helical trajectory, voxel size = 11.3 µm for *Hirondo* and *Chlorostilbon*, 23.3 µm for *Oriolus* and *Bombycilla* and 54.3 µm for other genera. The reconstruction software was RX Solutions XAct 2.0 r 8177. The dataset was then segmented, and surface meshes were generated using Avizo software.

3D Surface Geometric Morphometrics

Vertebrae exhibit a particularly complex shape that cannot be precisely recorded through traditional landmark-based procedures. Therefore, we applied a 3D surface sliding landmark approach (Bookstein 1997; Gunz et al. 2005) using three types of landmarks: homologous anatomical landmarks and sliding semilandmarks of curves and surfaces.

The anatomical landmarks and sliding semilandmarks of curves were manually digitized using the Landmark software (Wiley et al. 2005), and the sliding semilandmarks of surfaces were positioned using sliding landmarks and relaxation procedures. This was done following the protocol of Gunz et al. (2005), and the workflow is detailed by Botton-Divet et al. (2015). The sliding landmarks procedure was performed using the placePatch function of the Morpho package (Schlager 2013) in the free software R (R Core team 2017). We first designed a template following the method of Cornette et al. (2013). Second, the function placePatch automatically projected the sliding semilandmarks of surfaces from the template on all other scans via thin-plate spline deformation. To be more accurate, the template was deformed to correspond to the anatomical landmarks and sliding semilandmarks of the curves of the target specimen, and the coordinates of the sliding semilandmarks of the surfaces of the deformed template were then projected on the target specimen. Subsequently, relaxation against the template was performed using the relaxLM function from the same package, allowing sliding semilandmarks of surfaces to freely slide along the surface to minimize bending energy. The sliding and relaxation procedures were both repeated iteratively. Thereafter, to remove biases linked to the first relaxation against the template, a second spline relaxation procedure was executed against the mean of all objects

with the slider3d function from the same package. Sliding semilandmarks are geometric homologs, and because of these procedures, all landmarks of the dataset could be compared and analyzed using traditional morphometrics. In total, 16 anatomical landmarks, 651 sliding semilandmarks of curves and 159 sliding semilandmarks on surfaces were used (Fig. 1, Table 2).

All landmark coordinates were superimposed via generalized Procrustes analysis (GPA) to remove the nonshape effects of rotation, translation and scale (Rohlf and Slice 1990) using the gpagen function of the Geomorph package (Adams and Otárola-Castillo 2013).

All subsequent statistical treatments and analyses were also performed using the free software R (R Core team 2017).

Module Identification

We define a module as a set of CVs that share similar morphologies. To identify and characterize these modules, we used an unsupervised pattern recognition method: Gaussian mixture analysis (Fraley and Raftery 1998; Everitt and Dunn 2001). Gaussian mixture analysis is a classification method that identifies Gaussian subsets within the main Gaussian of the dataset without prior information on the objects. The Gaussian assumption is especially adapted to morphometric data. First, size elimination and projection into reduced space, as performed by principal component analysis (PCA), contribute to the normalization of the data (Diaconis and Freedman 1984). Then, unsupervised clustering is performed, which is a highly efficient method for datasets whose sizes and shapes may vary between groups (Baylac et al. 2003; Cordeiro-Estrela et al. 2006), as is the case for morphometric data.

We also performed PCA of the Procrustes coordinates using the plotTangentSpace function of the Geomorph package (Adams and Otárola-Castillo 2013). We retained 90% of the shape variability as shape variables. Only 90% of the variability was considered because the last principal components are generally considered noise (Baylac and Frieß 2005). For these variables, we performed a model-based clustering analysis, applying the Mclust function from the mclust library (Fraley and Raftery 2012). This function finds the number of clusters without a priori, according to the covariance structure of the dataset. It is based on an algorithm designed by Dasgupta and Raftery (1998), and generalized by Fraley and Raftery (1998). Here are the main steps of the algorithm, as written by Fraley and Raftery (1998): "(1) Determine a maximum number of clusters to consider (M) and a set of candidate parametrizations of the Gaussian model to consider. In general M should be as small as possible. (2) Do agglomerative hierarchical clustering for the unconstrained Gaussian model, and obtain the corresponding classifications for up to M groups. (3) Do EM (Expectation Maximization algorithm) for each parametrization and each number of clusters [from 2 to M] starting with the classification from hierarchical clustering. (4) Compute the BIC (Bayesian Information Criterion) for the one-cluster

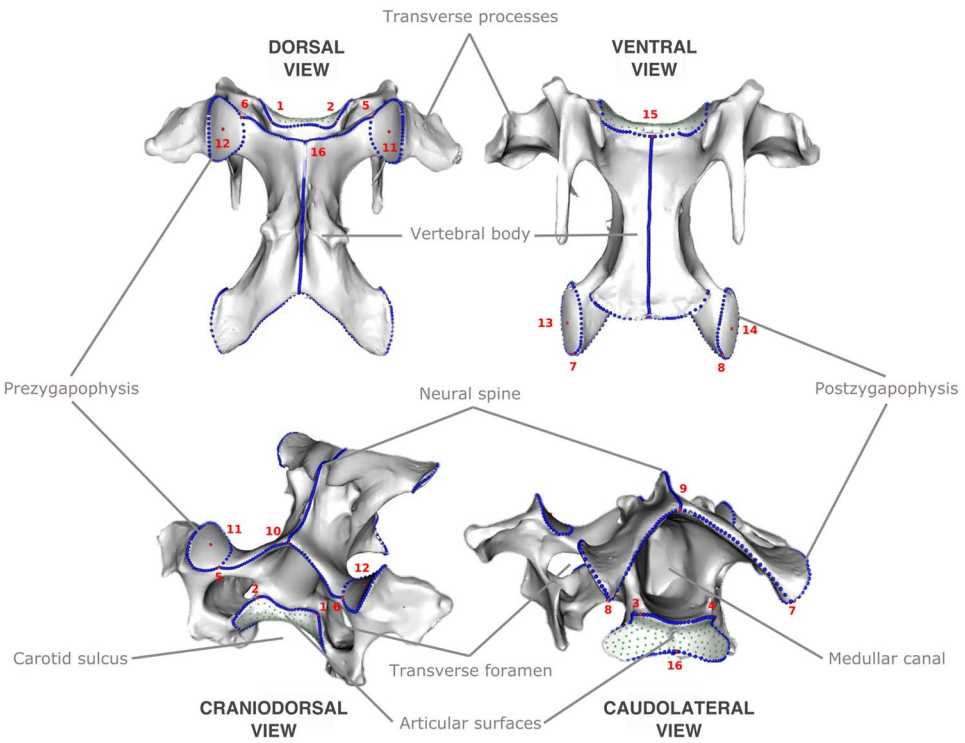

Fig. 1 Cervical vertebrae anatomy and landmarks locations used in our analysis (sixth vertebrae of *Gyps fulvus*). Red points: 16 anatomical landmarks; blue points: 651 sliding semilandmarks of curves; green points: 159 sliding semilandmarks of surfaces (Color figure online)

Table 2 Definition of the anatomical landmarks, semilandmarks of curves (define between anatomical landmarks) and semilandmarks of surfaces (define by semilandmarks of curves)

	Definitions
Anatomical Landmarks	
1	Maximum curvature of the dorsal and right part of the cranial articular surface
2	Maximum curvature of the dorsal and left part of the cranial articular surface
3	Maximum curvature of the dorsal and left part of the caudal articular surface
4	Maximum curvature of the dorsal and right part of the caudal articular surface
5	Junction of vertebral arch and left prezygapophyse facet
6	Junction of vertebral arch and right prezygapophyse facet
7	Junction of vertebral arch and right postzygapophyse facet
8	Junction of vertebral arch and left postzygapophyse facet
9	Caudal maximum curvature of vertebral arch
10	Cranial maximum curvature of vertebral arch
11	Middle of left prezygapophyse facet
12	Middle of right prezygapophyse facet
13	Middle of right postzygapophyse facet
14	Middle of left postzygapophyse facet
15	Middle ventral curvature of the cranial articular surface
16	Middle ventral curvature of the caudal articular surface
Semilandmarks of curves	
1–2–15	Outline of the cranial articular surface
3–4–16	Outline of the caudal articular surface
5–10–6	Border of the cranial face of the vertebral arch
8–9–7	Border of the caudal face of the vertebral arch
5	Outline of left prezygapophyse facet
6	Outline of right prezygapophyse facet
8	Outline of left postzygapophyse facet
7	Outline of right postzygapophyse facet
9–10	Central line along the dorsal face of the vertebral arch
15–16	Central line along the ventral face of the vertebral body
Semilandmarks of surfaces	
1–2–15	Cranial articular surface
3–4–16	Caudal articular surface

model for each parametrization and for the mixture likelihood with the optimal parameters from EM for [2 to M] clusters. This gives a matrix of BIC values corresponding to each possible combination of parametrization and number of clusters. (5) Plot the BIC values for each model. A decisive first local maximum indicates strong evidence for a model (parametrization + number of clusters)." In this study, the VEI model (model: λkA, distribution: diagonal, volume: variable, Shape: equal, orientation: coordinate axes) (Fraley and Raftery 2012) was used to parameterize the covariance matrix.

To quantify the significance of those modules, we tested the reciprocal influence of modules and species on the overall vertebrae shape. We performed a Procrustes MANOVA with permutation procedures, a resampling method that aim to validate the model by using random subsets of the data. We used the function 'procD.lm' from package 'geomorph' (Adams and Otárola-Castillo 2013). Then the proportion of variance that correspond to each of these factors was calculated according to the formula: SSf / SSt = V, where SSf is the sum of squares for the factor, SSt the total sum of squares and V the proportion of variance explained by the factor.

For each identified subset (i.e., module), we constructed 3D mean shape meshes. First, mean landmark coordinates were calculated using the mshape function of the Geomorph package (Adams and Otárola-Castillo 2013). Then, a thin plate spline deformation was applied on the closest mesh from the mean shape of the module (identified using the findMeanSpec function), so that the deformed mesh corresponded to the mean landmark coordinates calculated with the warpRefMesh function. Each mean mesh was exported using the mesh2ply function.

Shape Trajectories

To obtain a better overview of the diversity of the neck, we plotted the shape trajectories of each species using the ggplot and geom_segment functions from the ggplot2 package (Wickham 2015). Shape trajectories are the trajectories of shape changes between successive CVs in the PC1 vs. PC2 morphospace (raw PCAs with shape trajectories are available in SP Fig. 2) (i.e., the morphospace trajectory from the first to the last CV). This approach provides a simple visual representation of shape changes along the neck, as explained by Werneburg et al. (2015). We then visualized the order of the modules along the neck using the mean shape meshes of Fig. 2.

Influence of Phylogeny on the Modules

The phylogenetic influence on each module was tested, and the results are presented in Table 2. The hypothesis regarding the phylogenetic relationships of the birds considered in our study was based on molecular data (Hackett et al. 2008). A consensus topology (strict consensus tree) was generated from downloaded samples (100 randomly selected phylogenetic trees from the Global Bird Tree (Jetz et al. 2012) using the phytools, ape, picante and geiger packages in R (Paradis et al. 2004; Harmon et al. 2008; Kembel et al. 2010; Revell 2012). To quantify the phylogenetic influence, we used the K-statistic method developed by Blomberg et al. (2003) and adapted to multivariate data by Adams (2014), which quantifies the phylogenetic signal within datasets containing several variables such as shape. The phylogenetic signal was assessed for each module independently except for module 7, module 8 and module 9, for which the signal was not computable because these modules were present only in one or two species. A high K-value indicates a strong phylogenetic signal, meaning that the corresponding module is influenced by strong phylogenetic constraints. K-values were calculated using the physignal function in the Geomorph library (Adams and Otárola-Castillo 2013).

Reconstruction of the Osteological Neutral Posture for Each Module

To explore the effect of the specific morphology of each module on its curvature in the osteological neutral posture (Stevens and Parrish 1999), we reconstructed global mean modules and measured their curvature angle, both between two CVs and for the entire module. The reconstructions of the modules were generated by duplicating the mean shape meshes a number of times, where the number of duplications was equivalent to the number of CVs per module, which was estimated from an average calculation based on our sample. Using the software blender ver. 2.79 (Blender Foundation 2003–2018), we assembled the duplicated CVs in anatomical connection so that the articular surfaces of the vertebral body and the pre- and postzygapophyses of two successive CVs were in contact with each other without overhang. This arrangement based on osteological criteria does not take into account additional constraints/possibilities due to soft tissue such as muscles and ligaments.

Results

Module Identification

We identified nine statistically significant modules. Seven of them were found in the studied species (SP Fig. 1).

The manova testing the influence of modules and species revealed that both factors significantly influence vertebrae shape (modules: p-value < 0.05; species: p-value < 0.05). Modules explain 63% of vertebrae shape, while species explain 13%.

The comparison of the mean shape of each module presented in Fig. 2 reveals that the modules are characterized by specific morphological features. Transversal processes appear to be one of the less variable features from one module to another.

Module 1

The CVs of the first module are characterized by a well-developed neural spine that points vertically. They exhibit rather large, ventrally curved prezygapophyses and slightly ventrally inclined postzygapophyses. Another characteristic feature is the ventral process on the centrum. In dorsal view, the CVs present an X-shape.

Module 2

The characteristic features of the CVs in this module include the presence of well-developed transverse processes, including fused cervical ribs and a mostly enclosed carotid sulcus. In cranial view, the articular surface of the prezygapophyses is inclined medially. The orientation of the articular surface of the postzygapophyses is slightly ventrally inclined in lateral view. The neural spine is rather low.

Module 3

The CVs are compact with a high and wide vertebral body. In cranial view, the articular surface of the prezygapophyses exhibits a dorsomedial orientation. They are less concave than those of the second module. The articular surface of the postzygapophyses is rather horizontal in lateral view. The

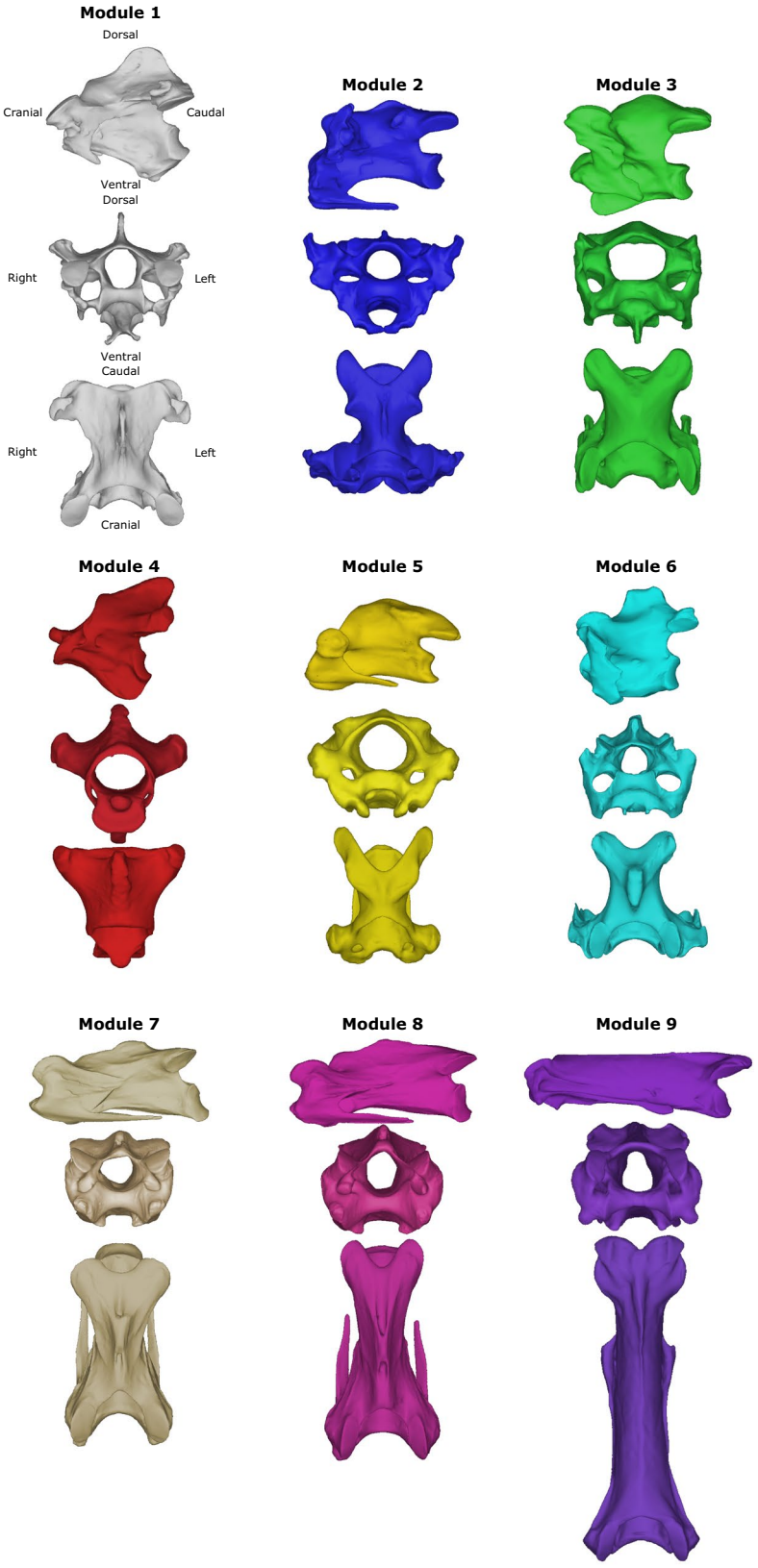

Fig. 2 Mean shape meshes of the nine modules identified by Gaussian mixture

medullar canal is oval, horizontally elongated, and hypapophysis is well developed.

Module 4

The fourth module comprises only one CV, which is the axis (the second cervical vertebra). Compared to the postaxis CVs in the neck, it is very peculiar in its morphology and consequently forms a group of its own. The most pronounced feature is the absence of a prezygapophysis and the presence of the odontoid process cranially articulating with the atlas (the first CV) and the occiput of the skull. In lateral view, the well-developed neural spine projects caudally, with the caudal border being almost aligned with the postzygapophyses. The axis presents a well-developed ventral process. Transverse foramina are missing. The postzygapophyses are ventrally oriented.

Module 5

The morphology of the CVs of module 5 resembles that of module 2, but the neural arch has a rounded shape in lateral view, and the spinal canal is rather large. The articular surface of the prezygapophyses has a dorsomediocaudal orientation; that of the postzygapophyses has a ventrolateral orientation. The carotid sulcus is marked.

Module 6

The CVs of this module are compact (similar to module 3) with well-developed neural spines. The articular surface of the prezygapophyses has a dorsomedial orientation in cranial view. The articular surface of the postzygapophyses presents a ventrolateral orientation. The spinal canal is rounded, and the carotid sulcus is slightly marked.

Module 7

The CVs are elongated and characterized by a rather small neural spine. The articular surface of the prezygapophysis is inclined dorsomedially, whereas the articular surface of the postzygapophyses are inclined ventrolaterally. The postzygapophyses are very short and are set back from the caudal end of the vertebral centrum. The carotid sulcus is marked. The transverse processes develop with long fused cervical ribs. This module was only identified in the neck of *Anhinga* and *Struthio* specimens.

Module 8

The CVs of module 8 also display an elongated morphology, even more so than those of module 7. The articular surface of the prezygapophyses is inclined ventrally in lateral view and medially in cranial view. The articular surface of the postzygapophyses is inclined ventrally. The carotid sulcus is marked. The transverse processes develop with long fused cervical ribs, which are shorter than those of module 7. The medullar canal is oval, being vertically elongated. This module was only identified in the neck of *Struthio* specimens.

Module 9

The CVs of module 9 are extremely elongated, more so than those of modules 7 and 8. In cranial and lateral view, the articular surface of the pre- and postzygapophyses are inclined ventrally. In particular, the postzygapophyses are very long and project caudally, extending over the caudal end of the vertebral centrum. The carotid sulcus is marked. This module was only found in the neck of *Anhinga* specimens.

Shape Trajectories

Species' shape trajectories—i.e., morphospace trajectory from the second to the last CV—are presented in Fig. 3.

All modules are present in more than one species except for modules 8 and 9, which are only present in *Anhinga*. The number of CVs constituting each module is quite stable; however, it is different between the modules. For instance, module 1 is generally composed of two or three CVs, and module 4 is always composed of one CV. The distribution of the modules along the neck is quite similar among species. For example, module 4 contains only the second cervical vertebra of each species, and module 1 is always found subsequent to module 4. Some other modules occupy the same place in the shape trajectory as modules 2 and 5.

The shape trajectories can be divided into two categories based on the shape of the trajectory. The first category includes trajectories that display a reversed C-shape (*Calyptomena, Bombycilla, Amazona, Dryocopus, Aptenodytes, Morus, Oriolus* and *Cacatua*). In some members of this group, the first and last vertebrae of the shape trajectory are truly close to each other in the morphospace. This is observed for *Aptenodytes, Dryocopus* and *Morus* (Fig. 3). In addition, *Morus* shows some peculiarities regarding the positions of the CVs of module 2 (Fig. 3). The second category of shape trajectories has a crushed reversed C-shape, meaning that the lower arc of the shape trajectories rises against the upper arc (*Chlorostilbon, Crypturellus, Gyps, Apteryx* and *Hirundo*). Among the members of this group, *Chlorostilbon* and *Apteryx* show peculiar shape trajectories (Fig. 3). Two species could not be assigned to one of these two general categories: *Anhinga* and *Struthio*.

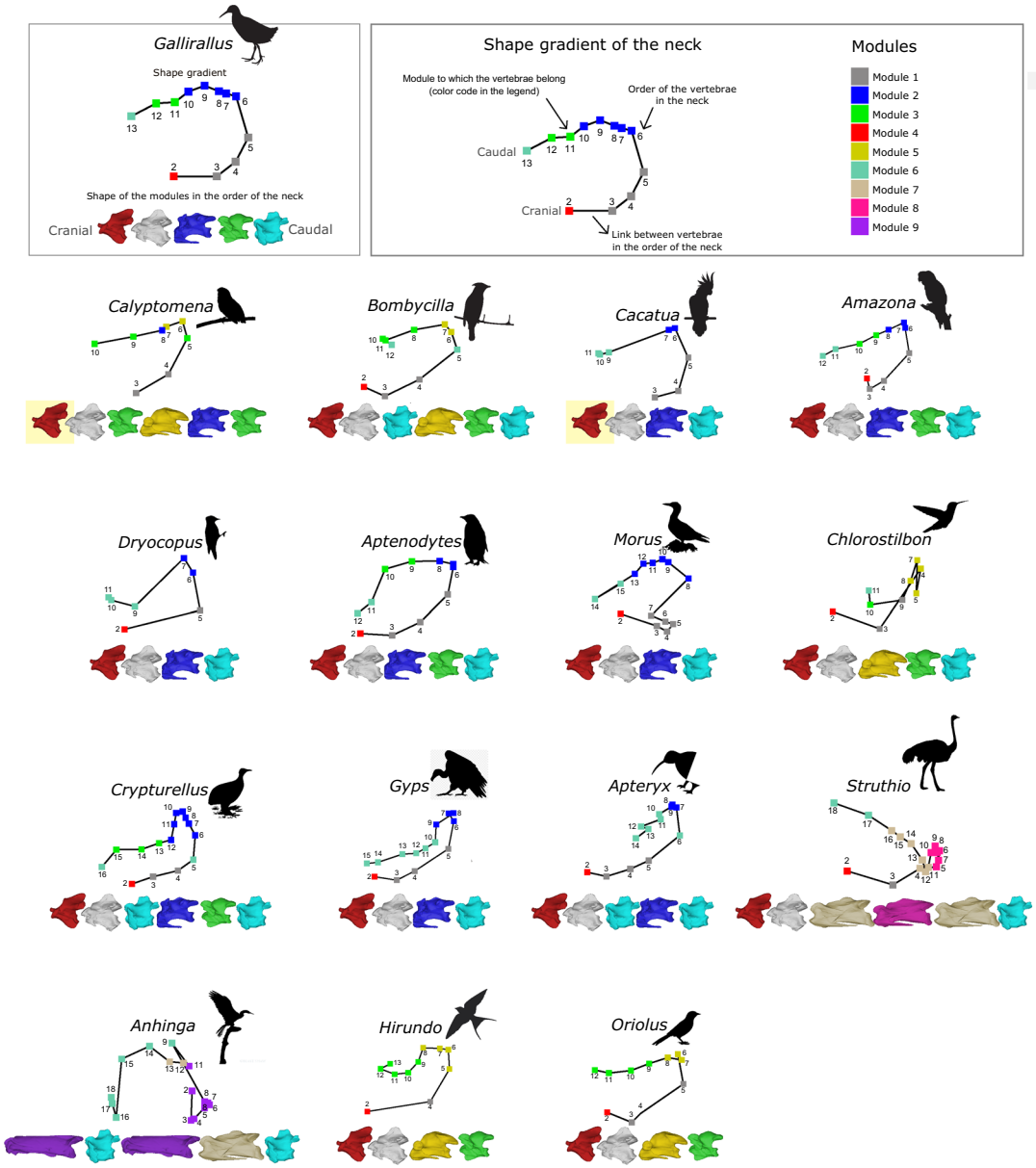

Fig. 3 Shape trajectories of the 16 species and order of the modules along the neck. Vertebrae with yellow background are missing modules (related to missing data) that we hypothesized to be present (Color figure online)

Influence of Phylogeny on Modules

The phylogenetic influence on each module was tested (Table. 3). The phylogenetic test was not applicable to module 7, module 8 or module 9 because they are species specific to *Anhinga* and *Struthio*. Modules 1, 2, 4 and 6 are significantly influenced by phylogeny, with a strong phylogenetic signal.

Table 3 Phylogenetic signal (K-value) and significance (p-value) within each modules

Module	1	2	3	4	5	6	7	8	9
K-value	0.92	0.99	0.93	0.93	0.97	0.91	NA	NA	NA
P-value	0.012*	0.021*	0.109	0.022*	0.184	0.047*	NA	NA	NA

*Significant phylogenetic signal

Reconstruction of the Osteological Neutral Posture for Each Module

The modules are variable in the number of CVs and result in different curvatures in an osteological neutral posture (Fig. 4). Module 4 was not subjected to this treatment because it is always composed of only one CV. There are three observable classes of modules: those that exhibit ventral curvature, such as modules 1 and 9 (21.09° to 21.44° of curvature, respectively, between two CVs); those with dorsal curvature, such as modules 2 and 5 (16.32° and 19.37°, respectively); and one that show very low curvature or does not show any as module 3, 6, 7 and 8 (from 0° to 6.47°). We observed that modules that share common postural properties in a relaxed posture occupy the same place in the neck. Modules in the ventral curvature belong to the

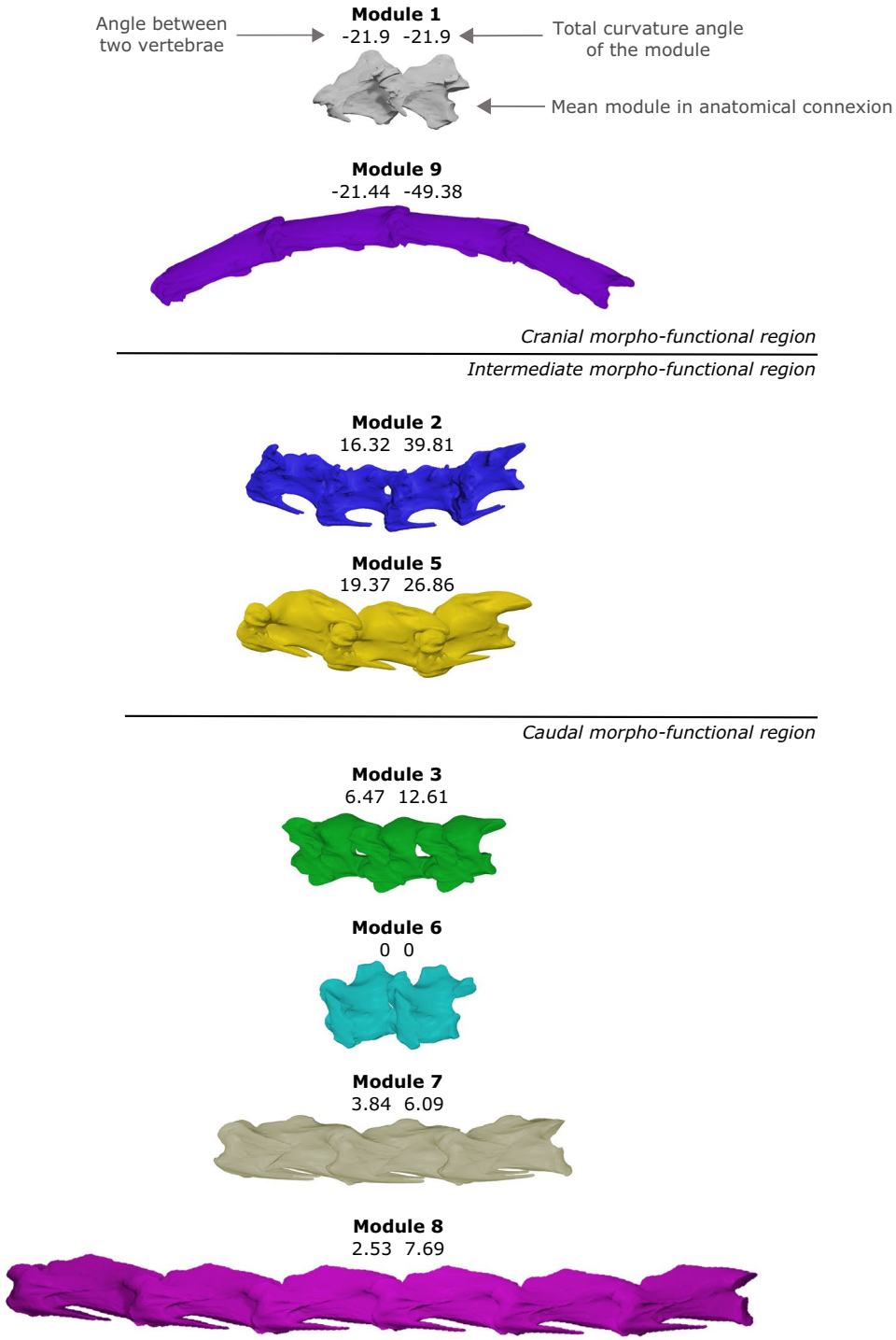

Fig. 4 Reconstruction of eight of the nine mean modules. Module 4 was not reconstructed because it was always composed of one vertebra. Curvature angles have been measured between two consecutive vertebrae and between the first and the last (i.e. total curvature angle of the module in relaxed posture)

cranial morphofunctional region, those with dorsal curvature belong to the intermediate region, and those with little or no curvature belong to the caudal region.

Discussion

To investigate modularity in the necks of birds, we applied a 3D SGM approach to the CVs of 16 species with varied feeding ecologies. We statistically identified nine modules. Seven of the modules are transpecific, while one is specific to *Anhinga* and one to *Struthio*, which are two genera with a long, peculiar neck morphology. First, we will discuss the observed morphological diversity at two different scales: modules (i.e., subsets of CVs) and combinations of modules (i.e., necks), and how it may be linked to feeding ecology, phylogeny and morphofunctional aspects. Then, we will discuss the three traditional functional regions of Boas in light of our results.

Modules (i.e., Subsets of CVs)

The modules are composed of CVs that occupy the same region of the neck (Fig. 3). Depending on their anatomical region, they display peculiar postural properties (Fig. 4). Thus, CVs are distributed in modules according to their postural characteristics, and not according to species. Vertebral shape itself is more explained by the transpecific modules (63%) than by species (13%). Therefore, modularity pattern along the neck is strongly linked to morphofunctional aspects. This finding supports the hypothesis that vertebral morphology and bending ability are tightly linked to posture and locomotion in vertebrates, as shown in cetaceans (Long et al. 1997), primates (Johnson and Shapiro 1998; Shapiro and Kemp 2019) and xenarthrans (Oliver et al. 2016).

The link between phylogeny and modularity patterns is more subtle. Some modules are under phylogenetic influence, while others are not (Table 3). Thus, phylogeny explains part of the shape variation between modules but does not fully explain the shape variation along the neck. This is in line with the conclusions of Brocklehurst et al. (2018), who postulated that phylogeny applies differentially along the vertebral column. To strengthen these findings, more species must be added to our dataset to further discuss the role of phylogeny in the regionalization of the neck.

The link between feeding ecology and the modularity pattern is less well supported. The modules are transversal across species (Fig. 3, SD Fig. 2), and considering that species represent feeding ecologies, we can deduce that the modular structure of the neck is not mainly linked to feeding ecology. Similar observations have been made in mammals, in which the patterns of modularity in the neck are highly conserved regardless of the species ecology (Arnold et al. 2016, 2017; Villamil 2018), in contrast to those observed in the rest of the column (Jones et al. 2018, 2019). To further extend these conclusions, they can be discussed in light of those reported for Felidae by Randau et al. (2017), who concluded that "ecological factors influence the shape of the vertebral column heterogeneously and that distinct vertebral sections may be under different selection pressures". We can therefore hypothesize that ecological factors might apply heterogeneously along the vertebral column, according to phylogeny. To test this hypothesis, it would be interesting to expand our dataset with other species to obtain statistically testable ecological groups. On the other hand, we can assume that because feeding ecology is not strongly linked to the modularity pattern, it could be linked to the remaining shape variability that exists within modules (SD Fig. 1).

Combinations of Modules (i.e., Necks)

Great shape variability is also observed at the scale of the neck. This diversity is represented by shape trajectories (Fig. 3), which visually describe morphological variations between CVs along the neck. Similar shape trajectories mean that neck morphologies are linked to similar phylogenetic, developmental and/or environmental factors (Werneburg et al. 2015) and vice versa. We identified two main categories of shape trajectories: reversed C shape and crushed reversed C shape (Fig. 3). The first group was composed of *Calyptomena, Bombycilla, Amazona, Dryocopus, Aptenodytes, Morus, Oriolus* and *Cacatua* and the second of *Crypturellus, Gyps, Apteryx, Hirundo* and *Chlorostilbon,* among which the last genus displays a particular shape trajectory. *Struthio* and *Anhinga* exhibit very specific shape trajectories and do not belong to one of these groups. These peculiarities may be linked to the particular elongated shape of their neck. Regarding feeding ecologies, the reversed C shape group contains opportunist and species that feed in water (divers and piscivores), while the crushed reversed C shape group contains opportunists, scavengers and nectarivores, among which the last group displays a peculiar trajectory. Therefore, the shape trajectory seems to be linked to feeding ecology. Modules may not appear to be related to ecology, but the chaining of modules (i.e., the neck) seems to be.

The Three Functional Regions Hypothesis

Each of the nine modules occupies a precise place in the species necks. Apart from module 1, the repartitioning of modules along the neck can generally be divided into three regions: (1) the cranial region, represented by modules 1 and 9 (Fig. 3), resulting in a ventrally bent neutral posture (Fig. 4); (2) the intermediate region, represented by modules 2 and 5 (Fig. 3), resulting in a dorsally bent neutral posture

(Fig. 4); and (3) the caudal region, represented by modules 3, 6, 7 and 8 (Fig. 3), resulting in a relatively unbent neutral posture (Fig. 4). Together, the ventrally bent cranial region, the dorsally bent intermediate region and the rather unbent caudal region of the cervical vertebral column appear to form the S-shaped neck of birds. These functional descriptions of the three regions of the neck in birds correspond to the observations made by Virchow (1910) and Boas (1929).

However, even though these three regions seem to present a clear functional definition, our results show that there is also a greater diversity than expected: we identified more modules than the regions (nine versus three). This implies the existence of (1) different modules occupying one same functional region and presenting similar postural properties and/or (2) subdivisions within Boas's functional regions (Fig. 3 and Fig. 4):

(1) Modules 2 and 5 occupy the intermediate region and result in a natural dorsally bent posture of approximately 30°. Modules 3, 6, 7 and 8 occupy the caudal region and result in a rather unbent posture. These modules are redundant in terms of their position in the neck and posture. However, they also display significantly different morphologies. The CVs of module 2 exhibit well-developed transverse processes, including fused ribs and a mostly enclosed carotid sulcus. This is in contrast with the CVs of module 5, which display the opposite morphological features (no fused cervical ribs and an open carotid sulcus) (Fig. 2). The same applies to modules 3, 6, 7 and 8, which display progressive elongation along the cranio-caudal axis.
(2) Two redundant modules are commonly found in the same neck, as observed for modules 2 and 5 in the neck of *Calyptomena* or module 3 and module 6 in the neck of *Amazona*, *Aptenodytes, Chlorostilbon* and *Crypturellus*. Therefore, in some species, the functional regions are morphologically subdivided. These subdivisions consist only of redundant modules and therefore share similar (even if not identical) postural properties but present varied shapes. This finding is in line with those of Krings et al. (2014, 2017), who identified three to seven modules along the neck of owls based on morphological and functional studies.

In conclusion, our results are consistent with those of previous studies on the regionalization of the neck in birds (e.g., Virchow 1910; Boas 1929; Zweers et al. 1987; van der Leeuw et al. 2001; Tambussi et al. 2012; Cobley et al. 2013; Krings et al. 2017; Kambic et al. 2017). However, they indicate that the pattern of modularity is more complex than expected, including subdivisions of the traditional functional regions and module redundancy. We found a clear link between the modular regionalization and posture of the neck. This relationship has been observed in other tetrapod groups (Polly et al. 2001; Hautier et al. 2010; Asher et al. 2011; Arnold et al. 2016; Randau et al. 2017; Jones et al. 2019). The patterns of regionalization in these groups are different, but they display similar pattern complexity.

Conclusion

In conclusion, despite the great variability of birds in terms of body size, ecology and the number and shape of CVs, the modularity pattern of the neck appears to be shared between species. Our innovative approach for addressing modularity using clustering proved to be relevant for the vertebral column, and nine modules were identified. Seven were transpecific, while one was specific to *Anhinga* and one to *Struthio*. The neck of each bird is composed of at least four modules. This modularity pattern is tightly linked to morphofunctional aspects, a property shared with other vertebrate groups, but is also partially linked to phylogeny, which is applied heterogeneously along the column. Feeding ecology seems to be more closely related to the neck than to the modules themselves. Each module results in different naturally bent postures, replicating the characteristic S-shape of the neck of bird. These postural properties of modules along the neck correspond to Boas's (1929) functional regions. However, we also found a more complex pattern than expected: first, these regions are subdivided; then, one region can be occupied by different modules with same postural properties between one species and another.

Acknowledgements The authors thank Pr Christine Lefèvre for the access of specimens from the collections (Muséum National d'Histoire Naturelle, Paris). They also thank Amandine Blin from the 'plate-forme de morphométrie' of the UMS 2700 (CNRS, MNHN) for access to the surface scanner.

Funding This study was financially supported by the Action transversale du Muséum (ATM) and the Agence National de la Recherche (ANR): Project ID #ANR-16-CE33-0025 (AVINECK), Project Coordinator: A. Abourachid.

Compliance with Ethical Standards

Conflict of interest The authors declare that they have no conflict of interest.

References

Adams, D. C. (2014). A generalized K statistic for estimating phylogenetic signal from shape and other high-dimensional multivariate data. *Systematic Biology, 63*(5), 685–697.

Adams, D. C., & Otárola-Castillo, E. (2013). Geomorph: An R package for the collection and analysis of geometric morphometric shape data. *Methods in Ecology and Evolution, 4*(4), 393–399.

Alexander, R. M. (1985). Mechanics of posture and gait of some large dinosaurs. *Zoological Journal of the Linnean Society, 83*(1), 1–25.

Arnold, P., Esteve-Altava, B., & Fischer, M. S. (2017). Musculoskeletal networks reveal topological disparity in mammalian neck evolution. *BMC Evolutionary Biology, 17*(1), 251.

Arnold, P., Forterre, F., Lang, J., & Fischer, M. S. (2016). Morphological disparity, conservatism, and integration in the canine lower cervical spine: Insights into mammalian neck function and regionalization. *Mammalian Biology, 81*(2), 153–162.

Asher, R. J., Lin, K. H., Kardjilov, N., & Hautier, L. (2011). Variability and constraint in the mammalian vertebral column: Mammalian vertebral variability. *Journal of Evolutionary Biology, 24*(5), 1080–1090.

Baylac, M., & Frieß, M. (2005). Fourier descriptors, procrustes superimposition, and data dimensionality: An example of cranial shape analysis in modern human populations. In D. E. Slice (Ed.), *Modern morphometrics in physical anthropology* (pp. 145–165). Boston: Springer.

Baylac, M., Villemant, C., & Simbolotti, G. (2003). Combining geometric morphometrics with pattern recognition for the investigation of species complexes: Geometric morphometrics, pattern recognition and species complexes. *Biological Journal of the Linnean Society, 80*(1), 89–98.

Blender Foundation (2003–2018). Blender. *Stichting Blender Foundation,* Amsterdam,https://www.blender.org

Blomberg, S. P., Garland, T., & Ives, A. R. (2003). Testing for phylogenetic signal in comparative data: Behavioural traits are more labile. *Evolution, 57*(4), 717–745.

Boas, J. E. V. (1929). *Biologisch-anatomische Studien über den Hals der Vögel* (pp. 1–127). Köbenhavn: A.F. Host & Son.

Böhmer, C., Plateau, O., Cornette, R., & Abourachid, A. (2019). Correlated evolution of neck length and leg length in birds. *Royal Society open science, 6*(5), 181588.

Böhmer, C., Rauhut, O. W. M., & Wörheide, G. (2015). Correlation between Hox code and vertebral morphology in archosaurs. *Proceedings of the Royal Society B: Biological Sciences, 282*(1810), 20150077.

Bookstein, F. L. (1997). *Morphometric tools for landmarks data: geometry and biology*. Cambridge: Cambridge University Press.

Botton-Divet, L., Houssaye, A., Herrel, A., Fabre, A.-C., & Cornette, R. (2015). Tools for quantitative form description; an evaluation of different software packages for semi-landmark analysis. *PeerJ, 3*, e1417.

Bout, R. G. (1997). Postures of the avian craniocervical column. *Journal of Morphology, 231*, 287–295.

Brocklehurst, R. J., Schachner, E. R., & Sellers, W. I. (2018). Vertebral morphometrics and lung structure in non-avian dinosaurs. *Royal Society Open Science, 5*(10), 180983.

Cheverud, J. M. (1996). Developmental integration and the evolution of pleiotropy. *American Zoologist, 36*(1), 44–50.

Cobley, M. J., Rayfield, E. J., & Barrett, P. M. (2013). Inter-vertebral flexibility of the ostrich neck: Implications for estimating sauropod neck flexibility. *PLoS ONE, 8*(8), e72187.

Cordeiro-Estrela, P., Baylac, M., Denys, C., & Marinho-Filho, J. (2006). Interspecific patterns of skull variation between sympatric Brazillian vesper mice: Geometric morphometrics assessment. *Journal of Mammalogy, 87*(6), 1270–1279.

Cornette, R., Baylac, M., Souter, T., & Herrel, A. (2013). Does shape co-variation between the skull and the mandible have functional consequences? A 3D approach for a 3D problem. *Journal of Anatomy, 223*(4), 329–336.

Daeschler, E. B., Shubin, N. H., & Jenkins, F. A. (2006). A Devonian tetrapod-like fish and the evolution of the tetrapod body plan. *Nature, 440*(7085), 757–763.

Dasgupta, A., & Raftery, A. E. (1998). Detecting features in spatial point processes with clutter via model-based clustering. *Journal of the American statistical Association, 93*, 294–302.

de Azevedo, T. P., Witten, P. E., Huysseune, A., Bensimon-Brito, A., Winkler, C., To, T. T., et al. (2012). Interrelationship and modularity of notochord and somites: A comparative view on zebrafish and chicken vertebral body development: Modularity of notochord and somites in zebrafish and chicken. *Journal of Applied Ichthyology, 28*(3), 316–319.

Diaconis, P., & Freedman, D. (1984). Asymptotics of graphical projection pursuit. *The Annals of Statistics, 12*(3), 793–815.

Dilger, W. C. (2010). The comparative ethology of the African Parrot Genus *Agapornis*. *Zeitschrift Für Tierpsychologie, 17*(6), 649–685.

Ericsson, R., Knight, R., & Johanson, Z. (2013). Evolution and development of the vertebrate neck. *Journal of Anatomy, 222*(1), 67–78.

Everitt, B., & Dunn, G. (2001). *Applied multivariate data analysis* (2nd ed.). Chichester: Wiley.

Fraley, C., & Raftery, A. E. (1998). How many clusters? Which clustering meSthod? Answers via model-based cluster analysis. *The Computer Journal, 41*(8), 578–588.

Fraley, C., & Raftery, A. E. (2012). *mclust Version 4 for R: Normal mixture modeling for model-based clustering, classification, and density estimation*. Department of Statistics, University of Washington, Technical Report no. 597.

Galis, F. (1999). Why do almost all mammals have seven cervical vertebrae? Developmental constraints, Hox genes, and cancer. *Journal of Experimental Zoology, 285*(1), 19–26.

Graf, W., Waele, C. D., & Vidal, P. P. (1994). Functional anatomy of the head-neck movement system of quadrupedal and bipedal mammals. *Journal of Anatomy, 186*, 55–74.

Guinard, G. (2012). Evolutionary concepts meet the neck of penguins (Aves: Sphenisciformes), towards a "survival strategy" for evo-devo. *Theory in Biosciences, 131*(4), 231–242.

Guinard, G., & Marchand, D. (2010). Modularity and Complete Natural Homeoses in Cervical Vertebrae of Extant and Extinct Penguins (Aves: Sphenisciformes). *Evolutionary Biology, 37*(4), 210–226.

Guinard, G., Marchand, D., Courant, F., Gauthier-Clerc, M., & Le Bohec, C. (2010). Morphology, ontogenesis and mechanics of cervical vertebrae in four species of penguins (Aves: Spheniscidae). *Polar Biology, 33*(6), 807–822.

Gunz, P., Mitteroecker, P., & Bookstein, F. L. (2005). Semilandmarks in three dimensions. In D. E. Slice (Ed.), *Modern morphometrics in physical anthropology* (pp. 73–98). Boston: Springer.

Hackett, S. J., Kimball, R. T., Reddy, S., Bowie, R. C. K., Braun, E. L., Braun, M. J., et al. (2008). A Phylogenomic study of birds reveals their evolutionary history. *Science, 320*(5884), 1763–1768.

Hallgrímsson, B., Jamniczky, H., Young, N. M., Rolian, C., Parsons, T. E., Boughner, J. C., et al. (2009). Deciphering the palimpsest: Studying the relationship between morphological integration and phenotypic covariation. *Evolutionary Biology, 36*(4), 355–376.

Harmon, L. J., Weir, J. T., Brock, C. D., Glor, R. E., & Challenger, W. (2008). GEIGER: Investigating evolutionary radiations. *Bioinformatics, 24*(1), 129–131.

Hautier, L., Weisbecker, V., Sanchez-Villagra, M. R., Goswami, A., & Asher, R. J. (2010). Skeletal development in sloths and the evolution of mammalian vertebral patterning. *Proceedings of the National Academy of Sciences, 107*(44), 18903–18908.

Head, J. J., & Polly, P. D. (2015). Evolution of the snake body form reveals homoplasy in amniote Hoxgene function. *Nature, 520*, 86–89.

Heidweiller, J., Van Der Leeuw, A. H. J., & Zweers, G. A. (1992). Cervical kinematics during drinking in developing chickens. *Journal of Experimental Zoology, 262*(2), 135–153.

Jetz, W., Thomas, G. H., Joy, J. B., Hartmann, K., & Mooers, A. O. (2012). The global diversity of birds in space and time. *Nature, 491*(7424), 444–448.

Johnson, S. E., & Shapiro, L. J. (1998). Positional behavior and vertebral morphology in atelines and cebines. *American Journal of Physical Anthropology, 105*, 333–354.

Jones, K. E., Angielczyk, K., & Pierce, S. (2019). Vertebral regionalization facilitates functional diversification of the mammalian axial skeleton. *The FASEB Journal, 33*, 613.

Jones, K. E., Benitez, L., Angielczyk, K. D., & Pierce, S. E. (2018). Adaptation and constraint in the evolution of the mammalian backbone. *BMC Evolutionary Biology, 18*(1), 172.

Long, J. H., Pabst, D. A., Shepherd, W. R., & Mclellan, W. A. (1997). Locomotor desing of dolphin vertebral columns: bending mechanics and morphology of *Dolphinus delphis*. *The Journal of Experimental Biology, 200*, 65–81.

Kambic, R. E., Biewener, A. A., & Pierce, S. E. (2017). Experimental determination of three-dimensional cervical joint mobility in the avian neck. *Frontiers in Zoology, 14*(1), 37.

Kembel, S. W., Cowan, P. D., Helmus, M. R., Cornwell, W. K., Morlon, H., Ackerly, D. D., et al. (2010). Picante: R tools for integrating phylogenies and ecology. *Bioinformatics, 26*(11), 1463–1464.

Klingenberg, C. P. (2008). Morphological Integration and Developmental Modularity. *Annual Review of Ecology, Evolution, and Systematics, 39*(1), 115–132.

Klingenberg, C. P. (2010). Evolution and development of shape: integrating quantitative approaches. *Nature Reviews Genetics, 11*, 623–635.

Klingenberg, C. P. (2014). Studying morphological integration and modularity at multiple levels: Concepts and analysis. *Philosophical Transactions of the Royal Society B: Biological Sciences, 369*(1649), 20130249–20130249.

Klingenberg, C. P., & Marugán-Lobón, J. (2013). Evolutionary covariation in geometric morphometric data: Analyzing integration, modularity, and allometry in a phylogenetic context. *Systematic Biology, 62*(4), 591–610.

Krings, M., Nyakatura, J. A., Boumans, M. L. L. M., Fischer, M. S., & Wagner, H. (2017). Barn owls maximize head rotations by a combination of yawing and rolling in functionally diverse regions of the neck. *Journal of Anatomy, 231*(1), 12–22.

Krings, M., Nyakatura, J. A., Fischer, M. S., & Wagner, H. (2014). The cervical spine of the american barn owl (Tyto furcata pratincola): I. Anatomy of the vertebrae and regionalization in their S-shaped arrangement. *PLoS ONE, 9*(3), e91653.

Muller, J., Scheyer, T. M., Head, J. J., Barrett, P. M., Werneburg, I., Ericson, P. G. P., et al. (2010). Homeotic effects, somitogenesis and the evolution of vertebral numbers in recent and fossil amniotes. *Proceedings of the National Academy of Sciences, 107*(5), 2118–2123.

Oliver, J. D., Jones, K. E., Hautier, L., Loughry, W. J., & Pierce, S. E. (2016). Vertebral bending mechanics and xenarthrous morphology in the nine-banded armadillo (*Dasypus novemcinctus*). *The Journal of Experimental Biology, 219*(19), 2991–3002.

Olson, E. C., & Miller, R. L. (1958). *Morphological integration*. Chicago: University of Chicago Press.

Paradis, E., Claude, J., & Strimmer, K. (2004). APE: Analyses of phylogenetics and evolution in R language. *Bioinformatics, 20*(2), 289–290.

Pierce, S. E., Ahlberg, P. E., Hutchinson, J. R., Molnar, J. L., Sanchez, S., Tafforeau, P., et al. (2013). Vertebral architecture in the earliest stem tetrapods. *Nature, 494*(7436), 226–229.

Polly, P. D., Head, J. J., & Cohn, M. J. (2001). Testing modularity and dissociation: the evolution of regional proportions in snakes. In M. L. Zelditch (Ed.), *Beyond heterochrony: The evolution of development* (pp. 305–335). New York: Wiley.

R Core Team. (2017). R: A language and environment for statistical computing. Retrieved April 2, 2018, from https://www.R-project.org/.

Randau, M., Cuff, A. R., Hutchinson, J. R., Pierce, S. E., & Goswami, A. (2017). Regional differentiation of felid vertebral column evolution: A study of 3D shape trajectories. *Organisms Diversity & Evolution, 17*(1), 305–319.

Revell, L. J. (2012). phytools: An R package for phylogenetic comparative biology (and other things): Phytools: R package. *Methods in Ecology and Evolution, 3*(2), 217–223.

Riedl, R. (1978). *Order in living organisms: a systems analysis of evolution*. New York: Wiley.

Rohlf, F. J., & Slice, D. (1990). Extensions of the procrustes method for the optimal superimposition of landmarks. *Systematic Zoology, 39*(1), 40.

Romer, A. S. (1950). *The vertebrate body*. Philadelphia: W. B. Saunders Company.

Shapiro, L. J., & Kemp, A. D. (2019). Functional and developmental influences on intraspecific variation in catarrhine vertebrae. *American Journal of Physical Anthropology, 168*(1), 131–144.

Schlager, S. (2013). Morpho: Calculations and visualisations related to geometric morphometrics. Retrieved April 2, 2018, from https://sourceforge.net/projects/morpho-rpackage/.

Stevens, K. A., & Parrish, J. M. (1999). Neck Posture and feeding habits of two jurassic sauropod dinosaurs. *Science, 284*(5415), 798–800.

Tambussi, C. P., de Mendoza, R., Degrange, F. J., & Picasso, M. B. (2012). Flexibility along the neck of the neogene terror bird *Andalgalornis steulleti* (Aves Phorusrhacidae). *PLoS ONE, 7*(5), e37701.

van der Leeuw, H. J., Bout, R. G., & Zweers, G. A. (2001). Control of the cranio-cervical system during feeding in birds. *American Zoologist, 41*, 1352–1363.

Villamil, C. I. (2018). Phenotypic integration of the cervical vertebrae in the Hominoidea (Primates): Cervical vertebrae integration in *Apes*. *Evolution, 72*(3), 490–517.

Virchow, H. (1910). *Über die Bewegungsmöglichkeiten an der Wirbelsäule von Spheniscus*. Sitzungsberichte der Gesellschaft Naturforschender Freunde zu Berlin. 1: 4–19.

Werneburg, I., Wilson, L. A. B., Parr, W. C. H., & Joyce, W. G. (2015). Evolution of neck vertebral shape and neck retraction at the transition to modern turtles: An integrated geometric morphometric approach. *Systematic Biology, 64*(2), 187–204.

West-Eberhard, M. J. (2003). *Developmental plasticity and evolution*. Oxford: Oxford University Press.

Wickham, H. (2015). *ggplot2: Elegant graphics for data analysis*. Berlin: Springer.

Wiley, D. F., Amenta, N., Alcantara, D. A., Ghosh, D., Kil, Y. J., Delson, E., et al. (2005). Evolutionary Morphing. *VIS 05 IEEE Visualization*. doi: 10.1109/VISUAL.2005.1532826

Wilkinson, D. M., & Ruxton, G. D. (2012). Understanding selection for long necks in different taxa. *Biological Reviews, 87*(3), 616–630.

Zweers, G. A., Vanden Berge, J. C., & Koppendraier, R. (1987). Avian cranio-cervical systems. Part I: Anatomy of the cervical column in the chicken (*Gallus gallus L.*). *Acta Morphologica Neerlando-Scandinavica, 25*, 131–155.

Skull morphological evolution in Malagasy endemic Nesomyinae rodents

Léa Terray[1], Christiane Denys[1*], Steven M. Goodman[2,3], Voahangy Soarimalala[3,4], Aude Lalis[1&], Raphaël Cornette[1&]

[1] Institute of Systematics and Evolution of Biodiversity (UMR7205), MNHN, Paris, France

[2] Field Museum of Natural History, 1400 South Lake Shore Drive, Chicago, IL 60605, USA

[3] Association Vahatra, BP 3972, Antananarivo 101, Madagascar

[4]Institut des Sciences et Techniques de l'Environnement, University of Fianarantsoa, Madagascar

*****Corresponding author:

E-mail : christiane.denys@mnhn.fr (CD)

[&] These authors contributed equally to this work.

Keywords

endemic rodents; morphometrics; skull; size & shape; Madagascar

Abstract

Madagascar is a large island to the south-east of Africa and in many ways continental in size and ecological complexity. Here we aim to define how skull morphology of an endemic and monophyletic clade of rodents (sub-family Nesomyinae), that show considerable morphological variation, have evolved and how their disparity is characterized in context of the geographical and ecological complexity of the island. We performed a two-dimensional geometric morphometric analysis on 371 dorsal and 400 ventral skull images of 19 species (comprising all nine extant endemic genera) and tested the influence of three ecological parameters (climate, locomotor habitat and nychthemeral cycle) in a phylogenetic context on size and shape. The results indicate that
skull shape appears to importantly reflect phylogeny, whereas skull size does not carry a significant phylogenetic signal. Skull shape is significantly influenced by climate while, skull size is not impacted by any of the ecological factors tested, which is controversial to expectations in an insular context. In conclusion, Nesomyinae must have evolved under unusual types of local constraints, preventing this radiation from demonstrating strong ecological release.

Introduction

Madagascar is a large island [1] (nearly 590,000 km^2) situated about 400 km off the southeastern coast of Africa. It is the 4th largest island on the planet and aspects of its biogeography are unique among other large islands in the tropics. Indeed, Madagascar has a large surface area associated with geological and meteorological complexities: highly different environments co-exist on this island as rainforests, steppes or karstic deserts. Madagascar has greater ecosystem richness than any other island [2,3]. This fact is supported by the high rate of endemism observed at different taxonomic levels, resulting in this island being considered as a biodiversity hotspot [4,5]. This diversity is illustrated by the four extant groups of endemic living Malagasy land mammals (Lemuroidea, Eupleridae, Tenrecidae and Nesomyinae), representing several hundred of species [6,7].

Each endemic mammal clade is the result of an independent successful colonization event. Nesomyinae colonized Madagascar in the early Miocene and probably originated from eastern Africa [6,8,9]. This monophyletic group is divided into two main clades and is currently (as of late 2018) composed of nine genera and 30 recognized extant species, all living in the diverse native forest ecosystems of the island [10]. Because this sub-family is endemic to Madagascar, it represents a unique opportunity to characterize, at macroevolutionary level, its radiation and estimate the importance of ecology, considered in a phylogenetic context, in shaping morphological diversity. The skull is an ideal structure for this type of investigation. Because it carries structures related to sensory functions (vision, olfaction, taste, etc.), feeding, and locomotion [11–13], it is likely to be influenced by environmental factors [12,14–16].

In this paper, we addressed the following question: in this particular geographical and ecological context of Madagascar, what shaped the morphological diversity observed in extant Nesomyinae rodents? To better understand the patterns and processes of evolution of the Nesomyinae, we examined the two following sub-questions: 1) To what extent does the skull shape of Nesomyinae reflect their phylogenetic history? 2) Did environmental parameters significantly influenced the shape of the skull and if so, how? To answer those questions, we performed shape analysis of Nesomyinae skulls in dorsal and ventral views, using geometric morphometrics (here abbreviated as GM). Then, we assessed the significance of phylogenetic signal and tested the influence of ecology on the

skull shape and size. We expect that the skulls of different nesomyines, and especially size, to display adaptations to local environments, as insular context is known to favor rapid character displacement towards local optima [17]. However, Madagascar being a particular case with several geographical and ecological continental characteristics more at a continental level, typical insular evolutionary trends [17] might not be observed. In addition, skull morphology can also show low evolutionary lability because of the strong phylogenetic signal in teeth, that are morphologically conserved [11,18]. In this case, because of the strength of phylogenetic signal, we would expect Nesomyinae skull to be less influenced by ecological variability.

Materials and Methods

Sampling

We used a data set of Nesomyinae skull photographs taken with a macro-photographic CANON EOS including 371 dorsal and 400 ventral images. The images were collected in a standardized way to prevent any bias due to the effect of parallax [19]: in dorsal view the frontal part of the skull was horizontally oriented (parallel to the photographic plane), and in ventral view molar rows were oriented as to be parallel to the photographic plane. Juveniles (defined as having portions of the skull being unossified) and older individuals (with heavily worn teeth) are not included in our sample. To minimize any potential bias due to sexual dimorphism we have included for each species as many specimens as possible and of both sexes; although, we add that this subfamily is not known to show sexual dimorphism [20]. Several species are known by only one or few individuals, such as *Brachytarsomys villosa*. The list of specimens used herein is presented in supplementary material (**Table S1**). These are housed in the Field Museum of Natural History (FMNH), Chicago; The Natural History Museum (formerly British Museum of Natural History [BMNH]), London; the Mention Zoologie et Biodiversité Animale (formerly Département de Biologie Animale), Université d'Antananarivo (UADBA), Antananarivo, Madagascar; the Museum für Naturkunde (ZMB), Berlin; and the Muséum national d'Histoire naturelle (MNHN), Paris. A summary of the specimens is presented in **Table 1**.

65

66 **Table 1. Summary of the photographic sampling.** M: Male, F: female. Reference spec-
67 imen: holotype or paratype specimen.

	DORSAL VIEW			VENTRAL VIEW		
Species	**Number of individuals**	**Sex**	**Inclusion of referent specimen (Yes/No)**	**Number of individuals**	**Sex**	**Inclusion of referent specimen (Yes/No)**
Eliurus carletoni	28	F(14) M(13)	Yes	30	F(19) M(10)	Yes
Eliurus majori	29	F(14) M(13)	Yes	32	F(14) M(15)	Yes
Eliurus antsingy	5	F(2) M(3)	No	5	F(2) M(3)	No
Eliurus grandidieri	30	F(11) M(18)	Yes	33	F(13) M(19)	Yes
Eliurus minor	25	F(11) M(12)	Yes	26	F(11) M(13)	Yes
Eliurus myoxinus	25	F(13) M(10)	No	26	F(13) M(11)	No
Eliurus tanala	30	F(16) M(11)	Yes	31	F(15) M(13)	Yes
Eliurus webbi	22	F(7) M(14)	Yes	23	F(8) M(14)	Yes
Voalavo gymnocaudus	10	F(4) M(4)	Yes	11	F(4) M(4)	Yes
Gymnuromys roberti	33	F(21) M(10)	Yes	36	F(22) M(11)	Yes
Brachytarsomys albicauda	9	F(4) M(2)	Yes	9	F(4) M(2)	Yes
Brachytarsomys villosa	3	F(0) M(3)	Yes	3	F(0) M(3)	Yes

Brachyuromys betsileoensis	19	F(10) M(6)	Yes	21	F(11) M(7)	Yes
Brachyuromys ramirohitra	11	F(1) M(7)	Yes	13	F(3) M(7)	Yes
Nesomys audeberti	12	F(4) M(5)	No	11	F(3) M(5)	No
Nesomys rufus	31	F(18) M(11)	Yes	34	F(19) M(13)	No
Hypogeomys antimena	15	F(3) M(4)	Yes	11	F(3) M(3)	Yes
Monticolomys koopmani	14	F(7) M(6)	No	24	F(14) M(9)	No
Macrotarsomys bastardi	19	F(8) M(6)	Yes	20	F(7) M(8)	Yes
TOTAL	370	-	-	399	-	-

Morphometric analyses

GM method allows a rigorous quantitative analysis of the geometric relationships of shape and size variation of an organism by combining a geometric concept of form with multivariate statistical procedures [21]. To capture skull shape variation, we used a 2-dimensional landmark-based approach. In dorsal view, 27 anatomical landmarks were chosen, as well as 42 in ventral view (**Figure 1**). Landmarks were selected to correspond as closely as possible to anatomical homologies. Descriptions of each type of landmark are given in supplementary material (**Tables S2 and S3**). They have been digitized using the software tpsDig2 [22].

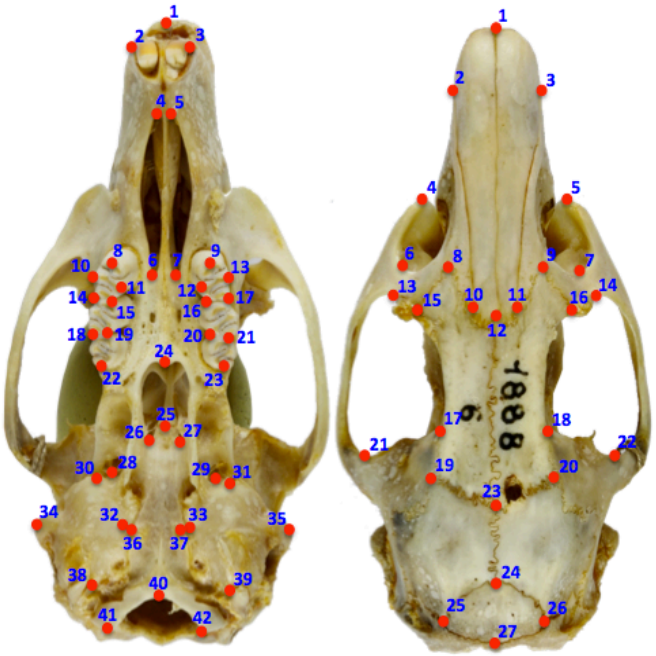

Fig. 1. Landmarks locations presented on a skull of *Hypogeomys antimena* (MNHN ZM-1888-6). Ventral view: 42 landmarks; dorsal view: 27 landmarks.

Ventral and dorsal data sets were analyzed separately. First, we performed a Generalized Procrustes Analysis (GPA). This method allows removal of effects due to scale, translation and rotation, maintaining only the geometric shape of objects and making comparisons possible [23]. This procedure was realized using the *gpagen* function of the *geomorph* library [24] under the free software R (R Core Team 2016).

We only examined the symmetric component of shape. Asymmetric component was explored using MorphoJ [25] and represents respectively 4.7% of shape variation in the ventral cranium and 5.8% in the dorsal cranium. It was removed using *bilat.symmetry* from *geomorph* [24]. Further statistical testing has also been performed under the free software R.

In order to reduce data dimensionality, principal component analyses (PCA) were performed on shape. PCA is a tool that uses the eigenvectors and eigenvalues of the covariance (or correlation) matrix to reduce the data dimensionality of a multivariate data set. The principal components are new uncorrelated variables (vectors loaded on the original variables) which successively maximize variance. This step was carried out using the *gm.prcomp* function of the *geomorph* library [24]. Visualizations of those PCA with all

99 individuals are presented in supplementary material (**Figure S1**). To reduce the number
100 of variables we retained 95% of shape variation, the latest principal components being
101 usually considered as negligible because they explain very little of the global shape vari-
102 ation [26]. Further analyses have been carried out on principal components instead of
103 Procrustes coordinates.
104 Sexual dimorphism in ventral and dorsal view was tested when information was
105 available (12 species: *Eliurus carletoni*, *Eliurus majori*, *Eliurus grandidieri*, *Eliurus ta-*
106 *nala*, *Eliurus minor*, *Eliurus myoxinus*, *Eliurus webbi*, *Gymnuromys roberti*, *Brachy-*
107 *uromys betsileoensis*, *Nesomys rufus*, *Monticolomys koopmani* and *Macrotarsomys bas-*
108 *tardi*). On shape we performed a Procrustes ANOVA with the function *procD.lm* from
109 the package *geomorph* [24] using the formula: shape ~ sex + species + sex:species. For
110 size we used the *lm* function from the *stats* package using the formula: size ~ sex + species
111 + sex:species. In both cases, the "sex" term was examined to assess the presence of sexual
112 dimorphism, and the interaction term to assess if sexual dimorphism is different between
113 species.
114 Allometry is the part of shape due to the influence of size [27]. If the Procrustes
115 superimposition method does separate size and shape, it does not remove allometry. Al-
116 lometry at the interspecific level was investigated with *procD.lm* from *geomorph* [24]
117 using the formula: shape ~ size + species + size:species. The log centroid size was used
118 as an estimator of size. Interactions between species and size were examined to asses
119 homogeneity of allometric slopes between species. This aspect was explored on all spec-
120 imens of our sample in dorsal and ventral views.
121 All subsequent analyses have been performed on species means that include all
122 specimens of a given taxa. For each data set comparative analyses were carried out on 1)
123 shape, which correspond to the principal components computed on the symmetric com-
124 ponent of Procrustes coordinates, and on 2) the centroid size, which is also obtained from
125 the Procrustes superimposition method and is defined as the square root of the sum of
126 square distance of each landmark from the centroid of the object.
127
128 Phylogenetic signal

As a basis for phylogenetic analyses we used the phylogeny of muroid rodents of Steppan et al. [28], which is based on 900 muroid species. The tree was pruned to keep only species of interest using the function *keep.tip* of the library *ape* [29].

To quantify phylogenetic signal in size we used the K-statistic method for univariate traits [30]. To quantify it on shape we used the same method extended to multivariate data by Adams [31]. This approach compares observed traits variations to their expected variations under Brownian motion. If K-value = 1 the considered trait evolved according to Brownian motion. If tested groups resemble each other more than expected, i.e. strong phylogenetic signal, K-value >> 1. On the contrary, K-value close to 0 indicates no phylogenetic signal. This signal has been computed with *physignal* from *geomorph* [24].

To visualize to what extend shape reflect phylogeny, we performed PCA on mean shape per species and projected phylogeny on it. This step was performed using *phylomorphospace* from the *phytools* library [32]. Method for ancestral states reconstruction, morphometric branch lengths estimation and phylomorphospace reconstruction are described in Sidlauskas [33]. Visualization of shape variation along axes were obtained using *plotRefToTarget* from *geomorph* [24] and are deformations in comparison to the global mean shape.

Influence of ecological factors

We tested the three best informed and relevant ecological parameters whose influence on mammalian skull morphology has been well documented: climate [34–36], locomotor habitat [37–40,12] and nychthemeral cycle [41,42]. Nesomyinae species occur in different natural vegetational zones of Madagascar, showing considerable local environmental variation [43] and, hence, these factors are good candidates to reflect adaptation. Based on recognized ecological characteristics of Nesomyinae [43], we assigned categories to characterize the three parameters : locomotor habitat (“terrestrial”, “arboreal”, and “semi-arboreal”), nychthemeral cycle (“nocturnal”, “twilight”, and “arrhythmic”) and climate (“tropical wet” and “hot and dry”) (**Table 2**). Specimens have been assigned to climatic areas based on the locality of their collection (**Table S1**).

Table 2. Species and their associated ecological characteristics. Areas are generalized from collection localities, climate data are from the Direction Générale de la Météorologie de Madagascar [44] and data concerning locomotor habits and nychthemeral cycle are from Goodman and Soarimalala (2011) [43].

Species	Area(s)	Climate	Locomotor habitat	Nycthemeral cycle
Eliurus carletoni	West coast	Tropical wet	Semi-arboreal	Nocturnal
Eliurus majori	East coast	Tropical wet	Arboreal	Nocturnal
Eliurus antsingy	West coast	Hot and dry	Terrestrial	Nocturnal
Eliurus grandidieri	East coast	Tropical wet	Terrestrial	Nocturnal
Eliurus minor	East coast	Tropical wet	Arboreal	Nocturnal
Eliurus myoxinus	East coast / West coast	Hot and dry	Arboreal	Nocturnal
Eliurus tanala	East coast	Tropical wet	Semi-arboreal	Nocturnal
Eliurus webbi	East coast	Tropical wet	Arboreal	Nocturnal
Voalavo gymnocaudus	East coast	Tropical wet	Arboreal	NA
Gymnuromys roberti	East coast / West coast / Central Highlands	NA	Terrestrial	Nocturnal
Brachytarsomys albicauda	East coast	Tropical wet	Arboreal	Nocturnal
Brachytarsomys villosa	East coast	Tropical wet	Arboreal	Nocturnal
Brachyuromys betsileoensis	East coast	Tropical wet	Terrestrial	Arrhythmic
Brachyuromys ramirohitra	East coast / Central Highlands	Tropical wet	Terrestrial	Arrhythmic
Nesomys audeberti	East coast	Tropical wet	Terrestrial	Twilight
Nesomys rufus	East coast / Central Highlands	Tropical wet	Terrestrial	Twilight
Hypogeomys antimena	West coast	Hot and dry	Terrestrial	Nocturnal
Monticolomys koopmani	East coast	Tropical wet	Terrestrial	NA

Macrotarsomys bastardi	West coast / South	Hot and dry	Terrestrial	Nocturnal

To quantify the influence of ecological factors on size, we performed ANOVA (F test), analyses of variance, which aims to determine whether qualitative factors (ecological factors) have significant effects on one quantitative variable (size). F is the ratio between inter- and intra-group variability. Thus, the more the average sizes of two groups are different, the higher the F statistic will be. Regarding shape we used MANOVA analyses (Wilks test). MANOVA, multivariate analysis of variances, is the extension of the ANOVA to multivariate data. It computes the λ of Wilks, which measures the part of intra-class inertia in total inertia. λ is comprised between 0 and 1, a value close to 0 indicating a good discrimination between the groups. When morphological descriptors found to carry significant phylogenetic signals we used phylogenetics MANOVA ($MANOVA^{phy}$), which takes phylogeny into account for p-value estimation. We used *manova.gls* from *MvMORPH* [45]. Fit of generalized least square linear model was performed using penalized likelihood method which allows to better manage the biases due to the number of traits approaching the number of species [46]. Prior, four evolutionary models were tested and compared with the Generalized Information Criterion (GIC): Brownian Motion (BM) in which the quantity of evolutionary change in a trait is relative to branch length, Ornstein-Uhlenbeck (OU) which takes into account stabilizing/divergent selection and stasis implying that traits can evolve towards one or more optima, Early Burst (EB) that assumes an exponential reduction in diversification rates over time and Pagel's lambda transformation (L) which scales the internal branches of the phylogeny thus reducing the expected covariance between species due to evolutionary history. To do that we used *GIC* from *MvMORPH* [45]. When no significant phylogenetic signal was found in morphological descriptors, the influence of ecological factors was determined using the function *aov* of the *Stats* library. For each case, ecological factors and their interaction with the log centroid size was tested using the formula: shape ~ size + ecology + size:ecology. Knowing that organisms reach different equilibrium sizes on islands as compared to continents, that is to say gigantism vs. dwarfism [17,47], the interaction between ecological factors and size could provide additional insight into these patterns. For each model effect size was computed using the *effectsize* function from *MvMORPH* [45], which provide the estimator τ^2 that take into account the penalized likelihood framework

and can be interpreted relatively. The higher τ^2, the stronger the association, and $\tau^2<0$ means no association. Because of missing data two species (*Voalavo gymnocaudus* and *Monticolomys koopmani*) were removed from nychthemeral cycle analyses. *Gymnuromys roberti* was removed from climate analyses as it is broadly distributed across different climatic zones.

When tests were significant, shape variations related to factors were investigated. We computed mean shape per category of each factor using *mshape* from *geomorph* [24].

Results

Morphometric analyses

No sexual dimorphism was detected in any of the species tested in dorsal size (sex : F = 2.86, p-value = 0.092; species: F = 55.37, p-value < 2e-16***; interaction: F = 1.57, p-values = 0.072), dorsal shape (sex: R^2 = 0.0012, p-value = 0.15; species: R^2 = 0.77, p-value =0.001**, interaction: R^2 = 0.013, p-value = 0.39), ventral size (sex: F = 0.008, p-value = 0.93; species: F = 42.24, p-value < 2e-16*** ; interaction: F = 0.77, p-value = 0.73), nor ventral shape (sex: R^2 = 0.00071, p-value = 0.28; species: R^2 = 0.8, p-value = 0.001**, interaction: R^2 = 0.0089, p-value = 0.84).

The test of allometry was statistically significant in dorsal (size: R^2=0.13, p-value=0.001**; species: R^2=0.65, p-value=.001**; interaction: R^2=0.024, p-value=0.001**) and ventral view (size: R^2=0.051, p-value=0.001**; species: R^2=0.75, p-value=0.001**; interaction: R^2=0.024, p-value=0.001**). Interaction between size and species is statistically significant in both cases, meaning that allometric slopes are heterogeneous between species. Plots of species allometric slopes are presented in **Figure S2**.

Phylogenetic signal

Results of K-statistics are presented in **Table 3**. In both data sets, centroid size has no statistically significant phylogenetic signal while a strong signal was detected in shape.

Table 3. Phylogenetic signal detected in size and shape. Asterisks indicates level of significance (*<0.05, **<0.01, ***<0.001). (+): a statistically significant phylogenetic signal was detected; (-): no statistically significant phylogenetic signal was detected.

	Data set	K value	P-value
Shape	Dorsal	0.90	0.001**
	Ventral	0.96	0.001**
Centroid size	Dorsal	0.50	0.097
	Ventral	0.53	0.064

In **Figure 2** and **Figure 3** the PCA with phylogenetic projection performed on respectively dorsal and ventral data sets are presented.

Regarding dorsal data set, the two first axes of the PCA in total encompass 54.4% of the variability (**Figure 2**). The first axis, which explains 32.3% of the total shape variation, display variation in relative widths of the anterior and posterior portions of the skull. For species situated in the negative area of the axis, the back of the skull is narrower, nasal bones longer (with no general elongation of the skull), and orbits in a more anterior position. In contrast, for species in the positive part of the axis the posterior portion of the skull is proportionally wider, nasal bones shorter and orbits in a more posterior position. This axis distinguishes the two Nesomyinae clades. The second axis of the PCA explains 22.2% of total shape variation. For species situated in the negative part of this axis, the posterior part of the skull is proportionally wider at the level of the jugal bone, braincase narrower and skull shorter in length. For the species situated in the positive part of the axis the braincase is wider and skull proportionally longer. This axis separates *Brachytarsomys villosa* and *Brachytarsomys. albicauda* and *Hypogeomys antimena* from the other species. The distribution of species represented by their morphological average in morphological space reflect their phylogenetic relationship, as expected given the high phylogenetic signal (**Table 3**). A PCA on the third and fourth axes, explaining respectively 13.3% and 7.6% of shape variation, is presented in supplementary material (**Figure S3**).

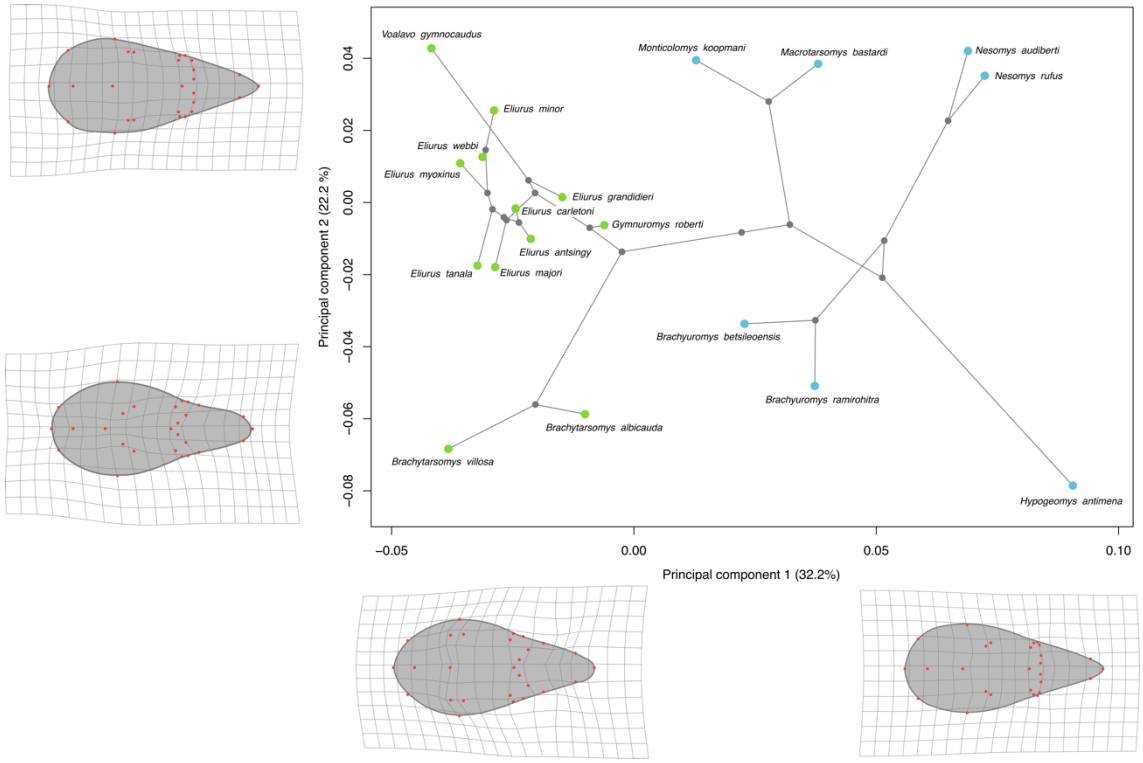

Fig. 2. Visualization of the two first axes of the PCA performed on dorsal shape with phylogenetic projection. Colored points represent the morphological average of all individuals of a species. Colors indicate the two principal clades among Nesomyinae. Blue: clade formed by the genus *Brachyuromys, Nesomys, Macrotarsomys, Monticolomys*, and *Hypogeomys*; green: clade formed by the genus *Brachytarsomys, Eliurus, Gymnuromys,* and *Voalavo*. Warpgrids indicate shape variation along axis with maximum deformation observed at each extremity of the axis.

Concerning the ventral data set the two first axes carry 61.5% of the total shape variation (**Figure 3**). The first axis explains 38.0% of the variability and the general patterns are consistent with the observed shape variation in dorsal view. For species situated in the positive part of this axis, the posterior portion of the skull is proportionally wider and rostrum large and rounded. In the negative part of this axis the posterior portion of the skull is proportionally narrower and rostrum narrow and pointed. This axis clearly separates the two Nesomyinae clades. The second axis of the PCA accounts for 23.5% of the total shape variation and the major shape variation concerns the relative length of the

skull. For species situated in the negative part of the axis the tympanic bullae are proportionally larger, rostrum longer and more pointed, and incisor foramens longer as compared to species in the positive of the axis. The distribution of species in morphological space reflect their phylogenetic relationship, as expected given the high phylogenetic signal (**Table 3**). A PCA on the third and fourth axes, explaining respectively 7.9% and 7.2% of shape variation, is presented in supplementary material (**Figure S4**).

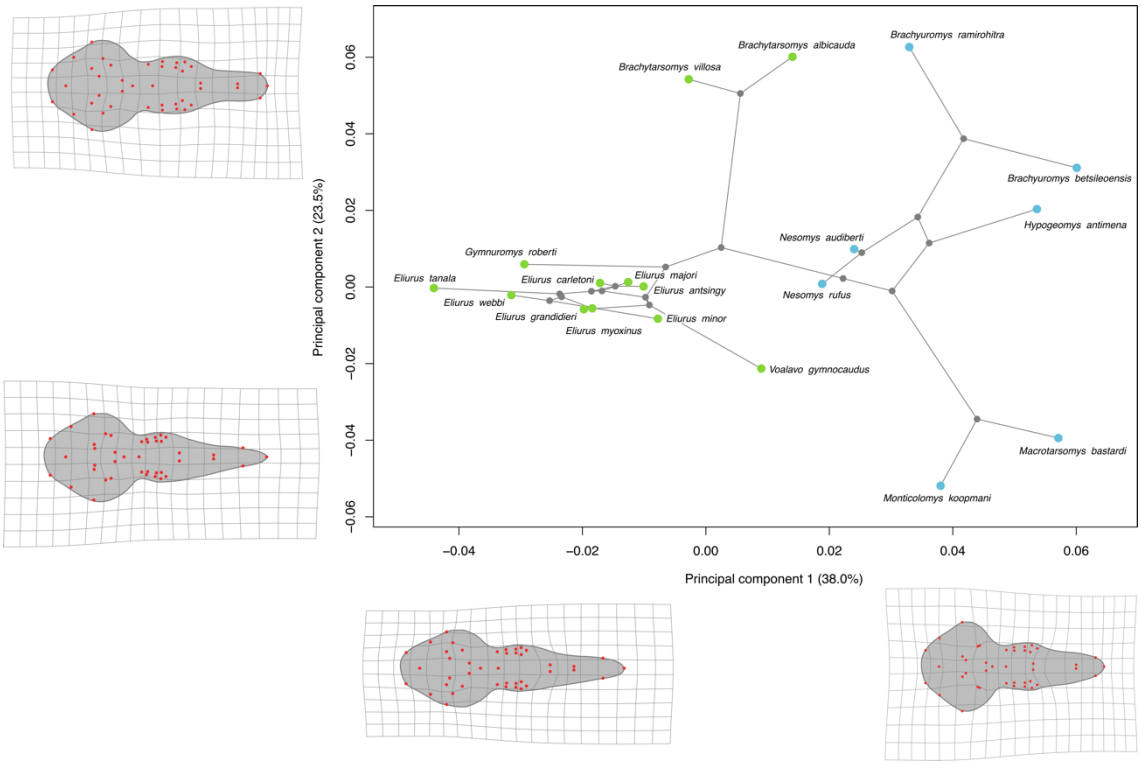

Fig. 3. Visualization of the two first axes of the PCA performed on ventral shape with phylogenetic projection. Colored points represent the morphological average of all individuals of a species. Colors indicate the two principal clades among Nesomyinae. Blue: clade formed by the genus *Brachyuromys, Nesomys, Macrotarsomys, Monticolomys*, and *Hypogeomys*; green: clade formed by the genus *Brachytarsomys, Eliurus, Gymnuromys,* and *Voalavo*. Warpgrids indicate shape variation along axis with maximum deformation observed at each extremity of the axis.

Influence of ecological factors

Results of ANOVA and MANOVA^{phy} performed on size and shape of both data sets are presented in **Table 4**.

When testing the association between ecological factors and skull shape, the estimated pseudo-likelihood of the phylogenetic MANOVA indicated that EB was the best fitted model in all cases (even if the GIC criterion showed small differences): climate and dorsal view (BM: pseudo-likelihood = 562.25, GIC = -1133.31; OU/Lambda: pseudo-likelihood = 562.25, GIC = -1131.31; EB: pseudo-likelihood = 564.35, GIC = -1130.90), climate and ventral view (BM: pseudo-likelihood = 697.52, GIC = -1405.42; OU/Lambda: pseudo-likelihood = 697.52, GIC = -1403.42; EB: pseudo-likelihood = 704.08, GIC = -1404.68), locomotor habitat and dorsal view (BM: pseudo-likelihood = 576.32, GIC = -1140.09; OU/Lambda: pseudo-likelihood = 576.32, GIC = -1138.09; EB: pseudo-likelihood = 578.30, GIC = -1139.40), locomotor habitat and ventral view (BM: pseudo-likelihood = 670.62, GIC = -1359.84; OU/Lambda: pseudo-likelihood = 670.62, GIC = -1357.84; EB: pseudo-likelihood = 676.37, GIC = -1364.19), nychthemeral cycle and dorsal view (BM: pseudo-likelihood = 518.82, GIC = -1054.35; OU: pseudo-likelihood = 518.82, GIC = -1052.35; Lambda: pseudo-likelihood = 519.18, GIC = -1050.22; EB: pseudo-likelihood = 527.03, GIC = -1068.31) and nychthemeral cycle and ventral view (BM: pseudo-likelihood = 618.50, GIC = -1255.56; OU: pseudo-likelihood = 618.50, GIC = -1253.56; Lambda: pseudo-likelihood = 618.51, GIC = -1253.60; EB: pseudo-likelihood = 633.82, GIC = -1272.96).

Climate is the only factor that has a statistically significant influence on shape. In ventral the main effect and the interaction with size are significant, meaning that shape variation related to size cannot be differentiated to shape variation related to climate. In dorsal there is no main effect of climate but the main effect of size and the interaction term are significant meaning that there is a crossover interaction. The effect of size on shape is opposite depending on the climate [48].

Table 4. Tests of ecological factors on shape and size. Level of significance: *<0.05, **<0.01, ***<0.001. Bold indicates relevant results regarding ecological factors. For linear models, we provide the multiple R^2. For models fitted with penalized likelihood we provide τ^2, the multivariate effect size estimated from the permuted data.

			Ecological factors		
	Data set		**Climate**	**Locomotor habitat**	**Nychthemeral Cycle**
Shape (MANOVA^{phy})	Dorsal	Ecological factor	$\lambda = 0.48$ $\tau^2 = 0.12$ P = 0.34	$\lambda = 0.4$ $\tau^2 = -0.20$ P = 0.89	$\lambda = 0.10$ $\tau^2 = 0.35$ P = 0.083
		Size	$\lambda = 0.24$ $\tau^2 = 0.54$ P = 0.011*	$\lambda = 0.20$ $\tau^2 = 0.62$ P = 0.006**	$\lambda = 0.076$ $\tau^2 = 0.86$ P = 0.001**
		Interaction	**$\lambda = 0.32$** $\tau^2 = 0.42$ **P = 0.045***	$\lambda = 0.20$ $\tau^2 = 0.14$ P = 0.29	$\lambda = 0.38$ $\tau^2 = -0.22$ P = 0.85
	Ventral	Ecological factor	**$\lambda = 0.34$** $\tau^2 = 0.36$ **P = 0.050***	$\lambda = 0.22$ $\tau^2 = 0.071$ P = 0.40	$\lambda = 0.16$ $\tau^2 = 0.18$ P = 0.29
		Size	$\lambda = 0.18$ $\tau^2 = 0.67$ P = 0.003**	$\lambda = 0.17$ $\tau^2 = 0.68$ P = 0.0029**	$\lambda = 0.076$ $\tau^2 = 0.85$ P = 0.001**
		Interaction	**$\lambda = 0.29$** $\tau^2 = 0.45$ **P = 0.043***	$\lambda = 0.16$ $\tau^2 = 0.20$ P = 0.16	$\lambda = 0.15$ $\tau^2 = 0.27$ P = 0.27
Centroid size (ANOVA)	Dorsal		F = 0.025 $R^2 = 0.0016$ P = 0.88	F = 0.33 $R^2 = 0.039$ P = 0.73	F = 0.73 $R^2 = 0.094$ P = 0.50
	Ventral		F = 0.013 $R^2 = 0.0008$ P = 0.91	F = 0.19 $R^2 = 0.023$ P = 0.83	F = 0.33 $R^2 = 0.045$ P = 0.73

Shape changes related to climate are presented in **Figure 4**. In the ventral cranium species living in "tropical wet" climates have an elongated skull, with a proportionally longer and larger rostra and smaller tympanic bullae compared to species living in "hot and dry" climates. In dorsal cranium species living in "tropical wet" climates have an elongated nasal bone compared to species living in "hot and dry" climates.

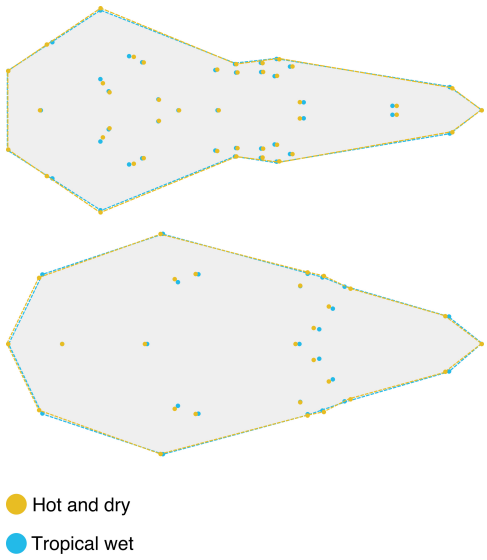

Fig. 4. Significant shape changes related to climate. Left: ventral shape; right: dorsal shape.

Discussion

Phylogenetic signal and ecological influence on skull size

No significant phylogenetic signal was detected in skull size (**Table 3**). Size might be conditioned by a factor/factors other than phylogenetic history. However, conversely to what is expected in insular context none of the three tested ecological factors was found to have a significant impact on skull size either (**Table 4**). Hence, either ecological space is not partitioned by size in Nesomyinae, either size may have been driven by other ecological parameters than those tested, as diet. However, diet is highly variable in rodents [43,49], and more data on the feeding habits of Nesomyinae are needed to test it reliably.

Phylogenetic signal and ecological influence on skull shape

Skull shape display significant phylogenetic signals (**Table 3**). Skull shape seems to be mainly driven by its evolutionary history. It is confirmed by our PCA results: in dorsal and ventral view the distribution of species in morphological space is congruent with phylogeny (**Figs 2 and 3**). Phylogenetically close species are also morphologically close, such as *Monticolomys koopmani* and *Macrotarsomys bastardi,* or all species belonging to same genus (*Eliurus, Brachytarsomys, Brachyuromys, Nesomys*). In ventral

view, *Nesomys rufus* is in the center of the PCA, as it represents the standard ventral shape of a Nesomyinae skull at least based on species present in our dataset. Given that these species are morphologically distinct, their dissimilarities appear rather low compared to their measured molecular distance [8]. The morphological proximity of species could be explained by a partition of resources through different behavior or activity pattern, rather than morphological character displacement. Another hypothesis, not tested in this paper, is that this morphological similarity might be due to convergence, as it has been observed in other endemic mammal lineages such as shrew tenrecs of the genus *Microgale* [50], mouse lemurs of the genus *Microcebus* [51], and long-fingered bats of the genus *Miniopterus* [52].

The evolutionary model that best fits our sample is the early burst model of diversification, and not Brownian motion as it was expected considering the high phylogenetic signal (**Table 3**). Maybe the climate variable provided a stronger explanatory power for skull shape variation, as suggested by Giacomini et al. (2021) [53] who obtained similar results. This mode of evolution usually involves ecological opportunities for concerned species and is typically observed in adaptive radiations [54,55]. Thus, despite the strong phylogenetic signal displayed by skull shape, it is likely that they are also subjected to adaptation.

Climate was found to significantly influenced shape in ventral cranium and to significantly interact with the influence of size on the shape of dorsal cranium. Two structures are mainly impacted: proportional size of the tympanic bullae and elongation of the rostrum. Species living in arid or semi-desertic environments ("hot and dry") display wider tympanic bullae than those living in humid environments ("Tropical wet") (**Figure 4**). A significant influence of climate on this structure is not surprising considering that it is highly sensible to the opening/closing of the environment where the animal lives, as it has been observed in gerbilles and other mammals [56–58]. Associated adaptations could also be related to the margins of the foramen magnum which are neighboring structures of tympanic bullae. Tropical areas are mainly covered with forests while arid areas are more often open environments. Evolving in such different environments requires different mobility abilities. The implication of the foramen magnum in mobility abilities have already been demonstrated in other studies on mammals [59,60] and is often related to head posture [12,37,38]. Variation in the elongation of the rostrum might be related to the

differences of available resources in varied environmental conditions. Shape variation associated with the width and length of the rostrum can be related to feeding habits. In rodents, it has been observed that herbivores display longer tooth rows and wider skull and rostrum [61]. However, it is well known that diet is spatially and temporally variable in rodents [49]. As far as we know, most Nesomyines are known to be omnivorous and their diet vary seasonally according to available resources [43]. The influence of climate on shape also strongly interacts with size. Then, climate seems also to affect the allometric pattern of the skull. The differences in allometric patterns between species are, at least in part, explained by differences in the climate of their living environment.

Temporal perspectives of Nesomyinae skull evolution

We analyzed the extant diversity of Nesomyinae to understand patterns and processes of their diversification since their colonization of Madagascar. However, the current representatives may not depict the maximum diversity of this clade since their arrival, thus biasing our interpretations. Several recent changes must have impacted Nesomyinae shape diversity such as human arrival on the island, natural climatic changes, anthropogenic vicissitudes and the introduction of invasive murids [62–65]. In the Quaternary subfossil record of Madagascar, one notably large-bodied nesomyine is known, *Hypogeomys australis* (Grandidier, 1903), which was notably larger than the only extant member of this genus, *Hypogeomys antimena,* the largest living rodent on the island. In addition, in the subfossil record is the largest known *Nesomys* species, *Nesomys narindaensis* [64], notably bigger than other extant members of this genus, which would include *Nesomys lambertoni* at less than 250 g [43]. Other large-bodied nesomyine species may have gone extinct, but the absence of paleontological data in the Neogene of Madagascar and the scarcity of the Quaternary material hinders any detailed interpretation of past nesomyine diversity and evolution. Among Madagascar endemic mammals, there were giants forms, all extinct in the Late Pleistocene-Holocene, such as *Hypogeomys australis*, of about 2 kg; lemurs, *Archaeoindris* up to 200 kg, and a carnivoran, *Cryptoprocta spelea*, the largest Holocene land predator of Madagascar [63,66,67]. Today, the extant *Hypogeomys antimena* only reaches a maximum body mass of slightly greater than 1 kg [43]. The continental African representatives of the Nesomyidae, the closest clades to the Malagasy Nesomyinae [8,28] all weigh under 100 g, with the exception *Cricetomys* species that

reach 2 kg. *Macrotarsomys* and *Monticolomys* are small genera whose molars are morphologically close to fossil genera such as *Protarsomys* and *Notocricetodon*, which date from the lower Miocene of East Africa and may be the ancestors of the Malagasy Nesomyinae [68,69]. According to molecular clock the crown-group diversification of Nesomyinae occurs around 12.8 Ma and the colonization of Madagascar between that date and 15.6 Ma [28,70]. *Protarsomys* and *Notocricetodon* (extinct Miocene genera) were small body-size rodents. This may indicate, despite geographical isolation, that at least molar morphology evolved in relative stasis for these genera since the Miocene, or represent an excellent example of convergence on opposite sides of the Mozambique Channel separated by about 20 Ma. The genus *Monticolomys*, which is consistently the sister taxon of *Macrotarsomys* in different molecular phylogenies [8,28,71], is morphologically close to *Macrotarsomys* [69]. Such congruence between phylogeny and a low morphological variability interpreted as preservation of an ancestral morphology in some lineages, may be the result of heavy constraints occurring on Nesomyinae skull morphology and no ecological release is readily apparent in this subfamily. Most of all Nesomyinae genera are represented by 1 to 3 species, with the exception of *Eliurus* whose diversity is 13 species [7]. This genus has a relatively homogenous skull shape and includes species ranging from 20 to 100 g. Its success may be related to its specialization towards arboreality during Cenozoic times in Madagascar.

Conclusion

Nesomyinae skull is a complex structure for which size and shape are not under the same constraints. Skull shape strongly reflects phylogeny, but is also substantially influenced by climate. Skull size revealed to carry a weak phylogenetic signal, as awaited in insular context, but unexpectedly show no adaptive signal regarding ecological factors examined. The large size of Madagascar, its ecological complexity and its particular colonization history of lineages may be associated with unusual types of constraints in island context, preventing the Nesomyinae radiation from displaying strong ecological release.

Acknowledgements

We are grateful to Frieder Mayer and Christiane Funk (Berlin, ZMB), to Paula Jenkins and Louise Tomsett (London, BMNH), to Julian Kerbis (Chicago, FMNH Museum), to Felix Rakotondraparany (Antananarivo, UADBA) who allowed us access to Nesomyinae collections under their care. This work was financially supported by the ATM (Transversal action program at the MNHN), Paris, and the LABEX BCDIV, CNRS, Paris. We are grateful to Ben Warren (ISYEB, MNHN) for his suggestions on the manuscript and to Kevin Le Verger (CR2P, MNHN) for conceptual discussions and advice. We also thank Dr Carlo Meloro, Dr Joshua X. Samuels and an anonymous reviewer for constructive and helpful comments on previous versions of the manuscript.

The protocols employed to treat these data provided here are available on line at:

https://www.protocols.io/view/geometric-morphometrics-nesomyinae-rodent-skulls-b2umqeu6

(dx.doi.org/10.17504/protocols.io.b2umqeu6)

The original TPS data and nexus file for the phylogenetic tree have been stored in OSF site:

https://osf.io/a8eth/?view_only=abd1896945ee4bbd83cbbbead4c736ea

References

1. Battistini R, Richard-Vindard G. Biogeography and ecology in Madagascar. Dr. W Junk B.V. Publishers. The Hague, The Netherlands; 1972.

2. Wittaker RJ. Island biogeography. ecology, evolution, and conservation. New York. Oxford University. 1998.

3. Jędrusik M. Madagascar – An Island or a Continent? On the Notions of 'Island' and 'Insularity.' Misc Geogr. 2018;13.

4. Goodman SM, Benstead JP. Updated estimates of biotic diversity and endemism for Madagascar. 2005; 5.

5. Myers N, Mittermeier RA, Mittermeier CG, da Fonseca GAB, Kent J. Biodiversity hotspots for conservation priorities. Nature. 2000;403: 853–858. doi:10.1038/35002501

6. Poux C, Madsen O, Marquard E, Vieites DR, de Jong WW, Vences M. Asynchronous Colonization of Madagascar by the Four Endemic Clades of Primates, Tenrecs, Carnivores, and Rodents as Inferred from Nuclear Genes. Baker A, editor. Syst Biol. 2005;54: 719–730. doi:10.1080/10635150500234534

7. Goodman SM, Raherilalao M, Wohlhauser S. Les aires protégées terrestres de Madagascar : leur histoire, description et biote / The terrestrial protected areas of Madagascar: Their history, description, and biota. Antananarivo: Association Vahatra. 2018.

8. Schenk JJ, Rowe KC, Steppan SJ. Ecological Opportunity and Incumbency in the Diversification of Repeated Continental Colonizations by Muroid Rodents. Syst Biol. 2013;62: 837–864. doi:10.1093/sysbio/syt050

9. Steppan SJ, Adkins RM, Spinks PQ, Hale C. Multigene phylogeny of the Old World mice, Murinae, reveals distinct geographic lineages and the declining utility of mitochondrial genes compared to nuclear genes. Mol Phylogenet Evol. 2005;37: 370–388. doi:10.1016/j.ympev.2005.04.016

10. Goodman SM, Soarimalala V. Systématique des rongeurs endémiques malgaches (famille des Nesomyidae : sous-famille des Nesomyinae) / Systematics of endemic Malagasy rodents (family Nesomyidae: subfamily Nesomyinae). Antananarivo: Association Vahatra. In: Goodman SM, Raherilalao M, Wohlhauser S, editors. Les aires protégées terrestres de Madagascar : leur histoire, description et biote / The terrestrial protected areas of Madagascar: Their history, description, and biota. Antananarivo: Association Vahatra. 2018. pp. 373–381.

11. Caumul R, Polly D. Phylogenetic and environmental components of morphological variation: skull, mandible and molar shape in marmots (Marmota, Rodentia). Evolution. 2005;59: 2460–2472.

12. Dumont M, Wall CE, Botton-Divet L, Goswami A, Peigné S, Fabre A-C. Do functional demands associated with locomotor habitat, diet, and activity pattern drive skull shape evolution in musteloid carnivorans? Biol J Linn Soc. 2016;117: 858–878. doi:10.1111/bij.12719

13. Kraatz B, Sherratt E. Evolutionary morphology of the rabbit skull. PeerJ. 2016; 23.

14. Yazdi T, Adriaens D. Patterns of skull shape variation in Meriones persicus (Rodentia: Muridae) in relation to geoclimatical conditions. 2011;7: 129–142.

15. Maestri R, Patterson BD, Fornel R, Monteiro LR, de Freitas TRO. Diet, bite force and skull morphology in the generalist rodent morphotype. J Evol Biol. 2016;29: 2191–2204. doi:10.1111/jeb.12937

16. Monteiro LR, Duarte LC, dos Reis SF. Environmental correlates of geographical variation in skull and mandible shape of the punar rat Thrichomys apereoides (Rodentia: Echimyidae). J Zool. 2003;261: 47–57. doi:10.1017/S0952836903003893

17. Lomolino MV. Body size evolution in insular vertebrates: generality of the island rule. J Biogeogr. 2005;32: 1683–1699. doi:10.1111/j.1365-2699.2005.01314.x

18. Ledevin R, Chevret P, Ganem G, Britton-Davidian J, Hardouin EA, Chapuis J-L, et al. Phylogeny and adaptation shape the teeth of insular mice. Proc R Soc B Biol Sci. 2016;283: 20152820. doi:10.1098/rspb.2015.2820

19. Mullin SK, Taylor PJ. The effects of parallax on geometric morphometric data. Comput Biol Med. 2002; 10.

20. Kappeler PL, Nunn CL, Vining AQ, Goodman SM. Evolutionary dynamics of sexual size dimorphism in non-volant mammals following their independent colonization of Madagascar. Sci Rep. 2019;9: 14.

21. Zelditch M, editor. Geometric morphometrics for biologists: a primer. Amsterdam ; Boston: Elsevier Academic Press; 2004.

22. Rohlf FJ. The tps series of software. Hystrix Ital J Mammal. 2015 [cited 12 Oct 2018]. doi:10.4404/hystrix-26.1-11264

23. Rohlf FJ, Slice D. Extensions of the Procrustes Method for the Optimal Superimposition of Landmarks. Syst Zool. 1990;39: 40. doi:10.2307/2992207

24. Adams DC, Otárola-Castillo E. geomorph: an R package for the collection and analysis of geometric morphometric shape data. Paradis E, editor. Methods Ecol Evol. 2013;4: 393–399. doi:10.1111/2041-210X.12035

25. Klingenberg CP. MorphoJ: an integrated software package for geometric morphometrics: COMPUTER PROGRAM NOTE. Mol Ecol Resour. 2011;11: 353–357. doi:10.1111/j.1755-0998.2010.02924.x

26. Baylac M, Frieß M. Fourier Descriptors, Procrustes Superimposition, and Data

539 Dimensionality: An Example of Cranial Shape Analysis in Modern Human Populations.
540 In: Slice DE, editor. Modern Morphometrics in Physical Anthropology. New York:
541 Kluwer Academic Publishers-Plenum Publishers; 2005. pp. 145–165. doi:10.1007/0-
542 387-27614-9_6

543 27. Klingenberg CP. Size, shape, and form: concepts of allometry in geometric mor-
544 phometrics. Dev Genes Evol. 2016;226: 113–137. doi:10.1007/s00427-016-0539-2

545 28. Steppan SJ, Schenk JJ. Muroid rodent phylogenetics: 900-species tree reveals
546 increasing diversification rates. Huchon D, editor. PLOS ONE. 2017;12: e0183070.
547 doi:10.1371/journal.pone.0183070

548 29. Paradis E, Claude J, Strimmer K. APE: Analyses of Phylogenetics and Evolution
549 in R language. Bioinformatics. 2004;20: 289–290. doi:10.1093/bioinformatics/btg412

550 30. Blomberg SP, Garland T, Ives AR. Testing for phylogenetic signal in compara-
551 tive data: behavioural traits are more labile. Evolution. 2003;57: 717–745.
552 doi:10.1111/j.0014-3820.2003.tb00285.x

553 31. Adams DC. A Generalized K Statistic for Estimating Phylogenetic Signal from
554 Shape and Other High-Dimensional Multivariate Data. Syst Biol. 2014;63: 685–697.
555 doi:10.1093/sysbio/syu030

556 32. Revell LJ. phytools: an R package for phylogenetic comparative biology (and
557 other things): phytools: R package. Methods Ecol Evol. 2012;3: 217–223.
558 doi:10.1111/j.2041-210X.2011.00169.x

559 33. Sidlauskas B. Continuous and arrested morphological diversification in sister
560 clades of characiform fishes: a phylomorphospace approach. Evolution. 2008;62: 3135–
561 3156.

562 34. Renaud S. Size and shape variability in relation to species differences and cli-
563 matic gradients in the African rodent Oenomys. J Biogeogr. 1999;26: 857–865.
564 doi:10.1046/j.1365-2699.1999.00327.x

565 35. Yom-Tov Y, Geffen E. Geographic variation in body size: the effects of ambient
566 temperature and precipitation. Oecologia. 2006;148: 213–218. doi:10.1007/s00442-006-
567 0364-9

568 36. Yom-Tov Y, Yom-Tov S. Climatic change and body size in two species of Japa-
569 nese rodents: climatic change and body size of rodents. Biol J Linn Soc. 2004;82: 263–
570 267. doi:10.1111/j.1095-8312.2004.00357.x

571 37. Ross CF, Ravosa MJ. Basicranial flexion, relative brain size, and facial kyphosis
572 in nonhuman primates. Am J Phys Anthropol. 1993;91: 305–324.

573 38. Lieberman DE, Ross CF, Ravosa MJ. The primate cranial base: Ontogeny, func-
574 tion, and integration. Yearb Phys Anthropol. 2000;43: 53.

575 39. Hautier L, Lebrun R, Cox PG. Patterns of covariation in the masticatory appa-
576 ratus of hystricognathous rodents: Implications for evolution and diversification. J Mor-
577 phol. 2012;273: 1319–1337. doi:10.1002/jmor.20061

578 40. Bertrand OC, Schillaci MA, Silcox MT. Cranial dimensions as estimators of
579 body mass and locomotor habits in extant and fossil rodents. J Vertebr Paleontol.
580 2016;36: e1014905. doi:10.1080/02724634.2015.1014905

581 41. Heesy CP. Ecomorphology of Orbit Orientation and the Adaptive Significance
582 of Binocular Vision in Primates and Other Mammals. Brain Behav Evol. 2008;71: 54–
583 67. doi:10.1159/000108621

584 42. Heesy CP, Ross CF. Evolution of activity patterns and chromatic vision in pri-
585 mates: Morphometrics, ge-netics and cladistics. J Hum Evol. 2001;40: 111–149.

586 43. Soarimalala V, Goodman SM. Les petits mammifères de Madagascar. Antanana-
587 rivo: Association Vahatra. 2011.

588 44. Direction Générale de la Météorologie de Madagascar: http://www.meteomada-
589 gascar.mg/services/applications/climatologie.

590 45. Clavel J, Escarguel G, Merceron G. mv MORPH : an R package for fitting multi-
591 variate evolutionary models to morphometric data. Poisot T, editor. Methods Ecol Evol.
592 2015;6: 1311–1319. doi:10.1111/2041-210X.12420

593 46. Clavel J, Aristide L, Morlon H. A Penalized Likelihood Framework for High-
594 Dimensional Phylogenetic Comparative Methods and an Application to New-World
595 Monkeys Brain Evolution. Harmon L, editor. Syst Biol. 2019;68: 93–116.
596 doi:10.1093/sysbio/syy045

597 47. Blondel J. Evolution and ecology of birds on Islands: Trends and prospects. Vie
598 Milieu 1980. 2000;50: 205–220.

599 48. Loftus GR. On interpretation of interactions. Mem Cognit. 1978;6: 312–319.
600 doi:10.3758/BF03197461

601 49. Sassi PL, Cuevas MF, Menéndez J, Dacar MA. Feeding strategies of a small
602 mammal (Phyllotis xanthopygus, Rodentia Cricetidae) at diverse altitud. Ethol Ecol
603 Evol. 2016;29: 351–366. doi:10.1080/03949370.2016.1188158

604 50. Olson LE, Goodman SM, Yoder AD. Illumination of cryptic species boundaries
605 in longtailed shrew tenrecs (Mammalia: Tenrecidae; Microgale), with new insights into
606 geographic variation and distributional constraints. Biol J Linn Soc. 2004;83: 1–22.

607 51. Weisrock DW, Rasoloarison RM, Fiorentino I, Ralison JM, Goodman SM, Kap-
608 peler PM, et al. Delimiting Species without Nuclear Monophyly in Madagascar's
609 Mouse Lemurs. Kayser M, editor. PLoS ONE. 2010;5: e9883. doi:10.1371/jour-
610 nal.pone.0009883

52. Christidis L, Goodman SM, Naughton K, Appleton B. Insights into the Evolution of a Cryptic Radiation of Bats: Dispersal and Ecological Radiation of Malagasy Miniopterus (Chiroptera: Miniopteridae). PLOS ONE. 2014;9: e92440. doi:doi:10.1371/journal.pone.0092440

53. Giacomini G, Herrel A, Chaverri G, Brown RP, Russo D, Scaravelli D, et al. Functional correlates of skull shape in Chiroptera: feeding and echolocation adaptations. Integr Zool. 2021; 1749-4877.12564. doi:10.1111/1749-4877.12564

54. Simpson GG. The Major Features of Evolution. Columbia University Press. New York: Columbia University Press; 1953.

55. Gavrilets S, Losos JB. Adaptive Radiation: Contrasting Theory with Data. Science. 2009;323: 732–737. doi:10.1126/science.1157966

56. Alhajeri BH, Hunt OJ, Steppan SJ. Molecular systematics of gerbils and deomyines (Rodentia: Gerbillinae, Deomyinae) and a test of desert adaptation in the tympanic bulla. J Zool Syst Evol Res. 2015;53: 312–330. doi:10.1111/jzs.12102

57. Darvish J. Morphometric comparison of fourteen species of the genius Meriones illiger, 1811 (Gerbillinae, Rodentia) from Asia and North Africa. Iran J Anim Biosyst. 2009;5: 59–77.

58. Huang G, Rosowski J, Ravicz M, Peake W. Mammalian ear specializations in arid habitats: structural and functional evidence from sand cat (Felis margarita). J Comp Physiol [A]. 2002;188: 663–681. doi:10.1007/s00359-002-0332-8

59. Ruth AA, Raghanti MA, Meindl RS, Lovejoy CO. Locomotor pattern fails to predict foramen magnum angle in rodents, strepsirrhine primates, and marsupials. J Hum Evol. 2016;94: 45–52. doi:10.1016/j.jhevol.2016.01.003

60. Camargo NF, Machado LF, Mendonça AF, Vieira EM. Cranial shape predicts arboreal activity of Sigmodontinae rodents. J Zool. 2019;308: 128–138. doi:10.1111/jzo.12659

61. Samuels JX. Cranial morphology and dietary habits of rodents. Zool J Linn Soc. 2009;156: 864–888. doi:10.1111/j.1096-3642.2009.00502.x

62. Crowley BE. A refined chronology of prehistoric Madagascar and the demise of the megafauna. Spec Theme Case Stud Neodymium Isot Paleoceanogr. 2010;29: 2591–2603. doi:10.1016/j.quascirev.2010.06.030

63. Goodman SM, Jungers W. Extinct Madagascar: Picturing the island's past. Chicago: University of Chicago Press. 2014.

64. Mein P, Sénégas F, Gommery D, Ramanivosoa B, Randrianantenaina H, Kerloc'h P. Nouvelles espèces subfossiles de rongeurs du Nord-Ouest de Madagascar. C R Palevol. 2010; 12.

65. Perez VR, Godfrey LR, Nowak-Kemp M, Burney DA, Ratsimbazafy J, Vasey

N. Evidence of early butchery of giant lemurs in Madagascar. J Hum Evol. 2005; 21.

66. Gommery D, Ramanivosoa B. Les lémuriens subfossiles dans le Nord-Ouest de Madagascar, du terrain à la diffusion des connaissances ou 15 ans de recherches franco-malgaches. Primatol ADRSC Marseille Fr. 2011. doi:10.4000/primatologie.670]

67. Meador LR, Godfrey LR, Rakotondramavo JC, Ranivoharimanana L, Zamora A, Sutherland MR, et al. Cryptoprocta spelea (Carnivora: Eupleridae): What Did It Eat and How Do We Know? J Mamm Evol. 2019;26: 237–251. doi:10.1007/s10914-017-9391-z

68. Lavocat R. Les rongeurs du Miocène d'Afrique orientale, vol. 1 Miocène inférieur. Ecole pratique des hautes études, Mém travInst Montpellier. 1973.

69. Carleton MD, Goodman SM. Systematic studies of Madagascar's endemic rodents (Muroidea: Nesomyinae): A new genus and species from the Central Highlands. Fieldiana, Zool n s. In: Goodman SM, editor. A floral and faunal inventory of the eastern slopes of the Reserve Naturelle In-tégrale d'Andringitra, Madagascar: With reference to elevational variation. Fieldiana, Zool n s. 1996. pp. 231–250.

70. Schenk JJ, Steppan SJ. The Role of Geography in Adaptive Radiation. Am Nat. 2018;192: 415–431. doi:10.1086/699221

71. Jansa SA, Goodman SM, Tucker PK. Molecular Phylogeny and Biogeography of the Native Rodents of Madagascar (Muridae: Nesomyinae): A Test of the Single-Origin Hypothesis. Cladistics. 1999;15: 253–270. doi:doi.org/10.1111/j.1096-0031.1999.tb00267.x.

Supporting Information

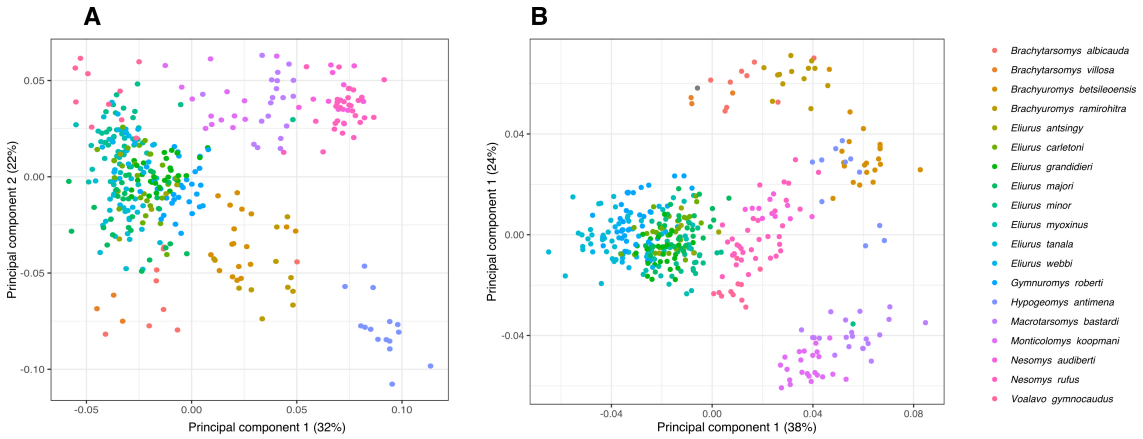

Fig. S1. Shape PCA individuals. PCA of dorsal (**A**) and ventral (**B**) view symmetric component of all individuals used for analysis.

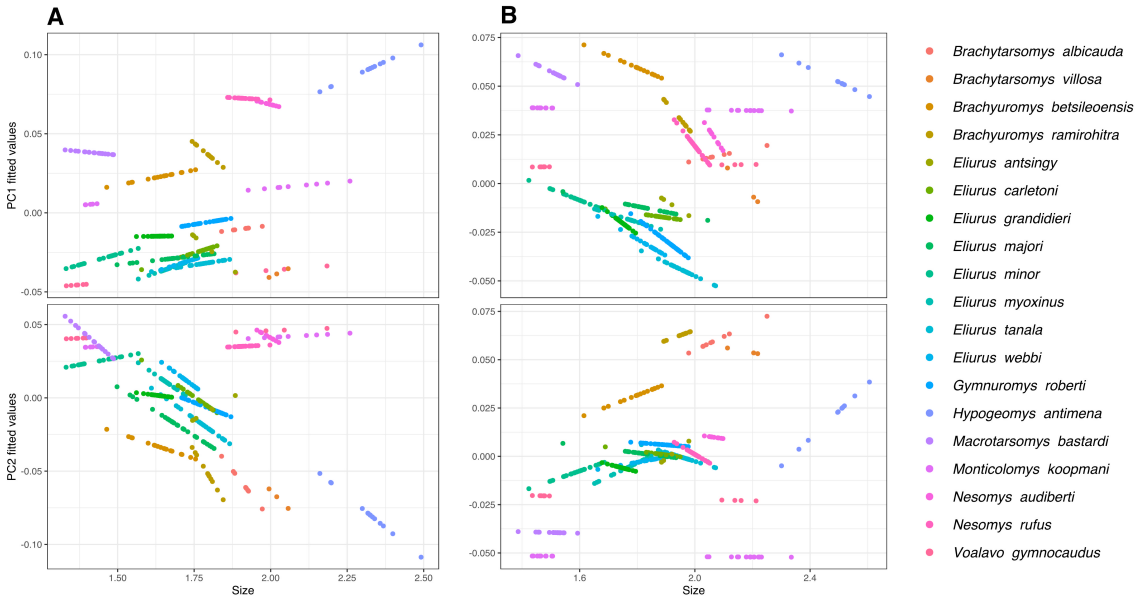

Fig. S2. Allometric slopes of species. Plots of PC1 and PC2 fitted values and the log centroid size in dorsal (**A**) and ventral (**B**) view.

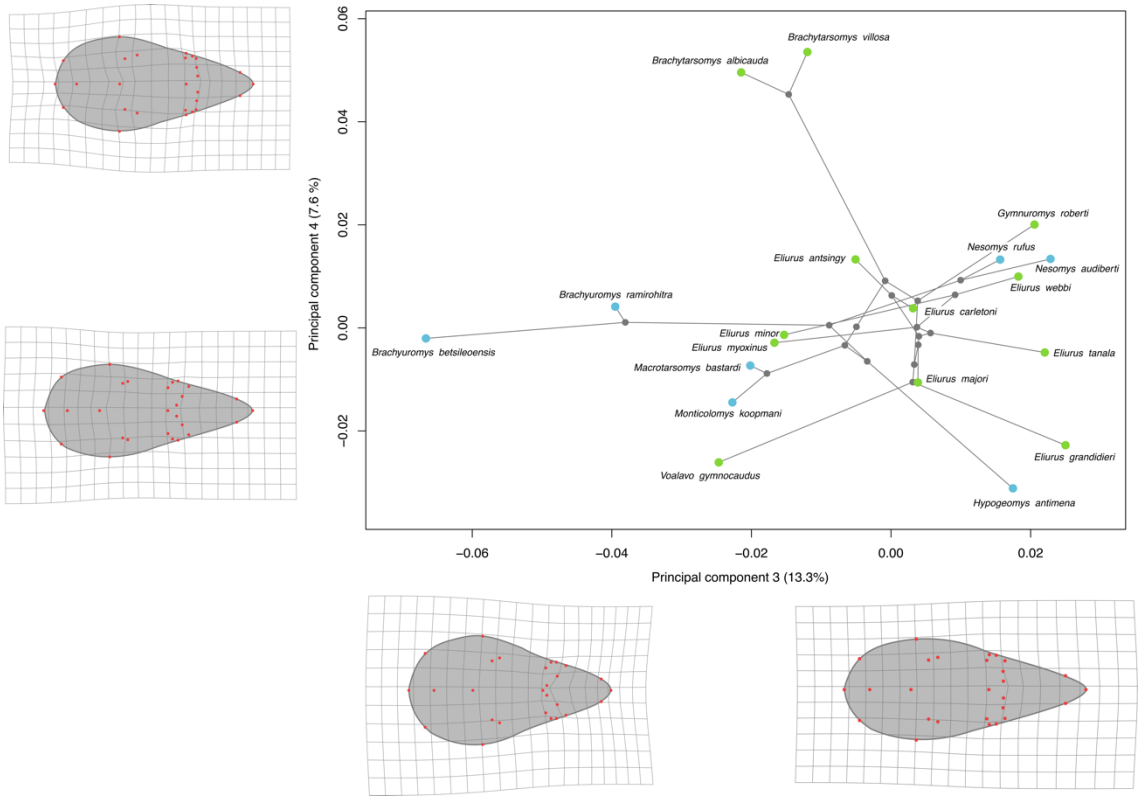

683
684

685 **Fig. S3. Visualization of the third and fourth axes of the PCA performed on dorsal**
686 **shape with phylogenetic projection.** Colored points represent the morphological aver-
687 age of all individuals of a species. Colors indicate the two principal clades among
688 Nesomyinae. Blue: clade formed by the genus *Brachyuromys, Nesomys, Macrotarsomys,*
689 *Monticolomys*, and *Hypogeomys*; green: clade formed by the genus *Brachytarsomys,*
690 *Eliurus, Gymnuromys,* and *Voalavo*. Warpgrids indicate shape variation along axis with
691 maximum deformation observed at each extremity of the axis.

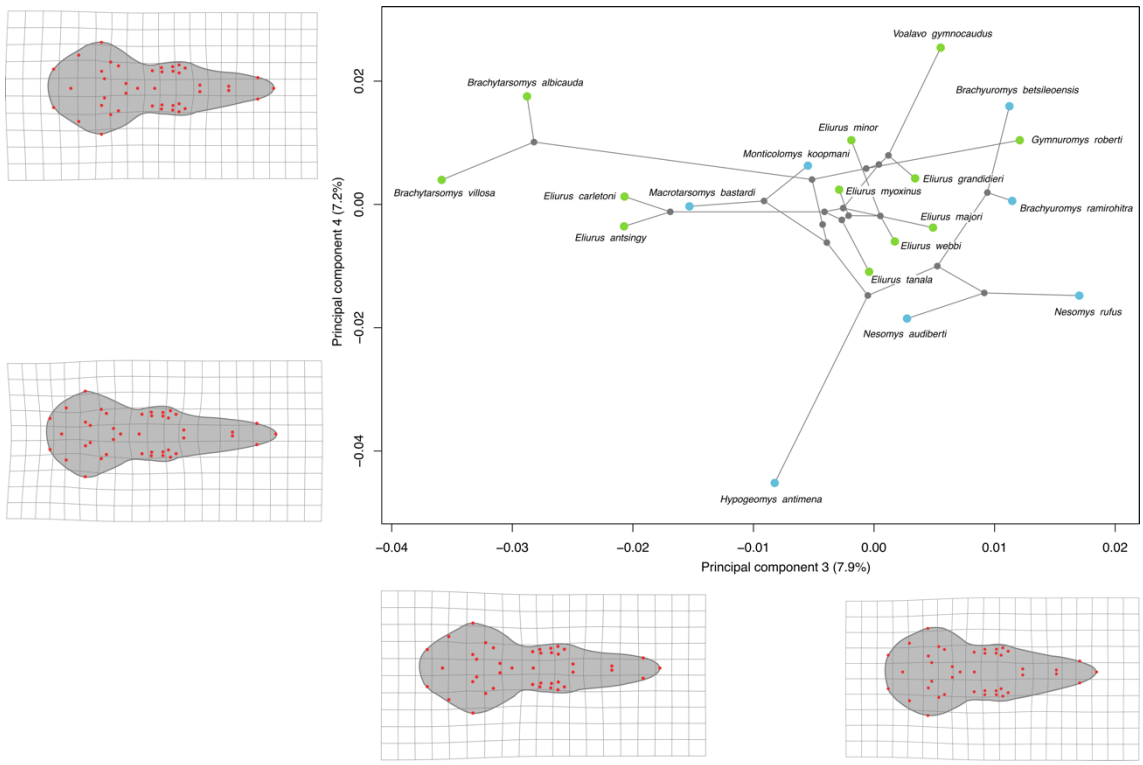

692
693

694 **Fig. S4. Visualization of the third and fourth axes of the PCA performed on ventral**
695 **shape with phylogenetic projection.** Colored points represent the morphological aver-
696 age of all individuals of a species. Colors indicate the two principal clades among
697 Nesomyinae. Blue: clade formed by the genus *Brachyuromys, Nesomys, Macrotarsomys,*
698 *Monticolomys*, and *Hypogeomys*; green: clade formed by the genus *Brachytarsomys,*
699 *Eliurus, Gymnuromys,* and *Voalavo*. Warpgrids indicate shape variation along axis with
700 maximum deformation observed at each extremity of the axis.

701

702 **Table. S1. Voucher specimen data**. List of used specimens and associated informations.
703 Lines in bold are type specimens (holotypes, syntypes or paratypes).
704

705 **Table. S2. Dorsal skull landmarks.** Descriptions and types of the 27 landmarks used for
706 the dorsal view.

707

708 **Table. S3. Ventral skull landmarks.** Descriptions and types of the 42 landmarks used
709 for the ventral view.